博士論文

ELASTIC STABILITY OF ARCHES WITH BUCKLING CONSTRAINT COMPONENTS AND THEIR APPLICATIONS

（座屈補剛されたアーチの弾性安定性

とその応用に関する研究）

陳　坤

ELASTIC STABILITY OF ARCHES WITH BUCKLING CONSTRAINT COMPONENTS AND THEIR APPLICATIONS

（座屈補剛されたアーチの弾性安定性とその応用に関する研究）

by

Kun CHEN

陳　坤

in

Department of Architecture

in

Graduate School of Engineering

of

The University of Tokyo

Doctoral Supervisor:

Professor Ken’ichi KAWAGUCHI

ABSTRACT

In this thesis, circular arches with symmetric closed cross section are taken as research objects, the elastic stability problems of circular arches with straight components and flexible components are mainly studied. The elastic stiffnesses of straight components play an important role in providing stiffening effects. In another aspect, for flexible components, if there are directly loads applied on flexible components, generating internal forces of flexible components may provide a type of stiffness (so-called stiffness of pseudo-spring) to stiffen arches.

The research work is done mainly in following aspects:

In Chapter 1, the background, the research purpose, the past researches and outline of this thesis are introduced.

In Chapter 2, according to two categorizing rules, one is the position of reaction force of braces, and the other one is the spatial relationship of the arch and braces, the stiffening patterns of single arch and cross arch are classified.

In Chapter 3, formulations of elements in finite element method are mainly discussed. Linear buckling analysis method by using FE approach to obtain the critical load and buckling mode for the bifurcation point is introduced. In order to treat the buckling problems of the circular arches and rings under uniform compression as linear buckling problems, modified matrixes considering the follower force effects of uniform compression are stated. Furthermore, formulations of linear beam element and linear truss element, formulations of geometric nonlinear beam element and geometric nonlinear truss element in FE approach are given.

In Chapter 4, theoretical approaches to analyze in-plane and out-of-plane elastic stability problems of circular arches under uniform compression are discussed. The static equilibrium differential equations built on the isolated infinitesimal body may be divided for in-plane stability and out-of-plane stability separately. Then related general solutions of displacements for in-plane stability and out-of-plane stability are given in explicit expressions. Buckling control equations for calculating the critical loads are also obtained, and specific numerical examples and FE method are used to verify these buckling control equations.

In Chapter 5, arch-spring models are proposed to simplify arches stiffened with straight braces. By using general solutions of displacements, the relationship of internal forces and these displacements on isolated infinitesimal body can be built, then the theoretical procedures for deducing the buckling control equations for in-plane stability and out-of-plane stability are given respectively. In addition, no matter in-plane stability or out-of-plane stability, spring ratios of the stiffnesses of the braces and arches are proved to be existing. Furthermore, stability problems of several stiffening patterns of single arch and cross arch, as well as hoop-rings stiffened with spokes, are analyzed.

In Chapter 6, the stiffening principle of flexible components is studied. Study work shows that the stiffening effects of elastic stiffnesses of flexible components can be ignored, and then the generating internal tension aroused by external loads mainly contributes to stiffening structures. Through an example of specific curved cables, explicit expressions of so-called stiffnesses of pseudo-springs are given. Validities of these stiffnesses of pseudo-springs are proved through comparison of the results obtained by theoretical analysis and by nonlinear FE method on a numerical example of a column model featuring with curved cables. And as applications, the stability problems of a guyed mast and a circular arch featuring with curved cables are analyzed. The variations of critical loads in these two structure systems show that the stiffening effects of curved cables are very similar to the one in the example involving column. A typical characteristic of the stiffening effect of curved cables is that there are optimal external loads on curved cables to obtain maximum critical loads. Oversize external loads on cables will decrease the critical loads, and they will also make the curved cables provide stiffening effect analogous to hinged ended.

In Chapter 7, three negatively pressured pneumatic structures utilized as first-aid shelters are constructed. During the experiments, stiffening pattern in setting ropes along the peripheral direction of multiple-arch skeleton can stop rotational buckling behavior and greatly increase the critical loads of the skeleton. Light-weight infrastructures are also verified available in the practice. Furthermore, arch model with pseudo-springs is proposed to simulate the stiffening effect of curved membrane in negatively pressured pneumatic structure in numerical analysis, and vertical load pattern and radical load pattern in numerical analysis are compared. Finally, through a load test experiment processed in a column structure featuring with curved cables, the changing of buckling shapes of the column is observed when the loads on curved cables are increasing, and the stiffnesses of pseudo-springs are proved to be existing in curved cables.

In Chapter 8, the conclusions of this thesis and future work are discussed.

ACHIEVEMENTS

Journal Papers:

1) Wang Xiaodun, Liu Zhansheng, **Chen Kun**. Study of the construction of cable supported structure. Industrial Construction, Vol. 40, No. 8, pp.35~41, 2010

*2) **Chen Kun**, Hong Wenhan, Kawaguchi Ken'ichi. Fundamental study on the buckling behavior and reinforcement for the skeleton supporting a negatively pressured pneumatic structure. Research Report on Membrane Structure 2011, No. 25, pp.17~24, 2012

*3) **Chen Kun,** Kawaguchi Ken'ichi. Fundamental study on stiffening effect of tensioned components under load. Research Report on Membrane Structure 2012, No. 26, pp. 13~19, 2013

*4) **Chen Kun**, Kawaguchi Ken'ichi. Preliminary research on stiffening effect of tensioned members with mechanism system and its applications. Journal of Structural Engineering(AIJ), Vol. 60B, pp. 179~187, 2014

*5) **Chen Kun**, Kawaguchi Ken'ichi. Preliminary study on stiffening effect of flexible tensioned components to the stability of slender structures. Journal of Building Structure, 2014 (Accepted)

Conference Papers:

1) Wang Xiaodun, **Chen Kun**, Chen Zhihua, Liu Zhansheng. Reliability welded joint of truss structure. National conference on modern steel structure 2009, pp.752~757, 2009

2) Wang Xiaodun, **Chen Kun**, Chen Zhihua, Liu Zhansheng, Ren Xiaofei. Fundamental properties of spherical lattice shell in the "lift-up" construction process. Steel Construction Conference 2010, pp. 628~634, 2010

*3) **Chen Kun**, Kawaguchi Ken'ichi, Hong Wenhan. Fundamental study on the buckling behavior and reinforcement for the skeleton supporting a negatively pressured pneumatic structure. Annual conference of AIJ 2012 Nagoya (Structure Ⅰ), pp. 929~930, 2012

*4) Hong Wenhan, Kawaguchi Ken'ichi, **Chen Kun.** Study on negatively pressured pneumatic structure by using solar power system. Annual conference of AIJ 2012 Nagoya (Environmental Engineering Ⅱ), pp. 517~518, 2012

Oral Sections:

*1) **Chen Kun,** Kawaguchi Ken'ichi, Hong Wenhan. Fundamental study on the buckling behavior and reinforcement for the skeleton supporting a negatively pressured pneumatic structure. Annual conference of AIJ 2012, Sep. 2012, Nagoya

*2) **Chen Kun**, Kawaguchi Ken'ichi. Fundamental study on the stiffening effect of mechanism tensioned components under load .The Japan Society of Mechanical Engineers (No. 13-88 Conference) 22th spatial engineering conference [SEC'13], Dec. 2012, Tokyo

*3) **Chen Kun**, Kawaguchi Ken'ichi. Preliminary research on stiffening effect of tensioned members with mechanism system and its applications. 60th Structural Engineering Symposium (AIJ), Apr. 2014, Kyoto

Patents:

1) Liu Zhansheng, Sun Guojun, Wang Xiaodun, Wang Lei, **Chen Kun**, Chen Zhihua. Patent for an invention: Cable expansion factor determination instrument, Patent number CN 101545879B, 2009

2) Wang Xiaodun, **Chen Kun**, Chen Zhihua, Sun Guojun, Liu Zhansheng, Ren Xiaofei. Patent for an invention: Multi-hinge-line lifting-up spherical lattice shell structure and construction method, Patent number CN 101956426B, 2010

(Noting: * is related to this thesis.)

ACKNOWLEDGEMENTS

This thesis is the summary of my 4-year researches as a doctoral candidate in Kawaguchi Laboratory in the University of Tokyo. My supervisor Prof. Kawaguchi Ken'ichi has been giving ardent and patient guidance in my researches all the time. Here I would like to give my most sincere thanks to him.

Prof. Chen Zhihua and Associate Prof. Wang Xiaodun, who are from Tianjin University in China, have given me lots of good advice on my researches, here I would like to express my gratitude to them.

Distinguished lecturer Mr. Ogi Yoshiro, technical staff Mr. Oya Shunji and assistant professor Mr. Akita Daisuke have given meticulous care to me. Ms. Uhara Yasuko, Ms. Kakimoto Mitsuyo and Ms. Kondo Yoko, who all are Secretaries in Kawaguchi Laboratory, have given lots of supports to me in varieties of ways. Here I would like to thank them.

Doctor Miki Masaaki is the one who led me to know the basic theories about finite element method and mechanics continuum, and he also gave me a lot of helps in composing the program codes. Mr. Ma Junbin, Mr. Cheng Chun, Mr. Nakaso Yosuke, who are all the doctoral candidates, have provided lots of helps in my daily life. And I also enjoy the time spent with Mr. Seo Namil, Mr. Hosomi Ryota, Mr. Hirotama Takuya, Miss Honda Ikuyo, who are all the master course students. Thanks for the masters Mr. Hong Wenhan and Mr. Afra participated in the experiments of negatively pressured pneumatic structures with me and provided pictures in this thesis. Thanks very much for all the students in Kawaguchi Laboratory.

Mr. Inoue Ken'ichi, who is from Jun Sato Structural Engineers, has been my tutor for one years when I came to Japan. He has helped me to accustom the daily life in Japan quickly. And he also took me to enjoy various entertainments in my leisure time. I would like to say thanks to him.

My parents, my girlfriend Miss Ren Xiaofei, and her parents have continuously given supports to me. They helped me conquer the adversity and gave me encouragement all the times. Here I would like to express my gratitude to them.

Finally, I would like to express my thanks to all the reviewers of this thesis. They are Prof. Kawaguchi Ken'ichi, Prof. Koshihara Mikio, Prof. Kuwamura Hitoshi, Prof. Takada Tsuyoshi, who are all from the University of Tokyo, and the Associate Prof. Yamamoto Kenji who is from Tokai University.

TABLE OF CONTENTS

ABSTRACT I

ACHIEVEMENTS III

ACKNOWLEDGEMENTS V

Chapter 1 Introduction 1

1.1 Background and research purpose 1

1.2 Review of past researches 4

1.2.1 Researches on the stability of arches and rings 4

1.2.2 Researches on the stability of arches with constraint components 5

1.2.3 Researches on numerical analysis of arches 6

1.2.4 Researches on negatively pressured pneumatic structures 6

1.2.5 Summaries of past researches 6

1.3 Outline of this thesis 7

Chapter 2 Category of Stiffening Patterns of Arches 9

2.1 Introduction 9

2.2 Two types of arches 9

2.3 Stiffening patterns 10

2.4 Summaries 12

Chapter 3 Formulations in Finite Element Method 13

3.1 Introduction 13

3.2 Linear buckling analysis 13

3.3 Formulations of linear elements 14

3.3.1 Linear beam element 14

3.3.2 Linear truss element 16

3.4 Formulations of geometric nonlinear elements 17

3.4.1 Geometric nonlinear beam element 17

3.4.2 Geometric nonlinear truss element 22

3.5 Modified matrixes 29

3.6 Numerical example 32

3.7 Summaries 33

Chapter 4 Theory of Elastic Stability of Arches 34

4.1 Introduction 34

4.2 Curvatures and moments 35

4.3 Equilibrium differential equations 37

4.3.1 In-plane 37

4.3.2 Out-of-plane 45

4.4 Summaries 56

Chapter 5 Stiffening Effect of Straight Components 57

5.1 Introduction 57

5.2 In-plane 57

5.2.1 Anti-symmetric buckling mode 57

5.2.2 Symmetric buckling mode 63

5.2.3 Combination analysis of two springs 67

5.2.4 Numerical examples 71

5.3 Out-of-plane 77

5.3.1 Buckling control equations........77

5.3.2 Numerical examples........81

5.4 Stiffening patterns of arches........83

5.4.1 Single arch........83

5.4.2 Cross arch........92

5.4.3 Hoop-ring........99

5.5 Summaries........103

Chapter 6 Stiffening Effect of Flexible Components........104

6.1. Introduction........104

6.2 Stiffening effects of elastic stiffness and internal force........105

6.3 Derivation of stiffness of pseudo-spring........107

6.3.1 In-plane........107

6.3.2 Out-of-plane........110

6.4 Judging the buckling plane........112

6.5 One pseudo-spring system........114

6.6 Numerical example........116

6.7 Applications of external force stiffening method........123

6.7.1 Guyed mast........124

6.7.2 Arch structure........126

6.8 Summaries........130

Chapter 7 Model Experiments........131

7.1 Introduction........131

7.2 Shelters with negatively pressured pneumatic structures........131

7.2.1 Hemispheric shelter 131

7.2.2 Rectangle shelter 137

7.2.3 Round shelter 140

7.3 Loading test experiment 148

7.4 Summaries 151

Chapter 8 Conclusions 153

8.1 Main conclusions 153

8.2 Future work 154

REFERENCES 155

Appendix A 171

Appendix B 176

Appendix C 187

Appendix D 194

Appendix E 198

Chapter 1 Introduction

1.1 Background and research purpose

Arch structure is a kind of light-weight structure that mainly transmits axial compression force to the boundary supports. Because of the concise beauty in architecture and high strength in structure, in Japan, China, Europe and other places in the world, arch structures such as arch bridges and roofs structures are widely utilized. However in the other aspect, with the decreasing of the weights of arches, large displacements and stability problems may also occur.

In order to solve such problems mentioned above, constraint components can be utilized to restrain the structural behaviors of arch structures. These constraint components can be sheeting, braces, or other secondary members, which will improve twist, rotation, warping deflection at local places of the arch structures, as well as prevent buckling behavior of the arch structures, as shown in Fig.1-1[144]. The existing components may also increase the resistance strength of the arch structures.

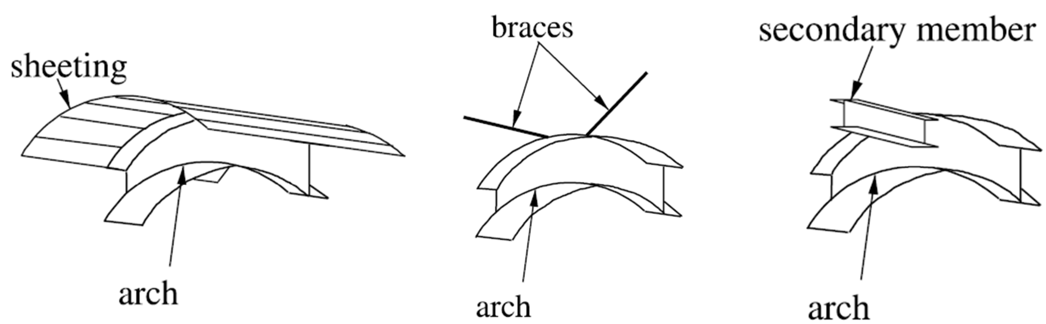

(a) (b) (c)

Fig.1-1 Constraint components at local places of the arch structures [144]

In another aspect, as noted above, the axial compression forces are the dominant forces for the arch structures, then infrastructures in the boundary are needed to react against the forces transmitted from arch, such as the horizontal reaction forces at the bases. If stiffening components such braces with rational combination of arch in the boundary of arch, the axial compression force at arch and tension force at braces can be mostly eliminated by making the best use of counterbalance effect of total internal force in entire structures, and more rational hybrid arches could be designed. Fig.1-2 shows the single arch with braces (a) and multiply arches with hoop-rings (b)[26].

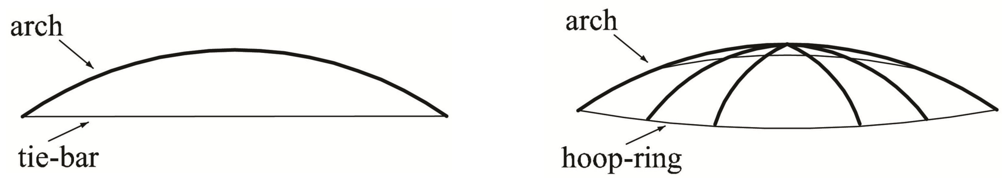

(a) (b)

Fig.1-2 Arches with components in the boundary [26]

Moreover, the straight strut can also be added at above brace to make the beam string structure consisting of arched beam in two-dimensional space (Fig.1-3(a)) [26]. And in three-dimensional space, suspen-dome pattern is available (Fig.1-3(b)) [26]. In addition, by combination of compression ring, tension ring and spoke (cable), a self-balance system called spoke structure can also be obtained (Fig.1-3(c)) [173].

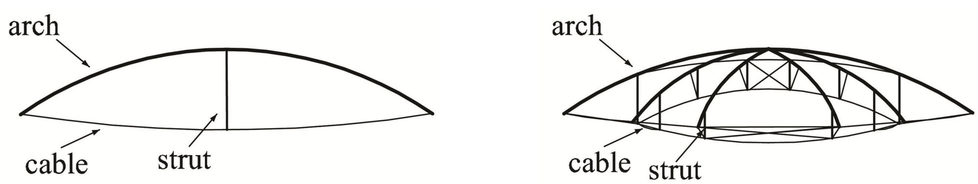

(a) [26] (b) [26]

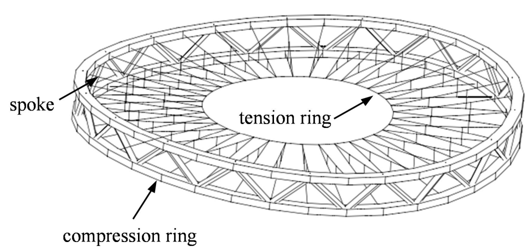

(c) [173]

Fig.1-3 Arch with components at boundary

In above narrative, constraint components themselves can be seen as rigid structures, however there are also existing flexible constraint components such as curved cables or curved membranes, and the tension in these components helps to maintain their geometric shapes. When these flexible components connect to the arch structure, these flexible components may not only transmit force to the arch, but also may provide stiffening effect to the arch. Fig.1-4(a) [148] and Fig.1-4(b) shows arch structures supported by cable-nets.

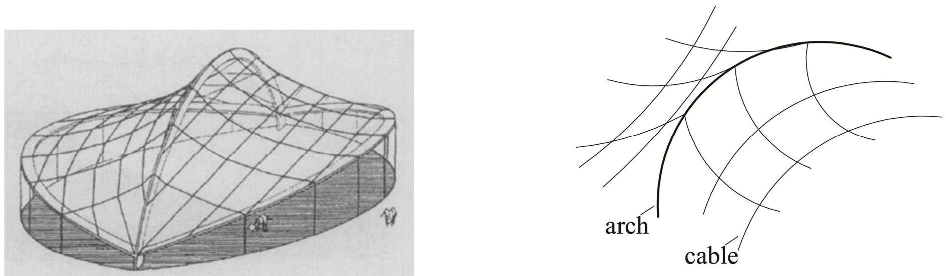

(a)[148] (b)

Fig.1-4 Arch structures supported by cable-nets

Therefore it is need further research to understand the stiffening effect of constraint components. From Fig.1-1 to Fig.1-4, the constraint components may be separated into two types: (1) rigid constraint components, such as sheetings, braces, struts, straight cables, these components themselves are structures, and their elastic stiffness is mainly utilized for stiffening; (2) flexible components, such as cable-nets, multistage cables, curved membranes, and prestress or external force should be applied to these components to generate internal tension to maintain their geometric shapes.

For straight components, it is eager to know rational arrangements of them for optimal stiffening effects. As it is not economical to use constraint components with infinity elastic stiffnesses, then determining the suitable elastic stiffnesses of components corresponding to rigidity of arch structures is very importance. However, for flexible components, whether or not they can be treated as a new type of constraint components; it is straightforward to judge that oversize tension in flexible components will do harm to the stability of arch structures, so whether there is existing an optimal tension in flexible components or not, which can only increase the stability of arch structures.

In theoretical discussion in this thesis, the arch structures are assumed as circular shapes and to have symmetric closed cross sections. And the types of buckling constraint components are supposed as braces and curved cables.

The research purpose of this thesis is stated as follows:

1) For straight buckling constraint components (ex. braces), theoretical procedures are aimed to be proposed to analyze in-plane stability and out-of-plane stability of the arch structures. Non-dimensional ratios of the elastic stiffnesses of the constraint components and the arches are aimed to be investigated by using formulations. Meanwhile, the stability problems of single arch and cross arch with different stiffening patterns are aimed to be

investigated respectively.

2) For flexible buckling constraint components (ex. curved cables), the theoretical procedures and approximate approaches are aimed to be proposed to calculate intrinsic stiffening stiffnesses, which are generated only by internal tension rather than elastic stiffnesses of the flexible components. And whether or not there is an optimal tension in curved cable to provide the best stiffening effect is aimed to be verified. Furthermore, the buckling behaviors of arch structures stiffened with flexible components are aimed to be analyzed.

3) In the practices of negatively pressured pneumatic structures, by using the straight components such as ropes to restrain the buckling modes of skeletons, the buckling phenomenons as well as the critical loads of skeletons are aimed to be investigated. And stiffening effects of membranes under negative draught head are aimed to be studied too. The realization possibility of light-weight infrastructures in this kind of pneumatic structure system is aimed to be verified. And simplified simulation models considering the stiffening effect of membranes in negatively pressured pneumatic structures are aimed to be proposed.

1.2 Review of past researches

1.2.1 Researches on the stability of arches and rings

The elastic stability theory of arch and ring has a long history. Levy [38] (1884) gave the solution for the bucking of a thin-walled ring loaded by a normal pressure in-plane. Love [38] (1944) derived the relationships for the forces and moment resultants in terms of curvatures, strains and twists for curved rods, and he also obtained the equilibriums equations. Timoshenko [42] (1961) developed the stability equations for thin bars, and he obtained closed-form solutions for the elastic buckling of a simply supported arch of narrow rectangular cross section in-plane and out-of-plane when the load condition is uniform bending and uniform compression. Vlasov [43] (1961) and Yoo [73] (1982) substituted the generalized strains of curved beam into the strains of a straight beam to obtain the equilibrium differential equations. Wah [47] (1967) used equations from free vibrations of circular rings to obtain buckling control equations in-plane and out-of-plane. George [48] (1967) made a theoretical investigation of stability of pressurized toroidal ring under uniform distributed line load considering finite shear stiffness, extensional stiffness. John [92] (1987) derived the axial and shear strains, and substituted those into second variation of total potential to obtain the buckling control equations. Tomas [63] (1979) used equations of equilibrium from nonlinear elastic theory to analyze the stability of thin-ring, and he also developed Wah's buckling theory in analyzing thick circular rings subjected to uniform compression. Yang [95] (1987) utilized the principle of virtual displacements to deduce nonlinear differential equations of equilibrium for a horizontal curved I beam. Rajasekaran [103] (1989) used the principle of virtual work for the derivation of thin-walled curved beam equations. This approach to the derivation and the associated physical interpretation is associated with geometric stiffness matrices in finite element continuum formulations. Xiang [108] (1991) gave a summary of stability theory of arch by using static method and energy method as well as nonlinear FE methods. Kang [116] (1993) used the principle of minimum total potential energy to derive equilibrium equations governing the linear, the bifurcation buckling and the large displacement behavior of thin-walled curved beams. Pi [150] (2004) derived the finite strains and the energy equations for flexural-torsional buckling of arches based on accurate orthogonal rotation matrix. Kang [165] (2007) directly used energy methods and approximate functions of buckling modes to get the critical loads.

1.2.2 Researches on the stability of arches with constraint components

Researchers studied the constraint effect of components in arch structures for a long time. Östlund [40] (1954) discussed lateral stability of bridge arches which are braced with transverse bars. Almeida [49] (1970) made his study on the lateral buckling of twin arch ribs with transverse bars. Sakimoto [72] (1982) investigated inelastic lateral instability of bridge arches associated with flexural-torsional deformation of the arch rib. Wen [94] (1987) studied the elastic stability of deck-type arch bridges. Xiang [108] (1991) studied the effect of horizontal beam to the lateral flexural-torsional buckling of hybrid arch. Nazmy [129] (1997) investigated design parameters on both strength and stability of a three-dimensional long-span steel arch bridge. Tanata [14] (2001) used numerical analysis and modeling tests to study the structural characteristics of tensegric truss arch. Ju [140] (2001) discussed the instability behavior of cable-arch structure by using large deflection finite element approach. Pi [144] (2001) discussed the elastic flexural-torsional buckling of continuously restrained arches of I-section in uniform bending and in uniform axial compression by using total potential formulation. Katoh [20] (2002) used numerical methods and experiments to study the effect of rigidity ratio, boundary condition and eccentricity to affect the buckling of beam string structure with arched beams. Wu [18] (2004) tested the static and dynamic behavior of a cable-stiffened arch models with experimental experiments and numerical analysis. Yang [154] (2005) studied in-plane stability of six types of circular arch stiffened by cables with respective different rise-span ratio and load actions by nonlinear FE approach, and he also investigated the in-plane stability of paraboloid and catenary arches stiffened by cables. Kang [165] (2007) talked about the arrangement of inclined cables to the stability of circular arch based on a cable-stayed bridge model by energy methods.

1.2.3 Researches on numerical analysis of arches

Dawe [53] (1974) proposed curved finite elements for shallow and deep arches respectively. Jones [59] (1977) used nonlinear FE approach to investigate the buckling strength of ring and shell. Robert [74] (1982) proposed matrices for change the nonlinear analysis of curved beam under uniform compression into linear eigenvalue problem. Prathap [87] (1986) designed a three-noded curved beam element with transverse shear formation from field-consistency principles. Wen [107] (1991) developed a nonlinear curved-beam finite element for three dimensional space system by using the principle of potential energy and polynomial functions. Fuji [11] (1998) proposed a computational procedure in nonlinear stability analysis of tracing the bifurcation points of a pined circular arch subject to stepwise changing loading modes. Raveendranath [136] (1999) proposed a two-noded shear flexible curved beam element with three degrees of freedom at each node based on curvilinear deep shell theory. Pi [170] (2010) also studied the effects of the pre-buckling response on the solution of the in-plane and out-of-plane uniform pressure loads of pin-ended elastic circular arches.

1.2.4 Researches on negatively pressured pneumatic structures

Negatively pressured pneumatic structure is a kind of pneumatic structure. Comparing to the positively pressured pneumatic structure (e.g. Tokyo dome), there are lack of examples of negatively pressured pneumatic structure. One deflect of positively pneumatic structure is that support structure of boundary will be very heavy in order to resist the inflation force of membrane. While for negatively pressured one, it is possible to reduce the weight of boundary, but at the same time skeleton is needed to resist the deflection force of membrane.

In Reference [25], Frei Otto proposed a conceptual design of the shape of a sing-layer and a double-layer negatively pressured pneumatic structure by directly utilizing the opposite curvature of positively pressured ones. He also wanted to build a roof with this system for an agricultural facility. Prof. Kawaguchi [21] designed the Power pavilion with negatively pressured type and put it in practice in 1970 Osaka World Exposition. Afra [35] and Hong [36] studied the possibility of build negatively pressured pneumatic structures with light-weight boundary condition, and they built several experimental models for first-aid shelters during 2012 and 2013.

1.2.5 Summaries of past researches

1) In past researches on the stability of arch structures with constraint components, stiffening effect of straight components are mostly studied. But there is lack of theoretical procedures to propose non-dimensional ratio of

elastic stiffness of straight components and arch structures in analyzing stability problems. In addition, there are not many researches carried out on the comparison of various stiffening patterns of arch structures.

2) There is lack of researches on the theoretical analysis to prove whether or not flexible components can provide stiffening effect to arch structures, and if they can, how to control the optimal tension on flexible components to provide best stiffening effect and do not do harm to the arch structures at the meantime, is also a problem to be discussed.

3) In negatively pressured pneumatic structures, curved membranes or cables under negatively draught head may provide stiffening effect to main skeletons. Few researches are carried on the negatively pressured pneumatic structures in the past. And simulation models of negatively pressured pneumatic structures are never mentioned in the past researches.

1.3 Outline of this thesis

In Chapter 1, the background, the research purpose, the past researches and outline of this thesis are introduced.

In Chapter 2, according to two categorizing rules, one is the position of reaction force of the brace, and the other one is the spatial relationship of the arch and the brace, the stiffening patterns of single arch and cross arch are classified.

In Chapter 3, formulations in finite element method are discussed. Linear buckling analysis method by using FE approach to obtain the critical load and buckling mode for the bifurcation point is introduced. In order to treat the buckling problems of the circular arches and rings under uniform compression as linear buckling problems, modified matrixes considering the follower force effects of uniform compression are stated. Furthermore, formulations of linear beam element and linear truss element, formulations of geometric nonlinear beam element and geometric nonlinear truss element in FE approach are given.

In Chapter 4, theoretical approaches to analyze in-plane and out-of-plane elastic stability of circular arches under uniform compression are discussed. The static equilibrium differential equations based on the isolated infinitesimal body may be divided separately for in-plane stability and out-of-plane stability. Then related general solutions of displacements for in-plane stability and out-of-plane stability are given in explicit expressions. Buckling control equations for calculating the critical loads are also obtained, and FE methods are used to verify these buckling control equations through specific numerical examples.

In Chapter 5, arch-spring models are proposed to simplify the arch structures stiffened with straight braces. By using general solutions of displacements, and the relationship of internal forces and these displacements can be built, then the theoretical procedures for deducing the buckling control equations for in-plane stability and out-of-plane stability are given respectively. No matter in-plane stability or out-of-plane stability, spring ratios of the stiffnesses of the braces and the arch structures are proved to be existing. Furthermore, stability problems of several stiffening patterns of single arch and cross arch, as well as hoop-rings stiffened with spokes are analyzed.

In Chapter 6, the stiffening principle of flexible components is studied. Study work shows that the stiffening effects of elastic stiffnesses of flexible components can be ignored, and then the generating internal tension aroused by external loads mainly contributes to stiffening structures. Through an example of specific curved cables, explicit expressions of so-called stiffnesses of pseudo-springs are given. Validities of these stiffnesses of pseudo-springs are proved through comparison of the results obtained by theoretical analysis and by nonlinear FE method on a numerical example of a column model featuring with curved cables. And as applications, the stability problems of a guyed mast and a circular arch featuring with curved cables are analyzed. The variations of critical loads in these two structure systems show that the stiffening effects of curved cables are very similar to the one in the example involving column. A typical characteristic of the stiffening effect of curved cables is that there are optimal external loads on curved cables to obtain maximum critical loads. Oversize external loads on cables will decrease the critical loads, and they will also make the curved cables provide stiffening effect analogous to hinged ended.

In Chapter 7, three negatively pressured pneumatic structures utilized as first-aid shelters are constructed. During the experiments, stiffening pattern in setting ropes along the peripheral direction of multiple-arch skeleton can stop rotational buckling behavior and greatly increase the critical loads of the skeleton. Light-weight infrastructures are also verified available in the practice. Furthermore, arch model with pseudo-springs is proposed to simulate the stiffening effect of curved membrane in negatively pressured pneumatic structure in numerical analysis, and vertical load pattern and radical load pattern in numerical analysis are compared. Finally, through a load test experiment processed in a column structure featuring with curved cables, the variation of buckling shapes of the column is observed when the loads on curved cables are increasing, and the stiffnesses of pseudo-springs are proved to be existing in curved cables.

In Chapter 8, the conclusions of this thesis and future work are discussed.

Chapter 2 Category of Stiffening Patterns of Arches

2.1 Introduction

Study on the stability problems of various stiffening patterns of arches is one of the research objects in this thesis. So in this chapter, and category of stiffening patterns of single arch and cross arch with circular shapes is the key content.

2.2 Two types of arches

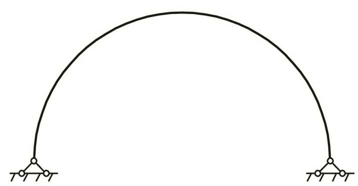

(a) Single arch

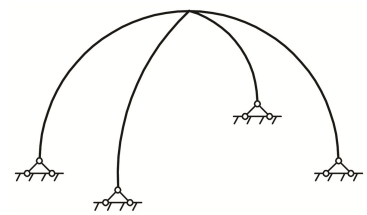

(b) Cross arch

Fig.2-1 Two types of arches

In Fig.2-1, two types of circular arches are enumerated: (a) single arch; (b) cross arch. Single arch can be seen as a as a basic unit for hybrid arches, such as cross arch, so that researches on single arch can help to understand the behavior of hybrid arches. Here three kinds of deformation of single arch under symmetric loads are enumerated. Fig.2-2(a) shows deformation of one arch under uniform load, the entire arch sunkens. And in Fig.2-2(b), when the loads near the boundary are larger than the ones near top, the arch hunches up at the top and sunken near the boundary. On contrast, in Fig.2-2(c) when the loads near the top are larger than the ones near the boundary, the arch sunkens at the top and hunches up near the boundary.

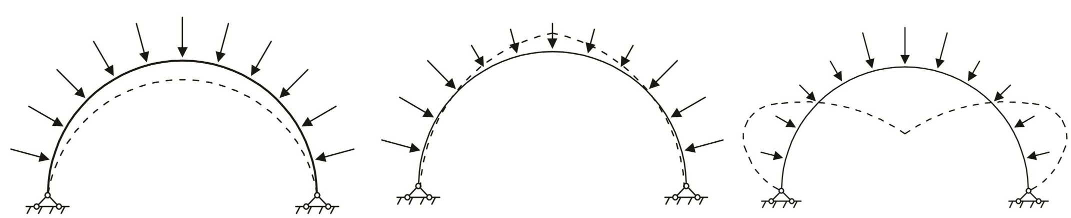

(a) Deformation shape 1 (b) Deformation shape 2 (c) Deformation shape 3

Fig.2-2 Three types of deformations

2.3 Stiffening patterns

When stiffeners are used to stiffen the arch structure, the mechanical behavior of arch will change according to different arrangements of arches. Reference [26] makes effort to divide the stiffening patterns of lattice shell structures with tensioned components. Referring to division methods in Reference [26], different stiffening patterns of single arch and cross arch are categorized. For convenience, here the constraint components in arches are assumed as all straight braces. And two rules are used for the categorizing. Examples in single arch are discussed firstly.

Rule one [26]: by judging the position of reaction force of braces, the stiffening patterns are divided into internal reaction type and external reaction type: (1) internal reaction type (Fig.2-3, Fig.2-4(a)): both sides of brace are connecting to the arch, and the reaction forces of brace happen only in the arch. (2) external reaction type (Fig.2-4(b), Fig.(2-5)): one side of brace is connecting to the arch, and the other side is connecting to a support in boundary. So the forces of braces will finally transmit to the boundary.

Rule two [26]: by considering the spatial relationship of single arch and braces in-plane, the stiffening patterns can be divided into two kinds: (1) longitudinal direction type: braces are set up along the longitudinal direction of the arch (Fig.2-3); (2) radial direction type (Fig.2-4): braces are set up in the radial direction of the arch.

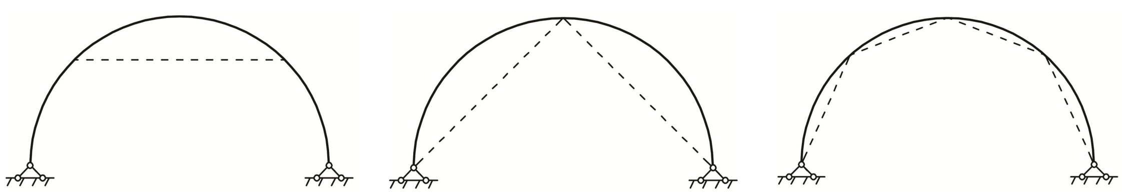

Fig.2-3 Longitudinal direction type/Internal reaction type of single arch

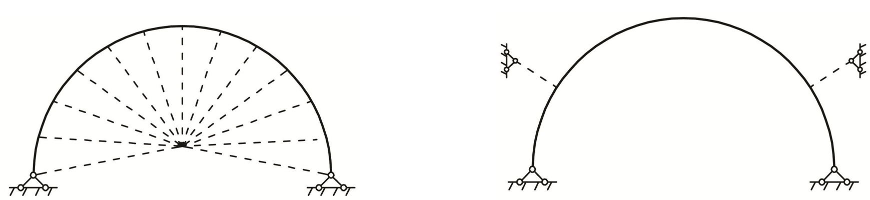

(a) Internal reaction type (b) External reaction type

Fig.2-4 Radial direction type of single arch

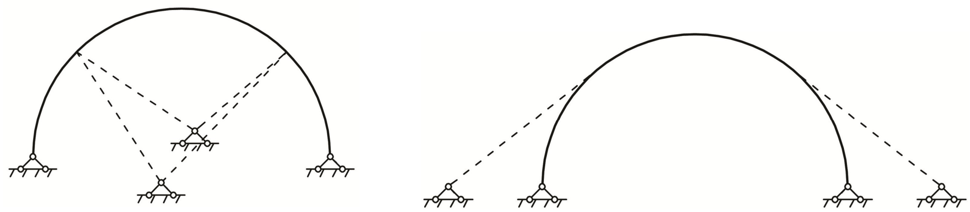

Fig.2-5 External reaction type of single arch

Similarly, in the case of cross arch, the category of internal reaction type (Fig.2-6, Fig.2-7(a)) and external reaction type (Fig.2-7(b), Fig.2-8) are also applicative. In addition, when considering the spatial relationship of arch and braces, the stiffening patterns can be divided into three kinds in cross arch: longitudinal direction type, latitudinal direction type and radial direction type. The definitions of them are as follows: (1) longitudinal direction type (Fig.2-6(a)): braces are set up along the longitude of arch. (2) peripheral direction type (Fig.2-6(b)): braces are set up along the latitude of arch. (3) Radial direction type (Fig.2-7): braces are setting up along radial direction.

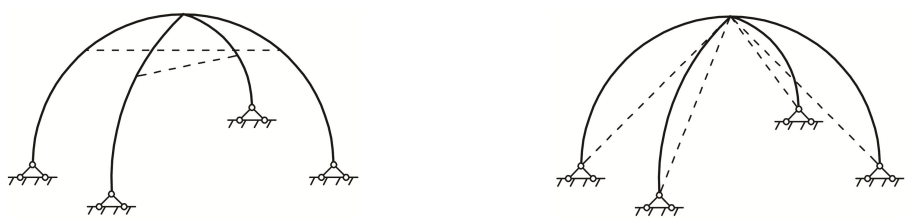

(a) Longitudinal direction type

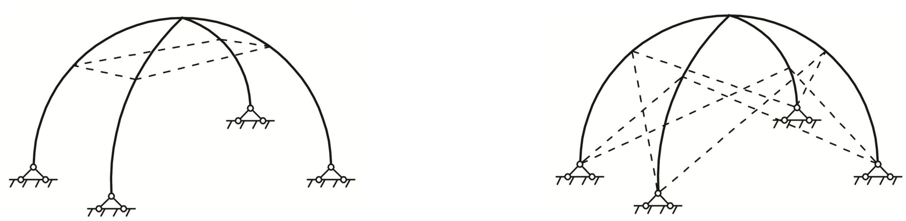

(b) Peripheral direction type

Fig.2-6 Internal reaction type of cross arch

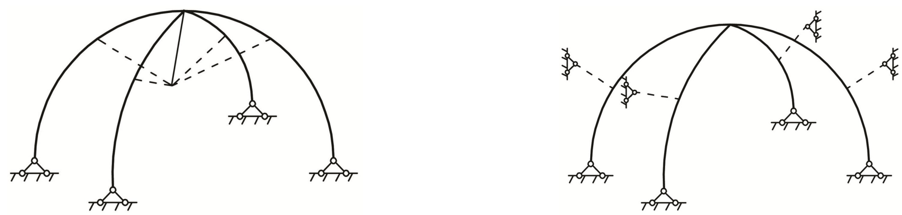

(a) Internal reaction type (b) External reaction type

Fig.2-7 Radial direction type of cross arch

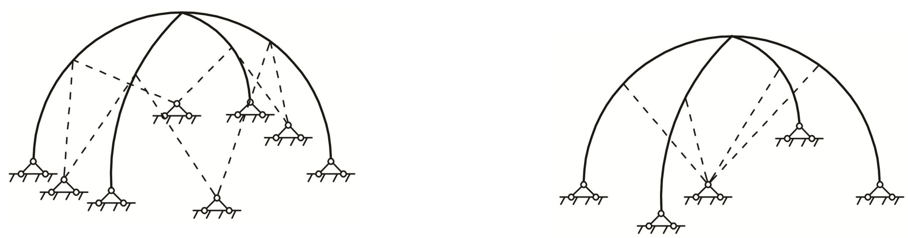

(a) Peripheral direction type (b) Radial reaction type

Fig.2-8 External reaction type of cross arch

2.4 Summaries

In this Chapter, stiffening patterns of single arch and cross arch are mainly classified according to two rules: one is by reaction force of the brace and the other one is by spatial positions of the brace and the arch. By using the first rule, internal reaction type and external reaction type are obtained. And by the latter rule, stiffening patterns of single arch are divided into longitudinal direction type and radial direction type. In another aspect, stiffening patterns of cross arch are divided into longitudinal direction type, peripheral direction type and radial direction type.

Chapter 3 Formulations in Finite Element Method

3.1 Introduction

In this chapter, formulations of elements utilized in finite element method (FE), such as linear beam element, linear truss element, geometric nonlinear beam element and geometric nonlinear truss element are introduced. In addition, for the stability problems of arches and rings under uniform compression, modified matrixes considering the follower force effect are introduced, with which the stability problems can be treated as the linear eigenvalue problems.

3.2 Linear buckling analysis

In a structure system, because of the work done by the external force, the potential energy function Π (=V-W) changes. Here V is the strain energy, W is the work done by the external force. The expression of potential energy function Π is [167]

$$\Pi = V - W = \frac{1}{2}\mathbf{u}^T \bullet \mathbf{K}_T \bullet \mathbf{u} - \mathbf{u}^T \bullet \mathbf{f} \tag{3.1}$$

Here $\mathbf{K}_T$ is the tangential stiffness matrix. $\mathbf{u}$ is the displacement vector, $\mathbf{f}$ is the nodal force vector. And $\mathbf{K}_T$ can be divided into the elastic stiffness matrix $\mathbf{K}_E$ and the geometric stiffness matrix $\mathbf{K}_G$ as follows:

$$\mathbf{K}_T = \mathbf{K}_E - \mathbf{K}_G \tag{3.2}$$

When the structure system arrives at an equilibrium state, the potential energy function will arrive at a stationary point, at this moment the first variation of potential energy function Π becomes 0, then the iterative equation can be obtained as

$$\mathbf{K}_T \bullet \mathbf{u} = \mathbf{f} \tag{3.3}$$

In order to get indifferent equilibrium state, the second variation of potential energy function Π should be 0, then the eigenvalue equation can be gotten as [34], [162]

$$(\mathbf{K}_E - \lambda_i \mathbf{K}_G) \bullet \boldsymbol{\psi}_i = 0 \tag{3.4}$$

In Eq.(3.4), λ_i is the i-th order eigenvalue, and $\boldsymbol{\psi}_i$ is the eigenvector corresponding to λ_i. In addition, the minimum positive number of λ_i is called first order critical load, and the corresponding vector is called first order buckling mode.

3.3 Formulations of linear elements

3.3.1 Linear beam element

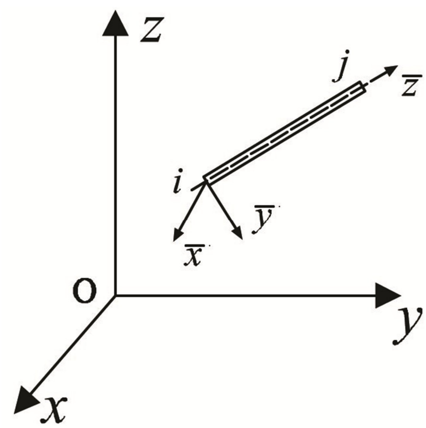

Fig.3-1 Global and local Cartesian coordinate system of 3D-beam element

Fig.3-1 shows the global and local Cartesian coordinate system of 3D-beam element with 2 nodes. In local Cartesian coordinate system, axis $\bar{z}$ is determined by the direction from node i to node j, axis $\bar{x}$ is perpendicular to axis $\bar{z}$, and axis $\bar{x}$ is parallel to plane xy in global Cartesian coordinate, axis $\bar{y}$ in local Cartesian coordinate is determined by right-handed screw rule [32].

Assuming the direction cosine of axis $\bar{z}$ in local Cartesian coordinate is

$$\bar{\mathbf{z}} = \begin{bmatrix} n_1 & n_2 & n_3 \end{bmatrix}^T \tag{3.5}$$

Assuming $\bar{x}$ is parallel to xoy plane, then the direction cosine of axis $\bar{x}$ can be obtained as

$$\bar{\mathbf{x}} = \begin{bmatrix} -\dfrac{n_2}{(n_1^2+n_2^2)^{1/2}} & \dfrac{n_1}{(n_1^2+n_2^2)^{1/2}} & 0 \end{bmatrix}^T \tag{3.6}$$

Finally direction cosine of axis $\bar{y}$ can be calculated as

$$\bar{\mathbf{y}} = \bar{\mathbf{z}} \times \bar{\mathbf{x}} \tag{3.7}$$

Noting matrix **r** as

$$\mathbf{r} = \begin{bmatrix} \bar{\mathbf{x}} & \bar{\mathbf{y}} & \bar{\mathbf{z}} \end{bmatrix} \tag{3.8}$$

According to the displacement sequence of Δx_i, Δy_i, Δz_i, $\Delta\theta_{xi}$, $\Delta\theta_{yi}$, $\Delta\theta_{zi}$, Δx_j, Δy_j, Δz_j, $\Delta\theta_{xj}$, $\Delta\theta_{yj}$, $\Delta\theta_{zj}$, the elastic stiffness matrix $\mathbf{K}_E$ and geometric stiffness matrix $\mathbf{K}_G$ of the linear beam element in 3D space are [3], [32]

$$\mathbf{K}_E = \begin{bmatrix}
\frac{12EI_x}{l^3} & & & & & & & & & & & \\
0 & \frac{12EI_y}{l^3} & & & & & & & & & & \\
0 & 0 & \frac{EA}{l} & & & & & & SYM. & & & \\
0 & -\frac{6EI_y}{l^2} & 0 & \frac{4EI_y}{l} & & & & & & & & \\
\frac{6EI_x}{l^2} & 0 & 0 & 0 & \frac{4EI_x}{l} & & & & & & & \\
0 & 0 & 0 & 0 & 0 & \frac{GJ}{l} & & & & & & \\
-\frac{12EI_x}{l^3} & 0 & 0 & 0 & -\frac{6EI_x}{l^2} & 0 & \frac{12EI_x}{l^3} & & & & & \\
0 & -\frac{12EI_y}{l^3} & 0 & \frac{6EI_y}{l^2} & 0 & 0 & 0 & \frac{12EI_y}{l^3} & & & & \\
0 & 0 & -\frac{EA}{l} & 0 & 0 & 0 & 0 & 0 & -\frac{EA}{l} & & & \\
0 & -\frac{6EI_y}{l^2} & 0 & \frac{2EI_y}{l} & 0 & 0 & 0 & \frac{6EI_y}{l^2} & 0 & \frac{4EI_y}{l} & & \\
\frac{6EI_x}{l^2} & 0 & 0 & 0 & \frac{2EI_x}{l} & 0 & -\frac{6EI_x}{l^2} & 0 & 0 & 0 & \frac{4EI_x}{l} & \\
0 & 0 & 0 & 0 & 0 & -\frac{GJ}{l} & 0 & 0 & 0 & 0 & 0 & \frac{GJ}{l}
\end{bmatrix}$$

(3.9)

$$
\mathbf{K}_G = \begin{bmatrix}
\frac{6N}{5l} & & & & & & & & & & & \\
0 & \frac{6N}{5l} & & & & & & & & & & \\
0 & 0 & 0 & & & & & & SYM. & & & \\
0 & -\frac{N}{10} & 0 & \frac{2Nl}{15} & & & & & & & & \\
\frac{N}{10} & 0 & 0 & 0 & \frac{2Nl}{15} & & & & & & & \\
-\frac{M_{xi}}{l} & \frac{M_{yi}}{l} & 0 & \frac{V_x l}{6} & \frac{V_y l}{6} & \frac{Nr_0^2}{l} & & & & & & \\
-\frac{6N}{5l} & 0 & 0 & 0 & -\frac{N}{10} & \frac{M_{xi}}{l} & \frac{6N}{5l} & & & & & \\
0 & -\frac{6N}{5l} & 0 & \frac{N}{10} & 0 & -\frac{M_{yi}}{l} & 0 & \frac{6N}{5l} & & & & \\
0 & 0 & 0 & 0 & 0 & 0 & 0 & 0 & 0 & & & \\
0 & -\frac{N}{10} & 0 & -\frac{Nl}{30} & 0 & -\frac{V_x l}{6} & 0 & \frac{N}{10} & 0 & \frac{2Nl}{15} & & \\
\frac{N}{10} & 0 & 0 & 0 & -\frac{Nl}{30} & -\frac{V_y l}{6} & -\frac{N}{10} & 0 & 0 & 0 & \frac{2Nl}{15} & \\
-\frac{M_{xj}}{l} & \frac{M_{yj}}{l} & 0 & -\frac{V_x l}{6} & -\frac{V_y l}{6} & -\frac{Nr_0^2}{l} & \frac{M_{xj}}{l} & -\frac{M_{yj}}{l} & 0 & \frac{V_x l}{6} & \frac{V_y l}{6} & \frac{Nr_0^2}{l}
\end{bmatrix} \tag{3.10}
$$

Here J is Saint-Venant torsion constant. G is the shear modulus, I_x and I_y are the moments of inertia. r_0 is the radius of gyration. And the components in Eq.(3.10) are

$$
\begin{cases}
r_0 = \sqrt{\dfrac{I_x + I_y}{A}} \\
N = N_{zi} = -N_{zj} \\
V_x = V_{xi} = -V_{xj} \\
V_y = V_{yi} = -V_{yj}
\end{cases} \tag{3.11}
$$

3.3.2 Linear truss element

By the hypothesis of small stain and small deformation, the elastic stiffness matrix $\mathbf{K}_E$ and geometric elastic stiffness matrix $\mathbf{K}_G$ of liner truss element in 3D space can refer to Reference [1], [2], [28]. Noting a direction cosine matrix as $\mathbf{C}$, and $\mathbf{C}$ is 3×1 matrix, and then other two matrixes are defined as

$$
\mathbf{k}_e = \frac{EA}{L}\mathbf{C}\bullet\mathbf{C}^T \tag{3.12}
$$

$$\mathbf{k}_g = \frac{N}{L}(\mathbf{I}_3 - \mathbf{C} \bullet \mathbf{C}^T) \tag{3.13}$$

In equations above, E is the Young's modulus, A is the area of cross section, L is the member length, N is the axial compression force, and $\mathbf{I}_3$ is a 3×3 unit matrix.

The elastic stiffness matrix $\mathbf{K}_E$ and geometric stiffness matrix $\mathbf{K}_G$ can be obtained as follows:

$$\mathbf{K}_E = \begin{bmatrix} \mathbf{k}_e & -\mathbf{k}_e \\ -\mathbf{k}_e & \mathbf{k}_e \end{bmatrix} \tag{3.14}$$

$$\mathbf{K}_G = \begin{bmatrix} \mathbf{k}_g & -\mathbf{k}_g \\ -\mathbf{k}_g & \mathbf{k}_g \end{bmatrix} \tag{3.15}$$

3.4 Formulations of geometric nonlinear elements

3.4.1 Geometric nonlinear beam element

In this section, geometric nonlinear beam element which has two nodes is introduced [86], [101]. And in this section, Eq.(3.16)~Eq.(3.55) refer to Reference [86]. This beam element is deduced through an updated Lagrangian approach, and it can be applied in analyzing the structure with large rotation and small strain. Fig.3-2 shows the displacements and internal forces of the beam element. In Fig.3-2, local Cartesian coordinate system $\bar{x}_1\bar{x}_2\bar{x}_3$ is set up on the beam element. $\bar{x}_1$ is along the connecting line of two nodes, $\bar{x}_2$ and $\bar{x}_3$ are along the direction of principle inertia axes in cross section respectively. And after deformation, usually two cross sections in one beam element are not parallel with each other anymore, $\bar{x}_2$ and $\bar{x}_3$ may be defined by the average values of principle inertia axes respectively.

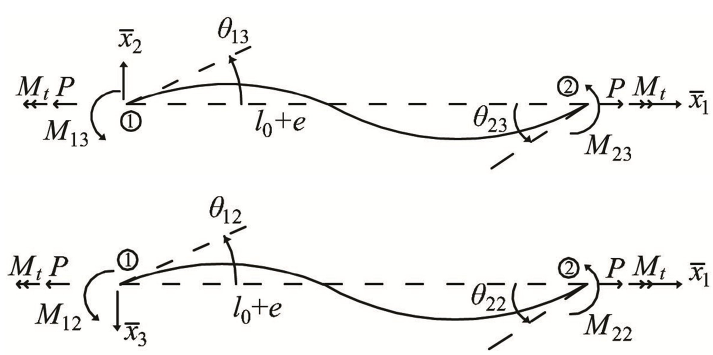

(a)

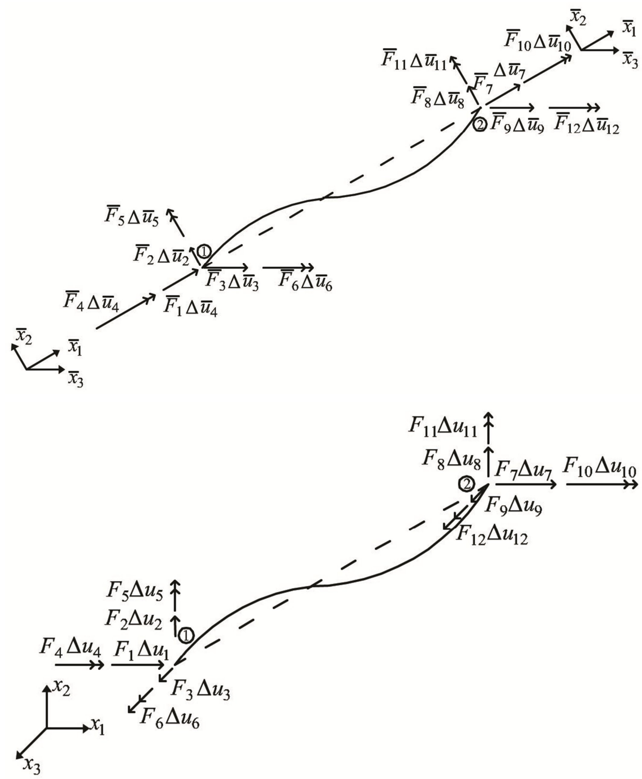

(b)

Fig.3-2 Displacements and internal forces of beam element [86], [101]

By utilizing the principle of minimum potential energy, the internal forces of beam element can be obtained as

$$M_{13} = (\frac{4EI_3}{l} + \frac{4Pl}{30})\theta_{13} + (\frac{2EI_3}{l} - \frac{Pl}{30})\theta_{23} \tag{3.16}$$

$$M_{23} = (\frac{2EI_3}{l} - \frac{Pl}{30})\theta_{13} + (\frac{4EI_3}{l} + \frac{4Pl}{30})\theta_{23} \tag{3.17}$$

$$M_{12} = (\frac{4EI_2}{l} + \frac{4Pl}{30})\theta_{12} + (\frac{2EI_2}{l} - \frac{Pl}{30})\theta_{22} \tag{3.18}$$

$$M_{22} = (\frac{2EI_2}{l} - \frac{Pl}{30})\theta_{12} + (\frac{4EI_2}{l} + \frac{4Pl}{30})\theta_{22} \tag{3.19}$$

$$M_t = (\frac{GJ}{l})\theta_t \tag{3.20}$$

$$P = EA[(\frac{e}{l}) + \frac{1}{30}(2\theta_{13}^2 - \theta_{13}\theta_{23} + 2\theta_{23}^2) + \frac{1}{30}(2\theta_{12}^2 - \theta_{12}\theta_{22} + 2\theta_{22}^2)] \tag{3.21}$$

Shear deformations and warping are neglected in equations above. Then firstly from the differential forms of Eq.(3.16)~Eq.(3.21), the relationship of internal forced and displacements can be obtained as

$$\Delta\mathbf{S} = \mathbf{K} \bullet \Delta\mathbf{V} \tag{3.22}$$

And components in Eq.(3.22) are

$$\Delta \mathbf{S} = \left[\Delta M_{13}, \Delta M_{23}, \Delta M_{12}, \Delta M_{22}, \Delta M_t, \Delta P\right]^T \tag{3.23}$$

$$\Delta \mathbf{V} = \left[\Delta \theta_{13}, \Delta \theta_{23}, \Delta \theta_{12}, \Delta \theta_{22}, \Delta \theta_t, \Delta e\right]^T \tag{3.24}$$

$$\mathbf{K} = \begin{bmatrix} K_{11} & K_{12} & K_{13} & K_{14} & K_{15} & K_{16} \\ & K_{22} & K_{23} & K_{24} & K_{25} & K_{26} \\ & & K_{33} & K_{34} & K_{35} & K_{36} \\ & SYM. & & K_{44} & K_{45} & K_{46} \\ & & & & K_{55} & K_{56} \\ & & & & & K_{66} \end{bmatrix} \tag{3.25}$$

And the components in Eq.(3.25) are

$$K_{11} = \frac{4EI_3}{l} + \frac{4EAe}{30} + \frac{EAl}{300}(8\theta_{13}^2 - 4\theta_{13}\theta_{23} + 3\theta_{23}^2) + \frac{EAl}{900}(8\theta_{12}^2 - 4\theta_{12}\theta_{22} + 8\theta_{22}^2) \tag{3.26}$$

$$K_{12} = \frac{2EI_3}{l} - \frac{EAe}{30} - \frac{EAl}{300}(2\theta_{13}^2 - 6\theta_{13}\theta_{23} + 2\theta_{23}^2) - \frac{EAl}{900}(2\theta_{12}^2 - \theta_{12}\theta_{22} + 2\theta_{22}^2) \tag{3.27}$$

$$K_{13} = \frac{EAl}{900}(16\theta_{13}\theta_{12} - 4\theta_{13}\theta_{22} - 4\theta_{12}\theta_{23} + \theta_{23}\theta_{22}) \tag{3.28}$$

$$K_{14} = \frac{EAl}{900}(-4\theta_{13}\theta_{12} + 16\theta_{13}\theta_{22} + \theta_{23}\theta_{12} - 4\theta_{23}\theta_{22}) \tag{3.29}$$

$$K_{15} = 0 \tag{3.30}$$

$$K_{16} = \frac{EA}{30}(4\theta_{13} - \theta_{23}) \tag{3.31}$$

$$K_{22} = \frac{4EI_3}{l} + \frac{4EAe}{30} + \frac{EAl}{300}(3\theta_{13}^2 - 4\theta_{13}\theta_{23} + 8\theta_{23}^2) + \frac{EAl}{900}(8\theta_{12}^2 - 4\theta_{12}\theta_{22} + 8\theta_{22}^2) \tag{3.32}$$

$$K_{23} = \frac{EAl}{900}(-4\theta_{12}\theta_{13} + \theta_{13}\theta_{22} + 16\theta_{23}\theta_{12} - 4\theta_{23}\theta_{22}) \tag{3.33}$$

$$K_{24} = \frac{EAl}{900}(\theta_{12}\theta_{13} - 4\theta_{13}\theta_{22} - 4\theta_{23}\theta_{12} + 16\theta_{23}\theta_{22}) \tag{3.34}$$

$$K_{25} = 0 \tag{3.35}$$

$$K_{26} = \frac{EA}{30}(-\theta_{13} + 4\theta_{23}) \tag{3.36}$$

$$K_{33} = \frac{4EI_2}{l} + \frac{4EAe}{30} + \frac{EAl}{900}(8\theta_{13}^2 - 4\theta_{12}\theta_{23} + 8\theta_{23}^2) + \frac{EAl}{300}(8\theta_{12}^2 - 4\theta_{12}\theta_{22} + 3\theta_{22}^2) \tag{3.37}$$

$$K_{34} = \frac{2EI_2}{l} - \frac{EAe}{30} - \frac{EAl}{900}(2\theta_{13}^2 - \theta_{13}\theta_{23} + 2\theta_{23}^2) - \frac{EAl}{300}(2\theta_{12}^2 - 6\theta_{12}\theta_{22} + 2\theta_{22}^2) \tag{3.38}$$

$$K_{35} = 0 \tag{3.39}$$

$$K_{36} = \frac{EA}{30}(4\theta_{12} - \theta_{22}) \tag{3.40}$$

$$K_{44} = \frac{4EI_2}{l} + \frac{4EAe}{30} + \frac{EAl}{900}(8\theta_{13}^2 - 4\theta_{13}\theta_{23} + 8\theta_{23}^2) + \frac{EAl}{300}(3\theta_{12}^2 - 4\theta_{12}\theta_{22} + 8\theta_{22}^2) \tag{3.41}$$

$$K_{45} = 0 \tag{3.42}$$

$$K_{46} = \frac{EA}{30}(-\theta_{12} + 4\theta_{22}) \tag{3.43}$$

$$K_{55} = \frac{GJ}{l} \tag{3.44}$$

$$K_{56} = 0 \tag{3.45}$$

$$K_{66} = \frac{EA}{l} \tag{3.46}$$

On the other hand, equilibrium equation in local Cartesian coordinate system is

$$\overline{\mathbf{F}} = \mathbf{G} \bullet \mathbf{S} \tag{3.47}$$

In Eq.(3.47), matrix $\mathbf{G}$ is

$$\mathbf{G} = \begin{bmatrix} 0 & \frac{1}{l} & 0 & 0 & 0 & 1 & 0 & -\frac{1}{l} & 0 & 0 & 0 & 0 \\ 0 & \frac{1}{l} & 0 & 0 & 0 & 0 & 0 & -\frac{1}{l} & 0 & 0 & 0 & 1 \\ 0 & 0 & -\frac{1}{l} & 0 & 1 & 0 & 0 & 0 & \frac{1}{l} & 0 & 0 & 0 \\ 0 & 0 & -\frac{1}{l} & 0 & 0 & 0 & 0 & 0 & \frac{1}{l} & 0 & 1 & 0 \\ 0 & 0 & 0 & -1 & 0 & 0 & 0 & 0 & 0 & 1 & 0 & 0 \\ -1 & 0 & 0 & 0 & 0 & 0 & 1 & 0 & 0 & 0 & 0 & 0 \end{bmatrix}^T \tag{3.48}$$

Noting displacement vector $\Delta\overline{\mathbf{u}}$ of node in local Cartesian coordinate system as

$$\Delta\overline{\mathbf{u}} = \begin{bmatrix} \Delta\overline{u}_1 & \Delta\overline{u}_2 & \cdots & \Delta\overline{u}_{12} \end{bmatrix}^T \tag{3.49}$$

Then $\Delta\mathbf{V}$ can be obtained as

$$\Delta\mathbf{V} = \mathbf{G}^T \bullet \Delta\overline{\mathbf{u}} \tag{3.50}$$

The differential equation of Eq.(3.47) is

$$\Delta\overline{\mathbf{F}} = \mathbf{G} \bullet \Delta\mathbf{S} + \Delta\mathbf{G} \bullet \mathbf{S} \tag{3.51}$$

The matrix $\Delta\mathbf{G}$ is

$$
\Delta\mathbf{G} = \begin{bmatrix}
-\rho_3/l & -\rho_3/l & -\rho_2/l & -\rho_2/l & 0 & 0 \\
-\delta/l^2 & -\delta/l^2 & 0 & 0 & 0 & -\rho_3 \\
0 & 0 & \delta/l^2 & \delta/l^2 & 0 & \rho_2 \\
0 & 0 & 0 & 0 & 0 & 0 \\
0 & 0 & 0 & 0 & 0 & 0 \\
0 & 0 & 0 & 0 & 0 & 0 \\
\rho_3/l & \rho_3/l & \rho_2/l & \rho_2/l & 0 & 0 \\
\delta/l^2 & \delta/l^2 & 0 & 0 & 0 & \rho_3 \\
0 & 0 & -\delta/l^2 & -\delta/l^2 & 0 & -\rho_2 \\
0 & 0 & 0 & 0 & 0 & 0 \\
0 & 0 & 0 & 0 & 0 & 0 \\
0 & 0 & 0 & 0 & 0 & 0
\end{bmatrix} \tag{3.52}
$$

In Eq.(3.52), $\delta = \Delta\bar{u}_7 - \Delta\bar{u}_1$, $\rho_2 = -(\Delta\bar{u}_9 - \Delta\bar{u}_3)/l$, $\rho_3 = (\Delta\bar{u}_8 - \Delta\bar{u}_2)/l$.

Substituting Eq.(3.22) into Eq.(3.51), the second term of Eq.(3.51) can change into expression of $\Delta\bar{\mathbf{u}}$.

$$
\Delta\overline{\mathbf{F}} = \mathbf{G}\bullet\mathbf{K}\bullet\Delta\mathbf{V} + \mathbf{D}\bullet\Delta\overline{\mathbf{u}} = (\mathbf{G}\bullet\mathbf{K}\bullet\mathbf{G}^T + \mathbf{D})\bullet\Delta\overline{\mathbf{u}} == \overline{\mathbf{K}}\bullet\Delta\overline{\mathbf{u}} \tag{3.53}
$$

Noting $a=(M_{12}+M_{22})/l^2$, $b=(M_{13}+M_{23})/l^2$, $c=P/l$, then matrix $\mathbf{D}$ in Eq.(3.53) is

$$
\mathbf{D} = \begin{bmatrix}
0 & b & -a & 0 & 0 & 0 & 0 & -b & a & 0 & 0 & 0 \\
 & c & 0 & 0 & 0 & 0 & -b & -c & 0 & 0 & 0 & 0 \\
 & & c & 0 & 0 & 0 & a & 0 & -c & 0 & 0 & 0 \\
 & & & 0 & 0 & 0 & 0 & 0 & 0 & 0 & 0 & 0 \\
 & & & & 0 & 0 & 0 & 0 & 0 & 0 & 0 & 0 \\
 & & & & & 0 & 0 & 0 & 0 & 0 & 0 & 0 \\
 & & & & & & 0 & b & -a & 0 & 0 & 0 \\
 & & SYM. & & & & & c & 0 & 0 & 0 & 0 \\
 & & & & & & & & c & 0 & 0 & 0 \\
 & & & & & & & & & 0 & 0 & 0 \\
 & & & & & & & & & & 0 & 0 \\
 & & & & & & & & & & & 0
\end{bmatrix} \tag{3.54}
$$

Transformation matrix of local Cartesian coordinate and global Cartesian coordinate is noted as

$$
\widetilde{\mathbf{R}} = \begin{bmatrix}
\mathbf{r} & & & \\
 & \mathbf{r} & & \\
 & & \mathbf{r} & \\
 & & & \mathbf{r}
\end{bmatrix} \tag{3.55}
$$

Here $\mathbf{r}$ is a direction matrix. This transformation matrix can be obtained in Reference [119]. Then tangential stiffness matrix in global Cartesian coordinate is

$$\mathbf{K}_g = \widetilde{\mathbf{R}} \cdot \overline{\mathbf{K}} \cdot \widetilde{\mathbf{R}}^T \tag{3.56}$$

3.4.2 Geometric nonlinear truss element

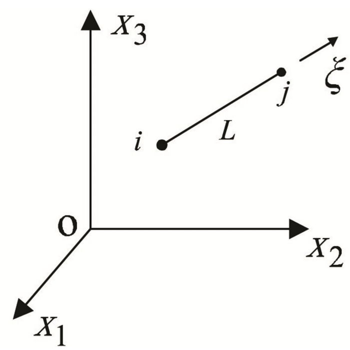

Fig.3-3 Truss element in 3D space [151]

Reference [151] introduced the formulation of geometric nonlinear truss element in 3D space. In this section, Eq.(3.57)~Eq.(3.86), Eq.(3.92)~Eq.(3.98) refer to Reference [151]. This formulation of truss element is an updated Lagrangian approach. Fig.3-3 shows a truss element with 2 nodes, the length of truss element is L, and i, j are the numbers of nodes. X_1, X_2, X_3 are axes in global Cartesian coordinate system. The displacement vector $\mathbf{u}$ at any position of truss element can be expressed by shape functions N_1 and N_2 as follows

$$\mathbf{u} = \begin{bmatrix} N_1 & 0 & 0 & N_2 & 0 & 0 \\ 0 & N_1 & 0 & 0 & N_2 & 0 \\ 0 & 0 & N_1 & 0 & 0 & N_2 \end{bmatrix} \cdot \begin{Bmatrix} u_1^1 \\ u_2^1 \\ u_3^1 \\ u_1^2 \\ u_2^2 \\ u_3^2 \end{Bmatrix} \tag{3.57}$$

Here the displacement vector $\mathbf{u}$ can be expressed as

$$\mathbf{u} = \begin{Bmatrix} u_1 \\ u_2 \\ u_3 \end{Bmatrix} \tag{3.58}$$

Shape functions N_1 and N_2 in natural coordinate system ξ are

$$N_1 = 1 - \frac{\xi}{L} \tag{3.59}$$

$$N_2 = \frac{\xi}{L} \tag{3.60}$$

Noting displacement vector of node $\mathbf{u}_e$ as

$$\mathbf{u}_e = \left\{ u_1^1 \quad u_1^2 \quad u_1^3 \quad u_2^1 \quad u_2^2 \quad u_2^3 \right\}^T \tag{3.61}$$

Green-Lagrange stain form moment t to t' is defined as

$$_t^{t'}\boldsymbol{\xi} = \left\{ _t^{t'}\xi_{11} \quad _t^{t'}\xi_{22} \quad _t^{t'}\xi_{33} \quad 2_t^{t'}\xi_{12} \quad 2_t^{t'}\xi_{13} \quad 2_t^{t'}\xi_{23} \right\}^T \tag{3.62}$$

$_t^{t'}\boldsymbol{\xi}$ can be divided into linear strain $_t\mathbf{e}$ and nonlinear strain $_t\boldsymbol{\eta}$.

$$_te_{ij} = \frac{1}{2}(u_{i,j} + u_{j,i}) \tag{3.63}$$

So that the linear strain $_t\mathbf{e}$ can be expressed as

$$_t\mathbf{e} = \left\{ _te_{11} \quad _te_{22} \quad _te_{33} \quad 2_te_{12} \quad 2_te_{13} \quad 2_te_{23} \right\}^T = \mathbf{L} \bullet \mathbf{u} = \mathbf{L} \bullet \mathbf{N} \bullet \mathbf{u}_e = \mathbf{B}_L \bullet \mathbf{u}_e \tag{3.64}$$

Variation and derivative of linear strain $_t\mathbf{e}$ is

$$\delta_t\mathbf{e} = \mathbf{B}_L \bullet \delta\mathbf{u}_e \tag{3.65}$$

$$_t\dot{\mathbf{e}} = \mathbf{B}_L \bullet \dot{\mathbf{u}}_e \tag{3.66}$$

Then noting

$$_t\eta_{ij} = \frac{1}{2}(u_{k,i} \bullet u_{k,j}) \tag{3.67}$$

So that the nonlinear strain $_t\boldsymbol{\eta}$ is

$$_t\boldsymbol{\eta} = \left\{ _t\eta_{11} \quad _t\eta_{22} \quad _t\eta_{33} \quad 2_t\eta_{12} \quad 2_t\eta_{13} \quad 2_t\eta_{23} \right\}^T = \frac{1}{2} \bullet \mathbf{A} \bullet \mathbf{H} \bullet \mathbf{u} = \frac{1}{2} \bullet \mathbf{A} \bullet \mathbf{B}_{NL} \bullet \mathbf{u}_e \tag{3.68}$$

Variation of nonlinear strain $_t\boldsymbol{\eta}$ is

$$\delta_t \boldsymbol{\eta} = \mathbf{A} \bullet \mathbf{H} \bullet \delta \mathbf{u} = \mathbf{A} \bullet \mathbf{B}_{NL} \bullet \delta \mathbf{u}_e \tag{3.69}$$

And the derivative of variation of nonlinear strain $_t\boldsymbol{\eta}$ is

$$(\delta_t \boldsymbol{\eta})^{\bullet} = \overline{\mathbf{A}} \bullet \mathbf{H} \bullet \delta \mathbf{u} = \overline{\mathbf{A}} \bullet \mathbf{B}_{NL} \bullet \delta \mathbf{u}_e \tag{3.70}$$

Here the components in equations above are

$$\mathbf{L} = \begin{bmatrix} \frac{\partial}{\partial^t X_1} & 0 & 0 & \frac{\partial}{\partial^t X_2} & \frac{\partial}{\partial^t X_3} & 0 \\ 0 & \frac{\partial}{\partial^t X_2} & 0 & \frac{\partial}{\partial^t X_1} & 0 & \frac{\partial}{\partial^t X_3} \\ 0 & 0 & \frac{\partial}{\partial^t X_3} & 0 & \frac{\partial}{\partial^t X_1} & \frac{\partial}{\partial^t X_2} \end{bmatrix}^T \tag{3.71}$$

$$\mathbf{B}_L = \mathbf{L} \bullet \mathbf{N} = \begin{bmatrix} \frac{\partial N_1}{\partial^t X_1} & 0 & 0 & \frac{\partial N_2}{\partial^t X_1} & 0 & 0 \\ 0 & \frac{\partial N_1}{\partial^t X_2} & 0 & 0 & \frac{\partial N_2}{\partial^t X_2} & 0 \\ 0 & 0 & \frac{\partial N_1}{\partial^t X_3} & 0 & 0 & \frac{\partial N_2}{\partial^t X_3} \\ \frac{\partial N_1}{\partial^t X_2} & \frac{\partial N_1}{\partial^t X_1} & 0 & \frac{\partial N_2}{\partial^t X_2} & \frac{\partial N_2}{\partial^t X_1} & 0 \\ \frac{\partial N_1}{\partial^t X_3} & 0 & \frac{\partial N_1}{\partial^t X_1} & \frac{\partial N_2}{\partial^t X_3} & 0 & \frac{\partial N_2}{\partial^t X_1} \\ 0 & \frac{\partial N_1}{\partial^t X_3} & \frac{\partial N_1}{\partial^t X_2} & 0 & \frac{\partial N_2}{\partial^t X_3} & \frac{\partial N_2}{\partial^t X_2} \end{bmatrix} \tag{3.72}$$

$$\mathbf{A} = \begin{bmatrix} \frac{\partial u_1}{\partial^t X_1} & 0 & 0 & \frac{\partial u_2}{\partial^t X_1} & 0 & 0 & \frac{\partial u_3}{\partial^t X_1} & 0 & 0 \\ 0 & \frac{\partial u_1}{\partial^t X_2} & 0 & 0 & \frac{\partial u_2}{\partial^t X_2} & 0 & 0 & \frac{\partial u_3}{\partial^t X_2} & 0 \\ 0 & 0 & \frac{\partial u_1}{\partial^t X_3} & 0 & 0 & \frac{\partial u_2}{\partial^t X_3} & 0 & 0 & \frac{\partial u_3}{\partial^t X_3} \\ \frac{\partial u_1}{\partial^t X_2} & \frac{\partial u_1}{\partial^t X_1} & 0 & \frac{\partial u_2}{\partial^t X_2} & \frac{\partial u_2}{\partial^t X_1} & 0 & \frac{\partial u_3}{\partial^t X_2} & \frac{\partial u_3}{\partial^t X_1} & 0 \\ \frac{\partial u_1}{\partial^t X_3} & 0 & \frac{\partial u_1}{\partial^t X_1} & \frac{\partial u_2}{\partial^t X_3} & 0 & \frac{\partial u_2}{\partial^t X_1} & \frac{\partial u_3}{\partial^t X_3} & 0 & \frac{\partial u_3}{\partial^t X_1} \\ 0 & \frac{\partial u_1}{\partial^t X_3} & \frac{\partial u_1}{\partial^t X_2} & 0 & \frac{\partial u_2}{\partial^t X_3} & \frac{\partial u_2}{\partial^t X_2} & 0 & \frac{\partial u_3}{\partial^t X_3} & \frac{\partial u_3}{\partial^t X_2} \end{bmatrix} \tag{3.73}$$

$$\overline{\mathbf{A}} = \begin{bmatrix} \frac{\partial^t \dot{u}_1}{\partial^t X_1} & 0 & 0 & \frac{\partial^t \dot{u}_2}{\partial^t X_1} & 0 & 0 & \frac{\partial^t \dot{u}_3}{\partial^t X_1} & 0 & 0 \\ 0 & \frac{\partial^t \dot{u}_1}{\partial^t X_2} & 0 & 0 & \frac{\partial^t \dot{u}_2}{\partial^t X_2} & 0 & 0 & \frac{\partial^t \dot{u}_3}{\partial^t X_2} & 0 \\ 0 & 0 & \frac{\partial^t \dot{u}_1}{\partial^t X_3} & 0 & 0 & \frac{\partial^t \dot{u}_2}{\partial^t X_3} & 0 & 0 & \frac{\partial^t \dot{u}_3}{\partial^t X_3} \\ \frac{\partial^t \dot{u}_1}{\partial^t X_2} & \frac{\partial^t \dot{u}_1}{\partial^t X_1} & 0 & \frac{\partial^t \dot{u}_2}{\partial^t X_2} & \frac{\partial^t \dot{u}_2}{\partial^t X_1} & 0 & \frac{\partial^t \dot{u}_3}{\partial^t X_2} & \frac{\partial^t \dot{u}_3}{\partial^t X_1} & 0 \\ \frac{\partial^t \dot{u}_1}{\partial^t X_3} & 0 & \frac{\partial^t \dot{u}_1}{\partial^t X_1} & \frac{\partial^t \dot{u}_2}{\partial^t X_3} & 0 & \frac{\partial^t \dot{u}_2}{\partial^t X_1} & \frac{\partial^t \dot{u}_3}{\partial^t X_3} & 0 & \frac{\partial^t \dot{u}_3}{\partial^t X_1} \\ 0 & \frac{\partial^t \dot{u}_1}{\partial^t X_3} & \frac{\partial^t \dot{u}_1}{\partial^t X_2} & 0 & \frac{\partial^t \dot{u}_2}{\partial^t X_3} & \frac{\partial^t \dot{u}_2}{\partial^t X_2} & 0 & \frac{\partial^t \dot{u}_3}{\partial^t X_3} & \frac{\partial^t \dot{u}_3}{\partial^t X_2} \end{bmatrix} \tag{3.74}$$

$$\mathbf{H} = \begin{bmatrix} \frac{\partial}{\partial^t X_1} & \frac{\partial}{\partial^t X_2} & \frac{\partial}{\partial^t X_3} & 0 & 0 & 0 & 0 & 0 & 0 \\ 0 & 0 & 0 & \frac{\partial}{\partial^t X_1} & \frac{\partial}{\partial^t X_2} & \frac{\partial}{\partial^t X_3} & 0 & 0 & 0 \\ 0 & 0 & 0 & 0 & 0 & 0 & \frac{\partial}{\partial^t X_1} & \frac{\partial}{\partial^t X_2} & \frac{\partial}{\partial^t X_3} \end{bmatrix}^T \tag{3.75}$$

$$\mathbf{B}_{NL} = \mathbf{H}\bullet\mathbf{N} = \begin{bmatrix} \frac{\partial N_1}{\partial^t X_1} & \frac{\partial N_1}{\partial^t X_2} & \frac{\partial N_1}{\partial^t X_3} & 0 & 0 & 0 & 0 & 0 & 0 \\ 0 & 0 & 0 & \frac{\partial N_1}{\partial^t X_1} & \frac{\partial N_1}{\partial^t X_2} & \frac{\partial N_1}{\partial^t X_3} & 0 & 0 & 0 \\ 0 & 0 & 0 & 0 & 0 & 0 & \frac{\partial N_1}{\partial^t X_1} & \frac{\partial N_1}{\partial^t X_2} & \frac{\partial N_1}{\partial^t X_3} \\ \frac{\partial N_2}{\partial^t X_1} & \frac{\partial N_2}{\partial^t X_2} & \frac{\partial N_2}{\partial^t X_3} & 0 & 0 & 0 & 0 & 0 & 0 \\ 0 & 0 & 0 & \frac{\partial N_2}{\partial^t X_1} & \frac{\partial N_2}{\partial^t X_2} & \frac{\partial N_2}{\partial^t X_3} & 0 & 0 & 0 \\ 0 & 0 & 0 & 0 & 0 & 0 & \frac{\partial N_1}{\partial^t X_1} & \frac{\partial N_2}{\partial^t X_1} & \frac{\partial N_3}{\partial^t X_1} \end{bmatrix}^T \tag{3.76}$$

As N_1 and N_2 are functions of natural coordinate ξ, so that derivatives about X_i (i=1, 2, 3) in global Cartesian coordinate system cannot be obtained directly. Then Chain rule is used to process a coordinate transformation.

$$\frac{\partial N_i}{\partial \xi} = \begin{bmatrix} \frac{\partial X_1}{\partial \xi} & \frac{\partial X_2}{\partial \xi} & \frac{\partial X_3}{\partial \xi} \end{bmatrix} \bullet \begin{bmatrix} \frac{\partial N_i}{\partial X_1} & \frac{\partial N_i}{\partial X_2} & \frac{\partial N_i}{\partial X_3} \end{bmatrix}^T = \mathbf{J}\bullet \begin{bmatrix} \frac{\partial N_i}{\partial X_1} & \frac{\partial N_i}{\partial X_2} & \frac{\partial N_i}{\partial X_3} \end{bmatrix}^T \tag{3.77}$$

In Eq.(3.77), **J** is

$$\mathbf{J} = \begin{bmatrix} \frac{\partial N_1}{\partial \xi} & \frac{\partial N_2}{\partial \xi} \end{bmatrix} \bullet \begin{bmatrix} X_1^1 & X_2^1 & X_3^1 \\ X_1^2 & X_2^2 & X_3^2 \end{bmatrix} = \begin{bmatrix} l & m & n \end{bmatrix} \tag{3.78}$$

In Eq.(3.78), l, m, n are direction cosine of the truss element. And there is

$$\mathbf{J}^T \bullet \mathbf{J} = \mathbf{I} \tag{3.79}$$

Here **I** is a unit matrix. Multiplying $\mathbf{J}^T$ at the two sides of Eq.(3.77) at the same time, we can obtain

$$\begin{bmatrix} \frac{\partial N_i}{\partial X_1} & \frac{\partial N_i}{\partial X_2} & \frac{\partial N_i}{\partial X_3} \end{bmatrix}^T = \begin{bmatrix} l\frac{\partial N_i}{\partial \xi} & m\frac{\partial N_i}{\partial \xi} & n\frac{\partial N_i}{\partial \xi} \end{bmatrix}^T \tag{3.80}$$

By using Eq.(3.59), Eq.(3.60) and Eq.(3.80), $\mathbf{B}_L$ and $\mathbf{B}_{NL}$ become

$$\mathbf{B}_L = \mathbf{L}\bullet\mathbf{N} = \begin{bmatrix} -\frac{l}{L} & 0 & 0 & \frac{l}{L} & 0 & 0 \\ 0 & -\frac{m}{L} & 0 & 0 & \frac{m}{L} & 0 \\ 0 & 0 & -\frac{n}{L} & 0 & 0 & \frac{n}{L} \\ -\frac{m}{L} & -\frac{l}{L} & 0 & \frac{m}{L} & \frac{l}{L} & 0 \\ -\frac{n}{L} & 0 & -\frac{l}{L} & \frac{n}{L} & 0 & \frac{l}{L} \\ 0 & -\frac{n}{L} & -\frac{m}{L} & 0 & \frac{n}{L} & \frac{m}{L} \end{bmatrix} \tag{3.81}$$

$$\mathbf{B}_{NL} = \mathbf{H}\bullet\mathbf{N} = \begin{bmatrix} -\frac{l}{L} & -\frac{m}{L} & -\frac{n}{L} & 0 & 0 & 0 & 0 & 0 & 0 \\ 0 & 0 & 0 & -\frac{l}{L} & -\frac{m}{L} & -\frac{n}{L} & 0 & 0 & 0 \\ 0 & 0 & 0 & 0 & 0 & 0 & -\frac{l}{L} & -\frac{m}{L} & -\frac{n}{L} \\ \frac{l}{L} & \frac{m}{L} & \frac{n}{L} & 0 & 0 & 0 & 0 & 0 & 0 \\ 0 & 0 & 0 & \frac{l}{L} & \frac{m}{L} & \frac{n}{L} & 0 & 0 & 0 \\ 0 & 0 & 0 & 0 & 0 & 0 & \frac{l}{L} & \frac{m}{L} & \frac{n}{L} \end{bmatrix} \tag{3.82}$$

The linear part $\mathbf{K}_L$ and the nonlinear part $\mathbf{K}_{NL}$ of tangential stiffness matrix can be obtained as

$$\mathbf{K}_L = \int_{^t v} ({}_t\mathbf{B}_L^T \bullet {}_t\overline{\mathbf{C}} \bullet {}_t\mathbf{B}_L) d^t v \tag{3.83}$$

$$\mathbf{K}_{NL} = \int_{^t v} \mathbf{B}_{NL}^T \bullet \overline{\boldsymbol{\tau}} \bullet \mathbf{B}_{NL} \, d^t v \tag{3.84}$$

Here ${}_t\overline{\mathbf{C}}$ is the component matrix of constitute tensor in global Cartesian coordinate system at time t, $\overline{\boldsymbol{\tau}}$ is the component matrix of Cauchy tensor in global Cartesian coordinate system.

$$ {}_t\overline{\mathbf{C}} = \begin{bmatrix} \overline{C}^{1111} & \overline{C}^{1122} & \overline{C}^{1133} & \overline{C}^{1112} & \overline{C}^{1113} & \overline{C}^{1123} \\ \overline{C}^{2211} & \overline{C}^{2222} & \overline{C}^{2233} & \overline{C}^{2212} & \overline{C}^{2213} & \overline{C}^{2223} \\ \overline{C}^{3311} & \overline{C}^{3322} & \overline{C}^{3333} & \overline{C}^{3312} & \overline{C}^{3313} & \overline{C}^{3323} \\ \overline{C}^{1211} & \overline{C}^{1222} & \overline{C}^{1233} & \overline{C}^{1212} & \overline{C}^{1213} & \overline{C}^{1223} \\ \overline{C}^{1311} & \overline{C}^{1322} & \overline{C}^{1333} & \overline{C}^{1312} & \overline{C}^{1313} & \overline{C}^{1323} \\ \overline{C}^{2311} & \overline{C}^{2322} & \overline{C}^{2333} & \overline{C}^{2312} & \overline{C}^{2313} & \overline{C}^{2323} \end{bmatrix} \tag{3.85}$$

$$ \overline{\boldsymbol{\tau}} = \begin{bmatrix} \overline{\tau}^{11} & \overline{\tau}^{12} & \overline{\tau}^{13} & 0 & 0 & 0 & 0 & 0 & 0 \\ \overline{\tau}^{12} & \overline{\tau}^{22} & \overline{\tau}^{23} & 0 & 0 & 0 & 0 & 0 & 0 \\ \overline{\tau}^{13} & \overline{\tau}^{23} & \overline{\tau}^{33} & 0 & 0 & 0 & 0 & 0 & 0 \\ 0 & 0 & 0 & \overline{\tau}^{11} & \overline{\tau}^{12} & \overline{\tau}^{13} & 0 & 0 & 0 \\ 0 & 0 & 0 & \overline{\tau}^{12} & \overline{\tau}^{22} & \overline{\tau}^{23} & 0 & 0 & 0 \\ 0 & 0 & 0 & \overline{\tau}^{13} & \overline{\tau}^{23} & \overline{\tau}^{33} & 0 & 0 & 0 \\ 0 & 0 & 0 & 0 & 0 & 0 & \overline{\tau}^{11} & \overline{\tau}^{12} & \overline{\tau}^{13} \\ 0 & 0 & 0 & 0 & 0 & 0 & \overline{\tau}^{12} & \overline{\tau}^{22} & \overline{\tau}^{23} \\ 0 & 0 & 0 & 0 & 0 & 0 & \overline{\tau}^{13} & \overline{\tau}^{23} & \overline{\tau}^{33} \end{bmatrix} \tag{3.86}$$

In Reference [128], the relationships of stress tensor, strain tensor and constitute tensor between global Cartesian coordinate system and local Cartesian coordinate system are given as follows:

$$\overline{\tau}^{ij} = (\overline{i}^{\,i} \bullet \hat{i}_a)(\overline{i}^{\,j} \bullet \hat{i}_b)\hat{\tau}_{ab} \tag{3.87}$$

$$\hat{e}_{cd} = (\overline{i}^{\,k} \bullet \hat{i}_c)(\overline{i}^{\,l} \bullet \hat{i}_d)\, \overline{e}_{kl} \tag{3.88}$$

$$\overline{\tau}^{ij} = \overline{C}^{ijkl} \bullet \overline{e}_{kl} \tag{3.89}$$

$$\hat{\tau}_{ab} = \hat{C}_{abcd} \bullet \hat{e}_{cd} \tag{3.90}$$

In Eq.(3.87) and Eq.(3.88), $\hat{i}_a$ and $\overline{i}^{\,i}$ are the unit vectors in local Cartesian coordinate and global Cartesian coordinate respectively.

Substituting Eq.(3.89) and Eq.(3.90) into Eq.(3.87), the relationship of component matrix of constitute tensor in global Cartesian coordinate system and local Cartesian coordinate system is

$$ {}_{t}\bar{C}^{ijkl} = {}_{t}\hat{C}_{abcd}(\bar{i}^{i} \bullet \hat{i}_{a})(\bar{i}^{j} \bullet \hat{i}_{b})(\bar{i}^{k} \bullet \hat{i}_{c})(\bar{i}^{l} \bullet \hat{i}_{d}) \tag{3.91} $$

As $\hat{C}_{1111} = E$ (E is Young's modulus), and defining

$$ \mathbf{p} = \left\{ l^2 \quad m^2 \quad n^2 \quad lm \quad ln \quad mn \right\} \tag{3.92} $$

Then the expression of matrix ${}_{t}\bar{\mathbf{C}}$ can be expressed as

$$ {}_{t}\bar{\mathbf{C}} = E\mathbf{p}^{T} \bullet \mathbf{p} \tag{3.93} $$

Assuming component $\hat{\tau}_{11}$ of Cauchy stress tensor in local Cartesian coordinate system at time t is τ, according to Eq.(3.87), the components of Cauchy stress tensor in global Cartesian coordinate at time t are

$$ \tilde{\boldsymbol{\tau}} = \left\{ \bar{\tau}^{11} \quad \bar{\tau}^{22} \quad \bar{\tau}^{33} \quad \bar{\tau}^{12} \quad \bar{\tau}^{13} \quad \bar{\tau}^{23} \right\}^{T} = \mathbf{p}^{T}\tau \tag{3.94} $$

The internal force vector $\mathbf{Q}$ in global Cartesian coordinate system is

$$ \mathbf{Q} = \int_{{}^{t}v} \mathbf{B}_{L}^{T} \bullet \tilde{\boldsymbol{\tau}} \, d^{t}v \tag{3.95} $$

Then if assuming $\mathbf{C} = [l, m, n]^T$, $\mathbf{k}_e = \dfrac{EA}{L}\mathbf{C}\cdot\mathbf{C}^T$, and a 3×3 unit matrix $\mathbf{I}_3$, then Eq.(3.83), Eq.(3.84) and Eq.(3.95) can be rewritten as

$$ \mathbf{K}_{L} = \begin{bmatrix} \mathbf{k}_e & -\mathbf{k}_e \\ -\mathbf{k}_e & \mathbf{k}_e \end{bmatrix} \tag{3.96} $$

$$ \mathbf{K}_{NL} = \frac{\tau A}{L} \begin{bmatrix} \mathbf{I}_3 & -\mathbf{I}_3 \\ -\mathbf{I}_3 & \mathbf{I}_3 \end{bmatrix} \tag{3.97} $$

$$ \mathbf{Q} = A\tau \left\{ -l \quad -m \quad -n \quad l \quad m \quad n \right\}^{T} \tag{3.98} $$

3.5 Modified matrixes

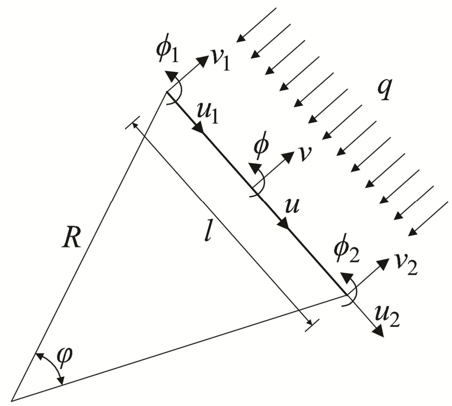

Fig.3-4 A straight beam element for the circular arch/ring [74]

In Eq.(3.4), the calculation of bifurcation points can be treated as linear eigenvalue problem. If the $\mathbf{K}_G$ in Eq.(3.4) are constituted for a unit value of pressure load, then the minimum positive eigenvalue λ can be considered as the critical load. And this solution of positive eigenvalue λ is only corresponding to the constant direction pressure [74]. In this section, Eq.(3.99)~ Eq.(3.108) refer to Reference [74].

But when the external load is uniform compression, because of the follower force effect, the normal eigenvalue approach in Eq.(3.4) cannot get an accurate solution. In order to make the normal eigenvalue approach available for the buckling analysis when external load is uniform compression, here modified matrixes [74] are introduced.

Considering the straight beam element in Fig.3-4, then energy expression association with changing direction of uniform compression in a circular arch or ring can be written as

$$\delta^2\Omega = \frac{q}{R}\int_0^l (u^2 - v^2)dx \tag{3.99}$$

Here q is the uniform compression in the radial direction of the arch/ring, and R is the radius of the arch/ring.

Assuming the generalized coordinate as

$$\mathbf{a} = \begin{bmatrix} a_1 & a_2 & a_3 & a_4 & a_5 & a_6 \end{bmatrix} \tag{3.100}$$

Then displacements u and v can be written as

$$u = \mathbf{N}_L \bullet \mathbf{a} \tag{3.101}$$

$$v = \mathbf{N}_C \bullet \mathbf{a} \tag{3.102}$$

Here $\mathbf{N}_L$ and $\mathbf{N}_C$ are

$$\mathbf{N}_L = [1 \quad x \quad 0 \quad 0 \quad 0 \quad 0] \tag{3.103}$$

$$\mathbf{N}_C = [0 \quad 0 \quad 1 \quad x \quad x^2 \quad x^3] \tag{3.104}$$

Then the Eq.(3.99) an be rewritten as

$$\delta^2\Omega = \mathbf{a}^T \mathbf{K}_{Cq} \bullet \mathbf{a} \tag{3.105}$$

In the Equation above, $\mathbf{K}_{Cqa}$ is

$$\mathbf{K}_{Cqa} = \frac{q}{R}\int_0^l (\mathbf{N}_L^T \bullet \mathbf{N}_L - \mathbf{N}_C^T \bullet \mathbf{N}_C)dx \tag{3.106}$$

Here q is the uniform compression, and R is the radius of arch or ring.

This is the desired matrix for uniform compression, except that it operates on the generalized coordinate rather than the local nodal coordinate. The transformation to local nodal coordinate in Fig.3-9 is stated as follows, which is obtained by evaluation $\mathbf{N}_L$, $\mathbf{N}_C$, and the $d\mathbf{N}_L/dx$ at the nodes.

$$\begin{bmatrix} u_1 \\ v_1 \\ \phi_1 \\ u_2 \\ v_2 \\ \phi_2 \end{bmatrix} = \begin{bmatrix} 1 & 0 & 0 & 0 & 0 & 0 \\ 0 & 0 & 1 & 0 & 0 & 0 \\ 0 & 0 & 0 & 1 & 0 & 0 \\ 1 & l & 0 & 0 & 0 & 0 \\ 0 & 0 & 1 & l & l^2 & l^3 \\ 0 & 0 & 0 & 1 & 2l & 3l^2 \end{bmatrix} \begin{bmatrix} a_1 \\ a_2 \\ a_3 \\ a_4 \\ a_5 \\ a_6 \end{bmatrix} \tag{3.107}$$

Noting $\mathbf{T}_a$ as the square matrix in Eq.(3.119), the referring to the local nodal coordinate , then the matrix in local nodal coordinate is

$$\mathbf{K}_{Cq} = \mathbf{T}_a^{-T} \bullet \mathbf{K}_{Cqa} \bullet \mathbf{T}_a^{-1} \tag{3.108}$$

If the linear beam element noted above is used, it is necessary to notice the difference of the setting of local coordinate system in Fig.3-1 and in Fig.3-4, and rearrange the position of components in Eq.(3.108).

In conclusion, when the external load is a uniform compression and straight beam element is used, then $(\mathbf{K}_{CG} - \mathbf{K}_{Cq})$ is need to be substituted for geometric elastic stiffness $\mathbf{K}_{CG}$ in local Cartesian coordinate system before $\mathbf{K}_{CG}$ in local Cartesian coordinate is transformed into $\mathbf{K}_G$ in global Cartesian coordinate.

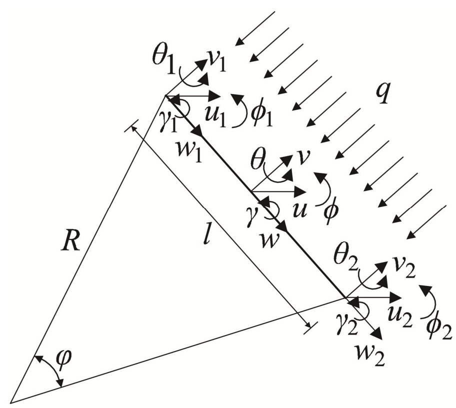

Fig.3-5 A straight beam element for a circular arch/ring

In addition, the same method can be used to deduce the modified matrix in 3D space. Assuming the generalized coordinate as

$$\bar{\mathbf{a}} = \begin{bmatrix} a_1 & a_2 & a_3 & a_4 & a_5 & a_6 & a_7 & a_8 & a_9 & a_{10} & a_{11} & a_{12} \end{bmatrix} \tag{3.109}$$

Then displacements u, v, w and γ can be written as

$$u = \mathbf{N}_u \bullet \bar{\mathbf{a}} \tag{3.110}$$

$$v = \mathbf{N}_v \bullet \bar{\mathbf{a}} \tag{3.111}$$

$$w = \mathbf{N}_w \bullet \bar{\mathbf{a}} \tag{3.112}$$

$$\gamma = \mathbf{N}_\gamma \bullet \bar{\mathbf{a}} \tag{3.113}$$

Here $\mathbf{N}_u$, $\mathbf{N}_v$, $\mathbf{N}_w$ and $\mathbf{N}_\gamma$ are

$$\mathbf{N}_u = [1 \quad x \quad x^2 \quad x^3 \quad 0 \quad 0 \quad 0 \quad 0 \quad 0 \quad 0 \quad 0 \quad 0] \tag{3.114}$$

$$\mathbf{N}_v = [0 \quad 0 \quad 0 \quad 0 \quad 1 \quad x \quad x^2 \quad x^3 \quad 0 \quad 0 \quad 0 \quad 0] \tag{3.115}$$

$$\mathbf{N}_w = [0 \quad 0 \quad 0 \quad 0 \quad 0 \quad 0 \quad 0 \quad 0 \quad 1 \quad x \quad 0 \quad 0] \tag{3.116}$$

$$\mathbf{N}_\gamma = [0 \quad 0 \quad 0 \quad 0 \quad 0 \quad 0 \quad 0 \quad 0 \quad 0 \quad 0 \quad 1 \quad x] \tag{3.117}$$

The other procedure is as same as the one in 2D space. And comparing the setting of local coordinate system in Fig.3-1 and in Fig.3-5, the setting of axes in these two configurations are the same, so there is no necessary to change the position of components in $\mathbf{K}_{Cq}$ any more.

3.6 Numerical example

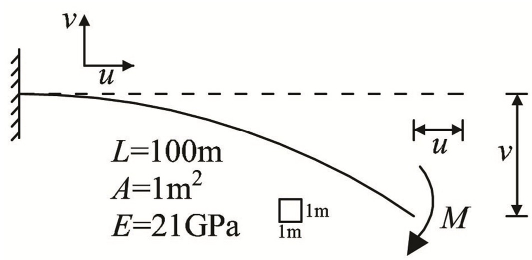

Fig.3-6 Cantilever beam under bending moment [159]

Fig.3-6 shows a cantilever under a bending moment at one side [159]. The value of moment is $M = n\pi EI/L$. Here E is the Young's modulus, I is the moment of inertia, L is the member length. Theoretical solution of this problem is $R = EI/M = L/n\pi$ [162]. Especially, when n=2, the equilibrium shape of beam is a closed arc.

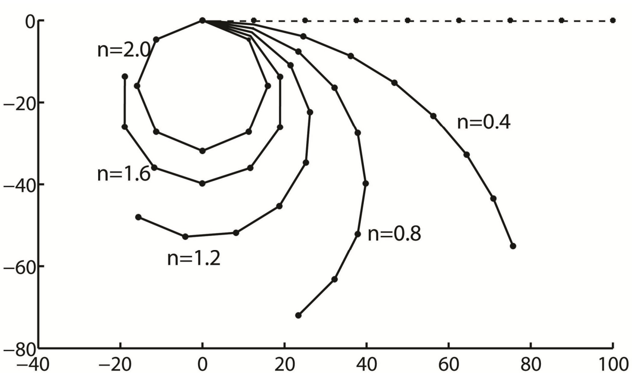

Fig.3-7 Shape of cantilever after deformation

The geometric nonlinear beam element in section 3.4.1 is used in this example. The entire cantilever is divided into 8 geometric nonlinear beam elements. Fig.3-7 shows the equilibrium shape of beam under different values of moments. And Table.3-1 shows the comparison of results obtained by FE method (author's program), by theoretical solutions and by past researches.

Table.3-1 Comparison of the results

n	u/L			v/L		
	FE.	Reference [159]	Theo. [162]	FE	Reference [159]	Theo. [162]
0.4	-0.243	-0.243	-0.243	-0.550	-0.550	-0.550
0.8	-0.766	-0.765	-0.766	-0.720	-0.722	-0.720
1.2	1.156	-1.158	-1.156	-0.480	-0.479	-0.480
1.6	1.189	-1.193	-1.189	-0.137	-0.140	-0.137
2.0	-0.998	-1.004	-1.000	0.000	-0.004	0.000

From Table.3-1, when n is smaller than 1.6 (including 1.6), FE results and theoretical solutions is almost identical. While n is larger than 1.6, the difference of the results between these two methods are very small and can be ignored. Analysis results of Reference [159] are also very close to FE results in this section.

3.7 Summaries

In this chapter, the FE methods to study the stability of the structures are introduced. And formulations of FE elements proposed in past researches are also given. The main work is summarized as follows:

1) The approach in solving linear eigenvalue problems to obtain the critical load and buckling mode by using FE method is introduced.

2) Formulations of the linear beam element and the linear truss element based on small deformation and small strain are given. Furthermore, formulations of geometric nonlinear beam element and geometric nonlinear truss element based on large deformation and small strain are also deduced.

3) In order to treat the buckling problems of the circular arch or ring under uniform compression as linear buckling problems rather than to use nonlinear FE analysis, modified matrixes considering follower force effect of uniform compression are introduced.

Chapter 4 Theory of Elastic Stability of Arches

4.1 Introduction

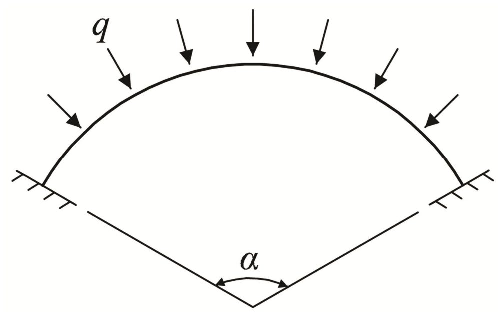

Fig.4-1 Circular arch under uniform compression

In this chapter the in-plane stability and out-of-plane stability of circular arches with symmetric closed cross section under uniform compression will be discussed. When uniform compression is applied to the line of the circular arch which is the same as the arch axis, before buckling phenomenon occurs, axial compression force can be considered as the main internal force in the arch, and the moments and shear forces in the arch can be ignored. Fig.4-1 shows the configuration of a circular arch under uniform compression.

Three kinds of methods are mainly used in theoretical analysis of elastic stability of arches. Firstly, researchers such as Wah[47], Yang[95], Rajasekaran[103], Kang[116], firstly proposed series of equilibrium differential equations for curved beams, then they used approximate functions of buckling modes to get the critical loads.

Secondly, researchers such as Tomas [63], Xiang[108] used isolated infinitesimal body of the arch to build static equilibrium differential equations. Especially, Tomas [63] utilized displacements in a Fourier series, Xiang[108] used approximate functions of buckling modes for the critical loads of in-plane stability. And Xiang[108] also used general solutions of displacements to get the critical loads of out-of-plane stability.

Thirdly, researchers such as John[92] and Kang[165] directly used energy methods to obtain critical loads for in-plane stability and out-of-plane stability of arches.

In this chapter, static methods introduced by Xiang[108] are utilized to get the equilibrium differential equations of the circular arch under uniform compression for in-plane stability and out-of-plane stability respectively. The circular arch is assumed to have symmetric closed cross section. Although Xiang[108] gave the general solutions of displacements for out-of-plane stability, he did not give the general solutions of displacements for in-plane stability. And then he used functions of buckling modes to obtain the critical loads. In this chapter, firstly the general solutions of the circular arch for in-plane and out-of-plane stability are deduced respectively. And then by using boundary conditions, buckling control equations for in-plane and out-of-plane stability are obtained respectively. In this chapter, Eq.(4.1)~Eq.(4.20), Eq.(4.39)~Eq.(4.80) refer to Reference [108].

4.2 Curvatures and moments

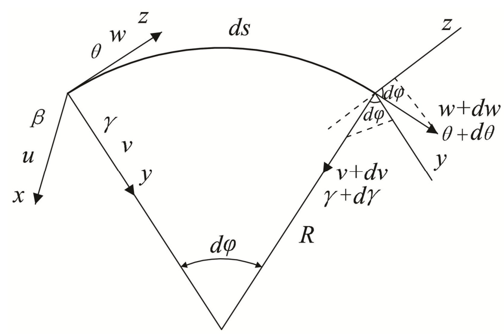

Fig.4-2 Displacements in the isolated infinitesimal body of the arch [108]

Fig.4-2 shows the displacements in the isolated infinitesimal body of the arch [108]. Translation displacements and rotational displacements in any cross section of the arch around x axis (perpendicular to the arch plane, lateral diction), y axis (pointing to the center of the arch in-plane, radial direction,) and z axis (tangential direction in -plane) are u, v, w and β, γ, θ respectively. Referring to coordinate system (x, y, z), coordinate system (ξ, η, ζ) is the substitution of former coordinate system in the arch after deformation occurs.

The rotational displacement around x axis is

$$\beta = -\frac{1}{ds}[(v+dv)\cos d\varphi + (w+dw)\sin d\varphi - v] \approx -(\frac{dv}{ds}+\frac{w}{R}) \tag{4.1}$$

And the increment of rotational displacement around y axis is

$$\Delta\gamma = (\gamma + d\gamma)\cos d\varphi + (\theta + d\theta)\sin d\varphi - \gamma \approx d\gamma + \theta d\varphi \tag{4.2}$$

And increment of rotational displacement around z axis is

$$\Delta\theta = -(\gamma + d\gamma)\sin d\varphi + (\theta + d\theta)\cos d\varphi - \theta \approx d\theta - \gamma d\varphi \tag{4.3}$$

The rotational displacement around y axis can be obtained by

$$\gamma = u' \tag{4.4}$$

Here K_x (excluding initial curvature $1/R$), K_y, and K_z are curvatures of axis x, axis y and axis z respectively. Then the values of curvatures around axis x, axis y and axis z are calculated as follows.

$$K_x = -\frac{d\beta}{ds} = \frac{d^2 v}{ds^2} + \frac{1}{R}\frac{dw}{ds} \tag{4.5}$$

$$K_y = \frac{\Delta\gamma}{ds} = \frac{d\gamma + \theta d\varphi}{ds} = \frac{d\gamma}{ds} + \frac{\theta}{R} = \frac{d^2 u}{ds^2} + \frac{\theta}{R} \tag{4.6}$$

$$K_z = \frac{\Delta\theta}{ds} = \frac{d\theta - \gamma d\varphi}{ds} = \frac{d\theta}{ds} - \frac{\gamma}{R} = \frac{d\theta}{ds} - \frac{1}{R}\frac{du}{ds} \tag{4.7}$$

In another aspect, moments M_ξ, M_η, M_ζ are the ones which appear in small length ds of the isolated infinitesimal body after deformation around axis ξ, axis η and axis ζ respectively. The directions of moments are stipulated in Fig.4-3 [108].

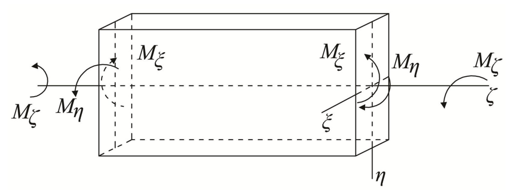

Fig.4-3 Moments in the isolated infinitesimal body [108]

And the material of the circular arch is assumed to conform to Hook's law. As the displacements are very small, the geometric shape of the cross section can be assumed unchanged after buckling. The relationship of curvatures and moments can be found as follows [108]:

$$\begin{cases} EI_x K_x = -M_\xi \\ EI_y K_y = M_\eta \\ GJ_z K_z - (EJ_w K_z')' = M_\varsigma \end{cases} \tag{4.8}$$

Here E is the Young's modulus, G is the shear modulus, I_x is moment of inertia around axis x, I_y is moment of inertia around axis y, J_z is Saint-Venant torsion constant, J_w is warping moment of inertia.

4.3 Equilibrium differential equations

4.3.1 In-plane

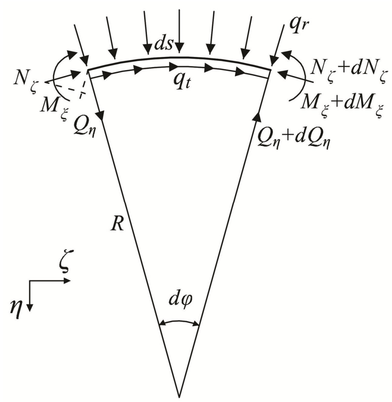

Fig.4-4 Equilibrium state of forces in-plane [108]

In Fig.4-4, shear force Q_η, axial compression force N_ς and bending moment M_ξ are in static equilibrium state under external load, q_r is distributed load in η direction and q_t is distributed load in ζ direction, m_ξ is the distributed bending moment around ξ axis [108]. From the static equilibrium conditions, we can obtain

$$\begin{cases} N_\varsigma + dN_\varsigma - N_\varsigma \cos d\varphi - Q_\eta \sin d\varphi - q_t ds = 0 \\ Q_\eta + dQ_\eta - Q_\eta \cos d\varphi + N_\varsigma \sin d\varphi - q_r ds = 0 \\ M_\xi + dM_\xi - M_\xi + Q_\eta ds + m_\xi ds = 0 \end{cases} \tag{4.9}$$

As $d\varphi$ is very small, here $\cos d\varphi \approx 1$, $\sin d\varphi \approx d\varphi$ are supposed. Meanwhile ignoring the effect of q_t and m_ξ, then the equations above become

$$\begin{cases} \dfrac{dN_\varsigma}{ds} = \dfrac{Q_\eta}{R} \\ \dfrac{dQ_\eta}{ds} = -\dfrac{N_\varsigma}{R} + q_r \\ \dfrac{dM_\xi}{ds} = -Q_\eta \end{cases} \tag{4.10}$$

In Eq.(4.10), Q_η of the third term is substituted into the one in the first term. Meanwhile taking one time derivative of the two sides of the third term and substituting the expression (dQ_η/ds) into the one in the second term, we can obtain

$$\begin{cases} \dfrac{dN_\varsigma}{ds} + \dfrac{1}{R}\dfrac{dM_\xi}{ds} = 0 \\ \dfrac{d^2 M_\xi}{ds^2} - \dfrac{N_\varsigma}{R} = -q_r \end{cases} \tag{4.11}$$

By combining these two terms in Eq.(4.11), we can obtain

$$\frac{d^3 M_\xi}{ds^3} + \frac{1}{R^2}\frac{dM_\xi}{ds} = -\frac{dq_r}{ds} \tag{4.12}$$

When the external load is uniform compression, referring to Reference [108], uniform compression q_r in η direction after buckling can be obtained as

$$q_r = q - NK_x \tag{4.13}$$

Here N=qR. Then substituting the first term of Eq.(4.8) and Eq.(4.13) into Eq.(4.12), we can obtain

$$-EI_x \frac{d^3 K_x}{ds^3} - EI_x \frac{1}{R^2}\frac{dK_x}{ds} = qR\frac{dK_x}{ds} \tag{4.14}$$

As the shape of the arch is assumed as circular, and $ds = Rd\varphi$ is a pre-established condition, then we know

$$\frac{d^n K_x}{ds^n} = \frac{1}{R^n}\frac{d^n K_x}{d\varphi^n} \tag{4.15}$$

Substituting Eq.(4.15) into Eq.(4.14), we can obtain

$$\frac{d^3 K_x}{d\varphi^3} + (1 + \frac{qR^3}{EI_x})\frac{dK_x}{d\varphi} = 0 \tag{4.16}$$

Love[38] and Timoshenko[42] assumed the circumferential strain of the centerline is 0 after buckling, by this assumption we can obtain

$$\frac{dw}{ds} = \frac{v}{R} \tag{4.17}$$

The same expression of Eq.(4.17) is

$$\frac{dw}{d\varphi} = v \tag{4.18}$$

Then substituting Eq.(4.18) into Eq.(4.5), then curvature K_x around axis x becomes

$$K_x = \frac{1}{R^2}\frac{d^2 v}{d\varphi^2} + \frac{1}{R^2} v \tag{4.19}$$

Substituting Eq.(4.19) into Eq.(4.16), we can obtain

$$\frac{d^5 v}{d\varphi^5} + \frac{d^3 v}{d\varphi^3} + (1 + \frac{qR^3}{EI_x})(\frac{d^3 v}{d\varphi^3} + \frac{dv}{d\varphi}) = 0 \tag{4.20}$$

Eq.(4.20) is the buckling control equation for in-plane stability of the arch. And Eq.(4.20) is identical to the expressions in Reference [103], Reference [108] and Reference [165]. But the general solution of Eq.(4.20) is not given by Xiang[108], and function of buckling mode is adapted in above three references. Due to the lack of general solution of Eq.(4.20), here the procedure to calculate the general solution of the displacement v is introduced.

When reviewing the derivation process of Eq.(4.20), we can find out that this equation originates from Eq.(4.16). Thus directly taking one time integration of two sides of Eq.(4.16), then we can obtain

$$\frac{d^2 K_x}{d\varphi^2} + (1 + \frac{qR^3}{EI_x})K_x = A_1 \tag{4.21}$$

Assuming a parameter τ as

$$\tau^2 = 1 + \frac{qR^3}{EI_x} \tag{4.22}$$

As Eq.(4.21) is a second order linear differential equation with constant coefficient, the general solution of K_x is

$$K_x = A_2 \sin\tau\varphi + A_3 \cos\tau\varphi + \frac{A_1}{\tau^2} \tag{4.23}$$

Then substituting Eq.(4.19) into Eq.(4.23), we can obtain

$$\frac{d^2 v}{d\varphi^2} + v = A_2 R^2 \sin\tau\varphi + A_3 R^2 \cos\tau\varphi + \frac{R^2}{\tau^2} A_1 \tag{4.24}$$

Eq.(4.24) can also be seen as a second order linear differential equation with constant coefficient, the general solution for this equation is

$$v = A_4 \sin\varphi + A_5 \cos\varphi + \frac{A_2 R^2}{1-\tau^2}\sin\tau\varphi + \frac{A_3 R^2}{1-\tau^2}\cos\tau\varphi + \frac{R^2}{\tau^2}A_1 \tag{4.25}$$

In order to simplify the expression of Eq.(4.25), here we note

$$\{A \quad B \quad C \quad D \quad E\} = \left\{A_4 \quad A_5 \quad \frac{A_2 R^2}{1-\tau^2} \quad \frac{A_3 R^2}{1-\tau^2} \quad \frac{R^2}{\tau^2}A_1\right\} \tag{4.26}$$

Then Eq.(4.25) becomes

$$v = A\sin\varphi + B\cos\varphi + C\sin\tau\varphi + D\cos\tau\varphi + E \tag{4.27}$$

Then taking one time integration of the two sides of Eq.(4.18), we can obtain the expression of w as

$$w = \int v d\varphi = -A\cos\varphi + B\sin\varphi - C\frac{\cos\tau\varphi}{\tau} + D\frac{\sin\tau\varphi}{\tau} + E\varphi + F \tag{4.28}$$

The first to third derivatives of Eq.(4.28) is

$$v' = A\cos\varphi - B\sin\varphi + C\tau\cos\tau\varphi - D\tau\sin\tau\varphi \tag{4.29}$$

$$v'' = -A\sin\varphi - B\cos\varphi - C\tau^2\sin\tau\varphi - D\tau^2\cos\tau\varphi \tag{4.30}$$

$$v''' = -A\cos\varphi + B\sin\varphi - C\tau^3\cos\tau\varphi + D\tau^3\sin\tau\varphi \tag{4.31}$$

From the third term of Eq.(4.10), we can obtain

$$Q_\eta = -\frac{dM_\xi}{ds} = \frac{EI_x}{R^3}\left(\frac{d^3v}{d\varphi^3} + \frac{dv}{d\varphi}\right) \tag{4.32}$$

1) Hinged ended in-plane

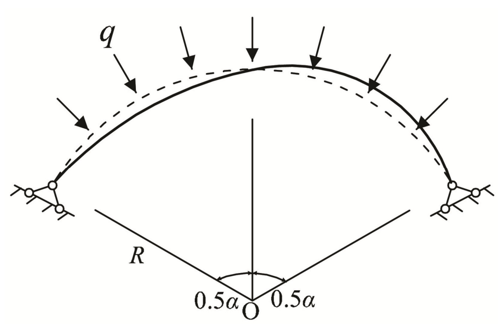

Fig.4-5 Buckling of the arch in-plane

In the account above, the general solutions of displacements v and w in-plane has been obtained. Now let's consider the boundary conditions. Firstly the boundary conditions of the circular arch are assumed as hinged ended, and the central angle of the arch is α, and uniform compression q is considered, as shown in Fig.4-5.

The expressions of hinged ended boundary conditions are

(1) $v = 0$, $v'' = 0$, $w = 0$ at $\varphi = 0$

(2) $v = 0$, $v'' = 0$, $w = 0$ at $\varphi = \alpha$

From these boundary conditions, we can obtain

$$\begin{cases} 0 = B + D + E \\ 0 = -B - D\tau^2 \\ 0 = -A - C\dfrac{1}{\tau} + F \\ 0 = A\sin\alpha + B\cos\alpha + C\sin\alpha\tau + D\cos\alpha\tau + E \\ 0 = -A\sin\alpha - B\cos\alpha - C\tau^2\sin\alpha\tau - D\tau^2\cos\alpha\tau \\ 0 = -A\cos\alpha + B\sin\alpha - C\dfrac{\cos\alpha\tau}{\tau} + D\dfrac{\sin\alpha\tau}{\tau} + E\alpha + F \end{cases} \tag{4.33}$$

According to the sequence of A, B, C, D, E and F, a matrix $\mathbf{S_{2D\text{-}H}}$ is assumed as

$$\mathbf{S_{2D\text{-}H}} = \begin{bmatrix} 0 & 1 & 0 & 1 & 1 & 0 \\ 0 & 1 & 0 & \tau^2 & 0 & 0 \\ 1 & 0 & \dfrac{1}{\tau} & 0 & 0 & -1 \\ \sin\alpha & \cos\alpha & \sin\alpha\tau & \cos\alpha\tau & 1 & 0 \\ \sin\alpha & \cos\alpha & \tau^2\sin\alpha\tau & \tau^2\cos\alpha\tau & 0 & 0 \\ -\cos\alpha & \sin\alpha & -\dfrac{\cos\alpha\tau}{\tau} & \dfrac{\sin\alpha\tau}{\tau} & \alpha & 1 \end{bmatrix} \tag{4.34}$$

Then the buckling control equation can be expressed as

$$\det(\mathbf{S_{2D\text{-}H}}) = 0 \tag{4.35}$$

Here a numerical example is used to prove the theoretical equation above. The example is given as follows:

Table.4-1 Materials parameters of the arch

	Young's modulus [GPa]	Poisson' ratio	Internal diameter [mm]	External diameter [mm]
Arch	205	0.3	6	12

The circular angel of arch is π. And its radius is 1m. The arch has a hollow circular constant cross section. Table.4-1 shows the materials parameters of arch in numerical example. In numerical analysis, 2D linear beam element in Section 3.3.1 and the modified matrix in Section 3.5 in Chapter 3 are used. Entire arch is divided into 48 and 192 linear beam elements, and each element has the same length.

In another aspect, we also use the large finite element analysis software ANSYS 12.1 for comparison. Element BEAM 188 is used for simulation. The division number of entire arch is 48 elements. In the later narrative, we use symbol "ANSYS" for the results obtained by ANSYS 12.1, and symbol "FE" for author's FE program.

Table.4-2 Comparison of the buckling modes (hinged ended: 48 elements)

First order	Second order	Third order
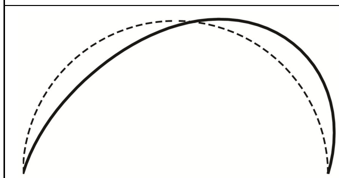 （FE）	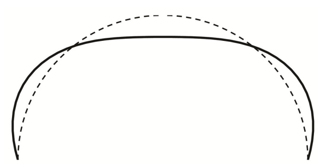 （FE）	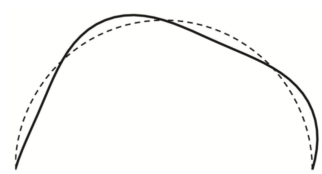 （FE）
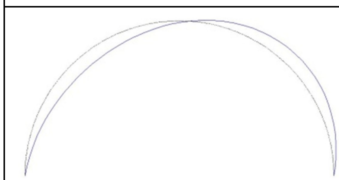 (ANSYS)	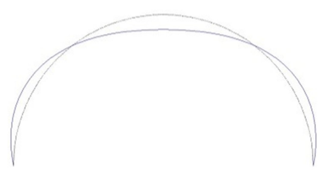 (ANSYS)	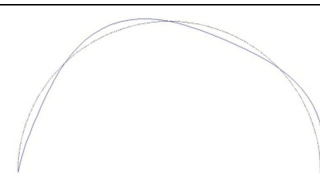 (ANSYS)

The buckling modes obtained by FE method and ANSYS with 48 elements are showed in Table.4-2. We can obtain the first and the third order buckling modes are anti-symmetric and the second order buckling mode is symmetric. The buckling modes obtained by FE method and ANSYS are almost identical to each other. And the comparison results by theoretical method, FE method and ANSYS are shown in Table.4-3. We can observe there is small difference between these three results.

Table.4-3 Comparison of the critical loads

		First order ($\frac{EI_x}{R^3}$)	Second order ($\frac{EI_x}{R^3}$)	Third order ($\frac{EI_x}{R^3}$)
Theory (q_{cr})		3.00	8.00	15.00
FE (q_{cr})	48 elements	3.06	8.15	15.30
	192 elements	3.01	8.04	15.07
ANSYS (q_{cr})	48 elements	3.00	8.03	15.11

In theoretical analysis, the first order critical load with central angel π is 3.00, this result is identical to the one obtained by Timoshenko[42]. And by comparing the results obtained by FE methods and ANSYS, we know that with the same division of elements (48 elem.), Element 188 in ANSYS has high accuracy. But when we compare the results obtained by FE methods with different divisions, we know higher division number will make the results closed to the ones in the theoretical analysis.

2) Fixed ended in-plane

When the boundary conditions in Fig.4-5 are fixed ended, the boundary conditions can be expressed as

(1) $v = 0$, $v' = 0$, $w = 0$ at $\varphi = 0$

(2) $v = 0$, $v' = 0$, $w = 0$ at $\varphi = \alpha$

From the boundary conditions, we can obtain

$$\begin{cases} 0 = B + D + E \\ 0 = A + C\tau \\ 0 = -A - C\dfrac{1}{\tau} + F \\ 0 = A\sin\alpha + B\cos\alpha + C\sin\alpha\tau + D\cos\alpha\tau + E \\ 0 = A\cos\alpha - B\sin\alpha + C\tau\cos\alpha\tau - D\tau\sin\alpha\tau \\ 0 = -A\cos\alpha + B\sin\alpha - C\dfrac{\cos\alpha\tau}{\tau} + D\dfrac{\sin\alpha\tau}{\tau} + \alpha E + F \end{cases} \tag{4.36}$$

Similar to the case when the boundary conditions are hinged ended, from the sequence of A, B, C, D, E and F, a matrix $\mathbf{S_{2D\text{-}F}}$ is assumed as

$$\mathbf{S_{2D\text{-}F}} = \begin{bmatrix} 0 & 1 & 0 & 1 & 1 & 0 \\ 1 & 0 & \tau & 0 & 0 & 0 \\ 1 & 0 & \dfrac{1}{\tau} & 0 & 0 & -1 \\ \sin\alpha & \cos\alpha & \sin\alpha\tau & \cos\alpha\tau & 1 & 0 \\ \cos\alpha & -\sin\alpha & \tau\cos\alpha\tau & -\tau\sin\alpha\tau & 0 & 0 \\ -\cos\alpha & \sin\alpha & -\dfrac{\cos\alpha\tau}{\tau} & \dfrac{\sin\alpha\tau}{\tau} & \alpha & 1 \end{bmatrix} \tag{4.37}$$

Then the buckling control equation can be expressed as

$$\det(\mathbf{S_{2D\text{-}F}}) = 0 \tag{4.38}$$

The same numerical example in hinged ended case is used here. Table.4-4 shows the Buckling modes with 48 elements. We know the first and third order of buckling modes are anti-symmetric, and the second order one is symmetric. The buckling modes calculated by FE method and ANSYS are almost identical to each other.

Table.4-4 Comparison of the buckling modes (fixed ended: 48 elements)

First order	Second order	Third order
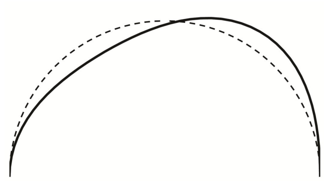 (FE)	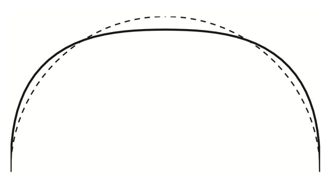 (FE)	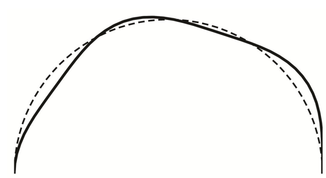 (FE)
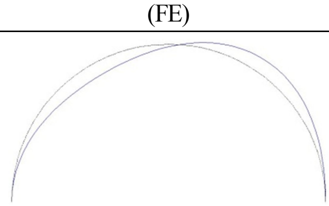 (ANSYS)	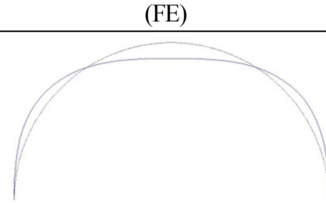 (ANSYS)	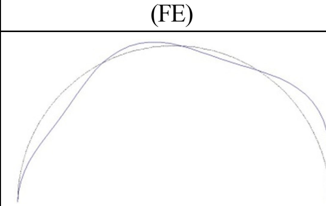 (ANSYS)

The comparison of the first order to the third order critical loads calculated by theoretical method, FE method and ANSYS are shown in Table. 4-5. In theoretical analysis, the first order critical load with central angel π is 8.00, this results is identical to the one obtained by Timoshenko[42]. And comparing the results of ANSYS and FE method, we know that with the same division of elements, ANSYS has higher accuracy. And comparing the FE results with different divisions, we observe FE and ANSYS results in higher division are closed to the ones in theoretical analysis.

Table.4-5 Comparison of the critical loads

		First order ($\frac{EI_x}{R^3}$)	Second order ($\frac{EI_x}{R^3}$)	Third order ($\frac{EI_x}{R^3}$)
Theory (q_{cr})		8.00	12.90	24.00
FE (q_{cr})	48 elements	8.15	13.15	24.49
	192 elements	8.04	12.96	24.12
ANSYS (q_{cr})	48 elements	8.03	12.99	24.31

As complements, in Appendix B we introduce other two methods to obtain critical loads for in-plane buckling in past researches, one is using function of buckling mode[108], [165], and the other one is utilizing simplified static equilibrium method [42].

4.3.2 Out-of-plane

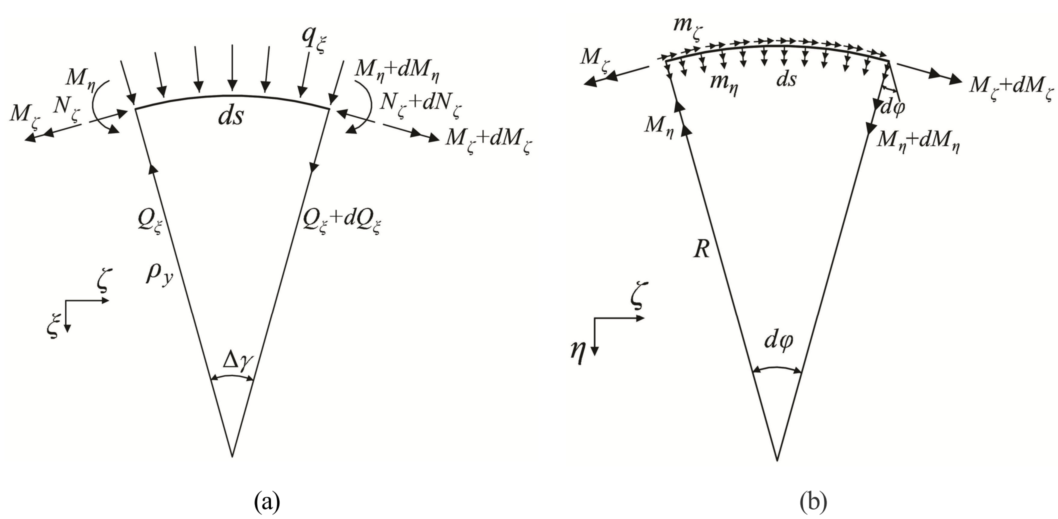

Fig. 4-7 Equilibrium state of forces out-of-plane [108]

In this section, out-of-plane stability of circular arch with symmetric closed cross section is analyzed. Fig.4-7 shows equilibrium state of circular arch in an infinitesimal length ds when flexural-torsional buckling happens out-of-plane [108]. These internal forces include lateral bending moment M_η, torsional moment M_ζ, lateral shear force Q_ξ, axis force N_ς, distributed load q_ξ, distributed moments m_η and m_ζ around axis η and axis ζ.

Researchers John [92], Rajasekaran [103], Pi [144] in their researches for the out-of-plane when the boundary conditions of the arch are hinged ended in-plane and simple ended out-of-plane, they thought that the moment

M_ξ (used for in-plane stability) around ξ axis is 0 and the axial compression force is $N_\varsigma = qR$. And Pi [150] stated the moment M_ξ (used in-plane stability) around ξ axis is very small when the boundary conditions of the arch are lateral fixed and he neglected the effect of M_ξ in studying the out-of-plane stability, and the axial compression force is assumed as $N_\varsigma = qR$. Wah [47], Tomas [63], Xiang [108], Kang [116] separated the buckling control equations of the circular arch for in-plane stability and out-of-plane stability respectively, and these researchers also assumed axial compression force of the arch is $N_\varsigma = qR$. In this section, the method introduced by Xiang [108] is utilized. Ignoring the effect of M_ξ when flexural-torsional buckling happens, we assume the axial compression force equals qR. From the static equilibrium condition in Fig.4-7, we can obtain

$$\sum F_\xi = 0 \tag{4.39}$$

$$\sum M_\eta = 0 \tag{4.40}$$

$$\sum M_\varsigma = 0 \tag{4.41}$$

From Eq.(4.39), we can obtain

$$\sum F_\xi = Q_\xi + dQ_\xi + q_\xi ds - N_\varsigma \sin\Delta\gamma - Q_\xi \cos\Delta\gamma = 0 \tag{4.42}$$

As $\Delta\gamma$ is small, we could assume $\sin\Delta\gamma \approx \Delta\gamma$, $\cos\Delta\gamma \approx 1$. And $\Delta\gamma = \dfrac{ds}{\rho_y} = K_y ds$. Eq.(4.42) can transform into the following equation.

$$\frac{dQ_\xi}{ds} + q_\xi - N_\varsigma K_y = 0 \tag{4.43}$$

In another aspect, from Eq.(4.40) we can obtain

$$\sum M_\eta = M_\eta + dM_\eta - M_\eta \cos d\varphi + M_\zeta \sin d\varphi + m_\eta ds + Q_\xi ds = 0 \tag{4.44}$$

As $\sin d\varphi \approx d\varphi$, $\cos d\varphi \approx 1$, neglecting the effect of m_η, so that Eq.(4.44) can transform into

$$\frac{dM_\eta}{ds} + \frac{M_\varsigma}{R} + Q_\xi = 0 \tag{4.45}$$

Finally from Eq.(4.41), we can obtain

$$\sum M_\varsigma = M_\varsigma + dM_\varsigma - M_\varsigma \cos d\varphi - M_\eta \sin d\varphi + m_\varsigma ds = 0 \tag{4.46}$$

Neglecting the effect of m_ζ, and Eq.(4.46) can transform into

$$\frac{dM_\varsigma}{ds} - \frac{M_\eta}{R} = 0 \tag{4.47}$$

The combination of Eq.(4.43) and Eq.(4.45) is

$$\frac{d^2 M_\eta}{ds^2} + \frac{1}{R}\frac{dM_\varsigma}{ds} + N_\varsigma K_y - q_\xi = 0 \tag{4.48}$$

Then buckling control equation can be expressed as

$$\begin{cases} \dfrac{d^2 M_\eta}{ds^2} + \dfrac{1}{R}\dfrac{dM_\varsigma}{ds} + N_\varsigma K_y - q_\xi = 0 \\ \dfrac{dM_\varsigma}{ds} - \dfrac{M_\eta}{R} = 0 \end{cases} \tag{4.49}$$

Substituting the expressions of M_η, M_ζ, K_y, and K_z into Eq.(4.49), we can obtain

$$\begin{cases} [EI_y(\dfrac{d^2u}{ds^2} + \dfrac{\theta}{R})]'' + [\dfrac{GJ_z}{R}(\dfrac{d\theta}{ds} - \dfrac{1}{R}\dfrac{du}{ds})]' + (\dfrac{d^2u}{ds^2} + \dfrac{\theta}{R})N_\varsigma - q_\xi = 0 \\ [GJ_z(\dfrac{d\theta}{ds} - \dfrac{1}{R}\dfrac{du}{ds})]' - \dfrac{EI_y}{R}(\dfrac{d^2u}{ds^2} + \dfrac{\theta}{R}) = 0 \end{cases} \tag{4.50}$$

And when out-of-plane buckling happens, $q_\xi \approx q\theta$ and $N_\varsigma = qR$ are pre-established conditions. Then Eq.(4.50) can be simplified as

$$\begin{cases} EI_y\dfrac{d^4u}{ds^4} + (qR - \dfrac{GJ_z}{R^2})\dfrac{d^2u}{ds^2} + (\dfrac{EI_y + GJ_z}{R})\dfrac{d^2\theta}{ds^2} = 0 \\ -(\dfrac{GJ_z + EI_y}{R})\dfrac{d^2u}{ds^2} + GJ_z\dfrac{d^2\theta}{ds^2} - \dfrac{EI_y}{R^2}\theta = 0 \end{cases} \tag{4.51}$$

Assuming two non-dimensional parameters λ and ω as

$$\lambda = \frac{EI_y}{GJ_z} \tag{4.52}$$

$$\omega = \frac{q}{EI_y / R^3} \tag{4.53}$$

Substituting the expressions of λ and ω into Eq.(4.51), we can obtain

$$\begin{cases} \lambda \dfrac{d^4u}{ds^4} + (\dfrac{\omega\lambda}{R^2} - \dfrac{1}{R^2})\dfrac{d^2u}{ds^2} + (\dfrac{\lambda+1}{R})\dfrac{d^2\theta}{ds^2} = 0 \\ -(\dfrac{1+\lambda}{R})\dfrac{d^2u}{ds^2} + \dfrac{d^2\theta}{ds^2} - \dfrac{\lambda}{R^2}\theta = 0 \end{cases} \tag{4.54}$$

As the shape of the arch is circular, we can obtain

$$\frac{d^n u}{ds^n} = \frac{1}{R^n}\frac{d^n u}{d\varphi^n} \tag{4.55}$$

$$\frac{d^n \theta}{ds^n} = \frac{1}{R^n}\frac{d^n \theta}{d\varphi^n} \tag{4.56}$$

By using Eq.(4.55) and Eq.(4.56), Eq. (4.54) can transform into

$$\begin{cases} \dfrac{d^4u}{d\varphi^4} + \dfrac{(\omega\lambda-1)}{\lambda}\dfrac{d^2u}{d\varphi^2} + \dfrac{(\lambda+1)R}{\lambda}\dfrac{d^2\theta}{d\varphi^2} = 0 \\ -\dfrac{1+\lambda}{R}\dfrac{d^2u}{d\varphi^2} + (\dfrac{d^2\theta}{d\varphi^2} - \lambda\theta) = 0 \end{cases} \tag{4.57}$$

Firstly, from the second term of Eq.(4.57), we can obtain

$$\frac{d^2u}{d\varphi^2} = \frac{R}{1+\lambda}\frac{d^2\theta}{d\varphi^2} - \frac{\lambda R}{1+\lambda}\theta \tag{4.58}$$

Taking one time integration of two sides of Eq.(4.58), we can obtain

$$\frac{du}{d\varphi} = \frac{R}{1+\lambda}\frac{d\theta}{d\varphi} - \frac{\lambda R}{1+\lambda}\int \theta d\varphi \tag{4.59}$$

Then taking one time integration of both sides of Eq.(4.59) again, we can obtain

$$u = \frac{R}{1+\lambda}\theta - \frac{\lambda R}{1+\lambda}\int(\int \theta d\varphi)d\varphi \tag{4.60}$$

Taking two times derivative of both sides of Eq.(4.58), we can obtain

$$\frac{d^4u}{d\varphi^4} = \frac{R}{1+\lambda}\frac{d^4\theta}{d\varphi^4} - \frac{\lambda R}{1+\lambda}\frac{d^2\theta}{d\varphi^2} \tag{4.61}$$

Substituting Eq.(4.58) and Eq.(4.61) into the first term of Eq.(4.57), we can obtain

$$\frac{d^4\theta}{d\varphi^4}+(\omega+2)\frac{d^2\theta}{d\varphi^2}+(1-\lambda\omega)\theta=0 \tag{4.62}$$

Eq.(4.62) is a fourth order linear differential equation with constant coefficient. Assuming parameters a and b as

$$a=\frac{\omega+2}{2} \tag{4.63}$$

$$b=1-\lambda\omega \tag{4.64}$$

Then the general solution of Eq.(4.62) can be obtained as

$$\theta=A\sin k_1\varphi+B\cos k_1\varphi+C\sinh k_2\varphi+D\cosh k_2\varphi \tag{4.65}$$

Here k_1 and k_2 are

$$k_1=\sqrt{a+\sqrt{a^2-b}} \tag{4.66}$$

$$k_2=\sqrt{-a+\sqrt{a^2-b}} \tag{4.67}$$

The first derivative and second derivative of two sides of Eq.(4.65) are

$$\frac{d\theta}{d\varphi}=Ak_1\cos k_1\varphi-Bk_1\sin k_1\varphi+Ck_2\cosh k_2\varphi+Dk_2\sinh k_2\varphi \tag{4.68}$$

$$\frac{d^2\theta}{d\varphi^2}=-Ak_1^2\sin k_1\varphi-Bk_1^2\cos k_1\varphi+Ck_2^2\sinh k_2\varphi+Dk_2^2\cosh k_2\varphi \tag{4.69}$$

Taking integration of two sides of Eq.(4.65) one time and two times respectively, we can obtain

$$\int\theta d\varphi=-\frac{A}{k_1}\cos k_1\varphi+\frac{B}{k_1}\sin k_1\varphi+\frac{C}{k_2}\cosh k_2\varphi+\frac{D}{k_2}\sinh k_2\varphi+E \tag{4.70}$$

$$\int(\int\theta d\varphi)d\varphi=-\frac{A}{k_1^2}\sin k_1\varphi-\frac{B}{k_1^2}\cos k_1\varphi+\frac{C}{k_2^2}\sinh k_2\varphi+\frac{D}{k_2^2}\cosh k_2\varphi+E\varphi+F \tag{4.71}$$

1) Hinged ended in-plane and simple ended out-of-plane

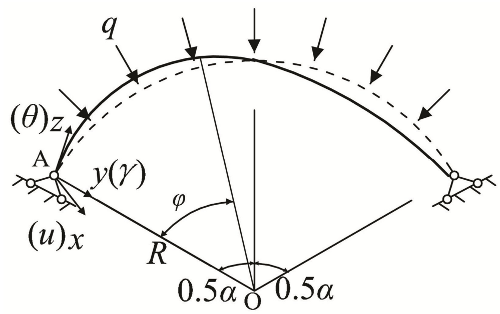

Fig.4-10 Buckling of the arch out-of-plane

Here an example shown in Fig.4-10 in 3D space is used to explain the applications of equations above. The circular angel of the arch is α. Uniform compression q is applied to the arch. Assuming the boundary conditions are hinged ended in-plane and simple ended out-of-plane. Here simple ended means the nodes at boundary can rotate along their principal axes but be unable to rotate along the tangents to their center line [42]. This kind of boundary conditions can be given as follows:

(1) $\theta = 0$ at $\varphi = 0$ and $\varphi = \alpha$

(2) $M_\eta = 0$ at $\varphi = 0$ and $\varphi = \alpha$

(3) $u = 0$ at $\varphi = 0$ and $\varphi = \alpha$

Firstly, let's talk about boundary condition (2). As M_η is 0, we can obtain $K_y = \dfrac{d^2u}{ds^2} + \dfrac{\theta}{R} = 0 \rightarrow \dfrac{d^2u}{d\varphi^2} = 0$.

Then from Eq.(4.58), $\dfrac{d^2\theta}{d\varphi^2} = 0$ can be obtained. Then the boundary condition (1) and (2) can be expressed as

$$\begin{cases} 0 = B + D \\ 0 = A\sin(\alpha k_1) + B\cos(\alpha k_1) + C\sinh(\alpha k_2) + D\cosh(\alpha k_2) \\ 0 = -Bk_1^2 + Dk_2^2 \\ 0 = -Ak_1^2\sin(\alpha k_1) - Bk_1^2\cos(\alpha k_1) + Ck_2^2\sinh(\alpha k_2) + Dk_2^2\cosh(\alpha k_2) \end{cases} \tag{4.72}$$

From equation set above we can obtain

$$\begin{cases} B = C = D = 0 \\ A\sin(\alpha k_1) = 0 \end{cases} \tag{4.73}$$

From the boundary condition (3), by using Eq.(4.60), we can obtain

$$\begin{cases} 0 = -\dfrac{B}{k_1^2} + \dfrac{D}{k_2^2} + F \\ 0 = -\dfrac{A}{k_1^2}\sin(\alpha k_1) - \dfrac{B}{k_1^2}\cos(\alpha k_1) + \dfrac{C}{k_2^2}\sinh(\alpha k_2) + \dfrac{D}{k_2^2}\cosh(\alpha k_2) + E\alpha + F \end{cases} \tag{4.74}$$

Substituting Eq.(4.73) into Eq.(4.74), we can obtain

$$E = F = 0 \tag{4.75}$$

Finally from the second term in Eq.(4.73), $\sin(\alpha k_1) = 0$. Then we know αk_1 is $n\pi$, we can obtain

$$k_1 = \frac{n\pi}{\alpha} \tag{4.76}$$

Substituting Eq.(4.76) into Eq.(4.66), we can obtain

$$(\frac{n\pi}{\alpha})^4 - 2a(\frac{n\pi}{\alpha})^2 + b = 0 \tag{4.77}$$

Then substituting expressions of a in Eq.(4.63) and b in Eq.(4.64) into Eq.(4.77), we can obtain

$$\omega = \frac{[(\frac{n\pi}{\alpha})^2 - 1]^2}{(\frac{n\pi}{\alpha})^2 + \lambda} \tag{4.78}$$

Finally substituting λ in Eq.(4.52) and ω in Eq.(4.53) into Eq.(4.78), the critical load q_{cr} can be expressed as

$$q_{cr} = \frac{EI_y}{R^3}\frac{[(\frac{n\pi}{\alpha})^2 - 1]^2}{(\frac{n\pi}{\alpha})^2 + \frac{EI_y}{GJ_z}} \tag{4.79}$$

When the central angle α is π. then the first order to the third order critical loads are

$$q_{cr}=\begin{cases}\dfrac{EI_y}{R^3}\dfrac{9}{4+\dfrac{EI_y}{GJ_z}}, \text{ the first order critical load}\\ \dfrac{EI_y}{R^3}\dfrac{64}{9+\dfrac{EI_y}{GJ_z}}, \text{ the second order critical load}\\ \dfrac{EI_y}{R^3}\dfrac{225}{16+\dfrac{EI_y}{GJ_z}}, \text{ the third order critical load}\end{cases} \tag{4.80}$$

The first term in Eq.(4.80) agrees with the value obtained by Timoshenko [42].

2) Fixed ended in-plane and out-of-plane

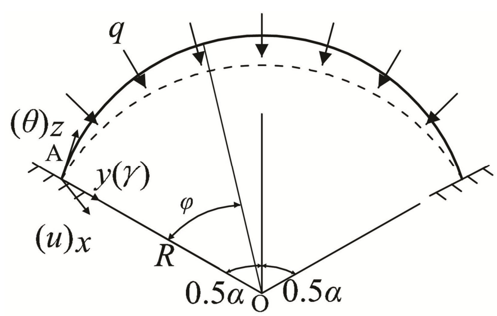

Fig.4-11 Buckling of the arch out-of-plane

When the boundary conditions are fixed ended in-plane and out-of-plane, as shown in Fig.4-11. And this type of boundary conditions can be given as follows:

(1) $\theta = 0$ at $\varphi = 0$ and $\varphi = \alpha$

(2) $u = 0$, $u' = 0$ at $\varphi = 0$ and $\varphi = \alpha$

The expressions of u' and u can be found in Eq.(4.59) and Eq.(4.60) respectively. Then using all the boundary conditions, we can obtain

$$\begin{cases} 0 = B + D \\ 0 = A\sin(\alpha k_1) + B\cos(\alpha k_1) + C\sinh(\alpha k_2) + D\cosh(\alpha k_2) \\ 0 = -\dfrac{B}{k_1^2} + \dfrac{D}{k_2^2} + F \\ 0 = -\dfrac{A}{k_1^2}\sin(\alpha k_1) - \dfrac{B}{k_1^2}\cos(\alpha k_1) + \dfrac{C}{k_2^2}\sinh(\alpha k_2) + \dfrac{D}{k_2^2}\cosh(\alpha k_2) + E\alpha + F \\ 0 = (Ak_1 + Ck_2) - \lambda(-\dfrac{A}{k_1} + \dfrac{C}{k_2} + E) \\ 0 = [Ak_1\cos(\alpha k_1) - Bk_1\sin(\alpha k_1) + Ck_2\cosh(\alpha k_2) + Dk_2\sinh(\alpha k_2)] \\ \quad -\lambda[-\dfrac{A}{k_1}\cos(\alpha k_1) + \dfrac{B}{k_1}\sin(\alpha k_1) + \dfrac{C}{k_2}\cosh(\alpha k_2) + \dfrac{D}{k_2}\sinh(\alpha k_2) + E] \end{cases} \tag{4.81}$$

According to the sequence of A, B, C, D, E and F, a matrix $\mathbf{S_{3D\text{-}F}}$ is assumed as

$$\mathbf{S_{3D\text{-}F}} = \begin{bmatrix} 0 & 1 & 0 & 1 & 0 & 0 \\ \sin(\alpha k_1) & \cos(\alpha k_1) & \sinh(\alpha k_2) & \cosh(\alpha k_2) & 0 & 0 \\ 0 & -\dfrac{1}{k_1^2} & 0 & \dfrac{1}{k_2^2} & 0 & 1 \\ -\dfrac{\sin(\alpha k_1)}{k_1^2} & -\dfrac{\cos(\alpha k_1)}{k_1^2} & \dfrac{\sinh(\alpha k_2)}{k_2^2} & \dfrac{\cosh(\alpha k_2)}{k_2^2} & \alpha & 1 \\ k_1 + \dfrac{\lambda}{k_1} & 0 & k_2 - \dfrac{\lambda}{k_2} & 0 & -\lambda & 0 \\ (k_1 + \dfrac{\lambda}{k_1})\cos(\alpha k_1) & -(k_1 + \dfrac{\lambda}{k_1})\sin(\alpha k_1) & (k_2 - \dfrac{\lambda}{k_2})\cosh(\alpha k_2) & (k_2 - \dfrac{\lambda}{k_2})\sinh(\alpha k_2) & -\lambda & 0 \end{bmatrix} \tag{4.82}$$

Then the buckling control equation which is the same expression of Eq.(4.81) is

$$\det(\mathbf{S_{3D\text{-}F}}) = 0 \tag{4.83}$$

We use a numerical model with same parameters in Section 4.3.1 here. And the results are shown in Table.4-9. In numerical analysis, the 3D beam elements without modified matrix are utilized. We only consider out-of-plane buckling modes but in-plane buckling modes are not stated. We analyze the two cases. The first one has the boundary conditions that are hinged ended in-plane and simple ended out-of-plane. And second one has the boundary conditions that are fixed ended in-plane and out-of-plane. For the first case, in software ANSYS, the tangential stiffness matrix of this kind of boundary conditions is singularity, then we do not give the solution by ANSYS in this case.

Table.4-6 shows the first order to third order buckling modes and critical loads when boundary conditions are hinged ended in-plane and simple ended out-of-plane. And Table.4-7 ~Table.4-9 show first order to third order buckling modes and critical loads respectively when boundary conditions are fixed ended both in-plane and out-of-plane.

Table.4-6 Buckling modes and critical loads

<table>
<tr><td colspan="5">Hinged ended in-plane and simple ended out-of-plane</td></tr>
<tr><td colspan="3">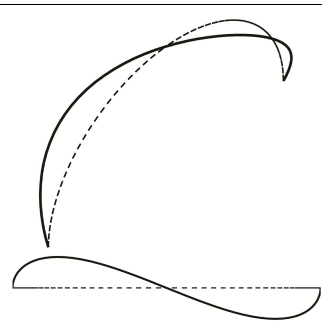
(48 elements)</td><td>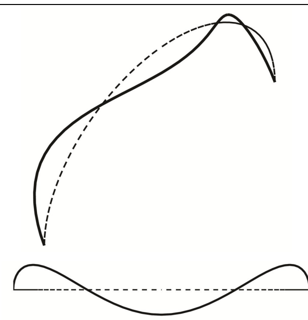
(48 elements)</td><td>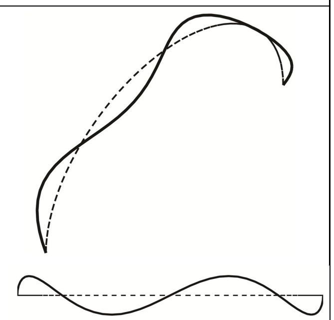
(48 elements)</td></tr>
<tr><td>Theory</td><td colspan="2">$q_{cr} = 1.70\frac{EI_y}{R^3}$</td><td>$q_{cr} = 6.21\frac{EI_y}{R^3}$</td><td>$q_{cr} = 13.00\frac{EI_y}{R^3}$</td></tr>
<tr><td rowspan="2">FE</td><td>48 elements</td><td>$q_{cr} = 1.73\frac{EI_y}{R^3}$</td><td>$q_{cr} = 6.34\frac{EI_y}{R^3}$</td><td>$q_{cr} = 13.28\frac{EI_y}{R^3}$</td></tr>
<tr><td>192 elements</td><td>$q_{cr} = 1.71\frac{EI_y}{R^3}$</td><td>$q_{cr} = 6.25\frac{EI_y}{R^3}$</td><td>$q_{cr} = 13.07\frac{EI_y}{R^3}$</td></tr>
</table>

Table.4-8 First order buckling modes and critical loads

<table>
<tr><td colspan="6">Fixed ended in-plane and out-of-plane</td></tr>
<tr><td colspan="3">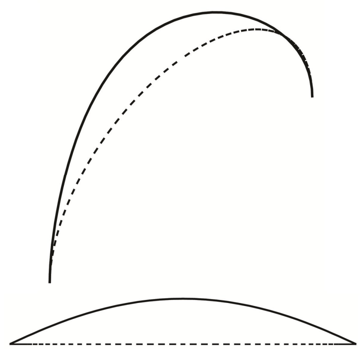
(FE: 48 elements)</td><td colspan="3">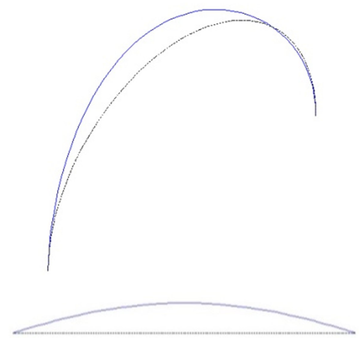
(ANSYS: 48 elements)</td></tr>
<tr><td colspan="2">Theory</td><td colspan="4">$q_{cr} = 2.47\frac{EI_y}{R^3}$</td></tr>
<tr><td rowspan="2">FE</td><td>48 elements</td><td>$q_{cr} = 2.52\frac{EI_y}{R^3}$</td><td rowspan="2">ANSYS</td><td rowspan="2">48 elements</td><td rowspan="2">$q_{cr} = 2.47\frac{EI_y}{R^3}$</td></tr>
<tr><td>192 elements</td><td>$q_{cr} = 2.48\frac{EI_y}{R^3}$</td></tr>
</table>

Table.4-8 Second order buckling modes and critical loads

<table>
<tr><td colspan="6">Fixed ended in-plane and out-of-plane</td></tr>
<tr><td colspan="3">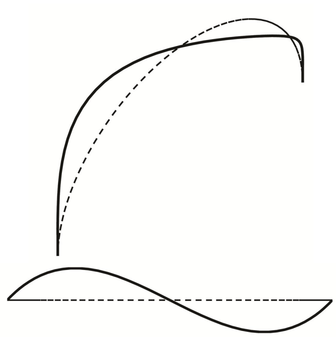
(FE: 48 elements)</td><td colspan="3">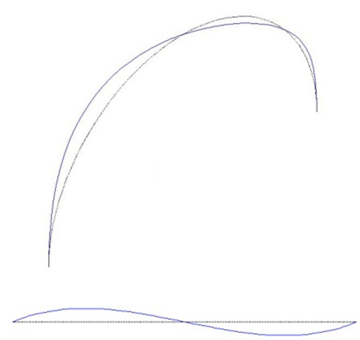
(ANSYS: 48 elements)</td></tr>
<tr><td colspan="2">Theory</td><td colspan="4">$q_{cr} = 5.71\frac{EI_y}{R^3}$</td></tr>
<tr><td rowspan="2">FE</td><td>48 elements</td><td>$q_{cr} = 5.83\frac{EI_y}{R^3}$</td><td rowspan="2">ANSYS</td><td rowspan="2">48 elements</td><td rowspan="2">$q_{cr} = 5.72\frac{EI_y}{R^3}$</td></tr>
<tr><td>192 elements</td><td>$q_{cr} = 5.74\frac{EI_y}{R^3}$</td></tr>
</table>

Table.4-9 Third order buckling modes and critical loads

<table>
<tr><td colspan="7">Fixed ended in-plane and out-of-plane</td></tr>
<tr><td colspan="3">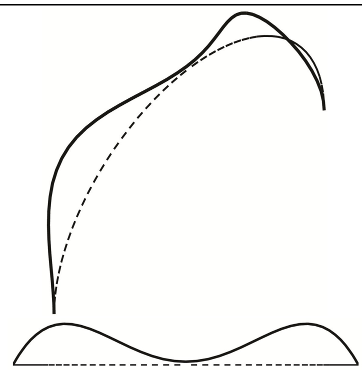
(FE: 48 elements)</td><td colspan="4">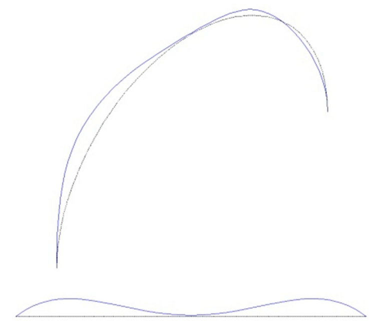
(ANSYS: 48 elements)</td></tr>
<tr><td colspan="2">Theory</td><td colspan="5">$q_{cr} = 13.32 \frac{EI_y}{R^3}$</td></tr>
<tr><td rowspan="2">FE</td><td>48 elements</td><td>$q_{cr} = 13.61 \frac{EI_y}{R^3}$</td><td rowspan="2">ANSYS</td><td rowspan="2">48 elements</td><td rowspan="2" colspan="2">$q_{cr} = 13.41 \frac{EI_y}{R^3}$</td></tr>
<tr><td>192 elements</td><td>$q_{cr} = 13.39 \frac{EI_y}{R^3}$</td></tr>
</table>

4.4 Summaries

In this chapter, static equilibrium conditions in the isolated infinitesimal body is used to deduce the equilibrium differential equations for in-plane and out-of-plane buckling of the arch under uniform compression respectively. The main achievement is summarized as follows:

1) General solutions of the displacements (v and w) for in-plane stability and of the displacements (θ and u) for out-of-plane stability are obtained respectively. By using these general solutions as well as boundary conditions, buckling control equations for in-plane and out-of-plane stability are able to be obtained.

2) By using numerical examples, the comparison of the results calculated by FE formulations in Chapter 2, by large finite element software ANSYS, and by the buckling control equations are carried out. These three results are very close to each other, and the theoretical procedures proposed in this chapter are verified.

Chapter 5 Stiffening Effect of Straight Components

5.1 Introduction

In Chapter 4, the elastic stability of the circular arch in-plane and out-of-plane under uniform compression are discussed. And the general solutions of displacements from equilibrium differential equations for in-plane stability and out-of-plane stability are obtained in explicit expressions respectively. In past research, researches mostly paid attention to the solution of first order critical load of arches or rings, because it is thought that only the first order buckling mode seems to happen in practice and higher buckling modes may not happen after all. But in this chapter, when constraint components are used to stiffen arches, buckling modes of arches may transfer from lower buckling modes to higher buckling modes, so theoretical solutions of second order critical loads and higher order critical loads are also very important for judging whether the numerical solutions obtained by FE methods are accurate or not.

The object of this chapter is to propose the theoretical approaches for analyzing the elastic stability problems of circular arches with straight components. And non-dimensional ratios (so-called spring ratios) of the stiffnesses of straight components and arches are aimed to be obtained. By taking braces as constraint components, arch-spring models are proposed and utilized for simplifications in theoretical procedures.

5.2 In-plane

5.2.1 Anti-symmetric buckling mode

1) Hinged ended in-plane

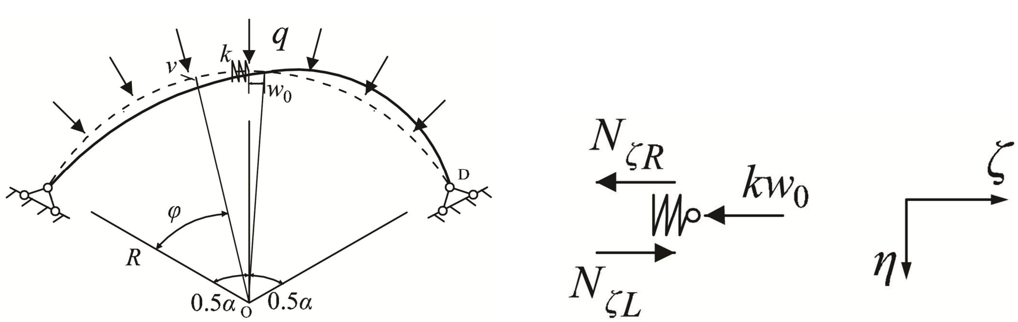

(a) (b)

Fig.5-1 Anti-symmetric arch-spring model

In Table.4-2 in Section 4.3.1 in Chapter 4, we know the first order and the third order buckling modes of the arch are anti-symmetric and the second order buckling modes is symmetric. Therefore two different kinds of methods are used to establish arch-spring models. Fig.5-1(a) shows an anti-symmetric arch-spring model. A spring with an elastic stiffness k is set up in horizontal direction at the middle of the arch. And uniform compression q is applied in the plane of the arch. Symbols "L" and "R" in subscripts are used to distinguish the displacements and forces at the left side and right side of the spring. From Eq.(4.27) in Chapter 4, the expressions of displacements are assumed as

$$v_L = A_1 \sin\varphi + B_1 \cos\varphi + C_1 \sin\tau\varphi + D_1 \cos\tau\varphi + E_1 \tag{5.1}$$

$$v_R = A_2 \sin\varphi + B_2 \cos\varphi + C_2 \sin\tau\varphi + D_2 \cos\tau\varphi + E_2 \tag{5.2}$$

Then the first to the fourth derivatives of v_L are

$$v_L' = A_1 \cos\varphi - B_1 \sin\varphi + C_1\tau \cos\tau\varphi - D_1\tau \sin\tau\varphi \tag{5.3}$$

$$v_L'' = -A_1 \sin\varphi - B_1 \cos\varphi - C_1\tau^2 \sin\tau\varphi - D_1\tau^2 \cos\tau\varphi \tag{5.4}$$

$$v_L''' = -A_1 \cos\varphi + B_1 \sin\varphi - C_1\tau^3 \cos\tau\varphi + D_1\tau^3 \sin\tau\varphi \tag{5.5}$$

$$v_L'''' = A_1 \sin\varphi + B_1 \cos\varphi + C_1\tau^4 \sin\tau\varphi + D_1\tau^4 \cos\tau\varphi \tag{5.6}$$

Similarly the first to the fourth derivatives of v_R are

$$v_R' = A_2 \cos\varphi - B_2 \sin\varphi + C_2\tau \cos\tau\varphi - D_2\tau \sin\tau\varphi \tag{5.7}$$

$$v_R'' = -A_2 \sin\varphi - B_2 \cos\varphi - C_2\tau^2 \sin\tau\varphi - D_2\tau^2 \cos\tau\varphi \tag{5.8}$$

$$v_R''' = -A_2 \cos\varphi + B_2 \sin\varphi - C_2\tau^3 \cos\tau\varphi + D_2\tau^3 \sin\tau\varphi \tag{5.9}$$

$$v_R'''' = A_2 \sin\varphi + B_2 \cos\varphi + C_2\tau^4 \sin\tau\varphi + D_2\tau^4 \cos\tau\varphi \tag{5.10}$$

In another aspect, referring to Eq.(4.28) in Chapter 4, the displacements w_L and w_R in tangential directions are

$$w_L = -A_1 \cos\varphi + B_1 \sin\varphi - C_1 \frac{\cos\tau\varphi}{\tau} + D_1 \frac{\sin\tau\varphi}{\tau} + E_1\varphi + F_1 \tag{5.11}$$

$$w_R = -A_2 \cos\varphi + B_2 \sin\varphi - C_2 \frac{\cos\tau\varphi}{\tau} + D_2 \frac{\sin\tau\varphi}{\tau} + E_2\varphi + F_2 \tag{5.12}$$

Fig.5-1(b) shows the equilibrium state of forces at the position of the spring in the horizontal direction, this equilibrium condition will be given as a boundary condition in latter narrative.

From the second term and third term of Eq.(4.10) in Chapter 4,we can obtain

$$N_{\varsigma} = R(-\frac{dQ_{\eta}}{ds} + q_r) = -\frac{dQ_{\eta}}{d\varphi} + Rq_r \tag{5.13}$$

$$Q_{\eta} = -\frac{dM_{\xi}}{ds} = \frac{EI_x}{R}\frac{dK_x}{d\varphi} = \frac{EI_x}{R^3}(\frac{d^3v}{d\varphi^3} + \frac{dv}{d\varphi}) \tag{5.14}$$

When the boundary conditions in Fig.5-1(a) are hinged ends, we can obtain

(1) $v_L = 0$, $v_L'' = 0$, $w_L = 0$ at $\varphi = 0$

(2) $v_R = 0$, $v_R'' = 0$, $w_R = 0$ at $\varphi = \alpha$

(3) $v_L = v_R$, $Q_{\eta L} = Q_{\eta R}$, $v_L' = v_R'$, $v_L'' = v_R''$, $w_L = w_R = w_0$, $-(Q_{\eta L})' = -(Q_{\eta R})' + kw_0$ at $\varphi = 0.5\alpha$

Then From boundary condition (1), we can obtain

$$\begin{cases} 0 = B_1 + D_1 + E_1 \\ 0 = -B_1 - D_1\tau^2 \\ 0 = -A_1 - C_1\dfrac{1}{\tau} + F_1 \end{cases} \tag{5.15}$$

From boundary condition (2), we can obtain

$$\begin{cases} 0 = A_2\sin\alpha + B_2\cos\alpha + C_2\sin\alpha\tau + D_2\cos\alpha\tau + E_2 \\ 0 = -A_2\sin\alpha - B_2\cos\alpha - C_2\tau^2\sin\alpha\tau - D_2\tau^2\cos\alpha\tau \\ 0 = -A_2\cos\alpha + B_2\sin\alpha - C_2\dfrac{\cos\alpha\tau}{\tau} + D_2\dfrac{\sin\alpha\tau}{\tau} + \alpha E_2 + F_2 \end{cases} \tag{5.16}$$

From boundary condition (3), we can obtain

$$
\begin{cases}
A_1 \sin 0.5\alpha + B_1 \cos 0.5\alpha + C_1 \sin 0.5\alpha\tau + D_1 \cos 0.5\alpha\tau + E_1 = \\
A_2 \sin 0.5\alpha + B_2 \cos 0.5\alpha + C_2 \sin 0.5\alpha\tau + D_2 \cos 0.5\alpha\tau + E_2 \\
-A_1 \cos 0.5\alpha + B_1 \sin 0.5\alpha - C_1\tau^3 \cos 0.5\alpha\tau + D_1\tau^3 \sin 0.5\alpha\tau = \\
-A_2 \cos 0.5\alpha + B_2 \sin 0.5\alpha - C_2\tau^3 \cos 0.5\alpha\tau + D_2\tau^3 \sin 0.5\alpha\tau \\
A_1 \cos 0.5\alpha - B_1 \sin 0.5\alpha + C_1\tau \cos 0.5\alpha\tau - D_1\tau \sin 0.5\alpha\tau = \\
A_2 \cos 0.5\alpha - B_2 \sin 0.5\alpha + C_2\tau \cos 0.5\alpha\tau - D_2\tau \sin 0.5\alpha\tau \\
-A_1 \sin 0.5\alpha - B_1 \cos 0.5\alpha - C_1\tau^2 \sin 0.5\alpha\tau - D_1\tau^2 \cos 0.5\alpha\tau = \\
-A_2 \sin 0.5\alpha - B_2 \cos 0.5\alpha - C_2\tau^2 \sin 0.5\alpha\tau - D_2\tau^2 \cos 0.5\alpha\tau \\
w_0 = -A_1 \cos 0.5\alpha + B_1 \sin 0.5\alpha - C_1 \dfrac{\cos 0.5\alpha\tau}{\tau} + D_1 \dfrac{\sin 0.5\alpha\tau}{\tau} + 0.5\alpha E_1 + F_1 \\
w_0 = -A_2 \cos 0.5\alpha + B_2 \sin 0.5\alpha - C_2 \dfrac{\cos 0.5\alpha\tau}{\tau} + D_2 \dfrac{\sin 0.5\alpha\tau}{\tau} + 0.5\alpha E_2 + F_2 \\
-\dfrac{EI_x}{R^3}(A_1 \sin 0.5\alpha + B_1 \cos 0.5\alpha + C_1\tau^4 \sin 0.5\alpha\tau + D_1\tau^4 \cos 0.5\alpha\tau) = \\
kw_0 - \dfrac{EI_x}{R^3}(A_2 \sin 0.5\alpha + B_2 \cos 0.5\alpha + C_2\tau^4 \sin 0.5\alpha\tau + D_2\tau^4 \cos 0.5\alpha\tau)
\end{cases}
\tag{5.17}
$$

According to the sequence of $A_1, B_1, C_1, D_1, E_1, F_1, A_2, B_2, C_2, D_2, E_2, F_2, w_0$, a matrix $\mathbf{S_{2D\text{-}AH}}$ is assumed as

$$
\mathbf{S_{2D\text{-}AH}} = \left[\begin{array}{cccccc c}
0 & 1 & 0 & 1 & 1 & 0 & \vdots \\
0 & 1 & 0 & \tau^2 & 0 & 0 & \vdots \\
1 & 0 & \dfrac{1}{\tau} & 0 & 0 & -1 & \vdots \\
0 & 0 & 0 & 0 & 0 & 0 & \vdots \\
0 & 0 & 0 & 0 & 0 & 0 & \vdots \\
0 & 0 & 0 & 0 & 0 & 0 & \vdots \\
\sin 0.5\alpha & \cos 0.5\alpha & \sin 0.5\alpha\tau & \cos 0.5\alpha\tau & 1 & 0 & \vdots \\
\cos 0.5\alpha & -\sin 0.5\alpha & \tau^3 \cos 0.5\alpha\tau & -\tau^3 \sin 0.5\alpha\tau & 0 & 0 & \vdots \\
\cos 0.5\alpha & -\sin 0.5\alpha & \tau \cos 0.5\alpha\tau & -\tau \sin 0.5\alpha\tau & 0 & 0 & \vdots \\
\sin 0.5\alpha & \cos 0.5\alpha & \tau^2 \sin 0.5\alpha\tau & \tau^2 \cos 0.5\alpha\tau & 0 & 0 & \vdots \\
\cos 0.5\alpha & -\sin 0.5\alpha & \dfrac{\cos 0.5\alpha\tau}{\tau} & -\dfrac{\sin 0.5\alpha\tau}{\tau} & -0.5\alpha & -1 & \vdots \\
0 & 0 & 0 & 0 & 0 & 0 & \vdots \\
\sin 0.5\alpha & \cos 0.5\alpha & \tau^4 \sin 0.5\alpha\tau & \tau^4 \cos 0.5\alpha\tau & 0 & 0 & \vdots
\end{array}\right.
$$

$$\left.\begin{array}{cccccccc}
\vdots & 0 & 0 & 0 & 0 & 0 & 0 & 0 \\
\vdots & 0 & 0 & 0 & 0 & 0 & 0 & 0 \\
\vdots & 0 & 0 & 0 & 0 & 0 & 0 & 0 \\
\vdots & \sin\alpha & \cos\alpha & \sin\alpha\tau & \cos\alpha\tau & 1 & 0 & 0 \\
\vdots & \sin\alpha & \cos\alpha & \tau^2\sin\alpha\tau & \tau^2\cos\alpha\tau & 0 & 0 & 0 \\
\vdots & -\cos\alpha & \sin\alpha & -\dfrac{\cos\alpha\tau}{\tau} & \dfrac{\sin\alpha\tau}{\tau} & \alpha & 1 & 0 \\
\vdots & -\sin 0.5\alpha & -\cos 0.5\alpha & -\sin 0.5\alpha\tau & -\cos 0.5\alpha\tau & -1 & 0 & 0 \\
\vdots & -\cos 0.5\alpha & \sin 0.5\alpha & -\tau^3\cos 0.5\alpha\tau & \tau^3\sin 0.5\alpha\tau & 0 & 0 & 0 \\
\vdots & -\cos 0.5\alpha & \sin 0.5\alpha & -\tau\cos 0.5\alpha\tau & \tau\sin 0.5\alpha\tau & 0 & 0 & 0 \\
\vdots & -\sin 0.5\alpha & -\cos 0.5\alpha & -\tau^2\sin 0.5\alpha\tau & -\tau^2\cos 0.5\alpha\tau & 0 & 0 & 0 \\
\vdots & 0 & 0 & 0 & 0 & 0 & 0 & 1 \\
\vdots & \cos 0.5\alpha & -\sin 0.5\alpha & \dfrac{\cos 0.5\alpha\tau}{\tau} & -\dfrac{\sin 0.5\alpha\tau}{\tau} & -0.5\alpha & -1 & 1 \\
\vdots & -\sin 0.5\alpha & -\cos 0.5\alpha & -\tau^4\sin 0.5\alpha\tau & -\tau^4\cos 0.5\alpha\tau & 0 & 0 & \dfrac{kR^3}{EI_x}
\end{array}\right]$$

$$(5.18)$$

Then the buckling control equation which is the same expression of Eq.(5.15)~Eq.(5.17) is

$$\det(\mathbf{S}_{\mathbf{2D\text{-}AH}}) = 0 \tag{5.19}$$

We spread out the equation above according to the last column of det($\mathbf{S}_{\mathbf{2D\text{-}AH}}$), and meanwhile a non-dimensional parameter r_x is assumed in Eq.(5.20).

$$r_x = \frac{k}{EI_x / R^3} \tag{5.20}$$

And this kind of non-dimensional parameters about the ratios of the elastic stiffnesses of springs (or braces) and arches is called "spring ratio" in latter narratives.

Then we can obtain

$$1\times\det(\mathbf{S}^{12}_{\mathbf{2D\text{-}AH1}}) + 1\times\det(\mathbf{S}^{12}_{\mathbf{2D\text{-}AH2}}) + r_x\det(\mathbf{S}^{12}_{\mathbf{2D\text{-}AH3}}) = 0 \tag{5.21}$$

Here det($\mathbf{S}^{12}_{\mathbf{2D\text{-}AH1}}$), det($\mathbf{S}^{12}_{\mathbf{2D\text{-}AH2}}$) and det($\mathbf{S}^{12}_{\mathbf{2D\text{-}AH3}}$) are cofactors of det($\mathbf{S}_{\mathbf{2D\text{-}AH}}$), the sizes of them are all 12×12. As these three cofactors only contain the unknown parameter τ and constant parameter α. We know τ is a function of uniform compression q, so from Eq.(5.21), we can judge that the critical load q_{cr} is determined by the spring ratio r_x.

2) Fixed ended in-plane

Now another case is considered, that is, the boundary conditions of the same circular arch in Fig.5-1(a) are fixed ended, this kind of boundary conditions can be expressed as

(1) $v_L = 0$, $v_L' = 0$, $w_L = 0$ at $\varphi = 0$

(2) $v_R = 0$, $v_R' = 0$, $w_R = 0$ at $\varphi = \alpha$

(3) $v_L = v_R$, $Q_{\eta L} = Q_{\eta R}$, $v_L' = v_R'$, $v_L'' = v_R''$, $w_L = w_R = w_0$, $-(Q_{\eta L})' = -(Q_{\eta R})' + kw_0$ at $\varphi = 0.5\alpha$

From boundary condition (1) and boundary condition (2), we can obtain

$$\begin{cases} 0 = B_1 + D_1 + E_1 \\ 0 = A_1 + C_1\tau \\ 0 = -A_1 - C_1\dfrac{1}{\tau} + F_1 \end{cases} \tag{5.22}$$

$$\begin{cases} 0 = A_2 \sin\alpha + B_2 \cos\alpha + C_2 \sin\alpha\tau + D_2 \cos\alpha\tau + E_2 \\ 0 = A_2 \cos\alpha - B_2 \sin\alpha + C_2\tau \cos\alpha\tau - D_2\tau \sin\alpha\tau \\ 0 = -A_2 \cos\alpha + B_2 \sin\alpha - C_2\dfrac{\cos\alpha\tau}{\tau} + D_2\dfrac{\sin\alpha\tau}{\tau} + \alpha E_2 + F_2 \end{cases} \tag{5.23}$$

Boundary condition (3) can be written as same as the one in Eq.(5.17). Then according to the sequence of A_1, B_1, C_1, D_1, E_1, F_1, A_2, B_2, C_2, D_2, E_2, F_2, w_0, a matrix $\mathbf{S_{2D\text{-}AF}}$ is assumed as

$$\mathbf{S_{2D\text{-}AF}} = \left[\begin{array}{cccccccc} 0 & 1 & 0 & 1 & 1 & 0 & \vdots \\ 1 & 0 & \tau & 0 & 0 & 0 & \vdots \\ 1 & 0 & \dfrac{1}{\tau} & 0 & 0 & -1 & \vdots \\ 0 & 0 & 0 & 0 & 0 & 0 & \vdots \\ 0 & 0 & 0 & 0 & 0 & 0 & \vdots \\ 0 & 0 & 0 & 0 & 0 & 0 & \vdots \\ \sin 0.5\alpha & \cos 0.5\alpha & \sin 0.5\alpha\tau & \cos 0.5\alpha\tau & 1 & 0 & \vdots \\ \cos 0.5\alpha & -\sin 0.5\alpha & \tau^3 \cos 0.5\alpha\tau & -\tau^3 \sin 0.5\alpha\tau & 0 & 0 & \vdots \\ \cos 0.5\alpha & -\sin 0.5\alpha & \tau \cos 0.5\alpha\tau & -\tau \sin 0.5\alpha\tau & 0 & 0 & \vdots \\ \sin 0.5\alpha & \cos 0.5\alpha & \tau^2 \sin 0.5\alpha\tau & \tau^2 \cos 0.5\alpha\tau & 0 & 0 & \vdots \\ \cos 0.5\alpha & -\sin 0.5\alpha & \dfrac{\cos 0.5\alpha\tau}{\tau} & -\dfrac{\sin 0.5\alpha\tau}{\tau} & -0.5\alpha & -1 & \vdots \\ 0 & 0 & 0 & 0 & 0 & 0 & \vdots \\ \sin 0.5\alpha & \cos 0.5\alpha & \tau^4 \sin 0.5\alpha\tau & \tau^4 \cos 0.5\alpha\tau & 0 & 0 & \vdots \end{array} \right.$$

$$\left.\begin{array}{cccccccc}
\vdots & 0 & 0 & 0 & 0 & 0 & 0 & 0 \\
\vdots & 0 & 0 & 0 & 0 & 0 & 0 & 0 \\
\vdots & 0 & 0 & 0 & 0 & 0 & 0 & 0 \\
\vdots & \sin\alpha & \cos\alpha & \sin\alpha\tau & \cos\alpha\tau & 1 & 0 & 0 \\
\vdots & \cos\alpha & -\sin\alpha & \tau\cos\alpha\tau & -\tau\sin\alpha\tau & 0 & 0 & 0 \\
\vdots & -\cos\alpha & \sin\alpha & -\dfrac{\cos\alpha\tau}{\tau} & \dfrac{\sin\alpha\tau}{\tau} & \alpha & 1 & 0 \\
\vdots & -\sin 0.5\alpha & -\cos 0.5\alpha & -\sin 0.5\alpha\tau & -\cos 0.5\alpha\tau & -1 & 0 & 0 \\
\vdots & -\cos 0.5\alpha & \sin 0.5\alpha & -\tau^3\cos 0.5\alpha\tau & \tau^3\sin 0.5\alpha\tau & 0 & 0 & 0 \\
\vdots & -\cos 0.5\alpha & \sin 0.5\alpha & -\tau\cos 0.5\alpha\tau & \tau\sin 0.5\alpha\tau & 0 & 0 & 0 \\
\vdots & -\sin 0.5\alpha & -\cos 0.5\alpha & -\tau^2\sin 0.5\alpha\tau & -\tau^2\cos 0.5\alpha\tau & 0 & 0 & 0 \\
\vdots & 0 & 0 & 0 & 0 & 0 & 0 & 1 \\
\vdots & \cos 0.5\alpha & -\sin 0.5\alpha & \dfrac{\cos 0.5\alpha\tau}{\tau} & -\dfrac{\sin 0.5\alpha\tau}{\tau} & -0.5\alpha & -1 & 1 \\
\vdots & -\sin 0.5\alpha & -\cos 0.5\alpha & -\tau^4\sin 0.5\alpha\tau & -\tau^4\cos 0.5\alpha\tau & 0 & 0 & \dfrac{kR^3}{EI_x}
\end{array}\right]$$

(5.24)

The buckling control equation is

$$\det(\mathbf{S}_{\mathbf{2D\text{-}AF}}) = 0 \tag{5.25}$$

Spreading out the equation above according to the last column of $\det(\mathbf{S}_{\mathbf{2D\text{-}AF}})$, we can obtain

$$1\times\det(\mathbf{S}^{12}_{\mathbf{2D\text{-}AF1}}) + 1\times\det(\mathbf{S}^{12}_{\mathbf{2D\text{-}AF2}}) + r_x\det(\mathbf{S}^{12}_{\mathbf{2D\text{-}AF3}}) = 0 \tag{5.26}$$

Here $\det(\mathbf{S}^{12}_{\mathbf{2D\text{-}AF1}})$, $\det(\mathbf{S}^{12}_{\mathbf{2D\text{-}AF2}})$ and $\det(\mathbf{S}^{12}_{\mathbf{2D\text{-}AF3}})$ are cofactors of $\det(\mathbf{S}_{\mathbf{2D\text{-}AF}})$, the sizes of them are all 12×12. As the same in case of hinged ended, the critical load q_{cr} of the arch is also determined by the spring ratio r_x.

5.2.2 Symmetric buckling mode

1) Hinged ended in-plane

Now the symmetric arch-spring model shown in Fig.5-2 (a) is discussed. And in Fig.5-2(a), a spring with elastic stiffness k is set up in vertical direction at the middle of the arch. Fig.5-2(b) shows equilibrium state of the forces at the position of the spring in vertical direction, and this equilibrium state of forces can be seen as one of the boundary conditions.

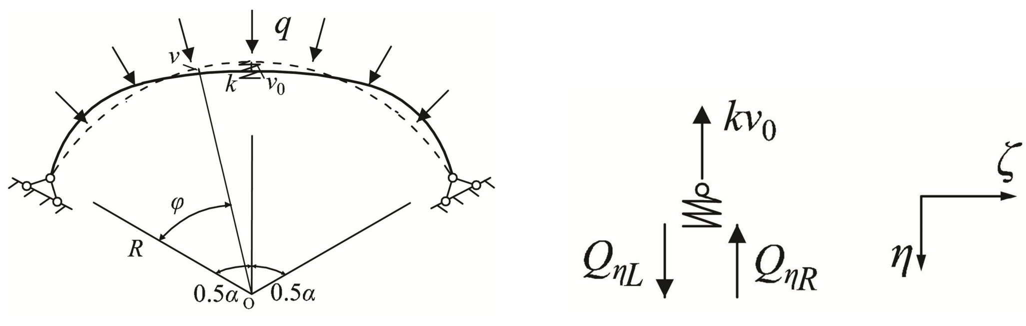

Fig.5-2 Symmetric arch-spring model

When the boundary conditions of the arch are hinged end, all boundary conditions can be expressed as

(1) $v_L = 0\,, v_L\,'' = 0\,, w_L = 0$ at $\varphi = 0$

(2) $v_R = 0\,, v_R\,'' = 0\,, w_R = 0$ at $\varphi = \alpha$

(3) $v_L = v_R = v_0\,, Q_{\eta L} = kv_0 + Q_{\eta R}\,, v_L\,' = v_R\,'\,, v_L\,'' = v_R\,''\,, w_L = w_R\,, (Q_{\eta L})' = (Q_{\eta R})'$ at $\varphi = 0.5\alpha$

The expressions of boundary condition (1) and (2) can be found in Eq.(5.15) and Eq.(5.16), so here only the boundary condition (3) is need to be considered, and it can be written as follows:

$$\begin{cases} v_0 = A_1 \sin 0.5\alpha + B_1 \cos 0.5\alpha + C_1 \sin 0.5\alpha\tau + D_1 \cos 0.5\alpha\tau + E_1 \\ v_0 = A_2 \sin 0.5\alpha + B_2 \cos 0.5\alpha + C_2 \sin 0.5\alpha\tau + D_2 \cos 0.5\alpha\tau + E_2 \\ -A_1 \cos 0.5\alpha + B_1 \sin 0.5\alpha - C_1\tau^3 \cos 0.5\alpha\tau + D_1\tau^3 \sin 0.5\alpha\tau = \\ \dfrac{kR^3}{EI_x} v_0 - A_2 \cos 0.5\alpha + B_2 \sin 0.5\alpha - C_2\tau^3 \cos 0.5\alpha\tau + D_2\tau^3 \sin 0.5\alpha\tau \\ A_1 \cos 0.5\alpha - B_1 \sin 0.5\alpha + C_1\tau \cos 0.5\alpha\tau - D_1\tau \sin 0.5\alpha\tau = \\ A_2 \cos 0.5\alpha - B_2 \sin 0.5\alpha + C_2\tau \cos 0.5\alpha\tau - D_2\tau \sin 0.5\alpha\tau \\ -A_1 \sin 0.5\alpha - B_1 \cos 0.5\alpha - C_1\tau^2 \sin 0.5\alpha\tau - D_1\tau^2 \cos 0.5\alpha\tau = \\ -A_2 \sin 0.5\alpha - B_2 \cos 0.5\alpha - C_2\tau^2 \sin 0.5\alpha\tau - D_2\tau^2 \cos 0.5\alpha\tau \\ -A_1 \cos 0.5\alpha + B_1 \sin 0.5\alpha - C_1 \dfrac{\cos 0.5\alpha\tau}{\tau} + D_1 \dfrac{\sin 0.5\alpha\tau}{\tau} + 0.5\alpha E_1 + F_1 = \\ -A_2 \cos 0.5\alpha + B_2 \sin 0.5\alpha - C_2 \dfrac{\cos 0.5\alpha\tau}{\tau} + D_2 \dfrac{\sin 0.5\alpha\tau}{\tau} + 0.5\alpha E_2 + F_2 \\ A_1 \sin 0.5\alpha + B_1 \cos 0.5\alpha + C_1\tau^4 \sin 0.5\alpha\tau + D_1\tau^4 \cos 0.5\alpha\tau = \\ A_2 \sin 0.5\alpha + B_2 \cos 0.5\alpha + C_2\tau^4 \sin 0.5\alpha\tau + D_2\tau^4 \cos 0.5\alpha\tau \end{cases} \tag{5.27}$$

According to the sequence of $A_1, B_1, C_1, D_1, E_1, F_1, A_2, B_2, C_2, D_2, E_2, F_2, v_0$, a matrix $\mathbf{S_{2D\text{-}SH}}$ is assumed as

$$
\mathbf{S}_{\mathbf{2D\text{-}SH}} = \left[\begin{array}{cccccc c}
0 & 1 & 0 & 1 & 1 & 0 & \vdots \\
0 & 1 & 0 & \tau^2 & 0 & 0 & \vdots \\
1 & 0 & \frac{1}{\tau} & 0 & 0 & -1 & \vdots \\
0 & 0 & 0 & 0 & 0 & 0 & \vdots \\
0 & 0 & 0 & 0 & 0 & 0 & \vdots \\
0 & 0 & 0 & 0 & 0 & 0 & \vdots \\
\sin 0.5\alpha & \cos 0.5\alpha & \sin 0.5\alpha\tau & \cos 0.5\alpha\tau & 1 & 0 & \vdots \\
0 & 0 & 0 & 0 & 0 & 0 & \vdots \\
\cos 0.5\alpha & -\sin 0.5\alpha & \tau^3\cos 0.5\alpha\tau & -\tau^3\sin 0.5\alpha\tau & 0 & 0 & \vdots \\
\cos 0.5\alpha & -\sin 0.5\alpha & \tau\cos 0.5\alpha\tau & -\tau\sin 0.5\alpha\tau & 0 & 0 & \vdots \\
\sin 0.5\alpha & \cos 0.5\alpha & \tau^2\sin 0.5\alpha\tau & \tau^2\cos 0.5\alpha\tau & 0 & 0 & \vdots \\
\cos 0.5\alpha & -\sin 0.5\alpha & \frac{\cos 0.5\alpha\tau}{\tau} & -\frac{\sin 0.5\alpha\tau}{\tau} & -0.5\alpha & -1 & \vdots \\
\sin 0.5\alpha & \cos 0.5\alpha & \tau^4\sin 0.5\alpha\tau & \tau^4\cos 0.5\alpha\tau & 0 & 0 & \vdots
\end{array}\right.
$$

$$
\left.\begin{array}{c ccccccc}
\vdots & 0 & 0 & 0 & 0 & 0 & 0 & 0 \\
\vdots & 0 & 0 & 0 & 0 & 0 & 0 & 0 \\
\vdots & 0 & 0 & 0 & 0 & 0 & 0 & 0 \\
\vdots & \sin\alpha & \cos\alpha & \sin\alpha\tau & \cos\alpha\tau & 1 & 0 & 0 \\
\vdots & \sin\alpha & \cos\alpha & \tau^2\sin\alpha\tau & \tau^2\cos\alpha\tau & 0 & 0 & 0 \\
\vdots & -\cos\alpha & \sin\alpha & -\frac{\cos\alpha\tau}{\tau} & \frac{\sin\alpha\tau}{\tau} & \alpha & 1 & 0 \\
\vdots & 0 & 0 & 0 & 0 & 0 & 0 & -1 \\
\vdots & \sin 0.5\alpha & \cos 0.5\alpha & \sin 0.5\alpha\tau & \cos 0.5\alpha\tau & 1 & 0 & -1 \\
\vdots & -\cos 0.5\alpha & \sin 0.5\alpha & -\tau^3\cos 0.5\alpha\tau & \tau^3\sin 0.5\alpha\tau & 0 & 0 & \frac{kR^3}{EI_x} \\
\vdots & -\cos 0.5\alpha & \sin 0.5\alpha & -\tau\cos 0.5\alpha\tau & \tau\sin 0.5\alpha\tau & 0 & 0 & 0 \\
\vdots & -\sin 0.5\alpha & -\cos 0.5\alpha & -\tau^2\sin 0.5\alpha\tau & -\tau^2\cos 0.5\alpha\tau & 0 & 0 & 0 \\
\vdots & -\cos 0.5\alpha & \sin 0.5\alpha & -\frac{\cos 0.5\alpha\tau}{\tau} & \frac{\sin 0.5\alpha\tau}{\tau} & 0.5\alpha & 1 & 0 \\
\vdots & -\sin 0.5\alpha & -\cos 0.5\alpha & -\tau^4\sin 0.5\alpha\tau & -\tau^4\cos 0.5\alpha\tau & 0 & 0 & 0
\end{array}\right]
$$

(5.28)

The buckling control equation is

$$\det(\mathbf{S}_{\mathbf{2D\text{-}SH}}) = 0 \tag{5.29}$$

Spreading out equation above according to the last column of det(**S_{2D-SH}**), and we can obtain

$$(-1)\times\det(\mathbf{S}^{12}_{\mathbf{2D\text{-}SH1}})+(-1)\times\det(\mathbf{S}^{12}_{\mathbf{2D\text{-}SH2}})+r_x\det(\mathbf{S}^{12}_{\mathbf{2D\text{-}SH3}})=0 \tag{5.30}$$

Here $\det(\mathbf{S}^{12}_{\mathbf{2D\text{-}SH1}})$, $\det(\mathbf{S}^{12}_{\mathbf{2D\text{-}SH2}})$ and $\det(\mathbf{S}^{12}_{\mathbf{2D\text{-}SH3}})$ are cofactors of $\det(\mathbf{S_{2D\text{-}SH}})$, the sizes of them are all 12×12. As same as the case in Section 5.2.1, the critical load q_{cr} of the arch is determined by the spring ratio r_x.

2) Fixed ended in- plane

When the boundary conditions of the arch in Fig.5-2(a) are fixed ended, this kind of boundary conditions can be expressed as

(1) $v_L=0$, $v_L'=0$, $w_L=0$ at $\varphi=0$

(2) $v_R=0$, $v_R'=0$, $w_R=0$ at $\varphi=\alpha$

(3) $v_L=v_R=v_0$, $Q_{\eta L}=kv_0+Q_{\eta R}$, $v_L'=v_R'$, $v_L''=v_R''$, $w_L=w_R$, $(Q_L)'=(Q_R)'$ at $\varphi=0.5\alpha$

The expressions of boundary condition (1)~(3) can be found in Eq.(5.22), Eq.(5.27) and Eq.(5.23) respectively. According to the sequence of A_1, B_1, C_1, D_1, E_1, F_1, A_2, B_2, C_2, D_2, E_2, F_2, v_1, a matrix $\mathbf{S_{2D\text{-}SF}}$ is assumed as

$$\mathbf{S_{2D\text{-}SF}}=\left[\begin{array}{cccccccc}
0 & 1 & 0 & 1 & 1 & 0 & \vdots \\
1 & 0 & \tau & 0 & 0 & 0 & \vdots \\
1 & 0 & \dfrac{1}{\tau} & 0 & 0 & -1 & \vdots \\
0 & 0 & 0 & 0 & 0 & 0 & \vdots \\
0 & 0 & 0 & 0 & 0 & 0 & \vdots \\
0 & 0 & 0 & 0 & 0 & 0 & \vdots \\
\sin 0.5\alpha & \cos 0.5\alpha & \sin 0.5\alpha\tau & \cos 0.5\alpha\tau & 1 & 0 & \vdots \\
0 & 0 & 0 & 0 & 0 & 0 & \vdots \\
\cos 0.5\alpha & -\sin 0.5\alpha & \tau^3\cos 0.5\alpha\tau & -\tau^3\sin 0.5\alpha\tau & 0 & 0 & \vdots \\
\cos 0.5\alpha & -\sin 0.5\alpha & \tau\cos 0.5\alpha\tau & -\tau\sin 0.5\alpha\tau & 0 & 0 & \vdots \\
\sin 0.5\alpha & \cos 0.5\alpha & \tau^2\sin 0.5\alpha\tau & \tau^2\cos 0.5\alpha\tau & 0 & 0 & \vdots \\
\cos 0.5\alpha & -\sin 0.5\alpha & \dfrac{\cos 0.5\alpha\tau}{\tau} & -\dfrac{\sin 0.5\alpha\tau}{\tau} & -0.5\alpha & -1 & \vdots \\
\sin 0.5\alpha & \cos 0.5\alpha & \tau^4\sin 0.5\alpha\tau & \tau^4\cos 0.5\alpha\tau & 0 & 0 & \vdots
\end{array}\right.$$

$$
\begin{matrix}
\vdots & 0 & 0 & 0 & 0 & 0 & 0 & 0 \\
\vdots & 0 & 0 & 0 & 0 & 0 & 0 & 0 \\
\vdots & 0 & 0 & 0 & 0 & 0 & 0 & 0 \\
\vdots & \sin\alpha & \cos\alpha & \sin\alpha\tau & \cos\alpha\tau & 1 & 0 & 0 \\
\vdots & \cos\alpha & -\sin\alpha & \tau\cos\alpha\tau & -\tau\sin\alpha\tau & 0 & 0 & 0 \\
\vdots & -\cos\alpha & \sin\alpha & -\dfrac{\cos\alpha\tau}{\tau} & \dfrac{\sin\alpha\tau}{\tau} & \alpha & 1 & 0 \\
\vdots & 0 & 0 & 0 & 0 & 0 & 0 & -1 \\
\vdots & \sin 0.5\alpha & \cos 0.5\alpha & \sin 0.5\alpha\tau & \cos 0.5\alpha\tau & 1 & 0 & -1 \\
\vdots & -\cos 0.5\alpha & \sin 0.5\alpha & -\tau^3\cos 0.5\alpha\tau & \tau^3\sin 0.5\alpha\tau & 0 & 0 & \dfrac{kR^3}{EI_x} \\
\vdots & -\cos 0.5\alpha & \sin 0.5\alpha & -\tau\cos 0.5\alpha\tau & \tau\sin 0.5\alpha\tau & 0 & 0 & 0 \\
\vdots & -\sin 0.5\alpha & -\cos 0.5\alpha & -\tau^2\sin 0.5\alpha\tau & -\tau^2\cos 0.5\alpha\tau & 0 & 0 & 0 \\
\vdots & -\cos 0.5\alpha & \sin 0.5\alpha & -\dfrac{\cos 0.5\alpha\tau}{\tau} & \dfrac{\sin 0.5\alpha\tau}{\tau} & 0.5\alpha & 1 & 0 \\
\vdots & -\sin 0.5\alpha & -\cos 0.5\alpha & -\tau^4\sin 0.5\alpha\tau & -\tau^4\cos 0.5\alpha\tau & 0 & 0 & 0
\end{matrix}\right]
$$

(5.31)

The buckling control equation is

$$\det(\mathbf{S_{2D\text{-}SF}}) = 0 \tag{5.32}$$

Spreading out the equation above according to the last column of det($\mathbf{S_{2D\text{-}SF}}$), we can obtain

$$(-1)\times\det(\mathbf{S^{12}_{2D\text{-}SF1}}) + (-1)\times\det(\mathbf{S^{12}_{2D\text{-}SF2}}) + r_x\det(\mathbf{S^{12}_{2D\text{-}SF3}}) = 0 \tag{5.33}$$

Here det($\mathbf{S^{12}_{2D\text{-}SF1}}$), det($\mathbf{S^{12}_{2D\text{-}SF2}}$)and det($\mathbf{S^{12}_{2D\text{-}SF3}}$) are cofactors of det($\mathbf{S_{2D\text{-}SF}}$), the sizes of them are all 12×12. As same as the case in Section 5.2.1, the critical load q_{cr} of the arch is determined by the spring ratio r_x.

5.2.3 Combination analysis of two springs

1) Hinged ended in-plane

In Section 5.2.1 and Section 5.2.2, the buckling control equations of arches are deduced when the buckling modes of arches are anti-symmetric and symmetrical respectively. It is straightforward to deduce one buckling equation to combine the cases of anti-symmetric and symmetrical modes together. The configuration of the arch and constraint springs is shown in Fig.5-3(a). And Fig.5-3(b) shows the equilibrium state of forces at the position of springs.

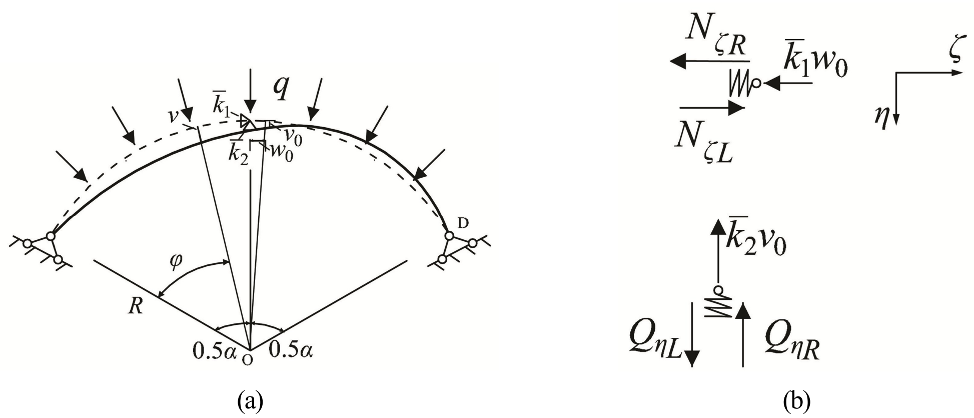

Fig.5-3 Circular arch stiffened by two springs

Assuming the boundary conditions of the arch are hinged ended, we can obtain

(1) $v_L = 0\,, v_L\,'' = 0\,, w_L = 0$ at $\varphi = 0$

(2) $v_R = 0\,, v_R\,'' = 0\,, w_R = 0$ at $\varphi = \alpha$

(3) $v_L = v_R = v_0\,, Q_{\eta L} = Q_{\eta R} + \bar{k}_2 v_0\,, v_L\,' = v_R\,'\,, v_L\,'' = v_R\,''\,, w_L = w_R = w_0\,, -(Q_{\eta L})' = -(Q_{\eta R})' + \bar{k}_1 w_0$

at $\varphi = 0.5\alpha$

Expressions of boundary condition (1) and (2) are in Eq.(5.15) and Eq.(5.16). And boundary condition (3) is

$$\begin{cases} v_0 = A_1 \sin 0.5\alpha + B_1 \cos 0.5\alpha + C_1 \sin 0.5\alpha\tau + D_1 \cos 0.5\alpha\tau + E_1 \\ v_0 = A_2 \sin 0.5\alpha + B_2 \cos 0.5\alpha + C_2 \sin 0.5\alpha\tau + D_2 \cos 0.5\alpha\tau + E_2 \\ -A_1 \cos 0.5\alpha + B_1 \sin 0.5\alpha - C_1\tau^3 \cos 0.5\alpha\tau + D_1\tau^3 \sin 0.5\alpha\tau = \\ \dfrac{\bar{k}_2 R^3}{EI_x} v_0 - A_2 \cos 0.5\alpha + B_2 \sin 0.5\alpha - C_2\tau^3 \cos 0.5\alpha\tau + D_2\tau^3 \sin 0.5\alpha\tau \\ A_1 \cos 0.5\alpha - B_1 \sin 0.5\alpha + C_1\tau \cos 0.5\alpha\tau - D_1\tau \sin 0.5\alpha\tau = \\ A_2 \cos 0.5\alpha - B_2 \sin 0.5\alpha + C_2\tau \cos 0.5\alpha\tau - D_2\tau \sin 0.5\alpha\tau \\ -A_1 \sin 0.5\alpha - B_1 \cos 0.5\alpha - C_1\tau^2 \sin 0.5\alpha\tau - D_1\tau^2 \cos 0.5\alpha\tau = \\ -A_2 \sin 0.5\alpha - B_2 \cos 0.5\alpha - C_2\tau^2 \sin 0.5\alpha\tau - D_2\tau^2 \cos 0.5\alpha\tau \\ w_0 = -A_1 \cos 0.5\alpha + B_1 \sin 0.5\alpha - C_1 \dfrac{\cos 0.5\alpha\tau}{\tau} + D_1 \dfrac{\sin 0.5\alpha\tau}{\tau} + 0.5\alpha E_1 + F_1 \\ w_0 = -A_2 \cos 0.5\alpha + B_2 \sin 0.5\alpha - C_2 \dfrac{\cos 0.5\alpha\tau}{\tau} + D_2 \dfrac{\sin 0.5\alpha\tau}{\tau} + 0.5\alpha E_2 + F_2 \\ -\dfrac{EI_x}{R^3}(A_1 \sin 0.5\alpha + B_1 \cos 0.5\alpha + C_1\tau^4 \sin 0.5\alpha\tau + D_1\tau^4 \cos 0.5\alpha\tau) = \\ \bar{k}_1 w_0 - \dfrac{EI_x}{R^3}(A_2 \sin 0.5\alpha + B_2 \cos 0.5\alpha + C_2\tau^4 \sin 0.5\alpha\tau + D_2\tau^4 \cos 0.5\alpha\tau) \end{cases} \tag{5.34}$$

According to the sequence of $A_1, B_1, C_1, D_1, E_1, F_1, A_2, B_2, C_2, D_2, E_2, F_2, v_0, w_0$, a matrix $\mathbf{S}_{\mathbf{2D\text{-}DH}}$ is assumed as

$$
\mathbf{S}_{\mathbf{2D\text{-}DH}} = \left[\begin{array}{ccccccc:ccccccc}
0 & 1 & 0 & 1 & 1 & 0 & 0 & 0 & 0 & 0 & 0 & 0 & 0 & 0 \\
0 & 1 & 0 & \tau^2 & 0 & 0 & 0 & 0 & 0 & 0 & 0 & 0 & 0 & 0 \\
1 & 0 & \frac{1}{\tau} & 0 & 0 & -1 & 0 & 0 & 0 & 0 & 0 & 0 & 0 & 0 \\
0 & 0 & 0 & 0 & 0 & 0 & \sin\alpha & \cos\alpha & \sin\alpha\tau & \cos\alpha\tau & 1 & 0 & 0 & 0 \\
0 & 0 & 0 & 0 & 0 & 0 & \sin\alpha & \cos\alpha & \tau^2\sin\alpha\tau & \tau^2\cos\alpha\tau & 0 & 0 & 0 & 0 \\
0 & 0 & 0 & 0 & 0 & 0 & -\cos\alpha & \sin\alpha & -\frac{\cos\alpha\tau}{\tau} & \frac{\sin\alpha\tau}{\tau} & \alpha & 1 & 0 & 0 \\
\sin 0.5\alpha & \cos 0.5\alpha & \sin 0.5\alpha\tau & \cos 0.5\alpha\tau & 1 & 0 & 0 & 0 & 0 & 0 & 0 & 0 & -1 & 0 \\
0 & 0 & 0 & 0 & 0 & 0 & \sin 0.5\alpha & \cos 0.5\alpha & \sin 0.5\alpha\tau & \cos 0.5\alpha\tau & 1 & 0 & -1 & 0 \\
\cos 0.5\alpha & -\sin 0.5\alpha & \tau^3\cos 0.5\alpha\tau & -\tau^3\sin 0.5\alpha\tau & 0 & 0 & -\cos 0.5\alpha & \sin 0.5\alpha & -\tau^3\cos 0.5\alpha\tau & \tau^3\sin 0.5\alpha\tau & 0 & 0 & \frac{\bar{k}_2 R^3}{EI_x} & 0 \\
\cos 0.5\alpha & -\sin 0.5\alpha & \tau\cos 0.5\alpha\tau & -\tau\sin 0.5\alpha\tau & 0 & 0 & -\cos 0.5\alpha & \sin 0.5\alpha & -\tau\cos 0.5\alpha\tau & \tau\sin 0.5\alpha\tau & 0 & 0 & 0 & 0 \\
\sin 0.5\alpha & \cos 0.5\alpha & \tau^2\sin 0.5\alpha\tau & \tau^2\cos 0.5\alpha\tau & 0 & 0 & -\sin 0.5\alpha & -\cos 0.5\alpha & -\tau^2\sin 0.5\alpha\tau & -\tau^2\cos 0.5\alpha\tau & 0 & 0 & 0 & 0 \\
\cos 0.5\alpha & -\sin 0.5\alpha & \frac{\cos 0.5\alpha\tau}{\tau} & -\frac{\sin 0.5\alpha\tau}{\tau} & -0.5\alpha & -1 & 0 & 0 & 0 & 0 & 0 & 0 & 0 & 1 \\
0 & 0 & 0 & 0 & 0 & 0 & \cos 0.5\alpha & -\sin 0.5\alpha & \frac{\cos 0.5\alpha\tau}{\tau} & -\frac{\sin 0.5\alpha\tau}{\tau} & -0.5\alpha & -1 & 0 & 1 \\
\sin 0.5\alpha & \cos 0.5\alpha & \tau^4\sin 0.5\alpha\tau & \tau^4\cos 0.5\alpha\tau & 0 & 0 & -\sin 0.5\alpha & -\cos 0.5\alpha & -\tau^4\sin 0.5\alpha\tau & -\tau^4\cos 0.5\alpha\tau & 0 & 0 & 0 & \frac{\bar{k}_1 R^3}{EI_x}
\end{array}\right] \tag{5.35}
$$

The buckling control equation is

$$\det(\mathbf{S_{2D\text{-}DH}}) = 0 \tag{5.36}$$

2) Fixed ended in-plane

When the boundary conditions are fixed ended, this kind of boundary conditions can be expressed as

(1) $v_L = 0$, $v_L' = 0$, $w_L = 0$ at $\varphi = 0$

(2) $v_R = 0$, $v_R' = 0$, $w_R = 0$ at $\varphi = \alpha$

(3) $v_L = v_R = v_0$, $Q_{\eta L} = Q_{\eta R} + \bar{k}_2 v_0$, $v_L' = v_R'$, $v_L'' = v_R''$, $w_L = w_R = w_0$, $-(Q_{\eta L})' = -(Q_{\eta R})' + \bar{k}_1 w_0$

at $\varphi = 0.5\alpha$

The expressions of boundary condition (1)~(3) can be found in Eq.(5.22), Eq.(5.23) and Eq.(5.34) respectively. According to the sequence of $A_1, B_1, C_1, D_1, E_1, F_1, A_2, B_2, C_2, D_2, E_2, F_2, v_0, w_0$, a matrix $\mathbf{S_{2D\text{-}DF}}$ is assumed as

$$\mathbf{S_{2D\text{-}DF}} = \begin{bmatrix}
0 & 1 & 0 & 1 & 1 & 0 & 0 & \vdots \\
1 & 0 & \tau & 0 & 0 & 0 & 0 & \vdots \\
1 & 0 & \dfrac{1}{\tau} & 0 & 0 & -1 & 0 & \vdots \\
0 & 0 & 0 & 0 & 0 & 0 & \sin\alpha & \vdots \\
0 & 0 & 0 & 0 & 0 & 0 & \cos\alpha & \vdots \\
0 & 0 & 0 & 0 & 0 & 0 & -\cos\alpha & \vdots \\
\sin 0.5\alpha & \cos 0.5\alpha & \sin 0.5\alpha\tau & \cos 0.5\alpha\tau & 1 & 0 & 0 & \vdots \\
0 & 0 & 0 & 0 & 0 & 0 & \sin 0.5\alpha & \vdots \\
\cos 0.5\alpha & -\sin 0.5\alpha & \tau^3 \cos 0.5\alpha\tau & -\tau^3 \sin 0.5\alpha\tau & 0 & 0 & -\cos 0.5\alpha & \vdots \\
\cos 0.5\alpha & -\sin 0.5\alpha & \tau \cos 0.5\alpha\tau & -\tau \sin 0.5\alpha\tau & 0 & 0 & -\cos 0.5\alpha & \vdots \\
\sin 0.5\alpha & \cos 0.5\alpha & \tau^2 \sin 0.5\alpha\tau & \tau^2 \cos 0.5\alpha\tau & 0 & 0 & -\sin 0.5\alpha & \vdots \\
\cos 0.5\alpha & -\sin 0.5\alpha & \dfrac{\cos 0.5\alpha\tau}{\tau} & -\dfrac{\sin 0.5\alpha\tau}{\tau} & -0.5\alpha & -1 & 0 & \vdots \\
0 & 0 & 0 & 0 & 0 & 0 & \cos 0.5\alpha & \vdots \\
\sin 0.5\alpha & \cos 0.5\alpha & \tau^4 \sin 0.5\alpha\tau & \tau^4 \cos 0.5\alpha\tau & 0 & 0 & -\sin 0.5\alpha & \vdots
\end{bmatrix}$$

$$
\left.\begin{matrix}
\vdots & 0 & 0 & 0 & 0 & 0 & 0 & 0 \\
\vdots & 0 & 0 & 0 & 0 & 0 & 0 & 0 \\
\vdots & 0 & 0 & 0 & 0 & 0 & 0 & 0 \\
\vdots & \cos\alpha & \sin\alpha\tau & \cos\alpha\tau & 1 & 0 & 0 & 0 \\
\vdots & -\sin\alpha & \tau\cos\alpha\tau & -\tau\sin\alpha\tau & 0 & 0 & 0 & 0 \\
\vdots & \sin\alpha & -\dfrac{\cos\alpha\tau}{\tau} & \dfrac{\sin\alpha\tau}{\tau} & \alpha & 1 & 0 & 0 \\
\vdots & 0 & 0 & 0 & 0 & 0 & -1 & 0 \\
\vdots & \cos 0.5\alpha & \sin 0.5\alpha\tau & \cos 0.5\alpha\tau & 1 & 0 & -1 & 0 \\
\vdots & \sin 0.5\alpha & -\tau^3\cos 0.5\alpha\tau & \tau^3\sin 0.5\alpha\tau & 0 & 0 & \dfrac{\overline{k}_2 R^3}{EI_x} & 0 \\
\vdots & \sin 0.5\alpha & -\tau\cos 0.5\alpha\tau & \tau\sin 0.5\alpha\tau & 0 & 0 & 0 & 0 \\
\vdots & -\cos 0.5\alpha & -\tau^2\sin 0.5\alpha\tau & -\tau^2\cos 0.5\alpha\tau & 0 & 0 & 0 & 0 \\
\vdots & 0 & 0 & 0 & 0 & 0 & 0 & 1 \\
\vdots & -\sin 0.5\alpha & \dfrac{\cos 0.5\alpha\tau}{\tau} & -\dfrac{\sin 0.5\alpha\tau}{\tau} & -0.5\alpha & -1 & 0 & 1 \\
\vdots & -\cos 0.5\alpha & -\tau^4\sin 0.5\alpha\tau & -\tau^4\cos 0.5\alpha\tau & 0 & 0 & 0 & \dfrac{\overline{k}_1 R^3}{EI_x}
\end{matrix}\right]
$$

(5.37)

Then the buckling control equation is

$$
\det(\mathbf{S}_{\mathbf{2D\text{-}DF}}) = 0 \tag{5.38}
$$

5.2.4 Numerical examples

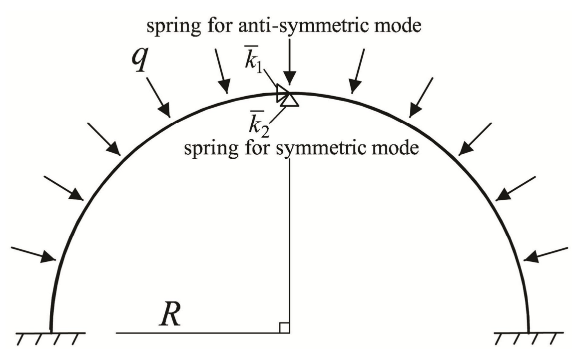

Fig.5-4 Numerical model of the arch in 2D plane

Firstly, the stability problems of the arch with only spring will be analyzed, which is set up in horizontal direction or vertical direction at the middle of the arch. Here two spring ratios r_1 and r_2 are assumed as

$$\begin{cases} r_1 = \dfrac{\overline{k}_1}{EI_x / R^3} \\ r_2 = \dfrac{\overline{k}_2}{EI_x / R^3} \end{cases} \tag{5.39}$$

Here a numerical example in Fig.5-4 is used to prove theoretical equations above. The materials parameters in this example are as same as the one stated in Chapter 4. The circular angel of the arch is π. The entire arch is divided into 48 linear beam elements with the same length respectively. The external load is assumed as uniform compression in-plane.

Table.5-1 shows the comparison of the results by Eq.(5.29) and Eq.(5.32), and by FE method. Symbols “1st order theo.”, “2nd order theo.” and “3rd order theo.” mean the first order, the second order and the third order critical loads of the arch without springs respectively, and these values are calculated in Section 4.3.1. Symbol “FE” means the results calculated by FE method. And symbol “Theo.” means the results calculated by the buckling control equations introduced in Section 5.2.1 or Section 5.2.2.

Firstly let’s observe the results of examples with hinged ended boundary conditions in Table.5-1(a). For anti-symmetric mode, the spring set up in horizontal direction in Fig.5-1 can cause the critical load to increase from the first order critical load to the second critical load. And for the spring set up in vertical direction in Fig.5-2, it can cause the critical load to increase from the second order critical load to the third critical load (the first order critical load is ignored here). In cases of anti-symmetric and symmetric modes, we obtain spring ratios r_1 and r_2 for the changing of buckling modes are about 23.67 and 57.25 respectively. Especially, in the latter narratives, the spring ratio for the last time of changing of buckling modes is called limiting spring ratio.

Furthermore, let’s observe the results of examples with fixed ended boundary conditions in Table.5-1(b). And the variation tendency of the critical loads in the examples of anti-symmetric mode and symmetric mode are similar to the cases which have the hinged ended boundaries. In cases of anti-symmetric and symmetric modes, limiting spring ratios r_1 and r_2 are obtained as about 37.73 and 87.15 respectively.

Table.5-1 Comparison of the results obtained by theory and FE

<table>
<tr><td colspan="2">(a) Hinged ended in-plane</td></tr>
<tr><td>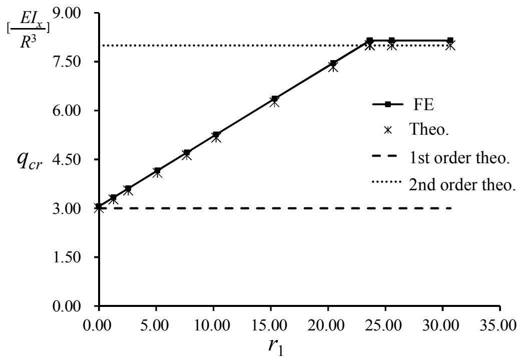
</td><td>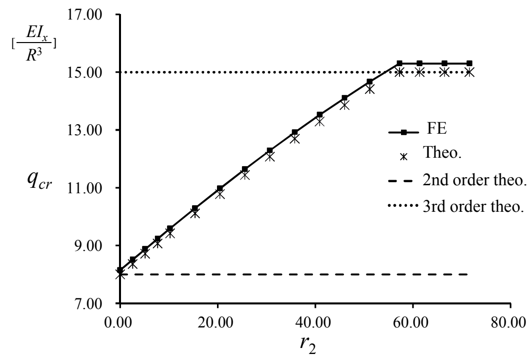
</td></tr>
<tr><td>(1) Anti-symmetric mode</td><td>(2) Symmetric mode</td></tr>
</table>

<table>
<tr><td colspan="2">(b) Fixed ended in-plane</td></tr>
<tr><td>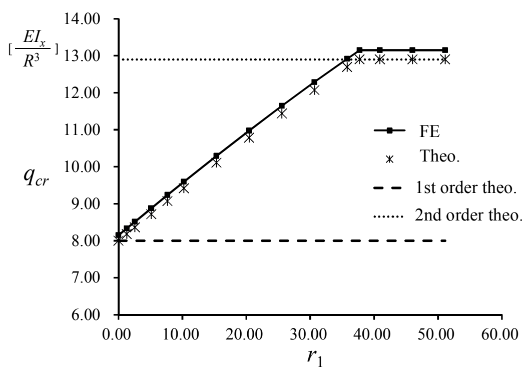
</td><td>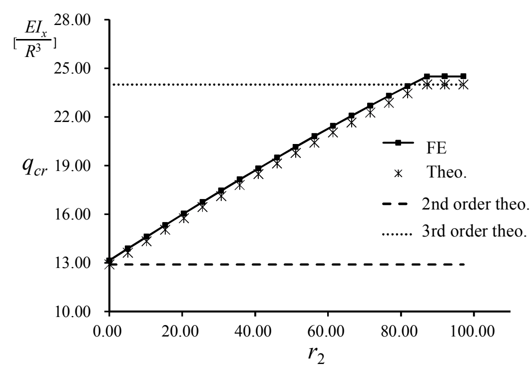
</td></tr>
<tr><td>(3) Anti-symmetric mode</td><td>(4) Symmetric mode</td></tr>
</table>

In another aspect, from Table.5-1 it is straightforward to observe that in these four configurations, the theoretical results are almost in accordance with the ones obtained by FE method. The small differences exist because of the different division numbers of beam elements in FE methods. And the higher division number of elements is, the higher accuracy of FE results becomes.

Next the cases with double springs at the same time are analyzed. Firstly the example with hinged ended boundary conditions is analyzed. We assume the spring ratio r_1 is a constant equaling 51.12 (spring stiffness $\overline{k}_1 = 10000N/m$), from the configuration (1) in Table.5-1, we know when r_1 is 51.12, we can ensure the first order buckling mode is symmetric mode, and then increase another parameter r_2 from 0 to observe the variation tendency of the first order critical load. The comparison of the results obtained by theoretical method in Eq.(5.36) and by FE method is shown in Fig.5-5. The variation of these two results is identical to each other, small differences between them attribute to the division number of elements in FE methods. In another aspect, from Fig.5-5, when r_1 is 51.12, we can observe the limiting spring ratio r_2 is 45.24 in FE analysis.

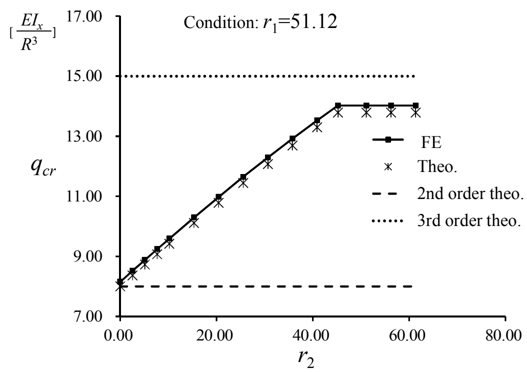

Fig.5-5 Comparison of the results with hinged ended boundaries

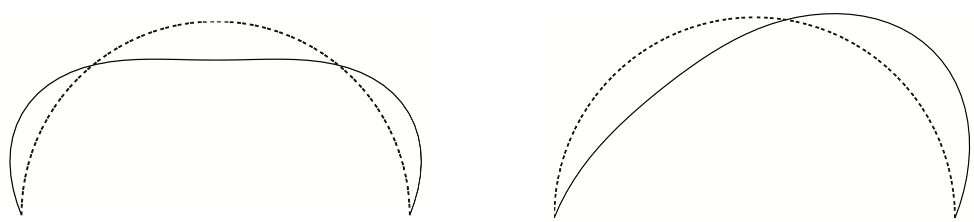

(a) r_1=51.12; r_2=0 (b) r_1=51.12; r_2=45.24

Fig.5-6 First order buckling modes (r_1=51.12)

Fig.5-6(a) and Fig.5-6(b) show the first order buckling modes when r_1 and r_2 are (r_1=51.12; r_2=0) and (r_1=51.12; r_2=45.24) respectively. The first order buckling mode in Fig.5-6(a) is symmetric, while the one in Fig.5-6(b) is anti-symmetric. Comparing the bucking modes in Table.4-2 in Chapter 4, we will find the buckling modes do not always change from lower buckling modes to higher bucking modes, the setting of springs will change the variation tendency oppositely.

Fig.5-7 shows the variation tendency of anti-symmetric modes. When r_1 and r_2 are both large enough, the corresponding first order buckling mode will coincide to the third order critical load when r_1 and r_2 are 0.

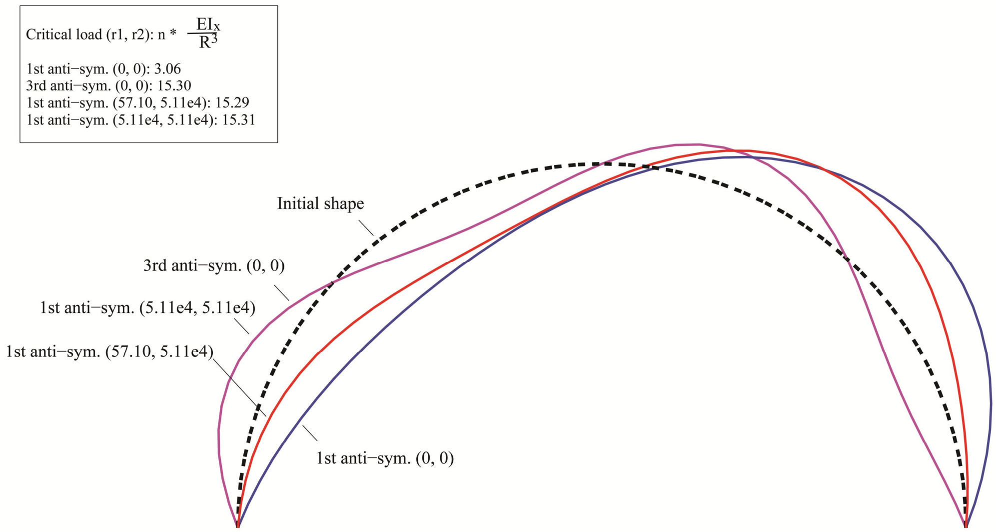

Fig.5-7 Variation of anti-symmetric modes with hinged ended boundaries

Next we discuss the case when the boundary conditions are fixed ended. Similar to the case with hinged ended boundary conditions, if we keep the spring ratio r_1 as 102.24 (spring stiffness $\overline{k}_1 = 20000N/m$), from configuration (3) in Table.5-1 we can ensure the first order buckling mode is symmetric mode, then we increase another spring ratio r_2 from 0 to get the first order critical load. The comparison of the results obtained by theoretical method in Eq.(5.38) and by FE method is shown in Fig.5-8.

From Fig.5-8, firstly we can observe the variation tendency of the results obtained by Eq.(5.38) and by FE method is almost identical to each other, the small differences also attributes to the division number of elements in FE methods. Secondly, we assume r_1 keeps 102.24, then the limiting spring ratios r_2 is about 40.18.

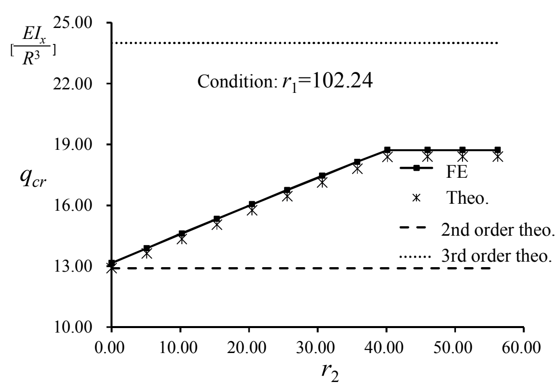

Fig.5-8 Comparison of the results with fixed ended boundaries

Fig.5-9(a) and Fig.5-9(b) show the first order buckling modes of arches when r_1 and r_2 are (r_1=102.24; r_2=0) and (r_1=102.24; r_2=40.18) respectively. The variation tendency of buckling modes is similar to the case with hinged ended boundary conditions, here we no longer describe reiteratively.

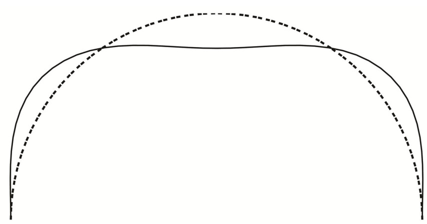

(a) r_1=102.24; r_2=0

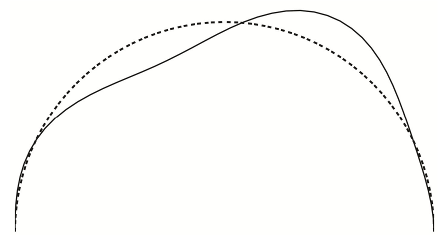

(b) r_1=102.24; r_2=40.18

Fig.5-9 First order buckling modes (r_1=102.24)

Fig.5-10 gives the variation of anti-symmetric buckling modes. Especially, when r_1 and r_2 are both large enough, the corresponding first order buckling mode will close to the third order critical mode in the case when r_1 and r_2 are 0, but these two buckling modes are not identical to each other. Especially, if r_1 and r_2 are both very large values, for example they both equals 5.11×10^4, then by FE method, the first order critical load is $22.59\dfrac{EI_x}{R^3}$, while the corresponding theoretical solution is $22.13\dfrac{EI_x}{R^3}$, this FE result is about 2.1% larger than theoretical result.

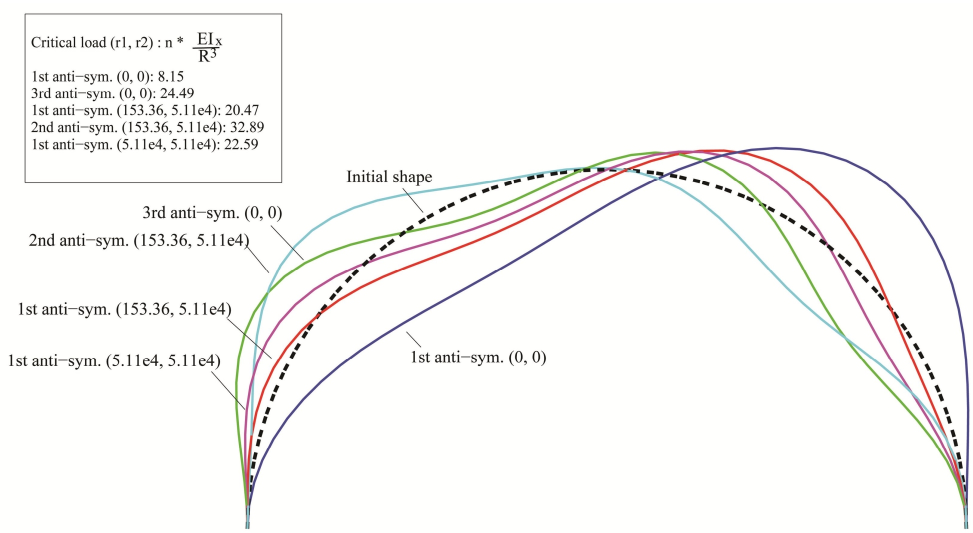

Fig.5-10 Variation of anti-symmetric modes with fixed ended boundaries

5.3 Out-of-plane

5.3.1 Buckling control equations

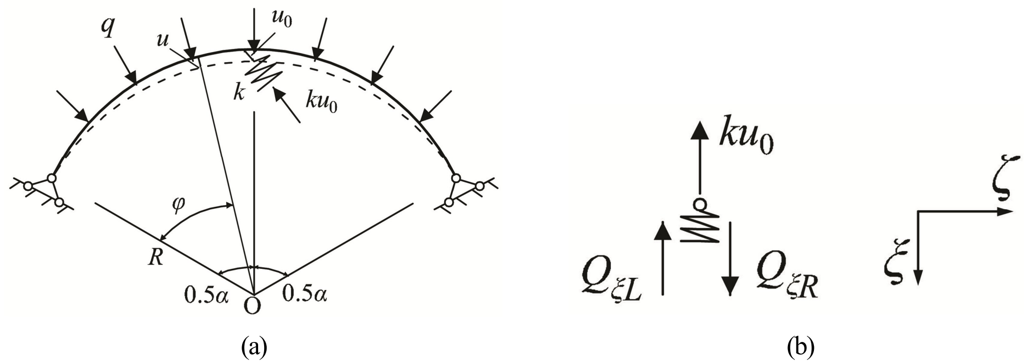

Fig.5-11 Arch-spring model out-of-plane

Fig.5-11(a) shows a circular arch stiffened with one spring k out-of-plane, and this spring is perpendicular to the plane of the arch. Fig.5-11(b) shows the equilibrium state of forces at the position of the spring. Symbols "L" and "R" in subscripts are used to distribute the displacements and forces at the left side and right side of the spring in Fig.5-11(b), then $Q_{\xi L}$ and $Q_{\xi R}$ are shear forces at the left and right side of the spring respectively.

Firstly substituting Eq.(4.58) into Eq.(4.6) in Chapter 4, and using $ds = Rd\varphi$, we can obtain

$$K_y = \frac{1}{R^2}\frac{d^2u}{d\varphi^2} + \frac{\theta}{R} = \frac{1}{R^2}\left(\frac{R}{1+\lambda}\frac{d^2\theta}{d\varphi^2} - \frac{\lambda R}{1+\lambda}\theta\right) + \frac{\theta}{R} = \frac{1}{R(1+\lambda)}\left(\frac{d^2\theta}{d\varphi^2} + \theta\right) \tag{5.40}$$

Then the first derivative of M_η in the second term of Eq.(4.8) is

$$\frac{dM_\eta}{d\varphi} = EI_y\frac{dK_y}{d\varphi} = \frac{EI_y}{R(1+\lambda)}\left(\frac{d^3\theta}{d\varphi^3} + \frac{d\theta}{d\varphi}\right) \tag{5.41}$$

In another aspect, using Eq.(4.45) and using identical equation $ds = Rd\varphi$, we can obtain

$$Q_\xi = -\frac{1}{R}\frac{dM_\eta}{d\varphi} - \frac{M_\varsigma}{R} \tag{5.42}$$

As a preparation, in chapter 4 the general solution of θ in Eq.(4.65) have been obtained. In addition, the first and second derivatives of θ for the central angel φ can be found in Eq.(4.68) and Eq.(4.69) in Chapter 4. The third derivative of θ is

$$\frac{d^3\theta}{d\varphi^3} = -Ak_1^3\cos k_1\varphi + Bk_1^3\sin k_1\varphi + Ck_2^3\cosh k_2\varphi + Dk_2^3\sinh k_2\varphi \tag{5.43}$$

And the expressions of θ_L and θ_R are

$$\theta_L = A_1\sin k_1\varphi + B_1\cos k_1\varphi + C_1\sinh k_2\varphi + D_1\cosh k_2\varphi \tag{5.44}$$

$$\theta_R = A_2\sin k_1\varphi + B_2\cos k_1\varphi + C_2\sinh k_2\varphi + D_2\cosh k_2\varphi \tag{5.45}$$

The boundary conditions of the arch in Fig.5-11(a) are assumed as hinged ended in-plane and fixed ended out-of-plane, then the expressions of the boundary conditions can be considered as follows:

(1) $\theta_L = 0\,, u_L = 0\,, u_L' = 0$ at $\varphi = 0$

(2) $\theta_R = 0\,, u_R = 0\,, u_R' = 0$ at $\varphi = \alpha$

(3) $u_L = u_R = u_0\,, u_L' = u_R'\,, Q_{\xi L} + ku_0 = Q_{\xi R}\,, \theta_L = \theta_R\,, \theta_L' = \theta_R'\,, \theta_L'' = \theta_R''$ at $\varphi = 0.5\alpha$

From boundary condition (1), we can obtain

$$\begin{cases} 0 = B_1 + D_1 \\ 0 = -\dfrac{B_1}{k_1^2} + \dfrac{D_1}{k_2^2} + F_1 \\ 0 = (A_1k_1 + C_1k_2) - \lambda(-\dfrac{A_1}{k_1} + \dfrac{C_1}{k_2} + E_1) \end{cases} \tag{5.46}$$

From boundary condition (2), we can obtain

$$\begin{cases} 0 = A_2\sin\alpha k_1 + B_2\cos\alpha k_1 + C_2\sinh\alpha k_2 + D_2\cosh\alpha k_2 \\ 0 = -\dfrac{A_2}{k_1^2}\sin\alpha k_1 - \dfrac{B_2}{k_1^2}\cos\alpha k_1 + \dfrac{C_2}{k_2^2}\sinh\alpha k_2 + \dfrac{D_2}{k_2^2}\cosh\alpha k_2 + \alpha E_2 + F_2 \\ 0 = [A_2k_1\cos(\alpha k_1) - B_2k_1\sin(\alpha k_1) + C_2k_2\cosh(\alpha k_2) + D_2k_2\sinh(\alpha k_2)] \\ -\lambda[-\dfrac{A_2}{k_1}\cos(\alpha k_1) + \dfrac{B_2}{k_1}\sin(\alpha k_1) + \dfrac{C_2}{k_2}\cosh(\alpha k_2) + \dfrac{D_2}{k_2}\sinh(\alpha k_2) + E_2] \end{cases} \tag{5.47}$$

From boundary condition (3) we can obtain

$$
\begin{cases}
u_0 = \dfrac{R}{1+\lambda}(A_1 \sin 0.5\alpha k_1 + B_1 \cos 0.5\alpha k_1 + C_1 \sinh 0.5\alpha k_2 + D_1 \cosh 0.5\alpha k_2) \\
-\dfrac{\lambda R}{1+\lambda}(-\dfrac{A_1}{k_1^2}\sin 0.5\alpha k_1 - \dfrac{B_1}{k_1^2}\cos 0.5\alpha k_1 + \dfrac{C_1}{k_2^2}\sinh 0.5\alpha k_2 + \dfrac{D_1}{k_2^2}\cosh 0.5\alpha k_2 + 0.5\alpha E_1 + F_1) \\
u_0 = \dfrac{R}{1+\lambda}(A_2 \sin 0.5\alpha k_1 + B_2 \cos 0.5\alpha k_1 + C_2 \sinh 0.5\alpha k_2 + D_2 \cosh 0.5\alpha k_2) \\
-\dfrac{\lambda R}{1+\lambda}(-\dfrac{A_2}{k_1^2}\sin 0.5\alpha k_1 - \dfrac{B_2}{k_1^2}\cos 0.5\alpha k_1 + \dfrac{C_2}{k_2^2}\sinh 0.5\alpha k_2 + \dfrac{D_2}{k_2^2}\cosh 0.5\alpha k_2 + 0.5\alpha E_2 + F_2) \\
-\dfrac{A_1}{k_1}\cos 0.5\alpha k_1 + \dfrac{B_1}{k_1}\sin 0.5\alpha k_1 + \dfrac{C_1}{k_2}\cosh 0.5\alpha k_2 + \dfrac{D_1}{k_2}\sinh 0.5\alpha k_2 + E_1 = \\
-\dfrac{A_2}{k_1}\cos 0.5\alpha k_1 + \dfrac{B_2}{k_1}\sin 0.5\alpha k_1 + \dfrac{C_2}{k_2}\cosh 0.5\alpha k_2 + \dfrac{D_2}{k_2}\sinh 0.5\alpha k_2 + E_2 \\
-\dfrac{EI_y}{R^2(1+\lambda)}(-A_1 k_1^3 \cos 0.5\alpha k_1 + B_1 k_1^3 \sin 0.5\alpha k_1 + C_1 k_2^3 \cosh 0.5\alpha k_2 + D_1 k_2^3 \sinh 0.5\alpha k_2) + ku_0 = \\
-\dfrac{EI_y}{R^2(1+\lambda)}(-A_2 k_1^3 \cos 0.5\alpha k_1 + B_2 k_1^3 \sin 0.5\alpha k_1 + C_2 k_2^3 \cosh 0.5\alpha k_2 + D_2 k_2^3 \sinh 0.5\alpha k_2) \\
A_1 \sin 0.5\alpha k_1 + B_1 \cos 0.5\alpha k_1 + C_1 \sinh 0.5\alpha k_2 + D_1 \cosh 0.5\alpha k_2 = \\
A_2 \sin 0.5\alpha k_1 + B_2 \cos 0.5\alpha k_1 + C_2 \sinh 0.5\alpha k_2 + D_2 \cosh 0.5\alpha k_2 \\
A_1 k_1 \cos 0.5\alpha k_1 - B_1 k_1 \sin 0.5\alpha k_1 + C_1 k_2 \cosh 0.5\alpha k_2 + D_1 k_2 \sinh 0.5\alpha k_2 = \\
A_2 k_1 \cos 0.5\alpha k_1 - B_2 k_1 \sin 0.5\alpha k_1 + C_2 k_2 \cosh 0.5\alpha k_2 + D_2 k_2 \sinh 0.5\alpha k_2 \\
-A\, k_1^2 \sin 0.5\alpha k_1 - B_1 k_1^2 \cos 0.5\alpha k_1 + C_1 k_2^2 \sinh 0.5\alpha k_2 + D_1 k_2^2 \cosh 0.5\alpha k_2 = \\
-A_2 k_1^2 \sin 0.5\alpha k_1 - B_2 k_1^2 \cos 0.5\alpha k_1 + C_2 k_2^2 \sinh 0.5\alpha k_2 + D_2 k_2^2 \cosh 0.5\alpha k_2
\end{cases}
$$

(5.48)

In order to simplify Eq.(5.48), here assuming symbols as

$$
\begin{cases}
g_1 = \sin \alpha k_1 \\
h_1 = \cos \alpha k_1 \\
g_2 = \sinh \alpha k_2 \\
h_2 = \cosh \alpha k_2 \\
m_1 = \sin 0.5\alpha k_1 \\
n_1 = \cos 0.5\alpha k_1 \\
m_2 = \sinh 0.5\alpha k_2 \\
n_2 = \cosh 0.5\alpha k_2
\end{cases}
\tag{5.49}
$$

According to the sequence of $A_1, B_1, C_1, D_1, E_1, F_1, A_2, B_2, C_2, D_2, E_2, F_2, u_0$, and a matrix $\mathbf{S_{3D\text{-}SF}}$ is assumed as

$$
\mathbf{S}_{\mathbf{3D\text{-}SF}} = \left[\begin{matrix}
0 & 1 & 0 & 1 & 0 & 0 & \vdots \\
0 & -\dfrac{1}{k_1^2} & 0 & \dfrac{1}{k_2^2} & 0 & 1 & \vdots \\
k_1+\dfrac{\lambda}{k_1} & 0 & k_2-\dfrac{\lambda}{k_2} & 0 & -\lambda & 0 & \vdots \\
0 & 0 & 0 & 0 & 0 & 0 & \vdots \\
0 & 0 & 0 & 0 & 0 & 0 & \vdots \\
0 & 0 & 0 & 0 & 0 & 0 & \vdots \\
m_1+\dfrac{\lambda}{k_1^2}m_1 & n_1+\dfrac{\lambda}{k_1^2}n_1 & m_2-\dfrac{\lambda}{k_2^2}m_2 & n_2-\dfrac{\lambda}{k_2^2}n_2 & -0.5\alpha\lambda & -\lambda & \vdots \\
0 & 0 & 0 & 0 & 0 & 0 & \vdots \\
-\dfrac{n_1}{k_1} & \dfrac{m_1}{k_1} & \dfrac{n_2}{k_2} & \dfrac{m_2}{k_2} & 1 & 0 & \vdots \\
k_1^3 n_1 & -k_1^3 m_1 & -k_2^3 n_2 & -k_2^3 m_2 & 0 & 0 & \vdots \\
m_1 & n_1 & m_2 & n_2 & 0 & 0 & \vdots \\
k_1 n_1 & -k_1 m_1 & k_2 n_2 & k_2 m_2 & 0 & 0 & \vdots \\
-k_1^2 m_1 & -k_1^2 n_1 & k_2^2 m_2 & k_2^2 n_2 & 0 & 0 & \vdots
\end{matrix}\right.
$$

$$
\left.\begin{matrix}
\vdots & 0 & 0 & 0 & 0 & 0 & 0 & 0 \\
\vdots & 0 & 0 & 0 & 0 & 0 & 0 & 0 \\
\vdots & 0 & 0 & 0 & 0 & 0 & 0 & 0 \\
\vdots & g_1 & h_1 & g_2 & h_2 & 0 & 0 & 0 \\
\vdots & -\dfrac{g_1}{k_1^2} & -\dfrac{h_1}{k_1^2} & \dfrac{g_2}{k_2^2} & \dfrac{h_2}{k_2^2} & \alpha & 1 & 0 \\
\vdots & k_1h_1+\dfrac{\lambda}{k_1}h_1 & -k_1g_1-\dfrac{\lambda}{k_1}g_1 & k_2h_2-\dfrac{\lambda}{k_2}h_2 & k_2g_2-\dfrac{\lambda}{k_2}g_2 & -\lambda & 0 & 0 \\
\vdots & 0 & 0 & 0 & 0 & 0 & 0 & -\dfrac{1+\lambda}{R} \\
\vdots & m_1+\dfrac{\lambda}{k_1^2}m_1 & n_1+\dfrac{\lambda}{k_1^2}n_1 & m_2-\dfrac{\lambda}{k_2^2}m_2 & n_2-\dfrac{\lambda}{k_2^2}n_2 & -0.5\alpha\lambda & -\lambda & -\dfrac{1+\lambda}{R} \\
\vdots & \dfrac{n_1}{k_1} & -\dfrac{m_1}{k_1} & -\dfrac{n_2}{k_2} & -\dfrac{m_2}{k_2} & -1 & 0 & 0 \\
\vdots & -k_1^3 n_1 & k_1^3 m_1 & k_2^3 n_2 & k_2^3 m_2 & 0 & 0 & \dfrac{(1+\lambda)R^2 k}{EI_y} \\
\vdots & -m_1 & -n_1 & -m_2 & -n_2 & 0 & 0 & 0 \\
\vdots & -k_1 n_1 & k_1 m_1 & -k_2 n_2 & -k_2 m_2 & 0 & 0 & 0 \\
\vdots & k_1^2 m_1 & k_1^2 n_1 & -k_2^2 m_2 & -k_2^2 n_2 & 0 & 0 & 0
\end{matrix}\right]
$$

(5.50)

The buckling control equation which is the same expressions of Eq.(5.46)~Eq.(5.48) is

$$\det(\mathbf{S}_{\mathbf{3D\text{-}SF}}) = 0 \tag{5.51}$$

Spreading out the left side of equation above according to the last column of det($\mathbf{S}_{\mathbf{3D\text{-}SF}}$), then we can obtain

$$-\frac{(1+\lambda)}{R}\det(\mathbf{S}^{12}_{\mathbf{3D\text{-}SF1}}) - \frac{(1+\lambda)}{R}\det(\mathbf{S}^{12}_{\mathbf{3D\text{-}SF2}}) + \frac{(1+\lambda)R^2 k}{EI_y}\det(\mathbf{S}^{12}_{\mathbf{3D\text{-}SF3}}) = 0 \tag{5.52}$$

Here det($\mathbf{S}^{12}_{\mathbf{3D\text{-}SF1}}$), det($\mathbf{S}^{12}_{\mathbf{3D\text{-}SF2}}$) and det($\mathbf{S}^{12}_{\mathbf{3D\text{-}SF3}}$) are cofactors of det($\mathbf{S}_{\mathbf{3D\text{-}SF}}$), the sizes of them are all 12×12. Then a spring ratio r_y is assumed as

$$r_y = \frac{k}{EI_y / R^3} \tag{5.53}$$

Then Eq.(5.52) is identical to the following equation

$$\det(\mathbf{S}^{12}_{\mathbf{3D\text{-}SF1}}) + \det(\mathbf{S}^{12}_{\mathbf{3D\text{-}SF2}}) - r_y \det(\mathbf{S}^{12}_{\mathbf{3D\text{-}SF3}}) = 0 \tag{5.54}$$

These three cofactors all contain parameters k_1 in Eq.(4.66) and k_2 in Eq.(4.67), and these two parameters also refer to the critical load q_{cr}, so the critical load q_{cr} for out-of-plane stability is determined by spring ratio r_y.

5.3.2 Numerical examples

The materials parameters and element division of the arch are as same as anterior numerical examples in this chapter. As the cross section of the arch is hollow circular section, so I_x=I_y=I is established. The central angle of the arch is π. The setting of the spring and external load are as same as the ones in Fig.5-11.

Firstly, let's talk about the example of the arch with hinged ended boundary conditions. The results calculated by theoretical method and by FE method is shown in Fig.5-12. Firstly we state the meanings of symbols in Fig.5-12. Symbol "FE" is the result obtained by FE method. Symbol "Theo.(3D)" is the first order critical load of the arch with stiffening spring out-of-plane, which is calculated by Eq.(5.51). Symbols "1st-Theo.(3D)" and "2nd-Theo.(3D)" are the first order and second order critical load of the arch without spring respectively, and buckling modes happen out-of-plane (Referring to Table.4-7, Table 4-8 in Chapter 4). Symbol "1st-Theo.(2D)" is the first order critical load of the arch without spring, and buckling mode happens in-plane (Referring to Table.4-3.)

From Fig.5-12, in FE analysis, when the spring ratio r_y is 0.84, the buckling mode changes from out-of-plane (refereeing to Table.4-7) to the one in-plane (referring to the mode in the first column in Table.4-2). Meanwhile the limiting spring ratio r_y is obtained as 0.84.

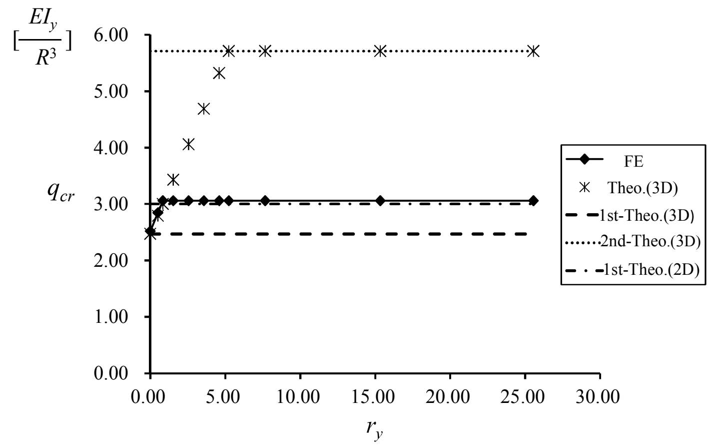

Fig.5-12 Relationship of r_y and q_{cr} with hinged ended boundaries in-plane

In another aspect, when the boundary conditions of the arch are both fixed ended in-plane and out-of-plane, the relationship of r_y and q_{cr} is shown in Fig.5-13. In numerical analysis, when r_y is 5.24, the buckling mode changes from translation mode out-of-plane (referring to Table.4-7) to rotational buckling mode out-of-plane (referring to Table.4-8). And limiting spring ratio r_y is 5.24 in this case.

In addition, because the “1st-Theo.(2D)” is higher than “2nd-Theo.(3D)”, then even we increase the stiffness of spring, the buckling phenomenon firstly happens out-of-plane rather than in-plane.

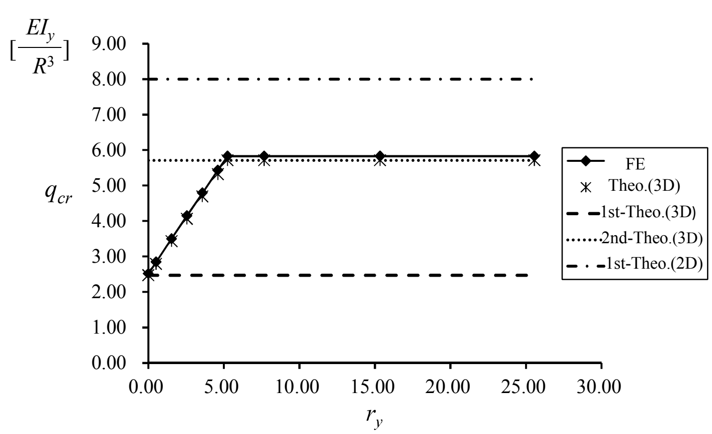

Fig.5-13 Relationship of r_y and q_{cr} with fixed ended boundaries in-plane

5.4 Stiffening patterns of arches

5.4.1 Single arch

a) Two-dimensional arch

In Section 2.3 of Chapter 2, the stiffening patterns of arches are classified. Then in this section, the stiffening effects of typical stiffening patterns will be discussed. Firstly, Fig.5-14 shows three basic stiffening patterns of single arch in-plane. In order to simplify the expressions in latter narrative, they are noted as Pattern A, Pattern B and Pattern C respectively. The anterior two patterns are longitudinal direction type (internal reaction type), and the latter one is radial direction type (external reaction type). And by the combination of the three basic stiffening patterns in Fig.5-14, we can obtain other three hybrid stiffening patterns in Fig.5-15. And in Fig.5-14 and Fig.5-15, the continuous line symbolizes the arch, and the broken line symbolizes the braces.

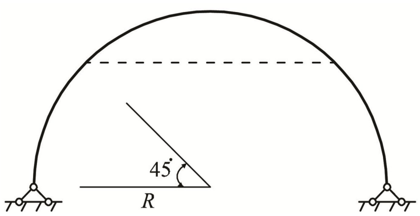

(a) Pattern A

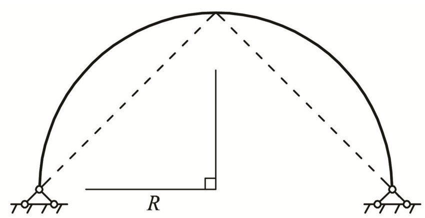

(b) Pattern B

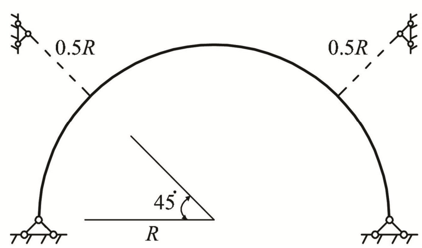

(c) Pattern C

Fig.5-14 Three basic stiffening patterns in-plane

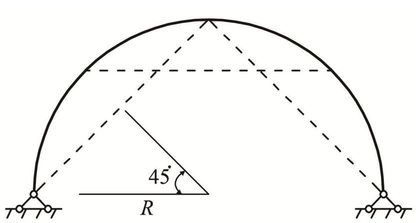

(a) Pattern AB

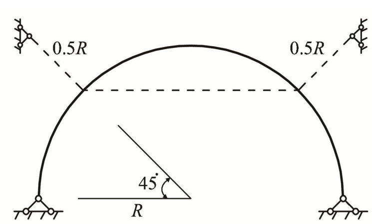

(b) Pattern AC

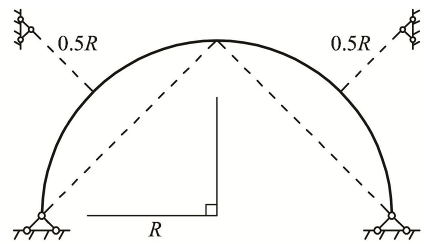

(c) Pattern BC

Fig.5-15 Three hybrid stiffening patterns in-plane

1) Hinged ended in-plane

Next we use FE method to discuss the stability of these stiffening patterns in Fig.5-14 and Fig.5-15. Firstly, we discuss two-dimensional arch when boundary conditions are hinged ended. The materials parameters of the arch are as same as the one shown in Table.4-1 in Chapter 4.The radius of the arch is 1m. The central angle of the arch is π. The entire arch is divided into 48 linear beam elements, and each beam element has the same length. And E_cA_c is the elastic stiffness of the brace, and E_cA_c can be seen as a variable in numerical analysis. Each brace is divided into one linear truss element. The external load is assumed as uniform compression.

Here "I" is used to symbolize the moment of inertia, as the cross section of the arch is hollow circular, and I_x=I_y=I is established. The moments of inertia I_x and I_y here are around axis x and axis y respectively, the configurations of axis x and axis y are shown in Fig.4-2 in Chapter 4. In Section 5.2 and Section 5.3, by theoretical analysis in arch-spring models, it is known that when using straight constraint components to stiffen the arch, no matter in-plane stability or out-of-plane stability of the arch, the spring ratio r_x in Eq.(5.20) or the spring ratio r_y in Eq.(5.53) can determine the critical loads of the arch. Then the stability problems of arches with different stiffening patterns are studied by FE methods, it is reasonable to use spring ratio which is ratio of the elastic stiffnesses of the brace and the arch. So a spring ratio r_p is defined as $r_p = (\frac{E_cA_c}{R})/(\frac{EI}{R^3})$ in FE analysis.

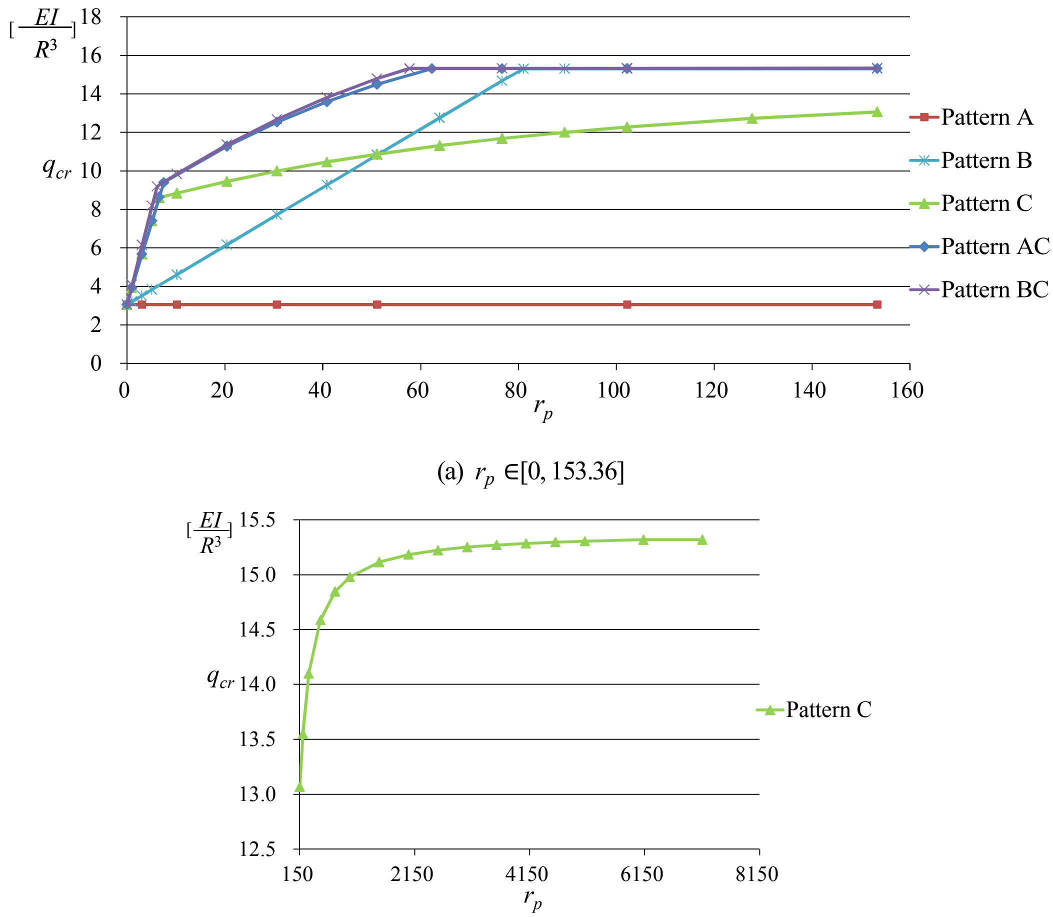

(a) r_p ∈[0, 153.36]

(b) r_p ∈[153.36, 7156.62]

Fig.5-16 Relationship of r_p and first order critical load q_{cr} (hinged ended)

Fig.5-16(a) and Fig.5-16(b) show the relationship of spring ratio r_p and the first order critical load q_{cr} when the boundary conditions of the arch are hinged ended. From Fig.5-16(a), we can see the first order critical load of Pattern A almost keeps constant even though r_p increases. And comparing the critical loads of other patterns, when r_p ∈[0, 51.12], the first order load of Pattern C is larger than the one in Pattern B; when r_p ∈(51.12, 153.36], the first order load of Pattern C is smaller than the one in Pattern B.

In another aspect, comparing the images in Fig.5-16(a), we can see the first order critical loads of Pattern AC and Patter BC are very close to each other. The first order critical loads of these two stiffening patterns are larger than the one in Pattern A, Pattern B or Pattern C. And the first order critical load of AB is almost identical to Pattern B, so it is not shown in Fig.5-16(a). In Fig.5-16(b), we can observe only when r_p is very large until the first order critical load of Pattern C approach maximum value. The theoretic analysis of Pattern C is discussed in

Appendix C.

In order to understand the variation tendency of first order critical load in Fig.5-16, here we take Pattern BC and Pattern C as examples to observe the variation of their first order buckling modes with the increasing of spring ratio r_p. Table.5-2 and Table.5-3 shows the variation of first order buckling modes of Pattern BC and Pattern C respectively.

Table.5-2 Variation tendency of buckling modes of pattern BC

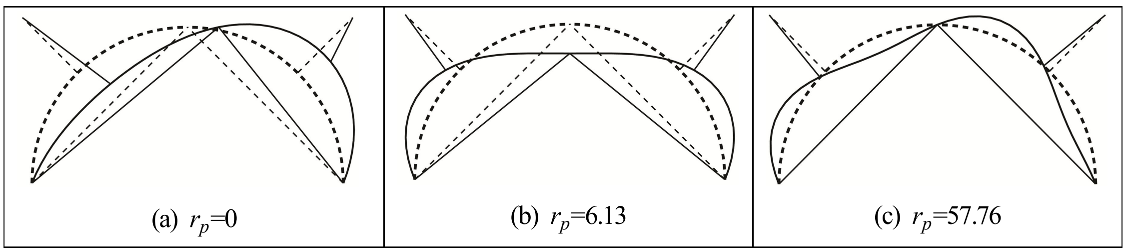

(a) r_p=0 (b) r_p=6.13 (c) r_p=57.76

Table.5-3 Variation tendency of buckling modes of pattern C

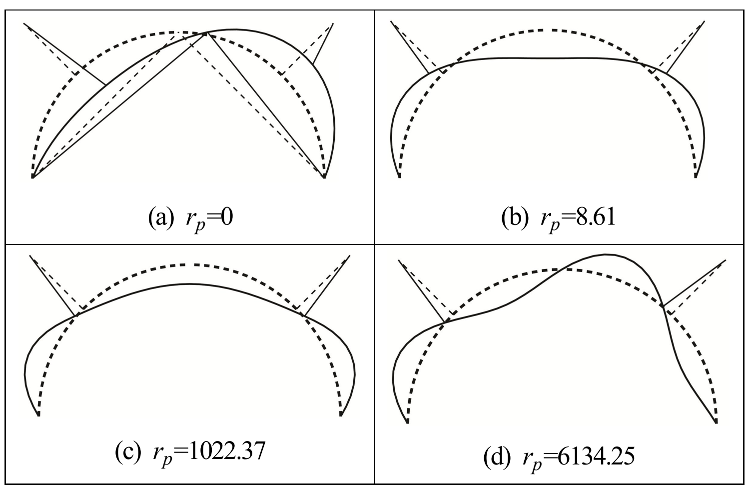

(a) r_p=0 (b) r_p=8.61

(c) r_p=1022.37 (d) r_p=6134.25

And Table.5-4 shows the finial shapes of the first order buckling modes of all stiffening patterns.

Table.5-4 Final first order buckling modes

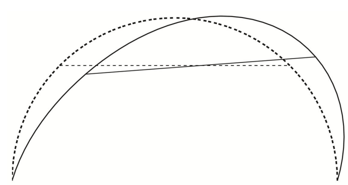 Pattern A	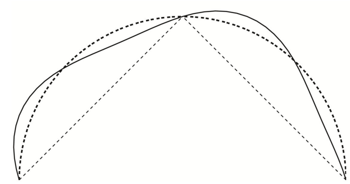 Pattern B	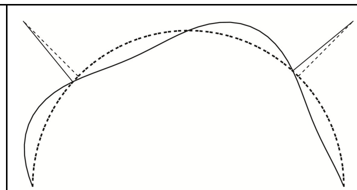 Pattern C
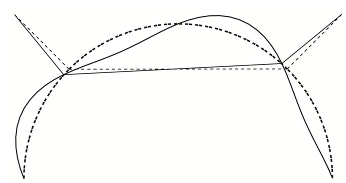 Pattern AC	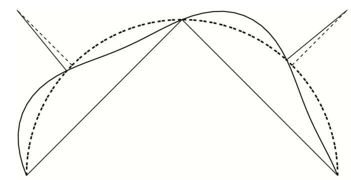 Pattern BC	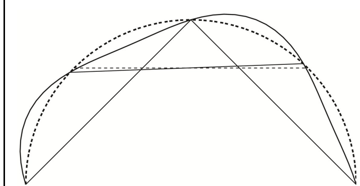 Pattern AB

2) Fixed ended in-plane

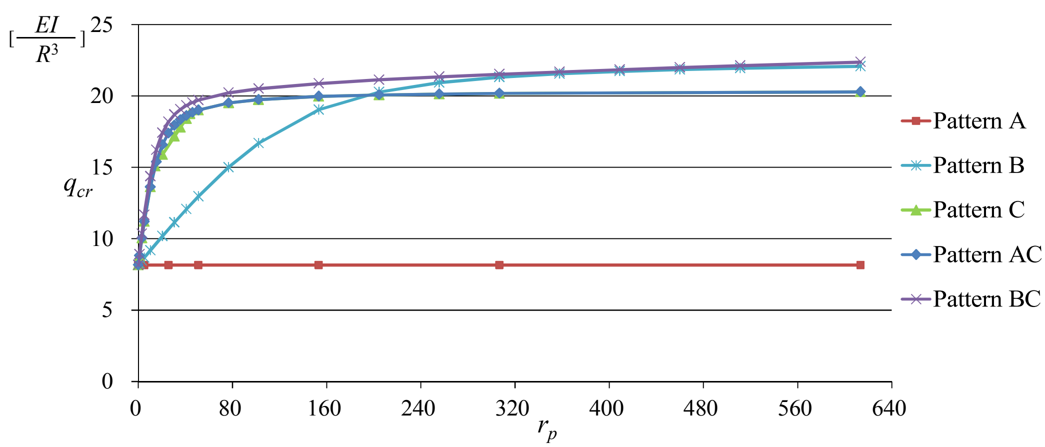

Fig.5-17 Relationship of r_p and first order critical load q_{cr} (fixed ended)

Now we consider the examples when the arches have fixed ended boundaries. Fig.5-17 shows the relationship of spring ratio r_p and first order critical load with fixed ended boundaries. From Fig.5-17(a), when $r_p \in$[0, 204.47], we can observe that the critical load from largest one to smallest one are Pattern BC, Pattern AC, Pattern C, Pattern B and Pattern A. In another aspect, in Fig.5-17(b), when $r_p \in$[204.47, 613.42], Pattern B will surpass Pattern C and Pattern AC when the value of r_p is about 204.47. The variation tendency of the first order critical load in Pattern AB is almost identical to the one in Pattern B, then the first order critical load of Pattern

AB is omitted in Fig.5-17.

Similar to the case with hinged ended boundaries, here we take the Pattern BC as an example, and then we observe the variation of first order buckling modes with the increasing of the spring ratio r_p. Table.5-5 shows the variations of the first order buckling modes of Pattern BC. And Table.5-6 shows the finial first order buckling modes of all stiffening patterns when r_p is very large.

Table.5-5 Variation tendency of buckling modes of pattern BC

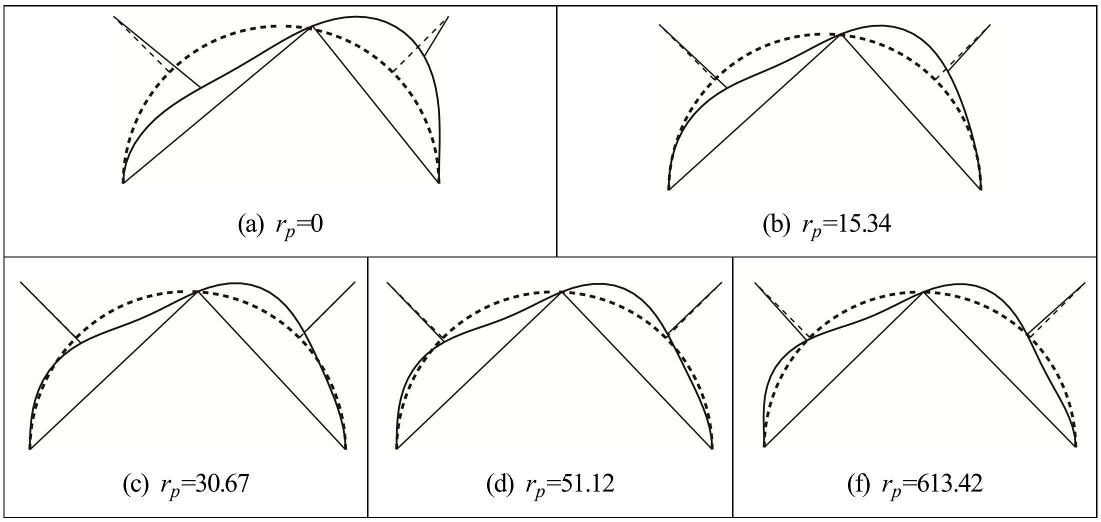

(a) r_p=0 (b) r_p=15.34

(c) r_p=30.67 (d) r_p=51.12 (f) r_p=613.42

Table.5-6 Final first order buckling modes

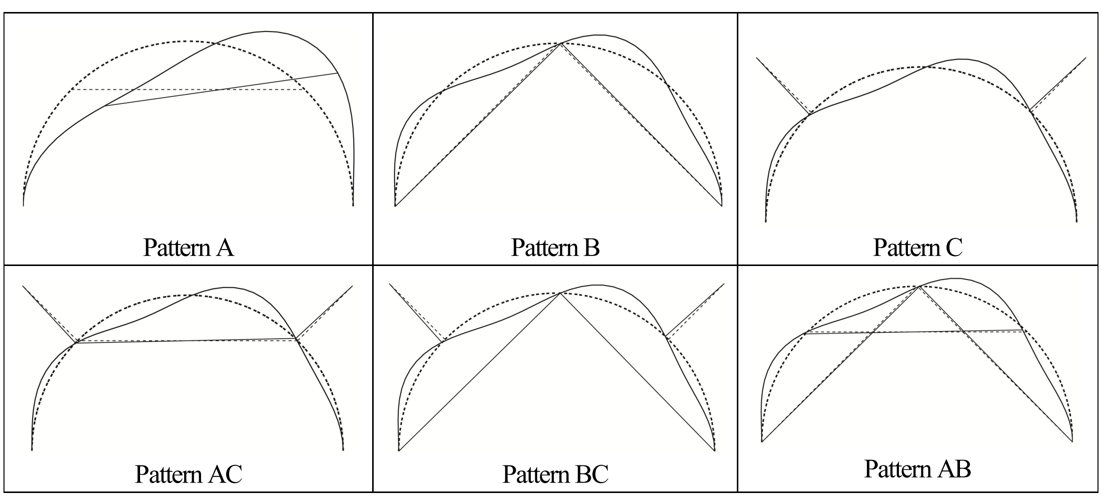

Pattern A Pattern B Pattern C

Pattern AC Pattern BC Pattern AB

b) Three-dimensional single arch

Fig.5-18 shows two stiffening patterns of three-dimensional single arch stiffened by braces out-of-plane. And Pattern D and Pattern E (external reaction types) are thought to be basic stiffening patterns of single arch out-of-plane.

In Pattern D, two braces are located at the two sides of the arch, the distance of the positions of the boundaries of braces is $2R$. The connecting line of the positions of the boundaries of braces is perpendicular to the plane of the arch.

In Pattern E, two braces located at each side of the arch symmetrically. The positions of braces connecting to the arch are at 45° central angle. The combination of Pattern D and Pattern E is shown in Fig.5-19. The materials parameters and division of elements in FE analysis are identical to the ones in numerical examples above.

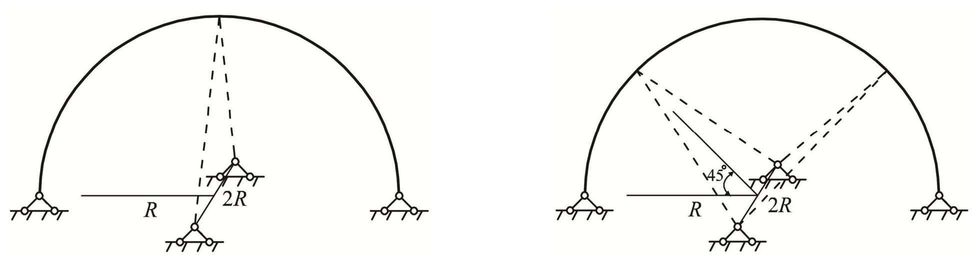

(a) Pattern D (b) Pattern E

Fig.5-18 Two basic stiffening patterns out-of-plane

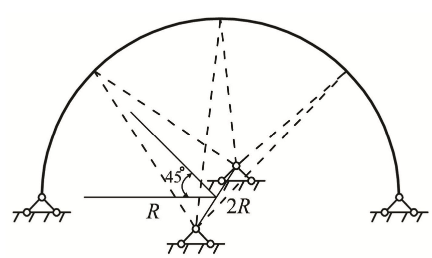

Pattern DE

Fig.5-19 Hybrid stiffening pattern out-of-plane

1) Hinged ended in-plane and fixed ended out-of-plane

Firstly, the boundary conditions of the arch are assumed as hinged ended in-plane and fixed ended out-of-plane, that is, among the six DOF of node at each side of boundary, only moment around ξ axis is free, other two rotational DOF and three translational DOF are all constraint.

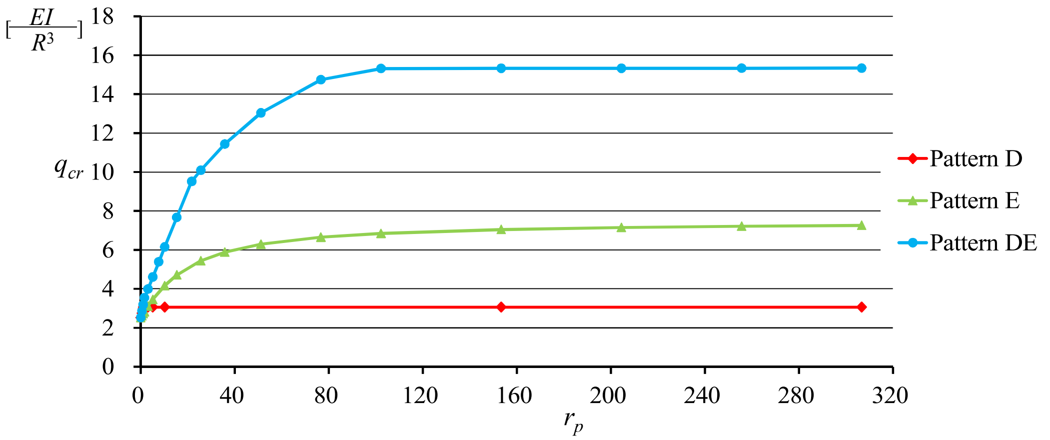

Fig.5-20 Relationship of r_p and first order critical load q_{cr}

Fig.5-20 shows the relationship of spring ratio r_p and first order critical load of q_{cr}. In Fig.5-20, the stiffening effect of Pattern DE is always the best. When r_p is smaller than 2.79, Pattern D is better than Pattern E. When r_p is larger than 1.19, the first order critical load q_{cr} of Patten D almost keeps constant.

In order to understand the configurations in Fig.5-20, here Pattern DE is taken as an example, and we observe the variation of first order buckling modes. Table.5-7 shows four different first order buckling modes of Pattern DE with the increasing of spring ratio r_p.

Table.5-7 Variation tendency of buckling modes of Pattern DE

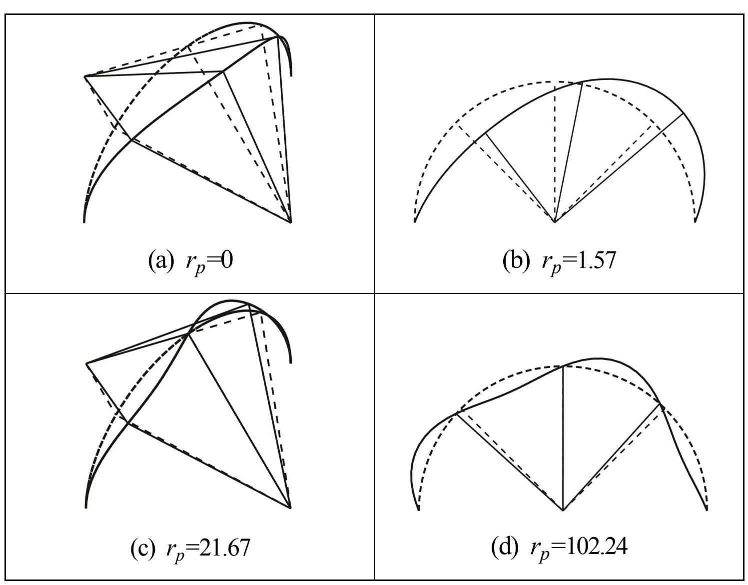

Table.5-8 shows the final first order buckling modes of all stiffening patterns, which are corresponding to the first order critical loads in Fig.5-20. When r_p is very large, we can observe that the first order buckling modes of Pattern D and Pattern DE happen in-plane, while the one of Pattern E happens out-of-plane.

Table.5-8 Final first order buckling modes

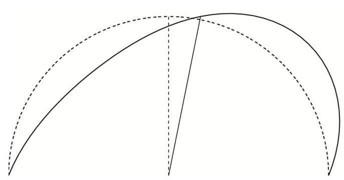	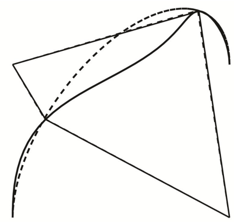	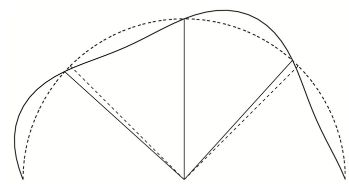
Pattern D	Pattern E	Pattern DE

2) Fixed ended in-plane and out-of-plane

Secondly, the boundary conditions of the arch are assumed as fixed ended both in-plane and out-of-plane, that is, among six DOF of node at each side of boundary are constrained.

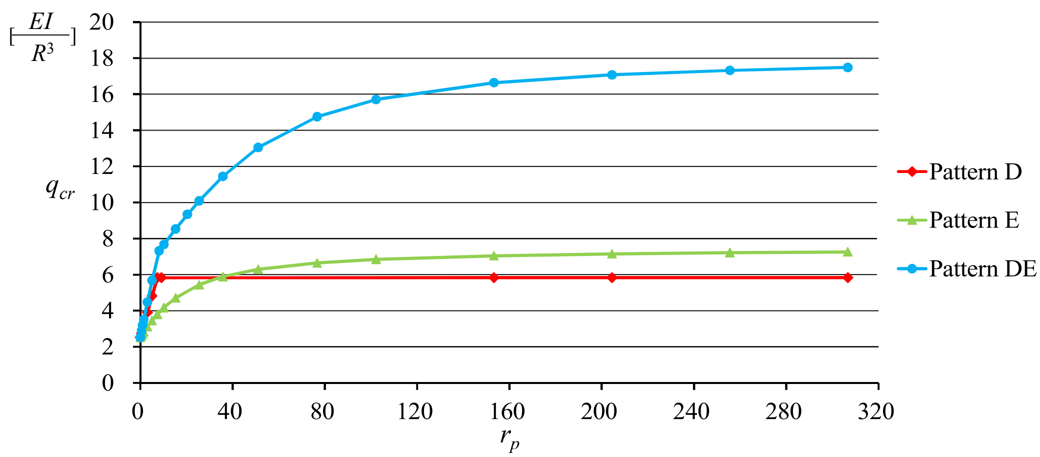

Fig.5-21 Relationship of r_p and first order critical loads q_{cr}

Fig.5-21 shows the relationship of the spring ratio r_p and the first order critical loads with fixed ended boundary conditions. In Fig.5-21, the stiffening effect of Pattern DE is the best. When r_p is smaller than 35.78, Pattern D is better than Pattern E, although for pattern D, its limiting spring ratio r_p is 7.41.

Similar to the case with hinged ended in-plane, here we also take Pattern DE as an example and we observe the variation of first order buckling modes. Table.5-9 shows four different first order buckling modes of Pattern DE with the increasing of spring ratio r_p.

Table.5-9 Variation tendency of buckling modes of Pattern DE

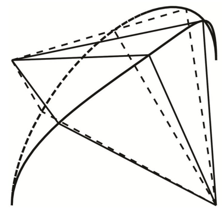 (a) r_p=0	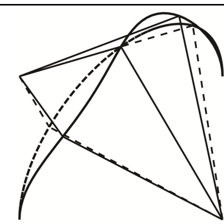 (b) r_p=8.18
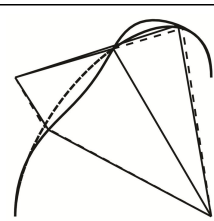 (c) r_p=102.24	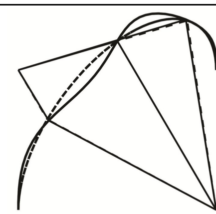 (d) r_p=306.71

Table.5-10 shows the final first order buckling modes of all stiffening patterns. When r_p is very large, the first order buckling modes of Pattern D, Pattern E and Pattern DE all happen out-of-plane.

Table.5-10 Final first order buckling modes

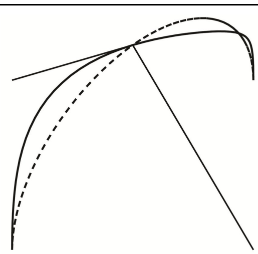 Pattern D	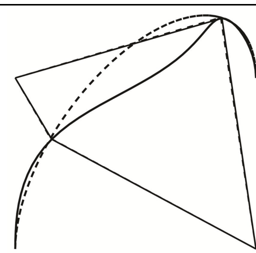 Pattern E	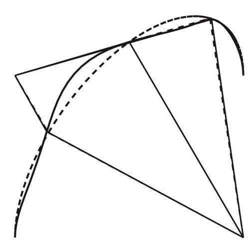 Pattern DE

5.4.2 Cross arch

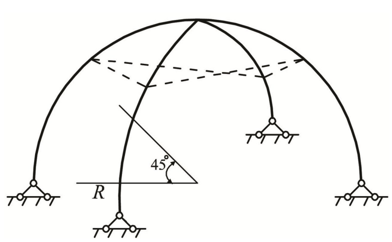

(a) Pattern F

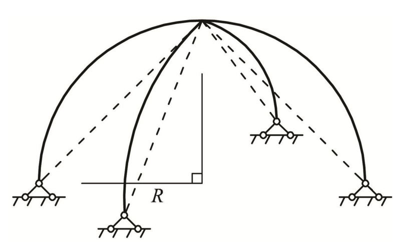

(b) Pattern G

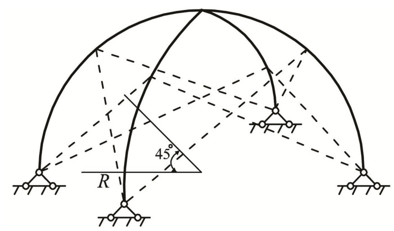

(c) Pattern H

Fig.5-22 Three basic stiffening patterns of cross arch

Now the stiffening effects of the braces in cross arch are discussed. In Fig.5-22, three basic stiffening patterns of cross arch are defined: Pattern F, Pattern G and Pattern H. In another aspect, according to the category rule introduced in Chapter 2, Pattern F and Pattern H are peripheral direction type, and Pattern G is longitudinal direction type. All of these three patterns are internal reaction type.

In addition, by combination of Pattern F and Pattern H, and Pattern G and Pattern H, we also propose two hybrid stiffening patterns as shown in Fig.5-23.

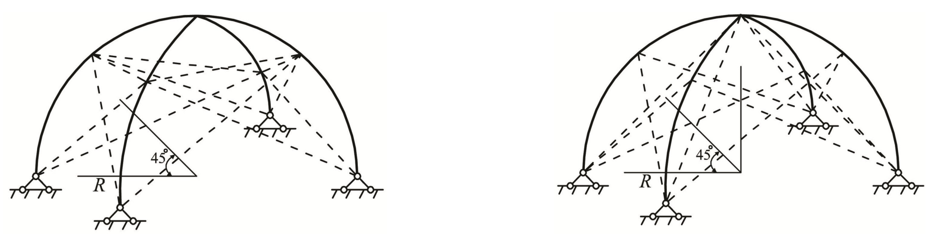

(a) Pattern FH (b) Pattern GH

Fig.5-23 Two hybrid stiffening patterns of cross arch

Firstly, let's talk about the case with hinged ended boundary conditions, that is, among the six DOF of node at each side, three translational DOF are constrained, and the other three rotational DOF are free. The materials parameters, uniform compression, and the shape of the arch are as same as the ones in above numerical analysis.

When there is no braces used to stiffen the cross arch, by FE method we can obtain the first to third order critical loads q_{cr} are $1.16\dfrac{EI}{R^3}$, $3.03\dfrac{EI}{R^3}$ and $4.67\dfrac{EI}{R^3}$ respectively(The theoretical solution for the first order critical load can refer to B.3 in Appendix B). The corresponding first order to third order buckling modes are shown in Fig.5-24 to Fig.5-26.

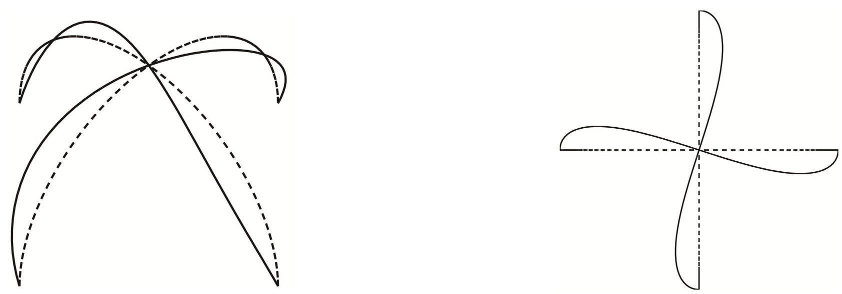

(a) Perspective drawing (b) Plane graph

Fig.5-24 First order buckling mode of cross arch

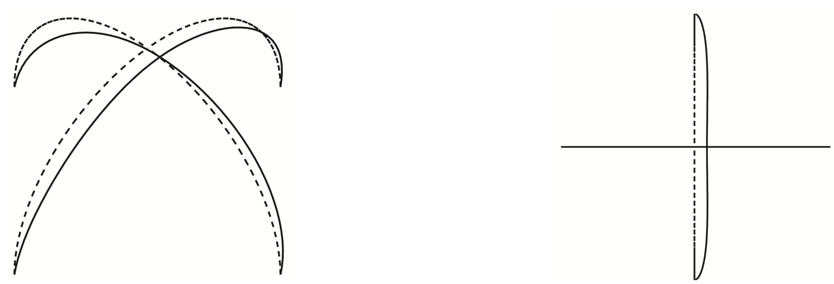

(a) Perspective drawing (b) Plane graph

Fig.5-25 Second order buckling mode of cross arch

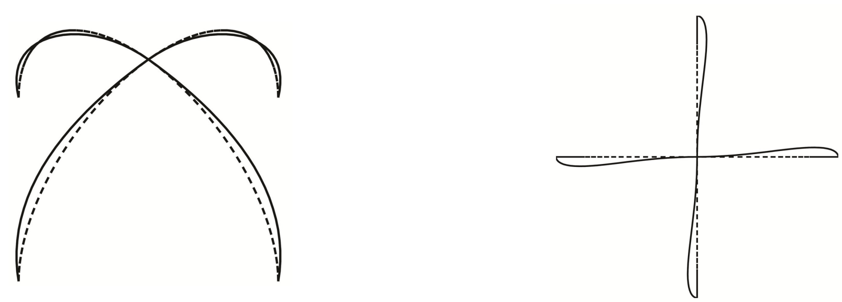

(a) Perspective drawing (b) Plane graph

Fig.5-26 Third order buckling mode of cross arch

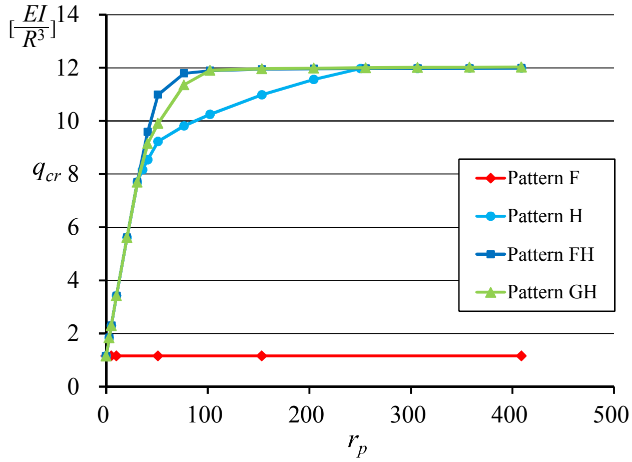

Fig.5-27 Relationship of r_p and first order critical load q_{cr} (hinged ended boundaries)

Fig.5-27 shows the relationship of spring ratio r_p and first order critical load q_{cr} when the boundary conditions of cross arch are hinged ended. From Fig.5-27, we can obtain that the first order critical load of Pattern F keeps constant even though spring ratio r_p increases. And Pattern G has the same critical load as Pattern F, here we omit Pattern G in Fig.5-27.

By comparing the first order critical loads of Pattern H, Pattern FH and Pattern GH, we can obtain when r_p is below 30.57, these three stiffening patterns have almost same first order critical load. When r_p is large than 30.57, the first order critical load of Pattern FH is largest, the value of Pattern GH is in the middle level, and value of Pattern H is the smallest. The maximum first order critical loads of these three patterns are almost identical.

In order to understand the configurations in Fig.5-27, here Pattern H is taken as an example, and the variation of first order buckling modes is aimed to be observed. Table.5-11 shows four different first order buckling modes of Pattern DE with the increasing of spring ratio r_p.

Table.5-11 Variation tendency of buckling modes of Pattern H

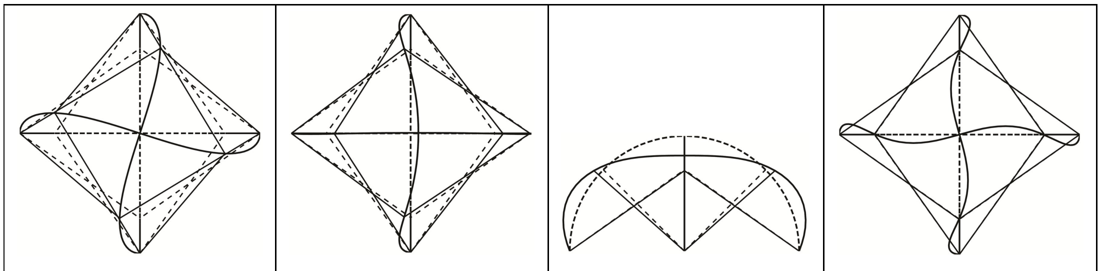

(a) r_p=0 (b) r_p=35.78 (c) r_p=76.68 (d) r_p=250.48

Table.5-12 shows the final first order buckling modes of call stiffening patterns. And Pattern F and Pattern G have the same buckling modes. The buckling modes of Pattern H, Pattern FH and Pattern GH are almost identical.

Table.5-12 Final first order buckling modes

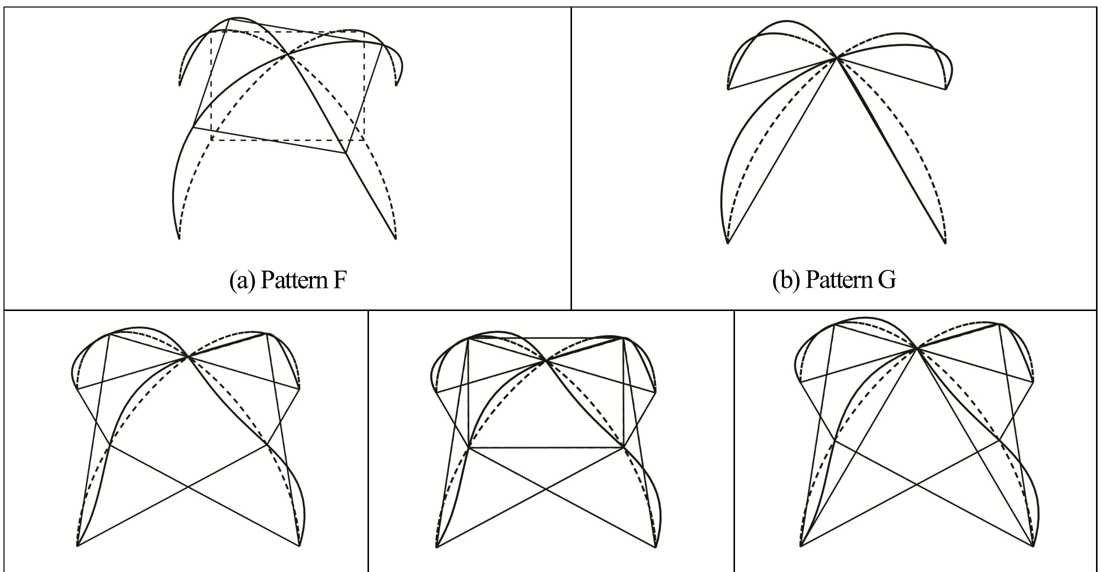

(a) Pattern F (b) Pattern G (c) Pattern H (d) Pattern FH (e) Pattern GH

Next let's talk about the cases when the arch has hinged ended boundary conditions, that is, among the six DOF of node at each boundary, the three translational DOF and three rotational DOF are all constrained. The materials parameters, uniform compression, and the shape of the arch are as same as the ones in above numerical analysis. When there is no braces, by FE method we can obtain the first to third order critical loads q_{cr} are $5.83\frac{EI}{R^3}$, $8.86\frac{EI}{R^3}$ and $13.15\frac{EI}{R^3}$ respectively. The corresponding buckling modes are shown in Fig.5-28 to Fig.5-30.

(a) Perspective drawing (b) Plane graph

Fig.5-28 First order buckling mode of cross arch

(a) Perspective drawing (b) Plane graph

Fig.5-29 Second order buckling mode of cross arch

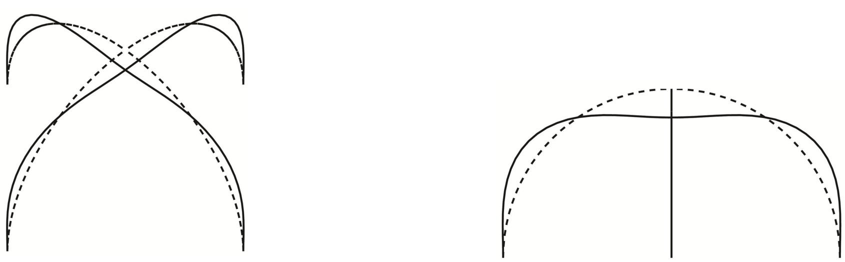

(a) Perspective drawing (b) Plane graph

Fig.5-30 Third order buckling mode of cross arch

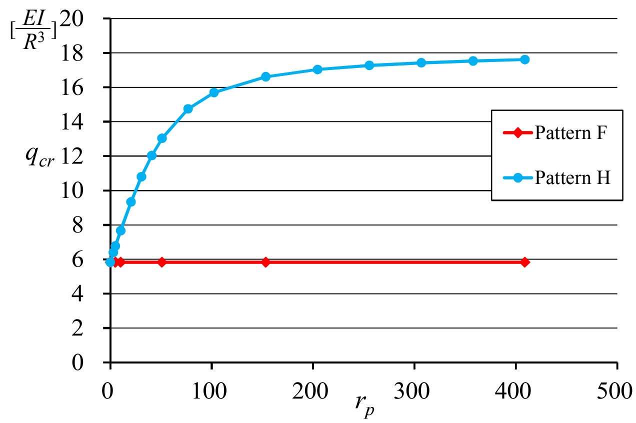

Fig.5-31 Relationship of r_p and the first order critical load q_{cr} (fixed ended boundaries)

Fig.5-31 shows the relationship of spring ratio r_p and first order critical load q_{cr} when the boundaries conditions of cross arch are fixed ended. The first order critical load of Pattern F keeps constant even though spring ratio r_p increases. And the first critical load of Pattern G is identical to the one of Pattern F, here its configuration is omitted.

And the first order critical loads of Pattern FH, Pattern GH are as same as the value of Pattern H, here their configurations are also omitted in Fig.5-31. And Pattern F and Pattern G have the same buckling modes. The buckling modes of Pattern H, Pattern FH and Pattern GH are identical.

Similar to the case with hinged ended boundaries, here we take the Pattern H as an example, and then we observe the variation of first order buckling modes with the increasing of spring ratio r_p. Table.5-13 shows three different first order buckling modes of Pattern H. And Table.5-14 shows the finial first order buckling modes of all stiffening patterns when r_p is very large.

Table.5-13 Variation tendency of buckling modes of pattern H

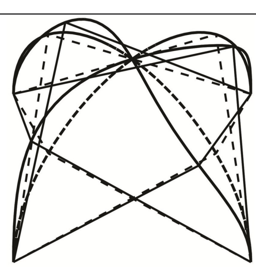 (a) r_p=0	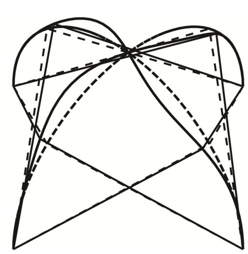 (b) r_p=76.68	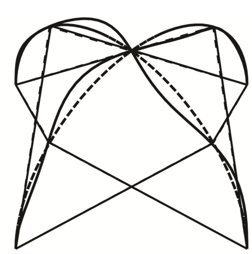 (c) r_p=408.95

Table.5-14 Final first order buckling modes

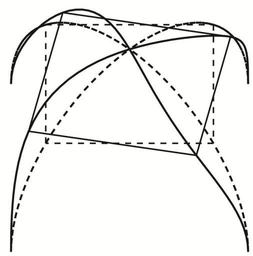 (a) Pattern F	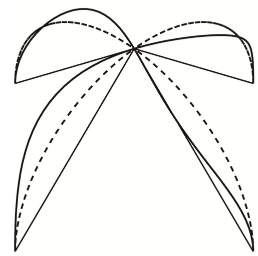 (b) Pattern G	
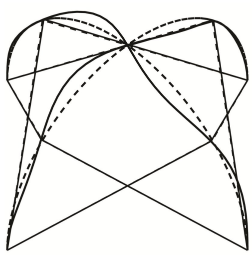 (c) Pattern H	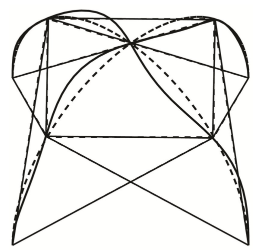 (d) Pattern FH	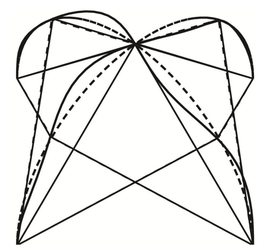 (e) Pattern GH

5.4.3 Hoop-ring

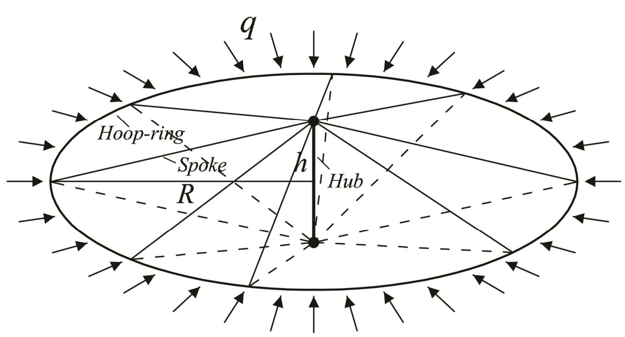

Fig.5-32 Hoop-ring stiffened with spokes

As an application, here the buckling behavior of hoop-ring stiffened by spokes is analyzed. Fig.5-32 shows one example of this kind of hoop-ring, 8 spokes are set up at each side of hoop-ring respectively, the central angel between adjacent spokes along circumferential direction is 45°. Uniform compression q is applied in the plane of hoop-ring.

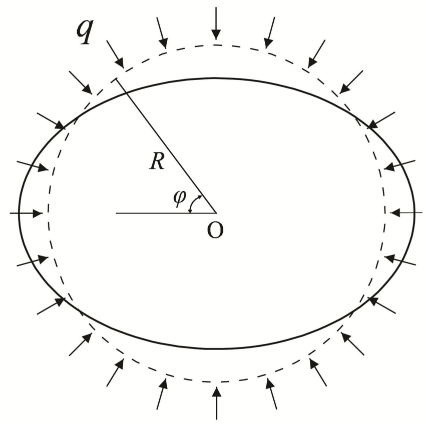

Fig.5-33 Buckling problem of ring in-plane

Firstly, let's deduce the critical load of ring in-plane. The configuration of ring is shown in Fig.5-33. The boundary conditions of symmetric buckling mode can be expressed as

(1) $w=0, v'=0, Q_\eta=0$ at $\varphi=0$

(2) $w=0, v'=0, Q_\eta=0$ at $\varphi=\pi$

From the Eq.(4.27), Eq.(4.28) and Eq.(4.32) in Chapter 4, we can find the expressions of displacements v , w, and shear force Q_η. From the boundary conditions, we can obtain

$$\begin{cases} 0=-A-\dfrac{C}{\tau}+F \\ 0=A+C\tau \\ 0=-A-C\tau^3 \\ 0=A-C\dfrac{\cos\pi\tau}{\tau}+D\dfrac{\sin\pi\tau}{\tau}+\pi E+F \\ 0=-A+C\tau\cos\pi\tau-D\tau\sin\pi\tau \\ 0=A-C\tau^3\cos\pi\tau+D\tau^3\sin\pi\tau \end{cases} \tag{5.55}$$

In Eq.(5.55), from the second term and third term, we can obtain A=C=0. Then from the first term we know F=0. Then the remaining parameters are D and E. If D is 0, then from the forth term, we can obtain E=0. As we know when buckling happens, A~F cannot be 0 at the same time, then we know D cannot be 0. As a result, from the fifth or sixth term, we can obtain

$$\sin\pi\tau=0 \tag{5.56}$$

As τ is larger than 1, the minimum positive integer for τ is 2, then we know the critical load q_{cr} is

$$q_{cr} = \frac{3EI_x}{R^3} \tag{5.57}$$

Eq.(5.57) is identical to the one obtained by Timoshenko [42].

And if there is no spokes in hoop-ring, for the stability of hoop-ring out-of-plane, we can find the first order critical load in the first term of Eq.(4.76) in Chapter 4

$$q_{cr} = \frac{EI_y}{R^3} \bullet \frac{9}{4 + EI_y / (GJ_z)} \tag{5.58}$$

Next a numerical example is used to calculate the first order critical loads and first order buckling modes for in-plane stability and out-of-plane stability. The radius of hoop-ring is 1m. The materials parameters of the hoop-ring are as same as the ones in numerical examples above. The entire hoop-ring is divided into 96 linear beam elements, and each element has the same length.

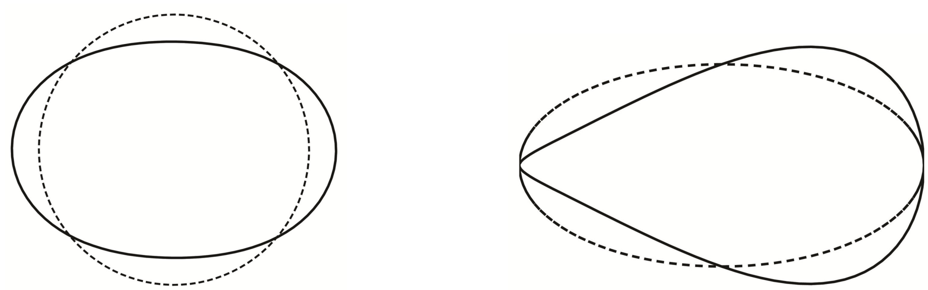

(a) (b)

Fig. 5-34 First order buckling modes in-plane and out-of-plane

Fig.5-34(a) shows the first order buckling mode in-plane, and the corresponding critical load is 3.0017 $\frac{EI_x}{R^3}$, which is almost identical to the one in Eq.(5.57). Fig.5-34(b) shows the first order buckling mode out-of-plane, the corresponding critical load q_{cr} is 1.6984 $\frac{EI_y}{R^3}$. In another aspect, from Eq.(5.58), we can obtain the theoretical critical load q_{cr} is 1.6981 $\frac{EI_y}{R^3}$.

Next the buckling of hoop-ring with 8 spokes in Fig.5-32 is discussed. From Eq.(C-6) in Appendix C, an equivalent elastic stiffness of spokes which mainly contributes the stiffening effect out-of-plane is given, and the value of this elastic stiffness in Fig.5-32 can be calculated as

$$k_E = \frac{2(0.5h)^2}{(0.25h^2 + R^2)} \frac{E_C A_C}{\sqrt{0.25h^2 + R^2}} \tag{5.59}$$

Here E_C is the Young's modulus of the spoke, A_C is the area of cross section. And a parameter b is assumed as $b=h/R$, then k_E transforms into

$$k_E = \frac{0.5b^2}{(0.25b^2 + 1)^{3/2}} \frac{E_C A_C}{R} \tag{5.60}$$

Assuming b=1, then we take $E_C A_C$ as a variable to observe variation of the first order critical loads. In theoretical analysis, when of hoop-ring wave is 8, from the third term of Eq.(4.76), the first order critical load is

$$q_{cr} = \frac{EI_y}{R^3} \frac{225}{16 + \dfrac{EI_y}{GJ_z}} = 13.0058 \frac{EI_y}{R^3} \tag{5.61}$$

A spring ratio r_y is assumed as

$$r_y = \frac{k_E}{EI_y / R^3} \tag{5.62}$$

Fig.5-35 shows relationship of parameter r_y and the critical load q_{cr}. And Fig.5-36 shows the variation of buckling modes.

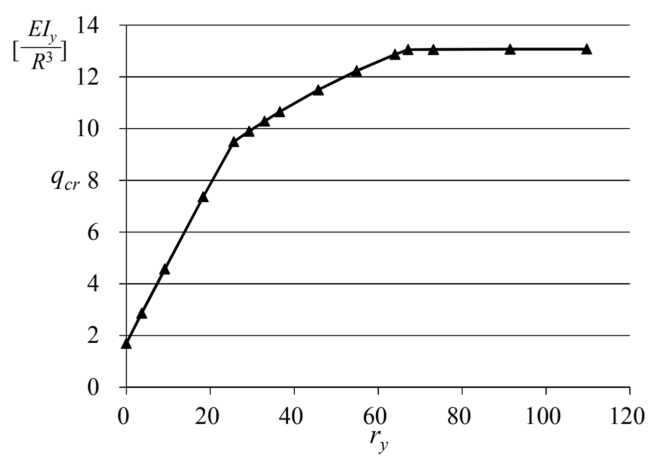

Fig.5-35 Relationship of parameter r_y and the first order critical load q_{cr}

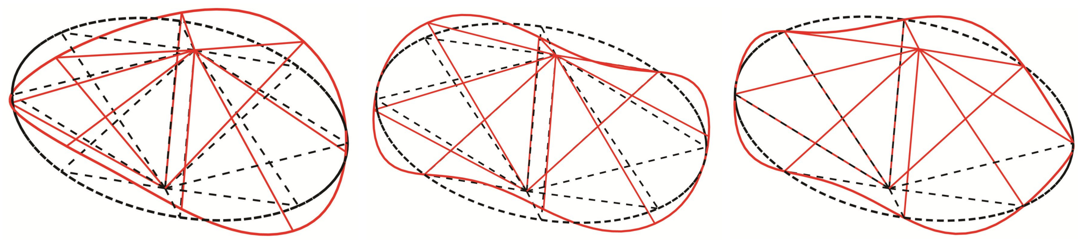

(a) r_y=0 (b) r_y=25.60 (c) r_y=67.12

Fig.5-36 Variation tendency of the first order buckling modes

5.5 Summaries

In this chapter, straight braces are used to stiffen the circular arch structures. And the stability problems of arches stiffened by braces are discussed. In addition, stability problems of various stiffening patterns of the single arch and cross arch, as well as hoop-rings stiffened by spokes are analyzed. The main achievements are stated as follows:

1) Arch-spring models for in-plane stability and out-of-plane stability of arches are proposed. By using general solutions of displacements obtained in Chapter 4, buckling control equations are able to be obtained. FE methods are used to verify these buckling control equations.

2) Spring ratio r_x of arch-spring model in-plane and spring ratio r_y of arch-spring model out-of-plane are available through the analysis of respective buckling control equations, and study work also shows that when the spring ratios are larger than limiting spring ratios, the critical loads of the arches cannot increase any more.

3) The variations of critical loads and buckling modes of various stiffening patterns of single arch and cross arch are analyzed, and study work shows by restraining their buckling modes efficiently can greatly increase the critical loads, and limiting spring ratios are also proved to be existing. The stiffening effect of spokes in hoop-ring structure is very similar to the stiffening effect of braces.

Chapter 6 Stiffening Effect of Flexible Components

6.1. Introduction

In Chapter 5, the stiffening effects of straight components are discussed. It is known that the elastic stiffness of the straight components play an important role in stiffening effect [15], [17], [26], [154], [165]. In this Chapter, stiffening effect of flexible components such as curved cables will be discussed. The obvious difference between straight components and flexible components is that the elastic stiffness of the latter one cannot attribute to the stiffening effect because they are in mechanistic state when buckling of main structures happens.

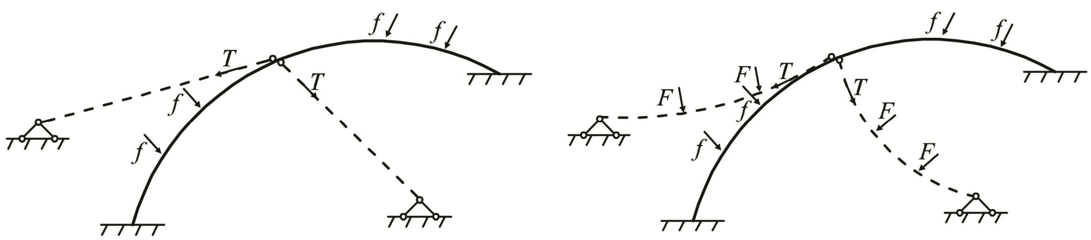

(a) Component stiffening method (b) External force stiffening method

Fig.6-1 Two kinds of stiffening methods

In order to distinguish the traditional stiffening methods by using straight component and the new method stated in this chapter, here we nominate these two methods respectively. The former one is called component stiffening method (Fig.6-1(a)), and the latter one called external force stiffening method (Fig.6-1(b)).

Table.6-1 Comparison of two stiffening methods

Stiffening methods	Transfer order of loads	Shape of components
Components stiffening method	Main Loads→ Arch→ brace	Straight line
External force stiffening method	Part of Loads→ brace→ Arch	Curved line

Next the characteristics of these two stiffening method shown in Table.6-1 will be discussed. In the case of component stiffening method, external forces are only applied to the arch, and the elastic stiffnesses of braces are directly used to stiffen the arch. And the shapes of braces are straight all the time. In another aspect, in the case of external force stiffening method, parts of external forces are directly applied to the cables, and the shapes of cables become curved; and other external forces are applied to the arch. In this chapter, the stiffening principle of flexible components will be discussed.

6.2 Stiffening effects of elastic stiffness and internal force

Before we discuss the flexible components' stiffening effect, we use a simple example to explain the effect of elastic stiffness and internal force in stiffening a column structure, as shown in Fig.6-2. To study the column structures can help us understand the case of arch structures.

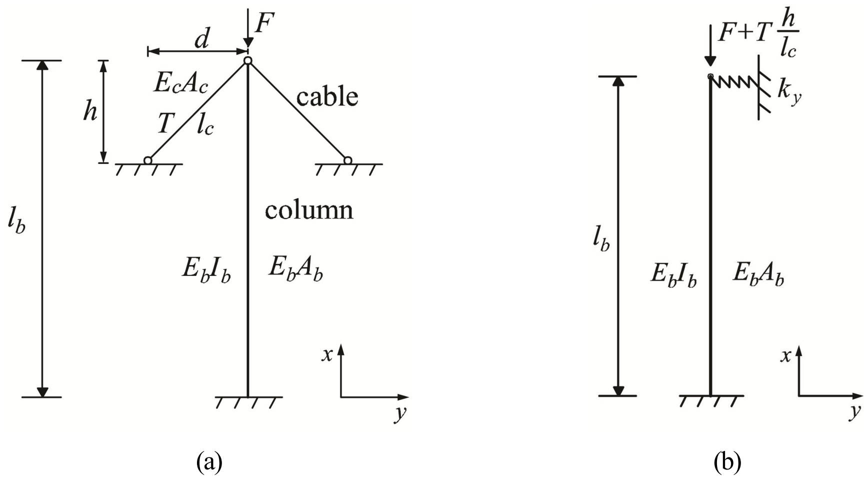

Fig.6-2 Column stiffened by straight cables

Symbols used in Fig.6-2(a) are as follows: for cables, E_c is the Young's modulus, A_c is the area of cross section, T is the internal force just prior to buckling, l_c is the member length. For column, E_b is the Young's modulus, A_b is the area of cross section, I_b is moment of inertia, l_b is the member length. A concentrated load F is applied at the top of column. We assume $E_bA_b \gg E_cA_c$, so that the component of elastic stiffnesses of cables in x direction can be ignored.

The model in Fig.6-2(a) is equivalent to a simple one in Fig.6-2(b), and k_y in Fig.6-2(b) is the entire stiffness aroused from cables, the calculation procedure is introduced in Appendix C. The value of k_y is

$$k_y = \frac{2d^2}{l_c^2}\frac{E_cA_c}{l_c} + \frac{2h^2}{l_c^2}\frac{T}{l_c} \tag{6.1}$$

k_y in the equation above can be divided into two parts: one is caused by the elastic stiffness E_cA_c, noting k_E; and another one is caused by internal force T, noting k_T. Then k_E and k_T are given as follows:

$$\begin{cases} k_E = \dfrac{2d^2}{l_c^2}\dfrac{E_cA_c}{l_c} \\ k_T = \dfrac{2h^2}{l_c^2}\dfrac{T}{l_c} \end{cases} \tag{6.2}$$

The sign of k_T relates to internal force T, and there is

$$\begin{cases} k_T > 0, \ \textit{if T is tension.} \\ k_T < 0, \ \textit{if T is compression.} \\ k_T = 0, \ \textit{if T is } 0. \end{cases} \tag{6.3}$$

In another aspect, the proportion of first term and second term in Eq. (6.2) is

$$\frac{k_T}{k_E} = \frac{\dfrac{2h^2}{l_c^2}\dfrac{T}{l_c}}{\dfrac{2d^2}{l_c^2}\dfrac{E_cA_c}{l_c}} = (\frac{h}{d})^2\frac{T}{E_cA_c} \tag{6.4}$$

Usually, $E_cA_c >> T$ is pre-established, so that the stiffness k_T originating from T can be ignored, the column is mainly stiffened by elastic stiffness k_E of cables.

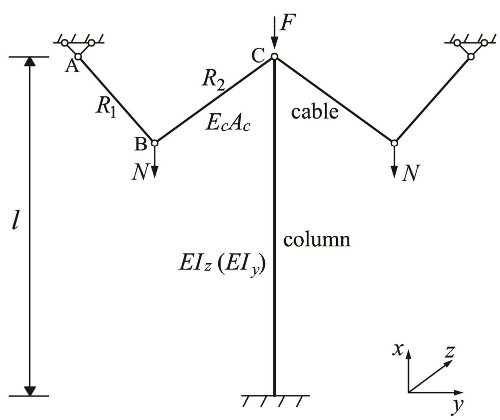

Fig.6-3 Column stiffened by curved cables

In contrast to the situation above, another situation is considered, that is, the stiffness k_T originating from internal force of cables contributes to stiffening the column, and stiffness k_E originating from the elastic stiffnesses of cables can be ignored. Fig.6-3 shows such an alternative stiffening method: a column is stiffened by curved cables, and concentrated loads N are directly applied to curved cables and another concentrated load F is applied at the top of the column. When buckling of the column happens, curved cables will experience mechanistic movements, and elastic stiffnesses of cables cannot provide stiffening effect to the column.

6.3 Derivation of stiffness of pseudo-spring

In this section, the stiffening effect of cables shown in Fig.6-3 is discussed. As mechanistic movements of curved cables happen after buckling of the column, it is necessary to consider the equilibrium shapes of cables and the column. Stability problems of the column in-plane and out-of-plane will be analyzed respectively.

6.3.1 In-plane

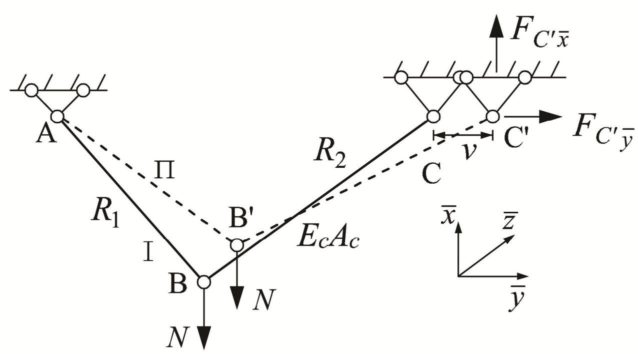

Fig.6-4 Mechanistic movements of cables in-plane

Firstly, the mechanistic movements of curved cables in-plane in 2D space are discussed. Axes $\bar{x}$, $\bar{y}$ and $\bar{z}$ in the local Cartesian coordinate system $\overline{xyz}$ in Fig.6-4 are parallel to axes x, y and z in global Cartesian coordinate system xyz in Fig.6-3 respectively. And symbols Ⅰ and Ⅱ in Fig.6-4 represent the equilibrium states before and after movements.

In Fig.6-4, point C is assumed to experience a movement with a displacement v along axis $\bar{y}$ in $\overline{xy}$ plane to a new position C'. Then point B also moves to a new position B'. Here the initial coordinates of A is (0, 0, 0), C is (0, $\bar{y}_C$, 0), and B' is ($\bar{x}_{B'}$, $\bar{y}_{B'}$, 0). Then it is straightforward to determine the coordinate of C' is (0, $\bar{y}_C+v$, 0).

The concentrated load N is assumed to be constant, the internal forces in cables during the shift from state Ⅰ to state Ⅱ will change to arrive at a new equilibrium state. As v is very small, if the lengths of cables are supposed to be almost identical in state Ⅰ and Ⅱ, then we can obtain

$$\begin{cases} \bar{x}_{B'}^2 + \bar{y}_{B'}^2 = R_1^2 \\ \bar{x}_{B'}^2 + (\bar{y}_{B'} - \bar{y}_C - v)^2 = R_2^2 \end{cases} \tag{6.5}$$

So that the coordinate of B' can be calculated as

$$\begin{cases} \overline{x}_{B'} = (-\sqrt{R_1^2 - \overline{y}_{B'}{}^2}) \\ \overline{y}_{B'} = \dfrac{R_1^2 - R_2^2 + (\overline{y}_C + v)^2}{2(\overline{y}_C + v)} \end{cases} \tag{6.6}$$

In the equilibrium state Ⅱ, from the relationship of reaction forces at point C' and equilibrium of moment at point A, we can obtain

$$\begin{cases} \dfrac{F_{C'\overline{x}}}{F_{C'\overline{y}}} = \dfrac{-\overline{x}_{B'}}{\overline{y}_C + v - \overline{y}_{B'}} \\ N\overline{y}_{B'} = F_{C'\overline{x}}(\overline{y}_C + v) \end{cases} \tag{6.7}$$

The solutions of Eq.(6.7) is

$$\begin{cases} F_{C'\overline{y}} = \dfrac{F_{C'\overline{x}}}{(\dfrac{-\overline{x}_{B'}}{\overline{y}_C + v - \overline{y}_{B'}})} \\ F_{C'\overline{x}} = \dfrac{N\overline{y}_{B'}}{\overline{y}_C + v} \end{cases} \tag{6.8}$$

Substituting Eq.(6.6) into Eq.(6.8), we can obtain

$$\begin{cases} F_{C'\overline{y}} = \dfrac{N((\overline{y}_C + v)^4 - (R_1^2 - R_2^2)^2)}{2(\overline{y}_C + v)^2\sqrt{4(\overline{y}_C + v)^2 R_1^2 - (R_1^2 - R_2^2 + (\overline{y}_C + v)^2)^2}} \\ F_{C'\overline{x}} = \dfrac{N}{2}(\dfrac{R_1^2 - R_2^2}{(\overline{y}_C + v)^2} + 1) \end{cases} \tag{6.9}$$

Based on the symmetry of curved cables shown in Fig.6-3, the resultant force F_y at point C' in y direction would be calculated as

$$\begin{aligned} F_y = F_{C'\overline{y}}(v) - F_{C'\overline{y}}(-v) = {} & \frac{N((\overline{y}_C + v)^4 - (R_1^2 - R_2^2)^2)}{2(\overline{y}_C + v)^2(\sqrt{4R_1^2(\overline{y}_C + v)^2 - (R_1^2 - R_2^2 + (\overline{y}_C + v)^2)^2})} \\ & - \frac{N((\overline{y}_C - v)^4 - (R_1^2 - R_2^2)^2)}{2(\overline{y}_C - v)^2(\sqrt{4R_1^2(\overline{y}_C - v)^2 - (R_1^2 - R_2^2 + (\overline{y}_C - v)^2)^2})} \end{aligned} \tag{6.10}$$

When the value of v approaches to 0, the limiting ratio of F_y and v is

$$\lim_{v \to 0} \frac{F_y}{v} = (\frac{2\overline{y}_C}{\sqrt{4R_1^2\overline{y}_C^2 - (R_1^2 - R_2^2 + \overline{y}_C^2)^2}} + \frac{2(R_1^2 - R_2^2)^2}{\overline{y}_C^3\sqrt{4R_1^2\overline{y}_C^2 - (R_1^2 - R_2^2 + \overline{y}_C^2)^2}}$$

$$+\frac{((R_1^2-R_2^2)^2-\overline{y}_C^4)(2R_1^2+2R_2^2-2\overline{y}_C^2))}{\overline{y}_C(4R_1^2\overline{y}_C^2-(R_1^2-R_2^2+\overline{y}_C^2)^2)^{(3/2)}})N \tag{6.11}$$

Here assuming a stiffness k_{xy} as

$$k_{xy}=(\frac{2\overline{y}_C}{\sqrt{4R_1^2\overline{y}_C^2-(R_1^2-R_2^2+\overline{y}_C^2)^2}}+\frac{2(R_1^2-R_2^2)^2}{\overline{y}_C^3\sqrt{4R_1^2\overline{y}_C^2-(R_1^2-R_2^2+\overline{y}_C^2)^2}}$$

$$+\frac{((R_1^2-R_2^2)^2-\overline{y}_C^4)(2R_1^2+2R_2^2-2\overline{y}_C^2)}{\overline{y}_C(4R_1^2\overline{y}_C^2-(R_1^2-R_2^2+\overline{y}_C^2)^2)^{(3/2)}})N \tag{6.12}$$

From Eq.(6.12), it is known that k_{xy} contains an independent variable N without the elastic stiffness E_cA_c of curved cables . For very small value of v, there is an approximate equation as follows:

$$F_y \approx k_{xy}v \tag{6.13}$$

Then k_{xy} can be seen as a relationship between force and displacement, which is similar to the elastic stiffness of a spring, so here k_{xy} is called “stiffness of pseudo-spring”. In other aspect, when the value of v is very small, the resultant force F_x in x direction is

$$F_x = F_{C'\overline{x}}(v)+F_{C'\overline{x}}(-v)\approx N(1+\frac{R_1^2-R_2^2}{\overline{y}_C^2}) \tag{6.14}$$

Especially, when $R_1 = R_2 = l_c$, we can obtain

$$k_{xy}=\frac{4Nl_c^2}{(4l_c^2-\overline{y}_C^2)^{(3/2)}} \tag{6.15}$$

$$F_x \approx N \tag{6.16}$$

6.3.2 Out-of-plane

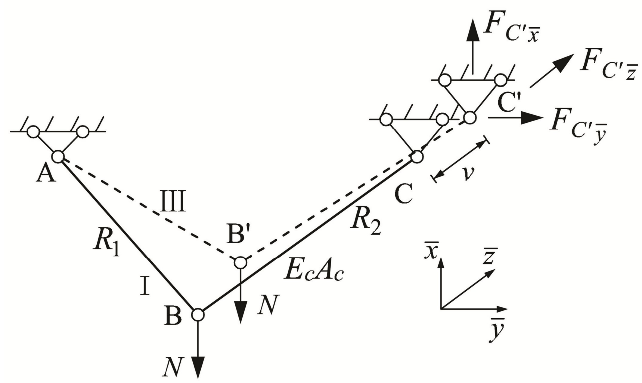

Fig.6-5 Mechanistic movements of curved cables out-of-plane

Fig.6-5 shows mechanistic movements of cables out-of-plane in 3D space. And symbols Ⅰ and Ⅲ represent the equilibrium states before and after movements. The coordinates of point A and point C are as same as the ones in Section 6.3.1. In local Cartesian coordinate system $\overline{xyz}$, the point C moves with a displacement v along axis $\bar{z}$ in $\overline{xz}$ plane to a new position C', and the coordinate of C' is (0, $\bar{y}_C$, v). Similar to the discussion in Section 6.3.1, the lengths of cables are supposed to be constant after movements. Assuming the coordinate of B' is ($\bar{x}_{B'}$, $\bar{y}_{B'}$, $\bar{z}_{B'}$). From the geometric relationship after movement, we can obtain

$$\begin{cases} \bar{x}_{B'}^2 + \bar{y}_{B'}^2 + \bar{z}_{B'}^2 = R_1^2 \\ \bar{x}_{B'}^2 + (\bar{y}_{B'} - \bar{y}_C)^2 + (\bar{z}_{B'} - v)^2 = R_2^2 \\ \dfrac{\bar{z}_{B'}}{\bar{y}_{B'}} = \dfrac{v}{\bar{y}_C} \end{cases} \tag{6.17}$$

So that the coordinate of B' can be obtained as

$$\begin{cases} \bar{x}_{B'} = -\sqrt{R_1^2 - \bar{y}_{B'}^2 - \bar{z}_{B'}^2} \\ \bar{y}_{B'} = \dfrac{(R_2^2 - R_1^2) - (\bar{y}_C^2 + v^2)}{-2\bar{y}_C - 2\dfrac{v^2}{\bar{y}_C}} \\ \bar{z}_{B'} = \dfrac{v}{\bar{y}_C}\bar{y}_{B'} \end{cases} \tag{6.18}$$

From the relationship of reaction force at point C' and equilibrium of moment at point A , we can obtain

$$\begin{cases} \dfrac{F_{C'\bar{z}}}{F_{C'\bar{x}}} = \dfrac{v - \bar{z}_{B'}}{-\bar{x}_{B'}} \\ \dfrac{F_{C'\bar{y}}}{F_{C'\bar{x}}} = \dfrac{\bar{y}_C - \bar{y}_{B'}}{-\bar{x}_{B'}} \\ N\sqrt{\bar{y}_{B'}^2 + \bar{z}_{B'}^2} = F_{C'\bar{x}}\sqrt{(\bar{y}_C^2 + v^2)} \end{cases} \tag{6.19}$$

Substituting Eq.(6.18) into Eq.(6.19), we can obtain the reaction forces at point C'

$$F_{C'\bar{x}} = N\frac{\sqrt{\bar{y}_{B'}^2 + \bar{z}_{B'}^2}}{\sqrt{(\bar{y}_C^2 + v^2)}} = N\frac{(R_2^2 - R_1^2) - (\bar{y}_C^2 + v^2)}{-2(\bar{y}_C^2 + v^2)} \tag{6.20}$$

$$F_{C'\bar{y}} = \frac{\bar{y}_C - \bar{y}_{B'}}{-\bar{x}_{B'}}F_{C'\bar{x}} = \frac{N\bar{y}_C((R_2^2 - R_1^2)^2 - (\bar{y}^2{}_C + v^2)^2)}{-2(\bar{y}_C^2 + v^2)\sqrt{4R_1^2(\bar{y}^2{}_C + v^2)^2 - ((R_2^2 - R_1^2) - (\bar{y}_C^2 + v^2))^2(\bar{y}^2{}_C + v^2)}} \tag{6.21}$$

$$F_{C'\bar{z}} = \frac{v - \bar{z}_{B'}}{-\bar{x}_{B'}}F_{C'\bar{x}} = \frac{vN((R_2^2 - R_1^2)^2 - (\bar{y}_C^2 + v^2)^2)}{-2(\bar{y}_C^2 + v^2)\sqrt{4R_1^2(\bar{y}^2{}_C + v^2)^2 - ((R_2^2 - R_1^2) - (\bar{y}_C^2 + v^2))^2(\bar{y}^2{}_C + v^2)}} \tag{6.22}$$

Considering the symmetry in Fig.6-3, then resultant force F_z at point C' in *z* direction is

$$F_z = 2F_{C'\bar{z}}(v) \tag{6.23}$$

$$\lim_{v\to 0}\frac{F_z}{v} = \frac{-N((R_2^2 - R_1^2)^2 - \bar{y}_C^4)}{\bar{y}_C^3\sqrt{4R_1^2\bar{y}_C^2 - (R_2^2 - R_1^2 - \bar{y}_C^2)^2}} \tag{6.24}$$

Similar to the notation of stiffness of pseudo-spring k_{xy} in-plane in 2D space, here we assume a stiffness of pseudo-spring k_{xz} out-of-plane in 3D space as

$$k_{xz} = \frac{-N((R_2^2 - R_1^2)^2 - \bar{y}_C^4)}{\bar{y}_C^3\sqrt{4R_1^2\bar{y}_C^2 - (R_2^2 - R_1^2 - \bar{y}_C^2)^2}} \tag{6.25}$$

From the expression of k_{xz} in Eq.(6.25), we know k_{xz} only contains an independent variable *N* without the elastic stiffness $E_c A_c$ of cables. For very small value of *v*, we can again use an approximate expression

$$F_z \approx k_{xz}v \tag{6.26}$$

In another aspect, for very small value of *v*, the resultant force F_x at point C' in direction *x* is

$$F_x = 2F_{C'\bar{x}}(v) \approx N(1 + \frac{R_1^2 - R_2^2}{\bar{y}_C^2}) \tag{6.27}$$

And resultant force F_y at point C' in direction y is

$$F_y = F_{C\bar{y}}(v) - F_{C\bar{y}}(v) = 0 \tag{6.28}$$

Especially, when $R_1 = R_2 = l_c$, Eq.(6.25) and Eq.(6.27) become

$$k_{xz} = \frac{N}{(4l_c^2 - \bar{y}_C^2)^{(1/2)}} \tag{6.29}$$

$$F_x \approx N \tag{6.30}$$

6.4 Judging the buckling plane

Now comparing the two stiffnesses of pseudo-springs k_{xy} in-plane and k_{xz} out-of-plane:

(1) If $N = 0$, then it is self-evident that $k_{xy} = k_{xz} = 0$.

(2) If $N \neq 0$, then the difference between k_{xy} and k_{xz} is

$$k_{xy} - k_{xz} = N\left(\frac{(\bar{y}_C^4 - 3(R_1^2 - R_2^2)^2)^2 + 8\bar{y}_C^2(R_1^2 - R_2^2)^3 - 12(R_1^2 - R_2^2)^4 + 16\bar{y}_C^2 R_2^2 (R_1^2 - R_2^2)^2}{\bar{y}_C^3 (4R_1^2\bar{y}_C^2 - (R_1^2 - R_2^2 + \bar{y}_C^2)^2)^{(3/2)}}\right) \tag{6.31}$$

It is necessary to judge the plus or minus sign of the right side of Eq.(6.31). Firstly, let's consider formula $(4R_1^2\bar{y}_C^2 - (R_1^2 - R_2^2 + \bar{y}_C^2)^2)$ in the denominator of Eq.(6.31).

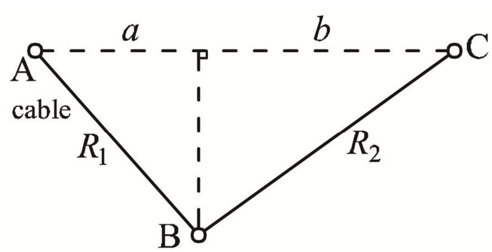

Fig.6-6 Initial geometric shape of curved cables

Fig.6-6 shows the initial geometric shape of curved cables in state I in Fig.6-4(or Fig.6-5). Based on this geometric shape, we can obtain

$$R_1^2 - a^2 = R_2^2 - b^2 \tag{6.32}$$

Substituting equation $b = \bar{y}_C - a$ into equation above, we can obtain

$$R_1^2 - R_2^2 + \overline{y}_C^2 = 2a\overline{y}_C \tag{6.33}$$

Then substituting Eq.(6.33) into $(4R_1^2\overline{y}_C^2 - (R_1^2 - R_2^2 + \overline{y}_C^2)^2)$, then we can obtain

$$4R_1^2\overline{y}_C^2 - (R_1^2 - R_2^2 + \overline{y}_C^2)^2 = 4\overline{y}_C^2(R_1^2 - a^2) > 0 \tag{6.34}$$

Secondly, the numerator in Eq.(6.31) is taken into consideration, assuming the numerator as a function *m*.

$$m = (\overline{y}_C^4 - 3(R_1^2 - R_2^2)^2)^2 + 8\overline{y}_C^2(R_1^2 - R_2^2)^3 - 12(R_1^2 - R_2^2)^4 + 16\overline{y}_C^2R_2^2(R_1^2 - R_2^2)^2 \tag{6.35}$$

In order to judge the plus-minus sign of m, here two parameters *s* and *g* are noted as follows.

$$\begin{cases} s = R_1^2 - R_2^2 \\ g = \overline{y}_C^2 \end{cases} \tag{6.36}$$

As $R_1^2 - R_2^2 + \overline{y}_C^2 > 0$ and $R_1^2 - R_2^2 - \overline{y}_C^2 < 0$, so that $|s| < g$.

Then substituting Eq.(6.36) into Eq.(6.35) and simplifying the function *m*, we can obtain

$$m = (g^2 - 3s^2)^2 + 4s^3(2g - 3s) + 16gs^2R_2^2 \tag{6.37}$$

In the equation above, the parameter s can be seen as a constant number, and the parameter g can be seen as an independent variable, meanwhile the function m can be seen as a dependent variable. The first and second derivatives of the function m are

$$\frac{dm}{dg} = 8s^3 + (16R_2 - 12g)s^2 + 4g^3 \tag{6.38}$$

$$\frac{d^2m}{dg^2} = 12g^2 - 12s^2 = 12(g^2 - s^2) > 0 \tag{6.39}$$

As $\frac{d^2m}{dg^2} > 0$, $\frac{dm}{dg}$ is a monotone increasing function, when $g = s$, $\frac{dm}{dg}$ arrives minimum.

$$\frac{dm}{dg}\Big|_{g=s} = 8s^3 + (16R_2 - 12s)s^2 + 4s^3 = 16R_2 > 0 \tag{6.40}$$

Because $\frac{dm}{dg} > 0$, so that the function *m* is monotone increasing too. When $g = s$, the function *m* arrives its minimum.

$$m\big|_{g=s} = 16s^3R_2^2 > 0 \tag{6.41}$$

It is clear that $m > 0$, since the numerator and the denominator in Eq.(6.31) are demonstrated to be positive, $k_{xy} > k_{xz}$ is therefore affirmed. If the cross section of the column is symmetric closed cross section, and moments of inertia around axis z and axis y have a relationship that I_z=I_y. Then buckling phenomenon of the 3D-column in Fig.6-3 may happen out-of-plane rather than in-plane as if the column has no preexisting imperfection.

6.5 One pseudo-spring system

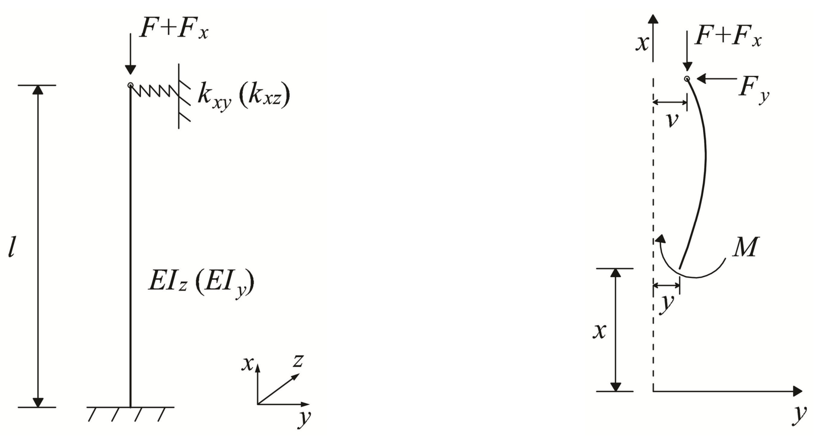

Fig.6-7 One pseudo-spring system

Firstly, in-plane stability of the column in Fig.6-3 in 2D space is considered. Fig.6-7(a) is a simplification of the model in Fig.6-3. In Fig.6-7(b), the effects of shearing deformation and shortening of beam axis are ignored, according to Eq.(C-19) in Appendix C, the equilibrium differential equation can be written as

$$y'' + \frac{F+F_x}{EI_z}y = -F_y\frac{(l-x)}{EI_z} + \frac{(F+F_x)v}{EI_z} \tag{6.42}$$

Assuming a parameter λ as

$$\lambda^2 = \frac{F+F_x}{EI_z} \tag{6.43}$$

Then substituting Eq.(6.13) and Eq.(6.43) into Eq.(6.42), we can obtain

$$y''+\lambda^2 y=-\frac{k_{xy}v}{EI_z}(l-x)+\lambda^2 v \tag{6.44}$$

The general solution of Eq.(6.44) is

$$y=A\cos\lambda x+B\sin\lambda x-\frac{k_{xy}v}{\lambda^2 EI_z}(l-x)+v \tag{6.45}$$

The boundary conditions in Fig.6-7(b) are

(1) $y=0, y'=0$ at $x=0$

(2) $y=v$ at $x=l$

Utilizing the above boundary conditions, we can obtain

$$[(\frac{k_{xy}l}{\lambda^2 EI_z}-1)\cos\lambda l-\frac{k_{xy}}{\lambda^3 EI_z}\sin\lambda l]v=0 \tag{6.46}$$

As the value of v is an arbitrary small displacement, then the solution of Eq.(6.46) is

$$(\frac{k_{xy}l}{\lambda^2 EI_z}-1)\cos\lambda l-\frac{k_{xy}}{\lambda^3 EI_z}\sin\lambda l=0 \tag{6.47}$$

Eq.(6.47) is the buckling control equation of in-plane stability of the column in 2D space. The relationship of the critical load F_{cr} and the concentrated load N is need to be examined.

(1) If $N=0$, then it is self-evident that $k_{xy}=0$. The buckling control equation in Eq.(6.47) becomes

$$\cos\lambda l=0 \tag{6.48}$$

The minimum positive value of λl satisfying Eq.(6.48) is 0.5π, the corresponding critical load F_{cr} is

$$F_{cr}=\frac{\pi^2 EI_z}{(2l)^2} \tag{6.49}$$

(2) If $N\neq 0$, then $k_{xy}\neq 0$. We assume two notations $u=\lambda l$, and $r=\frac{k_{xy}}{EI_z/l^3}$. Here u and r are non-dimensional parameters. Then the buckling control equation in Eq.(6.47) thus becomes

$$\tan u=u-\frac{u^3}{r} \tag{6.50}$$

As Eq.(6.50) is a transcendental equation, numerical method can be used for the value of u.

Assuming a pseudo-critical load $P_{cr} = u^2 \frac{EI_z}{l^2}$, so that from Eq.(6.43) the critical load F_{cr} can be calculated as

$$F_{cr} = P_{cr} - F_x \approx u^2 \frac{EI_z}{l^2} - N(1 + \frac{(R_1^2 - R_2^2)}{\overline{y}_C^2}) \tag{6.51}$$

In 3D-column analysis, for axial compression column with biaxial symmetric cross section, buckling modes of the column may be flexural buckling or torsional buckling. For example, flexural buckling typically occurs when the column has H-type cross section; torsional buckling is more common when the column has a crisscross cross section or X-type cross section. If only the flexural buckling of the column is considered, then k_{xz} is substituted for k_{xy}, and EI_y is substituted for EI_z, the critical load F_{cr} for out-of-plane stability can be obtained.

6.6 Numerical example

Here a numerical example in Fig.6-8 is used to show the variation tendency of the critical load F_{cr} and pseudo-critical load P_{cr} with the increasing of the concentrated load N.

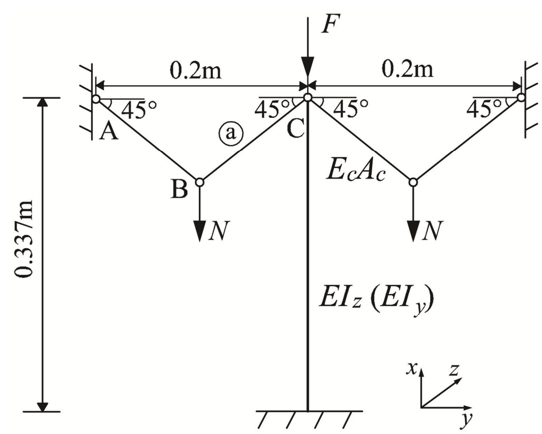

Fig.6-8 Column featuring with curved cables

Table.6-2 Materials parameters of numerical example

	Young's modulus [GPa]	Poisson' ratio	Internal diameter [mm]	External diameter [mm]
Cable	205	–	–	0.7
Column	2.82	0.38	4	6

The cross sections of the column and cables are hollow cross section and solid circular cross section respectively. The materials parameters of the column and cables are shown in Table.6-2. In the static analysis by using nonlinear FE method, the entire column is divided into 30 geometric nonlinear beam elements introduced in Section 3.4.1, and each beam element has the same length. And one cable is divided into one geometric nonlinear truss element only, which is introduced in Section.3.4.2. The column is supposed to have no preexisting imperfection in FE analysis.

a) In-plane stability

1) Theoretical solution

In Section 6.3, the solutions of stiffnesses of pseudo-springs k_{xy} in Eq. (6.12) and k_{xz} in Eq.(6.25) are given. And then in Section 6.5, a procedure to get the theoretical solution of the critical load F_{cr} in Eq.(6.51) is also discussed. As a preparation, parameters in Fig.6-8 (definitions of $\bar{y}_C$, l_c and l refer to Section 6.3) are obtained as

$$\begin{cases} \bar{y}_C = 2\cos 45^0 l_c = \sqrt{2} l_c \\ l_c = \dfrac{\sqrt{2}}{10}(\text{m}) \\ l = 0.337(\text{m}) \end{cases} \tag{6.52}$$

Firstly, let's consider the model in Fig6-8 in 2D space. Because the lengths of AB and BC are identical, then from Eq.(6.15), the theoretical stiffness of pseudo-spring k_{xy} is

$$k_{xy} = \frac{4Nl_c^2}{(4l_c^2 - \bar{y}_C^2)^{(3/2)}} = \sqrt{2}\frac{N}{l_c} = 10N \tag{6.53}$$

The non-dimensional parameter r can be obtained as

$$r = \frac{k_{xy}}{EI_z / l^3} = \frac{\sqrt{2}N / l_c}{EI_z / l^3} \tag{6.54}$$

In theoretical analysis, by substituting Eq.(6.54) into Eq.(6.50), u in Eq.(6.50) corresponding to different concentrated loads N can be obtained. Then substituting u into Eq.(6.51), the critical load F_{cr} can be obtained.

2) FE approach

For static analysis based on nonlinear FE method, when the critical load F_{cr} at the top of the column is aimed to be obtained, which corresponds to defined concentrated load N on the cables, two steps are used to get the critical load F_{cr} during the FE analysis process: Step 1: Keeping F as 0N, then we increase N from 0 to a predetermined value and the system of column and cables arrives an equilibrium state; Step 2: Keeping N to the new determined value, then we increase F from 0N to a new value where minimum positive eigenvalue of tangential stiffness matrix reaches 0. This freshly defined value of F is the critical load F_{cr}.

Here a specific example is given to show how to calculate the critical load F_{cr} by using nonlinear FE method. In this example, the concentrated load N is assumed as 5N. It is usually quite difficult to attain a minimum positive eigenvalue equaling 0. So as minimum positive eigenvalue of tangential stiffness matrix approaches 0, we will expect buckling of the column to have happened. Fig.6-9(a) and Fig.6-9(b) show the relationships of minimum positive eigenvalue of tangential stiffness matrix and the concentrated load N, and the concentrated load F respectively. By observing Fig.6-9(a) and Fig.6-9(b), the minimum positive eigenvalue firstly increases, and then decreases to 0. When the concentrated load N equals 5N, at the same time the concentrated load F equals 10.2N, the minimum eigenvalue in Fig.6-9(b) becomes 2.5×10^{-4}, so buckling of the column is thought to have occurred.

Fig.6-10 shows the relationship of displacement of point B in x direction with concentrated loads N and F. The displacement in x direction is monotone decreasing in step 1 and step 2.

Fig.6-11 shows the relationship of tension of cable ⓐ with concentrated loads N and F. In step 1 in Fig.6-11(a), when the concentrated load F remains 0N, tension is increasing in almost linear fashion with each increment added to the concentrated load N. However, in step 2 in Fig.6-11(b), when the concentrated load N remains 5N, even as the concentrated load F increases, tension of cable almost remains nearly unchanged.

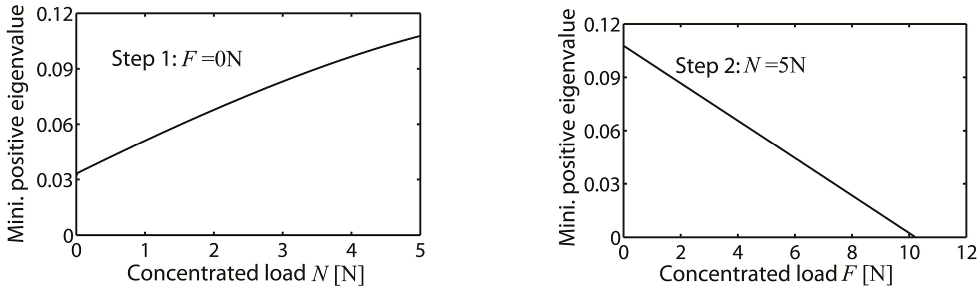

(a) (b)

Fig.6-9 Relationship of minimum positive eigenvalue with N and F

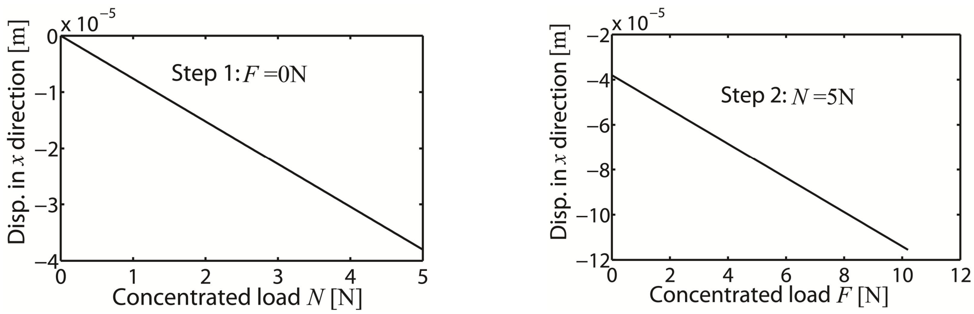

(a) (b)

Fig.6-10 Relationship of displacement with N and F

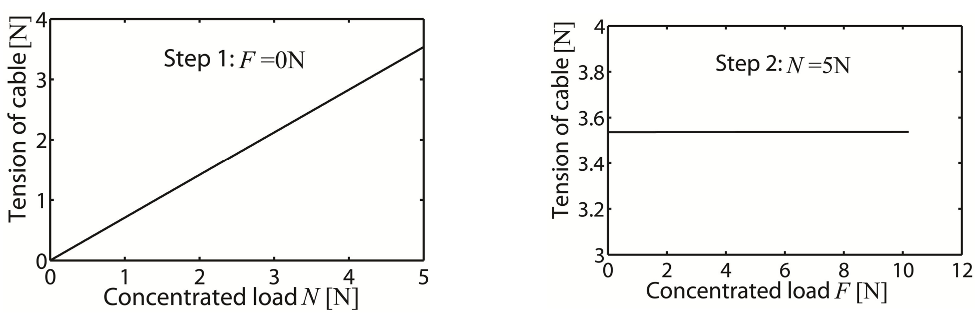

(a) (b)

Fig.6-11 Relationship of tension of cable with N and F

Fig.6-12 shows relationship of the non-dimensional parameter $\frac{N/l_c}{EI_z/l^3}$, the critical load F_{cr} and the pseudo-critical load P_{cr}. Symbols for "num." and "theo." represent the respective results by FE method and by theoretical analysis. P_1 is the critical load of axial compression column with only one side fixed and the other side free, and $P_1 = \pi^2 EI_z/(2l)^2$. And P_2 is the critical load of axial compression column with one side fixed and the other side restrained by hinged ended, and $P_2 = \pi^2 EI_z/(0.7l)^2$.

From Fig.6-12, it can be observed that the FE results of P_{cr} and F_{cr} are almost as same as the results obtained by theoretical method; and this affirms the validity of theoretical method proposed in this section and the stiffness of pseudo-spring in-plane proposed in Section 6.3.1. Therefore it can be concluded that it is tension rather than the intrinsic elastic stiffness of cables that contributes to the stiffening effect of the column.

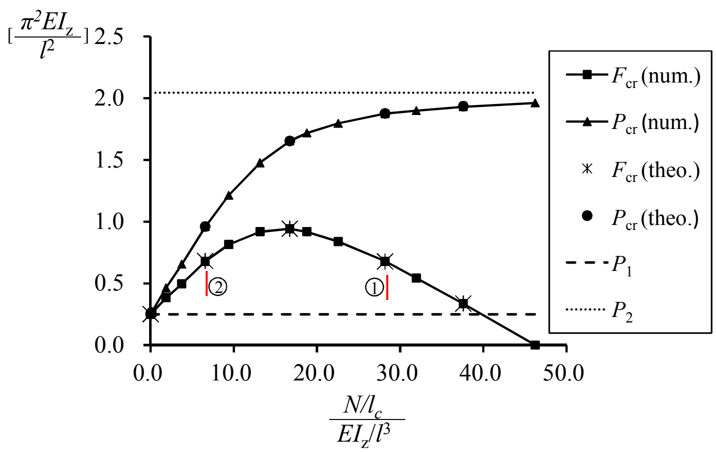

Fig.6-12 Relationship of $\frac{N/l_c}{EI_z/l^3}$, F_{cr} and P_{cr} in-plane

In another aspect, from variation tendency of pseudo-critical load P_{cr}(num.) in Fig.6-12, it can be observed that with the increment of $\frac{N/l_c}{EI_z/l^3}$, P_{cr} changes from P_1 to P_2; this means the side of the column connecting to the cables is restrained from a free situation to a state that is analogous to a hinged ended. And by inspecting the variation tendency of the critical load F_{cr}, when $\frac{N/l_c}{EI_z/l^3} \in [0,16.73)$, F_{cr} is monotone increasing; on contrast, when $\frac{N/l_c}{EI_z/l^3} \in [16.73, 46.24]$, F_{cr} is monotone decreasing. This suggests, although in limiting scope, that the concentrated load N can contribute to stiffening the column, but any overlarge value of the concentrated N will lead to a decrease in F_{cr}. The maximum value of the critical load F_{cr} is $0.94\pi^2 EI_z/l^2$, which is about $3.76P_1$ or $0.46P_2$. This means comparing to a column with one side fixed and the other side free, the maximum critical load F_{cr} of the column has increased about 2.76 times.

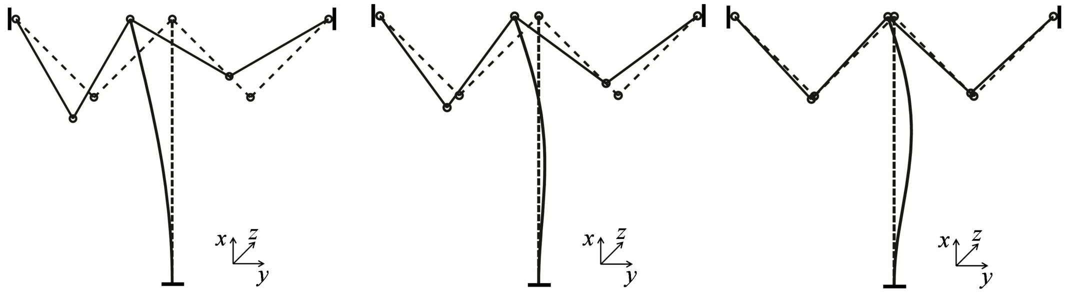

(a) N is small: $\frac{N/l_c}{EI_z/l^3}=0.02$ (b) F_{cr} is max.: $\frac{N/l_c}{EI_z/l^3}=16.73$ (c) $F_{cr}=0$: $\frac{N/l_c}{EI_z/l^3}=46.24$

Fig.6-13 First order buckling modes in-plane by FE method

Fig.6-13 shows the first order buckling modes by FE method. The broken line is the original shape and continuous line is the buckling mode. With the increment of the concentrated load N, the first order bucking modes have experienced transference in-plane.

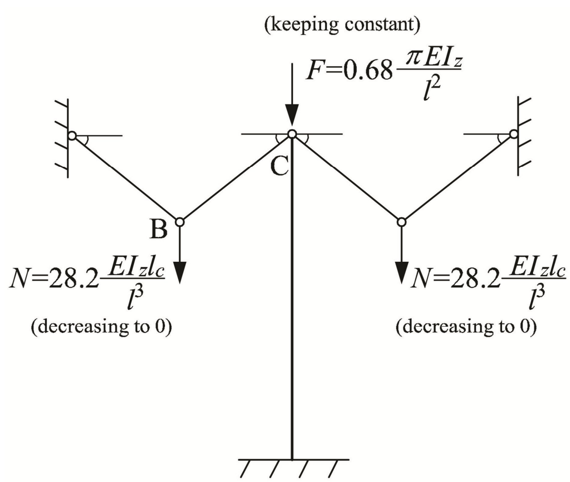

Fig.6-14 Off-loading schematic plot

In another aspect, although Fig.6-12 shows the critical loads F_{cr} corresponding to different concentrated loads N, it is also necessary to find out the safety zone of the whole structure. Here a off-loading schematic plot in Fig.6-14 to explain how to use the configuration in Fig.6-12. In this example, the load pattern in Fig.6-14 is identical to the position ① (28.20, 0.68) in Fig.6-12. In other word, when $\frac{N/l_c}{EI_z/l^3}=28.2$, $F=0.68\frac{\pi^2 EI_z}{l^2}$ can be obtained.

During the discussion, $F=0.68\frac{\pi^2 EI_z}{l^2}$ is assumed as constant, the concentrated loads N applied to the curved cables are decreased at the same time. The coordinate position ② in Fig.6-12 is (6.58, 0.68). When $\frac{N/l_c}{EI_z/l^3}$ is in the field (6.58 28.2), from Fig.6-12 it is known that if the column start to buckling, the values of F are all larger than $0.68\frac{\pi^2 EI_z}{l^2}$, this means the column is safe in all the load patterns when F=$0.68\frac{\pi^2 EI_z}{l^2}$, and $\frac{N/l_c}{EI_z/l^3} \in$ (6.58, 28.2); and the column will collapse in the load patterns when F=$0.68\frac{\pi^2 EI_z}{l^2}$, and $\frac{N/l_c}{EI_z/l^3} \in$ (0, 6.58). Therefore, Fig.6-12 is very useful to design the load patterns for keeping the column safe.

b) Out-of-plane stability

Next the buckling analysis in Fig.6-8 for out-of-plane stability of the column in 3D space is addressed. Similar to the case of in-plane stability of the column in 2D space, the two critical loads of the column are assumed to be $P_1 = \pi^2 EI_y/(2l)^2$, $P_2 = \pi^2 EI_y/(0.7l)^2$. In static analysis based on nonlinear FE method, the column is presumed to have no preexisting imperfection.

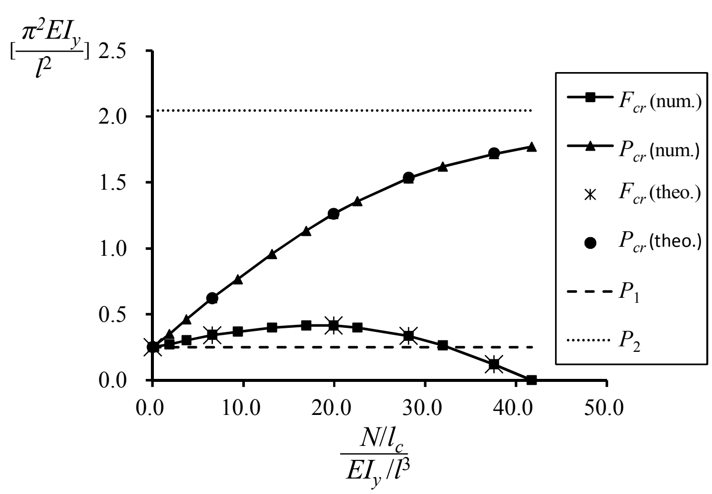

Fig.6-15 Relationship of $\frac{N/l_c}{EI_y/l^3}$, F_{cr} and P_{cr} out-of-plane

Fig.6-15 shows the relationship of non-dimensional parameter $\frac{N/l_c}{EI_y/l^3}$, the critical load F_{cr} and the pseudo-critical load P_{cr}. In Fig.6-15, the nonlinear numerical results of F_{cr} and P_{cr} are almost the same as the results obtained by theoretical methods introduced in this section noted above, so that correctness of the stiffness of pseudo-spring out-of-plane proposed in Section 6.3.2 is also proved.

The variation tendency of pseudo-critical load P_{cr}(num.) also changes from P_1 to P_2, but the maximum of

P_{cr}(num.) is $1.77\pi^2 EI_y/l^2$, while in 2D situation, the maximum of P_{cr}(num.) is $1.96\pi^2 EI_z/l^2$.

In another aspect, the critical load F_{cr}(num.) in Fig.6-15 also firstly increases and after reaching a maximum value $0.42\pi^2 EI_y/l^2$, which is about 1.68 times of P_1 and 0.21 times of P_2, and then it begins to decrease. Compared to the critical load P_1 of column with one side fixed and the other side free, the maximum of F_{cr} has increased about 0.68 times.

The maximum of F_{cr}(num.) is $0.94\pi^2 EI_z/l^2$ in 2D space, but when I_z=I_y is considered, F_{cr}(num.) in the out-of-plane case, it can be observed that the critical load is about 0.45 times the maximum of the critical load F_{cr}(num.) in-plane.

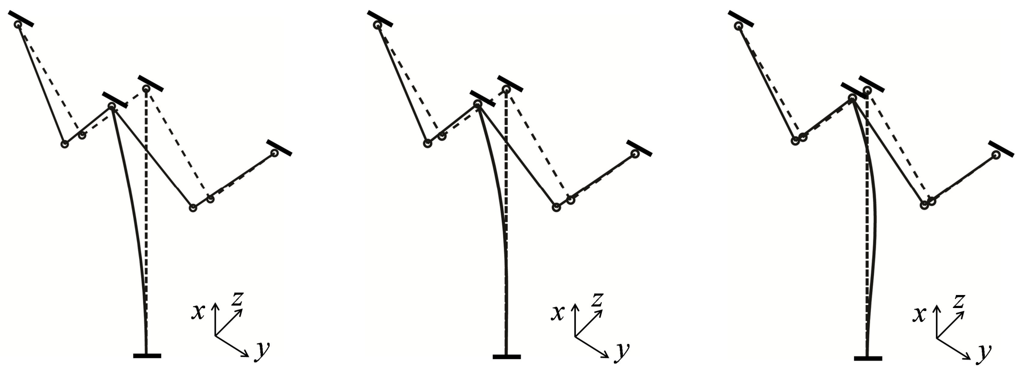

(a) N is small: $\frac{N/l_c}{EI_y/l^3}$ =0.02 (b) F_{cr} is max.: $\frac{N/l_c}{EI_y/l^3}$ =19.92 (c) F_{cr} is 0: $\frac{N/l_c}{EI_y/l^3}$ =41.73

Fig.6-16 First order buckling modes out-of-plane by n FE method

Fig.6-16 shows the transference of first order buckling modes. The broken line is the original shape and continuous line is buckling mode.

6.7 Applications of external force stiffening method

In this pursuit the stability problems of a guyed mast and an arch structure featuring with curved cables are analyzed. When external forces are applied directly to curved cables, curved cables under direct loads could provide a stiffening effect to the main structures. And the stiffening principle of the curved cables is similar to the example of the column in Section 6.5.

6.7.1 Guyed mast

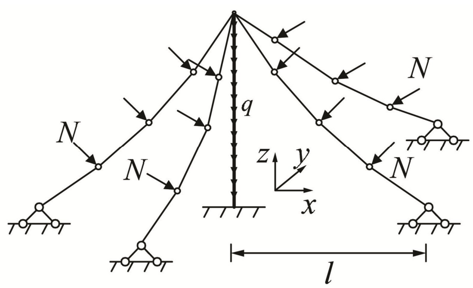

Fig.6-17 Guyed mast

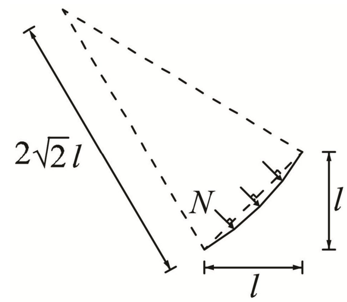

Fig.6-18 Shape of curved cables

Fig.6-17 shows a guyed mast with one side fixed and other side connecting to four curved cables symmetrically. Among the four cables, two of them are located in *xz* plane and other two cables are located in *xy* plane. In nonlinear FE analysis, each curved cable is divided into 4 geometric nonlinear truss elements, and each element has the same length. The entire column is divided into 30 geometric nonlinear beam elements, and each element has the same length. As for one curved cable, it is divided into 4 geometric nonlinear truss elements. Because each curved cable is flexible, the generalized inverse matrix is utilized to avoid the singularity of tangential stiffness matrix, and no elongation displacement method is adapted during calculation, which is introduced in Appendix A.

Concentrated loads *N* are applied to curved cables symmetrically, and the direction of the concentrated load *N* is perpendicular to a line connecting the endpoints of cables, e.g., direction of the concentrated load *N* in *xz* plane in -*x* position is $[1/\sqrt{2}, 0, -1/\sqrt{2}]$. During numerical analysis, the direction of the concentrated load *N* is presumed to be constant and follower force effect of concentrated load *N* is not considered here. In addition, the guyed mast has self-weight with the distributed load *q* in unit length.

Table.6-3 Materials parameters of the guyed mast

	Young's modulus [GPa]	Poisson' ratio	Internal diameter [mm]	External diameter [mm]
Cable	205	–	–	2
Column	205	0.3	20	40

The guyed mast exhibits buckling with the concentrated load *N* and self-weight distributed load *q*. The elevation of the guyed mast is 10m. Fig.6-18 shows the shape of curved cables, which is a part of circle. And Table.6-3 shows the materials parameters of the guyed mast in FE analysis. And nonlinear FE method is used to analyze buckling phenomenon of the guyed mast.

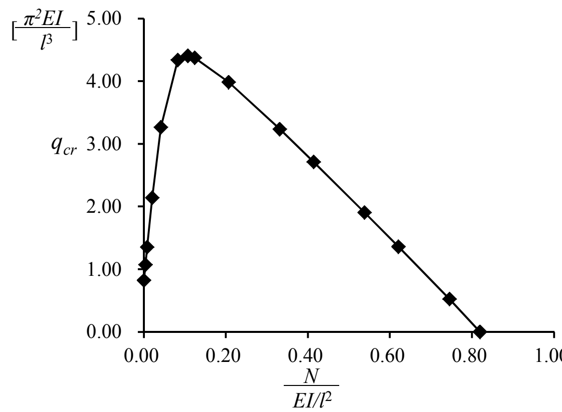

Fig.6-19 Relationship of $\frac{N}{EI/l^2}$ and critical distributed load q_{cr}

In Fig.6-19, I is moment of inertia, which has the same value as I_y and I_z. With increasing of non-dimensional parameter $\frac{N}{EI/l^2}$, the variation tendency of the critical distributed load q_{cr} is very similar to the variation tendency of F_{cr}(num.) in the numerical examples of the column in-plane in Section 6.6. When $\frac{N}{EI/l^2}$ is about 0, $q_{cr} = 0.82\pi^2 EI/l^4$; and when $\frac{N}{EI/l^2}$ is 0.1077, q_{cr} arrives the maximum value equaling $4.41\pi^2 EI/l^4$, which has increased 4.38 times comparing to the one in the situation when the concentrated load N is 0; and when $\frac{N}{EI/l^2}$ is 0.8198, q_{cr} equaling 0 is obtained.

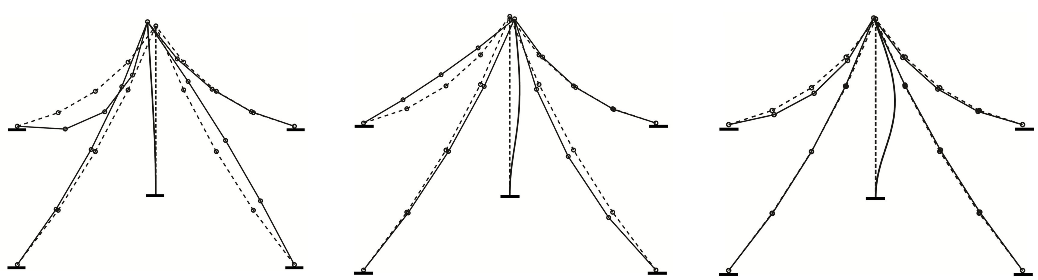

(a) N is small: $\frac{N}{EI/l^2} = 0.0004$ (b) q_{cr} is max.: $\frac{N}{EI/l^2} = 0.1077$ (c) q_{cr} is 0: $\frac{N}{EI/l^2} = 0.8198$

Fig.6-20 First order buckling modes by FE method

Fig.6-20 shows the transference of the first order buckling modes of the guyed mast. The broken line is the original shape and continuous line is the buckling mode.

6.7.2 Arch structure

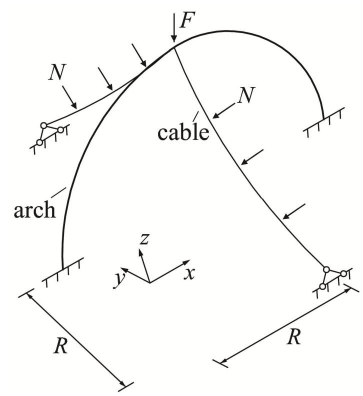

Fig.6-21 Arch featuring with curved cables

Fig.6-21 shows an arch structure featuring with one pair of curved cables. In fact, Fig.6-21 is a simplified special example of the arch with cable-nets shown in Fig.1-4 in Chapter 1. To analyze the buckling behavior of the arch in simple stiffening pattern shown in Fig.6-21 helps to understand the stiffening effect of cable-nets in Fig.1-4 in Chapter 1.

In Fig.6-21, two curved cables are located at the two sides of the arch in *yz* plane symmetrically. The shape of curved cables and direction of the concentrated loads *N* are as same as the ones in Fig.6-18. The radius *R* of the arch is 1 m. The central angel of the arch is π. In FE analysis, the entire arch is divided into 48 geometric nonlinear beam elements with 3.75° along circumferential direction of the arch, and each beam element has the same length. Each curved cable is divided into 4 geometric nonlinear truss elements, and each truss element has the same length. Excluding the concentrated loads *N* applied to curved cables, there is another concentrated load *P* applied to the top of the arch. The boundary conditions of the arch are assumed as fixed ended, and the boundary conditions of cables are assumed as hinged ended overall. Table.6-4 shows the materials parameters of the arch and cables in numerical example.

Table.6-4 Materials parameters of the arch and cables

	Young's modulus [GPa]	Poisson' ratio	Internal diameter [mm]	External diameter [mm]
Cable	205	–	–	1
Arch	205	0.3	6	7

Before the stability of the arch featuring with curved cables in Fig.6-21 is analyzed, the stability of single circular arch without stiffening cables in 3D space shown in Fig.6-22 should be discussed firstly.

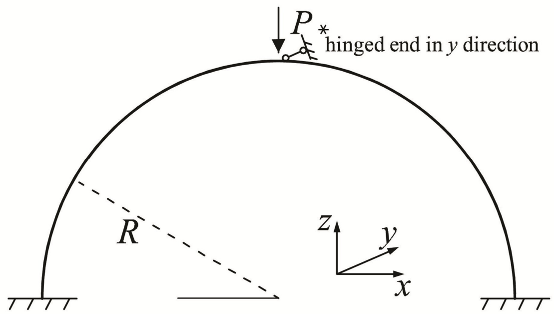

Fig.6-22 Circular arch model

At the top of the arch, a hinged ended is used to support the arch in *y* direction. A concentrated load *P* is applied at the top of the arch. The first order critical loads for the arch without and with hinged ended at the top are noted as P_1 and P_2 respectively. The other conditions, such as geometric shape, boundary conditions, materials parameters of the arch are as same as the ones in Fig.6-21.

Fig.6-23 shows the relationship of displacement and concentrated load in –*z* direction in three dimensional space. From Fig.6-23, P_1=46.8N, P_2=104.3N can be obtained.

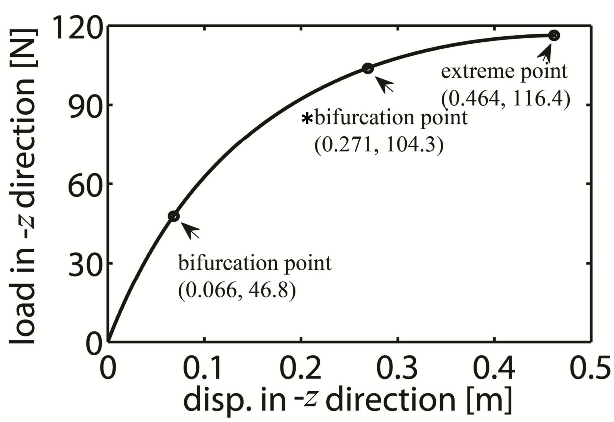

Fig.6-23 The relationship of displacement and load in –z direction

Then the stability of the model in Fig.6-21 is analyzed. Fig.6-24 shows the relationship of the concentrated load on cables and the critical load. The symbols in Fig.6-24 are noted as follows: F_{cr} is the first order critical load, which is applied at the top of the arch when buckling happens. F_z is the resultant force which is transmitted from cables to the top of the arch in -*z* direction. And P_{cr} is the pseudo-critical load, and $P_{cr}=F_{cr}+F_z$.

From Fig.6-24, it can be observed that with the increment of the concentrated load *N*, the critical load F_{cr} firstly increases, after it arrives maximum, it decreases to 0. When the concentrated load N is 4.7N, the critical load F_{cr} arrives maximum, and F_{cr}=75.0N. When the concentrated load N is 25.4N, the critical load F_{cr} equals 0N. In another aspect, the variation tendency of pseudo-critical load P_{cr} is from P_1 to P_2, that is, the increasing of concentrated load N on cables will provide a stiffening effect which is analogous to the case with hinged ended supports.

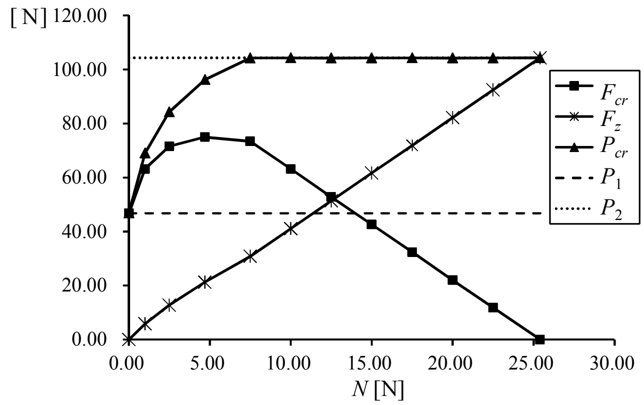

Fig.6-24 Relationship of the concentrated load on cables and the critical load

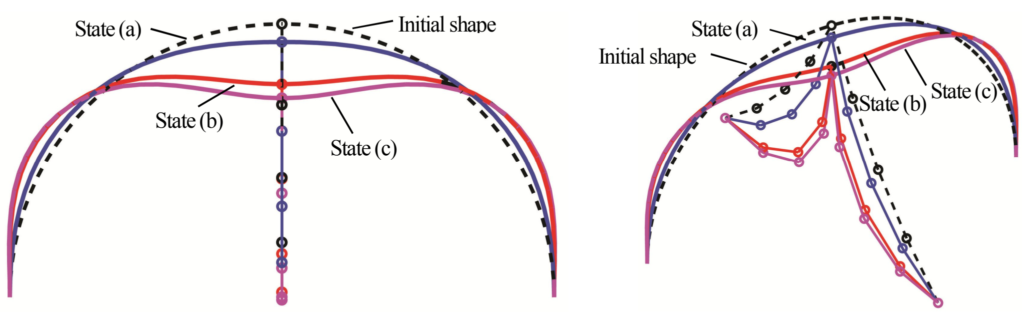

Fig.6-25 Equilibrium shapes of the arch before buckling

Fig.6-25 shows the Equilibrium shapes of the arch before buckling. Black broken line symbolizes the initial shape, and continuous lines (“blue line ”, “red line” and “violet line”) symbolize the equilibrium shapes before buckling happens. “State (a)” is the state when N=10^{-3}(N); F_{cr}=46.8(N); “State (b)” is the state when N=4.7(N); F_{cr}=75.0(N); and “State (c)” is when N=25.4(N); F_{cr}=0.0(N).

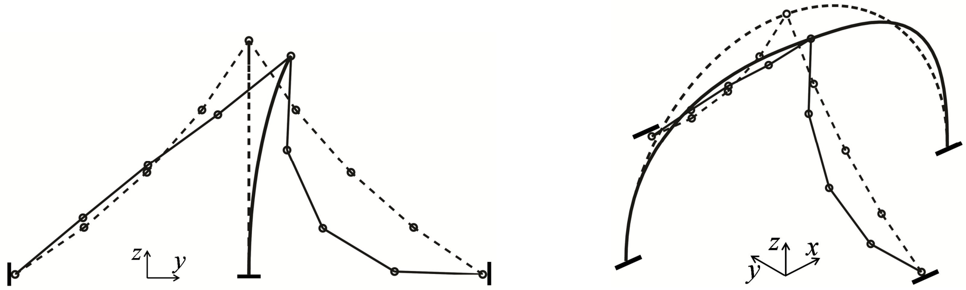

(a) N=10^{-3}(N); F_{cr}=46.8(N); P_{cr}=46.8(N)

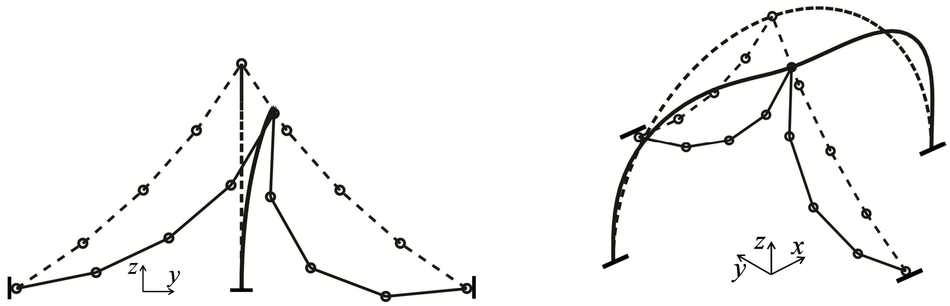

(b) N=4.7(N); F_{cr}=75.0(N); P_{cr}=96.2(N)

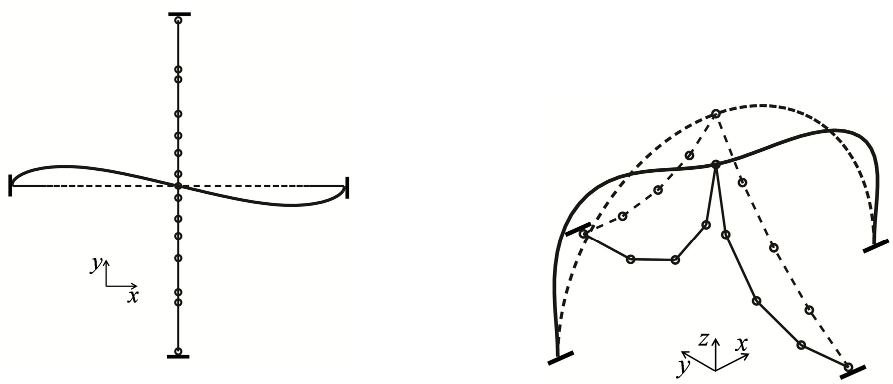

(c) N=25.4(N); F_{cr}=0.0(N); P_{cr}=104.3(N)

Fig.6-26 First order buckling modes of the arch with curved cables

Buckling modes (continuous line) corresponding to three equilibrium states in Fig.6-25 are shown in Fig.6-26. These buckling modes are plotted by directly adding the buckling modes on the equilibrium states before buckling. The broken line symbolizes the initial shape, and the continuous line symbolizes the buckling modes. From Fig.6-26(a) and Fig.6-26(b), for the two cases when N is small and F_{cr} arrives maximum, the buckling modes are translating to out-of-plane of the arch. Meanwhile, from Fig.6-26(c), for the case when F_{cr} is 0, the buckling mode is rotational shape (Fig.6-26(c)).

6.8 Summaries

In this chapter, a new concept of stiffening methods called external force stiffening method is proposed. The characteristic of this method is by applying external loads directly to flexible components to stiffen the structures. The major achievements are summarized as follows:

1) In external force stiffening method, the elastic stiffnesses of curved cables can no longer provide stiffening effect to structures, and the external force in components can produce a stiffness called stiffness of pseudo-spring to stiffen structures.

2) By using a column model featuring with curved cables, the stiffnesses of pseudo-springs both in-plane and out-of-plane are deduced. Meanwhile, the buckling control equations of this structure system are also derived. And by comparing the results obtained by nonlinear FE method and by theoretical approach, the validities of theoretical approach and formulations of stiffnesses of pseudo-springs are proved.

3) External force stiffening method can be applied to a guy mast structure and an arch structure featuring with curved cables. The stiffening effects of curved cables and variation of the critical load are very similar to the ones in anterior column's example. And transferences of buckling modes in these two application examples are also studied.

4) External force stiffening methods have a similar characteristic: if there are external loads applied to flexible components, and the other loads applied in main structure. Then in limiting scope, the external loads on flexible components can enhance the stability of structures, but these oversize external loads will also lower the stability of structures. In other word, there are optimal values of loads on flexible components to obtain the best stiffening effects.

Chapter 7 Model Experiments

7.1 Introduction

As in positively pressured pneumatic structure system, heavy and strong maintenance structure in boundary is needed to resist the inflation force of membrane. For this reason, it cannot uttermost exert the convenience of pneumatic structure. Then we begin to consider the possibility of the negatively pressured one for the application in the first-aid shelter, because in first-aid shelter the facility of construction work is mostly emphasized. In this chapter, we discuss three experimental shelters with negatively pressured pneumatic type. The main skeletons of these structures are made of arches. These three shelters are called hemispheric shelter, rectangle shelter and a round shelter respectively.

In the type of negatively pressured pneumatic structure, membranes or cables may deform into curved shape when they are under negative draught head. These kinds of flexible components under directly loading may provide stiffening effect to the main structure, as are discussed in the Chapter 6. Then a load test experiment is processed in a column structure featuring with curved cables to verify this view.

7.2 Shelters with negatively pressured pneumatic structures

7.2.1 Hemispheric shelter

The object of this experiment is to observe the buckling phenomenon of skeleton. In addition, ropes are used as a kind of constraint components to stiffen the skeleton and the stiffening effect of the ropes are investigated.

1) Model of the skeleton

Fig.7-1 Miniature model of hemispheric shelter

Fig.7-2 Special joint at the top

The shape of hemispheric shelter is a dome, the skeleton of which is made of 6 semi-circular arches. Fig.7-1 shows a miniature model. In experiments of the full-scale model, we made a special joint for all the semi-circle arches, as shown in Fig.7-2. And Fig.7-3 shows the PVC pipes, which are the materials of skeleton. The PVC pipes are hollow circular cross section, and the external diameter of pipes is 32cm, their thickness is 3.5cm. And Fig.7-4 shows the joints of PVC pipes. Fig.7-1 ~Fig.7-4, and the construction materials refer to Reference [36].

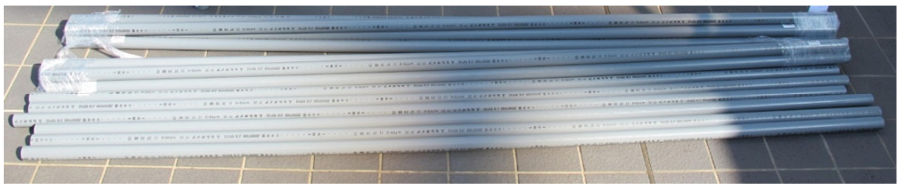

Fig.7-3 PVC pipes

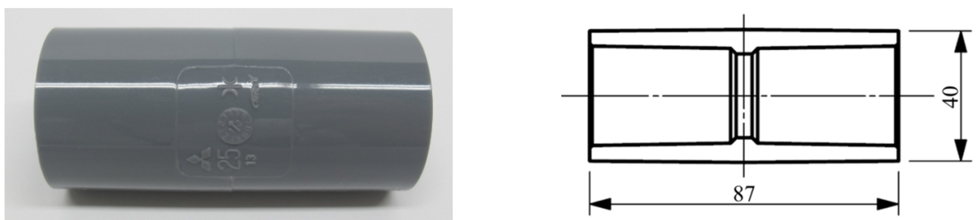

(a) (b)

Fig.7-4 Joint of PVC pipes

In the full-scale experiment is carried out at the terrace of EW building of the Institute of Industrial Science in the University of Tokyo in January 12th, 2012. The diameter of semi-circular arches in design is 6m. The shape of boundary is dodecagon, the radius of internal tangential circle is 3m.

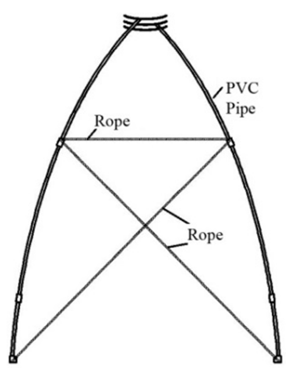

Fig.7-5 Setting of stiffening rope

Totally 36 cotton ropes are used to stiffen the skeleton of semi-circular arches. Fig.7-5 shows the arrangement of ropes between two adjacent arches. Two cross ropes are set up between adjacent arches. And one additional rope is put in horizontal direction.

The procedure of experiment is carried out as follows[30]:

Step 1): The positively pressured pneumatic structure is constructed. And PVC pipes are used to make 6 circular cross arches inside (Fig.7-6). The membrane contacts skeleton naturally without any connecting joints.

Step 2): The air to make the negatively pressured one is deflated. Gradually the skeleton began to resist the draught head and suddenly buckling phenomenon of skeleton happens (Fig.7-7). At this time, the draught head is measured as approximately -50Pa.

Step 3): The air is deflated again. The skeleton is modified to the shape in Fig.7-6, and then 36 ropes are utilized to stiffening the skeleton (Fig.7-5). After finishing the stiffening work, the air is deflated again. Fig.7-8 shows a stabilization state of skeleton with ropes. Buckling phenomenon occurs at approximately -70 Pa (Fig.7-9).

(a) Outside view (b) Inside view

Fig.7-6 Construction of skeleton (+110Pa)

(a) Outside view (b) Inside view

Fig.7-7 Buckling phenomenon in step 2 ($\approx$-50Pa)

(a) Outside view (b) Inside view

Fig.7-8 Stabilization state in step 3 (-30Pa~-40Pa)

(a) Outside view (b) Inside view

Fig.7-9 Buckling phenomenon in step 3 (≈-70Pa)

2) Numerical analysis

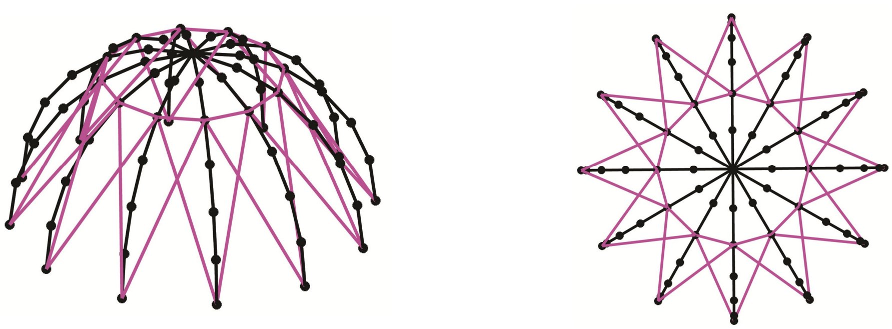

(a) Perspective drawing (b) Plane graph

Fig.7-10 Numerical model

Numerical analysis is carried out for comparison, its model is shown in Fig.7-10. The radius of semi-circular arches is 3m. In FE analysis, the entire arch is divided into 12 linear beam elements with same length. And each cable is divided into one linear truss element. And external loads are calculated by the draught head and approximate projection areas between two circular arches (the edges of triangle or quadrangle parallel to horizontal plane keep constant, the heights of them in projection plane are all assumed as one-sixth of the radius), and the external loads are applied in the radial direction[30]. The boundary conditions are assumed as hinged ended. The materials parameters are shown in Table.7-1. Young's modulus and Poisson's ratio of PVC pipes refer to standard of Japan PVC Pipe and Fittings Association.

Table.7-1 Materials parameters of numerical example

	Young's modulus [GPa]	Poisson's ratio	Internal diameter [mm]	External diameter [mm]
Rope	10.8[23]	–	–	10.5
Arch	3.33	0.38	25	32

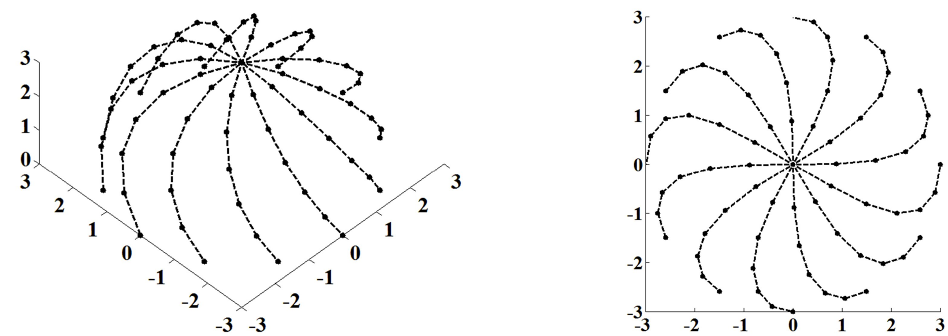

(a) Perspective drawing (b) Plane graph

Fig.7-11 First order buckling mode without ropes (First order critical load=-8.6Pa)

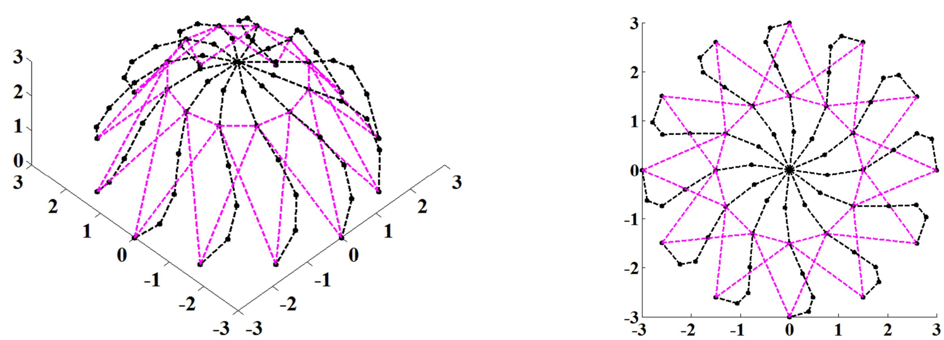

(a) Perspective drawing (b) Plane graph

Fig.7-12 First order buckling mode with ropes (First order critical load=-44.0Pa)

Fig.7-11 and Fig.7-12 shows the first order buckling modes of dome without and with stiffening ropes. Both shapes of these two modes are rotating along the longitudinal direction of dome. When there are stiffening ropes, during the static calculation, for -1Pa draught head, the internal force of inclined ropes and horizontal rope are positive value and negative value respectively. Then all the horizontal ropes are omitted in Fig.7-12 and the numerical model is modified (omitting the horizontal rope in Fig.7-5). The result of modified model is shown in Fig.7-13. In static analysis, the internal force of inclined cables becomes positive value for -1 Pa draught head.

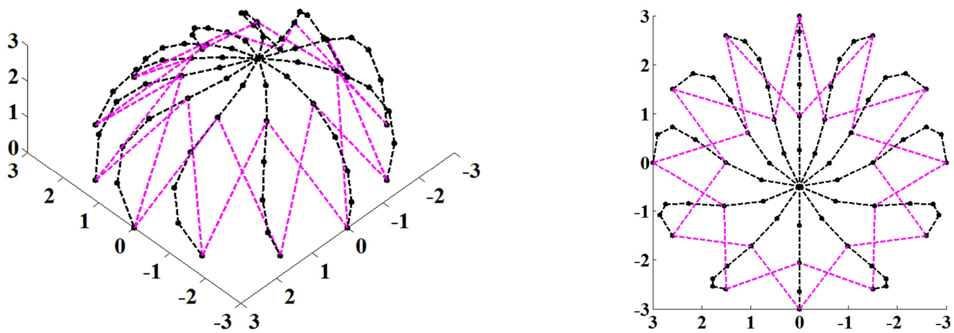

(a) Perspective drawing (b) Plane graph

Fig.7-13 First order buckling mode with ropes (First order critical load=-25.2Pa)

3) Summary of results of experiments and numerical analysis

a) The experiment results in Fig.7-7 and numerical result in Fig.7-11 are compared. The critical load in experiment is approximately -50Pa, while the numerical result is -8.6Pa, about 17% of experimental one. And the buckling phenomenon in experiment and the first order buckling mode in Fig.7-11 are both rotational modes along the longitudinal direction of dome.

b) When the buckling phenomenon in Fig.7-9 is investigated, we can observe most of the horizontal ropes are slack. So it is better to use the numerical results in Fig.7-13 for comparison. The critical load in experiment is approximately -70Pa, while in numerical analysis, the result is -25.2Pa, about 36% of experimental one. It can be observed the inclined ropes increase the strength of dome. While comparing the buckling modes in Fig.7-9 and in Fig.7-13, in Fig.7-9 the buckling phenomenon of dome is local buckling, e.g. pipes are indenting in specific arches, and in Fig.7-13 the buckling mode of dome is global buckling behavior translating along the axis of symmetry.

c) As the experimental model is only a testing model, and there are a lot of initial imperfection existing in the skeleton, and the internal force in every arches may have great difference and then focus on some specific components. In fact, the shapes of arches may not be semi-circular and the force transmitting to arch from membrane are unknown in experiments. The boundary conditions are also complex, which is not identical to hinged ended used in numerical analysis.

7.2.2 Rectangle shelter

In order to welcome the 2012 Open Campus of Institute of Industrial Science in June 1st and June 2nd in 2002, we constitute a new rectangle shelter for exhibition at the same place of former shelter. The dwelling space for dwelling is considered to be able to afford 5 people, which is assumed as be basic unit of family. Fig.7-14 shows the design sketch of rectangle shelter[35]. And Fig.7-15 shows a miniature model of skeleton[36]. In this section, Fig.7-14~Fig.7-15, Fig.7-17~Fig.7-21 are provided by two co-operators in the same experiment Afra [35] and Hong [36].

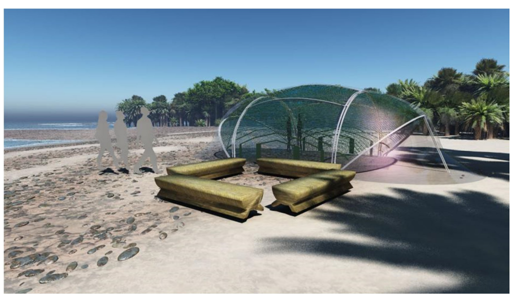

Fig.7-14 Design sketch of rectangle shelter

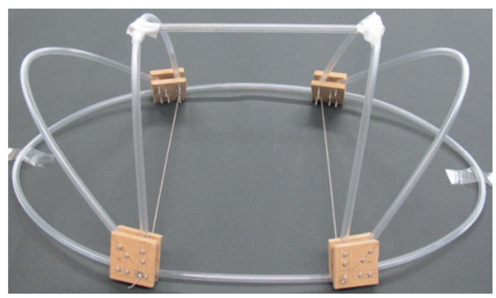

Fig.7-15 A miniature model of skeleton

The skeleton of shelter is mainly made by six semi-circular arches, two arches are on the ground, two arches is 45-degree inclining to the ground, two arches are perpendicular to the ground, and the other two are located at ground. In order to maintenance the shape of membranes and skeleton, we use net and ropes as constraint components between the skeletons. The skeleton are also made of PVC pipes as same as the ones used in former shelter. All the construction materials are stated in Reference [36]. The design size is shown in Fig.7-16.

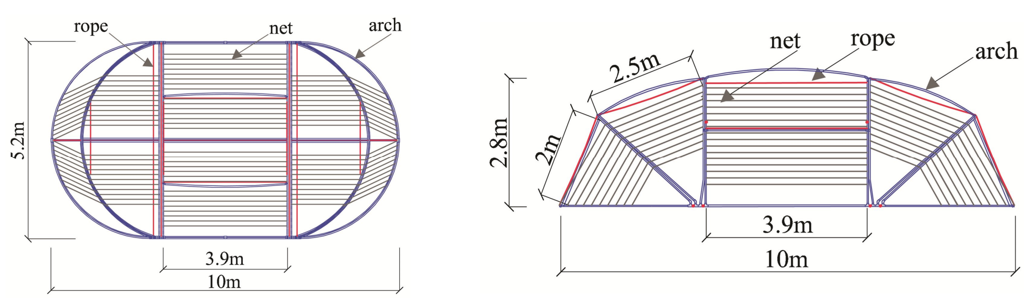

(a) Plane graph

(b) Vertical view

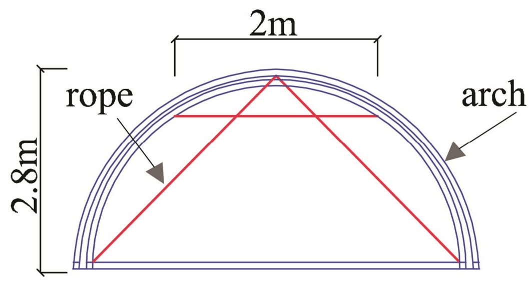

(c) Sectional view

Fig.7-16 Design size of rectangle shelter

The experiments are carried out two times. The first time is a pre-experiment, it is at 25th April, 2012. The constriction procedure are written explicitly by co-operators in this experiment Afra [35] and Hong [36]. The size of PVC membrane is a square with lateral length 14m. Fig.7-17 shows configuration of rectangle shelter in 25th April.

(a)

(b)

Fig.7-17 Rectangle shelter

During experiment, we extend the surplus membrane to the ground as long as possible, and then we deflate the air to turn the structure into a negatively pressured one (Fig.7-17(b)). During the increment of draught head, we could observe that PVC membrane in the ground is beginning to cling to the ground. Finally we succeed in making the negatively pressured pneumatic structure without additional maintenance structure in the boundary. And when the draught head is about -30 Pa, the buckling phenomenon happens obviously in the arches and then we stop deflating. Fig.7-18 shows the buckling phenomenon of skeleton. In another aspect, during the experimental experience in Fig.7-17 and Fig.7-18, we also find out that if the average length of surplus PVC membrane in the boundary is approximate 1.5m, the negatively pressured pneumatic structure is easily to realize.

Fig.7-18 Buckling of skeletons of rectangle shelter in April (≈-30Pa)

In addition, in order to estimate the effect of surplus PVC membrane in the boundary, we put the surplus PVC membrane inside of skeleton, as shown in Fig.7-19. But at this time, even though we try to deflate the air, but the draught head cannot be reduced. For investigation of the reason, we can consider that when surplus membranes are put inside of the skeleton, air leakage is very remarkable during deflating, so the negatively pressured pneumatic structure cannot be made successfully.

Fig.7-19 New folding method of membranes in the boundary

In the second time of experiment during 23th-25th May, 2012. This time we constitute negatively pressured one according to the original design sketch in Fig.7-15. And Fig.7-20 shows the accomplished skeleton and the whole structure with membranes. The construction works totally takes about 4hours with the help of 7 people.

(a)

(b)

Fig.7-20 Rectangle shelter in May

The deflating experiment is totally carried out three times. The explicit experimental process is introduced in

Reference [36]. Here only the experimental results are listed. Fig.7-21 shows three configurations during all the experiments in May, 2012. In Fig.7-21(a), when the draught head is -33Pa, no obvious buckling phenomenon is observed. When the draught head becomes about -42Pa, two horizontal bars between the semi-circular arches at the waist area indent suddenly. And the draught head is reduced to about -71Pa, the horizontal bar between the semi-circular arches at the peak area is indenting too. Meanwhile, we can observe buckling of the erected two semi-circular arches also happens.

(a) Stable state (Draught head≈-33Pa)	(b) Two horizontal bars buckling (Draught head≈-42Pa)	(c) Global buckling (Draught head≈-71Pa)

Fig.7-21 Deflating experiment in May

7.2.3 Round shelter

1) Constructions of round shelter in practice

(a) (b)

Fig.7-22 Design sketches of round shelter [35]

In the anterior two experiments in negatively pressured pneumatic structure, the skeletons are mainly constituted by PVC pipes, the buckling phenomenon of skeletons is observed. So this time we use mental materials with higher strength to constitute the skeleton. In this section, Fig.7-22~Fig.7-23, Fig.7-26~Fig.7-31 are provided by the co-operator in this experiment Afra [35]. Aluminum pipes are elected because of the light-weight merit. The external diameter of pipes is 32mm, and the thickness is 3mm. The design sketch of round shelter is shown in Fig.7-22.

Fig.7-23 shows the design size of round shelter [35]. The main skeleton of this shelter is made of five semi-circular arches. Four of them is used to constitute two circles. And other one is used to make the ceiling at the top. Ten ropes are used to connect the top arch to the circle at the middle.

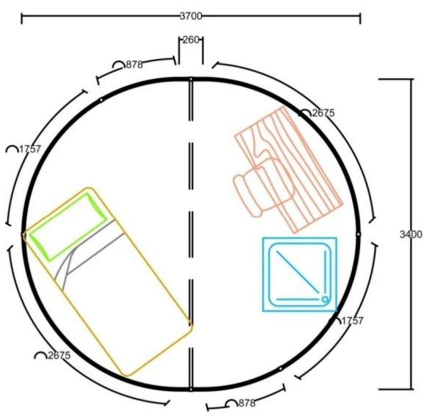

(a)

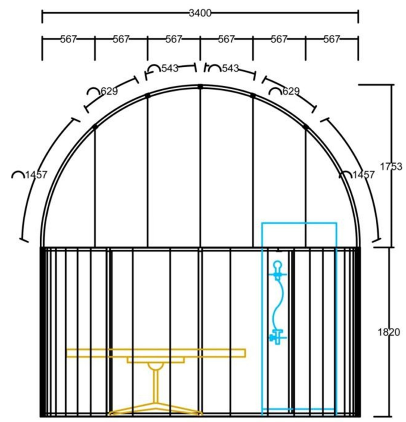

(b)

Fig.7-23 Design size of round shelter

We also design the specific columns and joints in the design, as shown in Fig.7-24. We divided the column into two types: type I and typeⅡ.And the number of type I column is 4, and of typeⅡcolumn is two. And Fig.7-25 shows two types of joints, the number of crisscross type joints and T-type joints are two respectively.

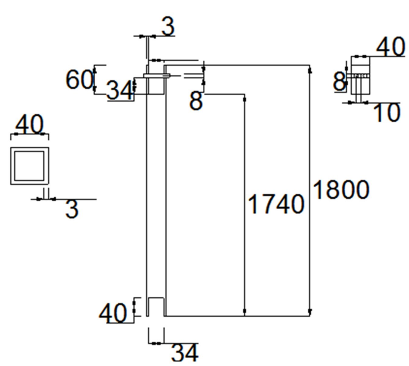

(a) Column type I

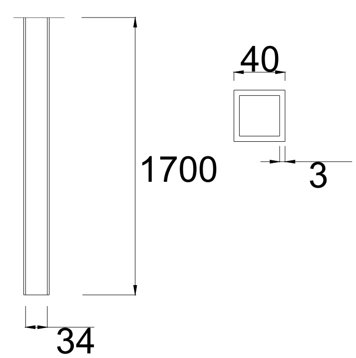

(b) Column typeⅡ

Fig.7-24 Two types of columns

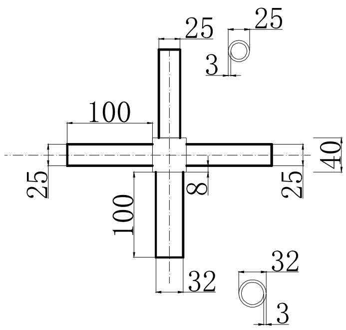

(a) Crisscross type joint

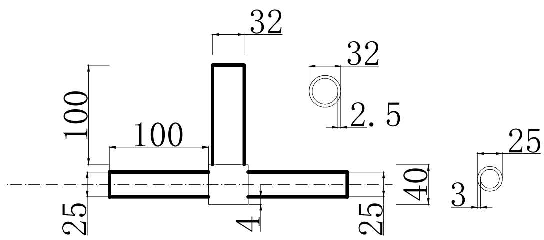

(b) T-type joint

Fig.7-25 Two types of joints

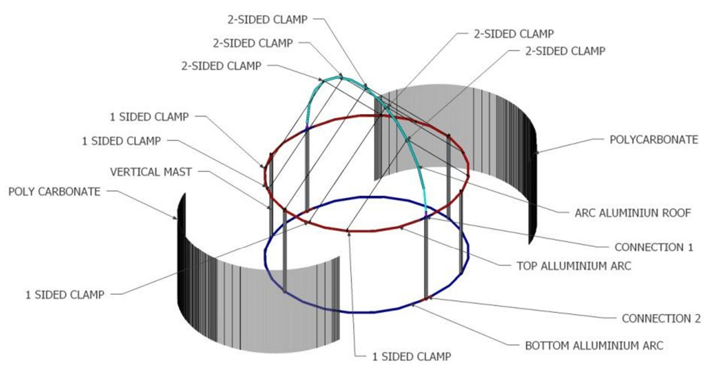

(a)

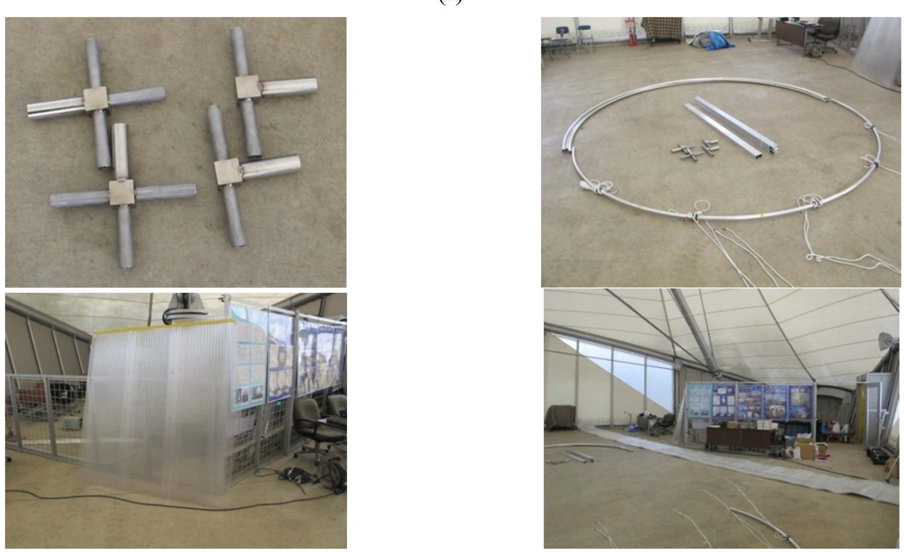

(b)

Fig.7-26 Components of round shelter

Fig.7-26(a) shows the constituted components of skeleton. And Fig.7-26(b) shows the actual objects used in construction. Polycarbonate sheets are used to make the wall of round shelter.

The experiment is carried out during 7th-11th in the buckling of white rhino at CHIBA Experimental Station in the University of Tokyo. During the construction process, as the dome has a height of about 3.5m, so it is hard to lift up whole heavy PVC membrane after the accomplishment of entire skeleton. Then we think out a method in the construction. The construction procedure is carried out in four steps as follows:

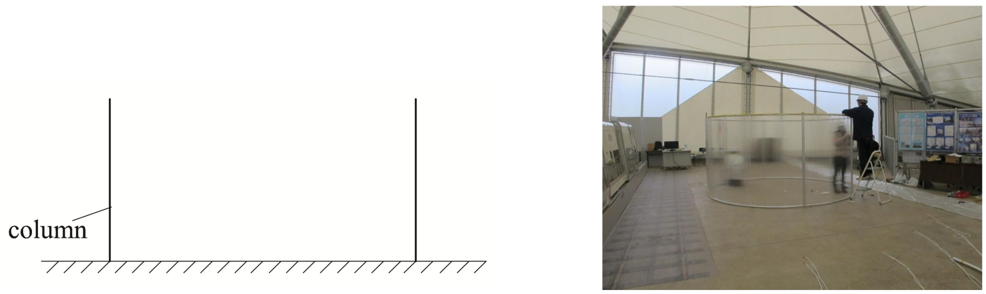

(a) Step one

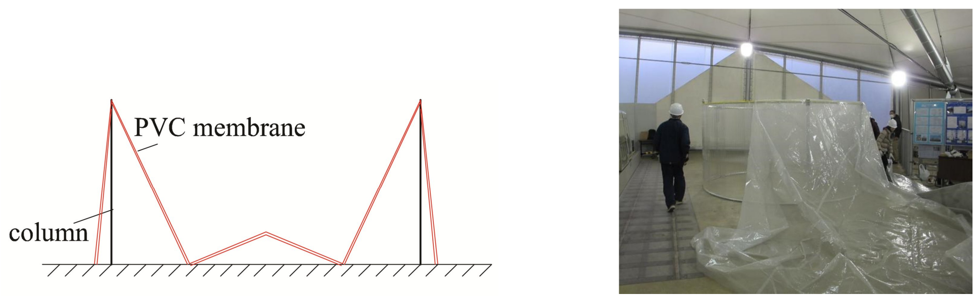

(b) Step two

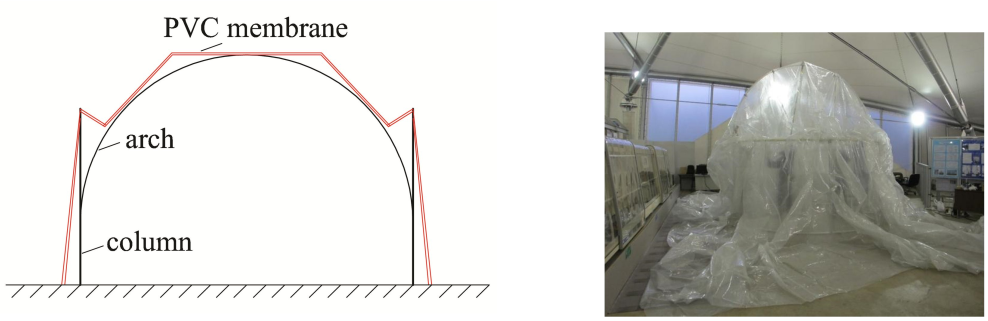

(c) Step three

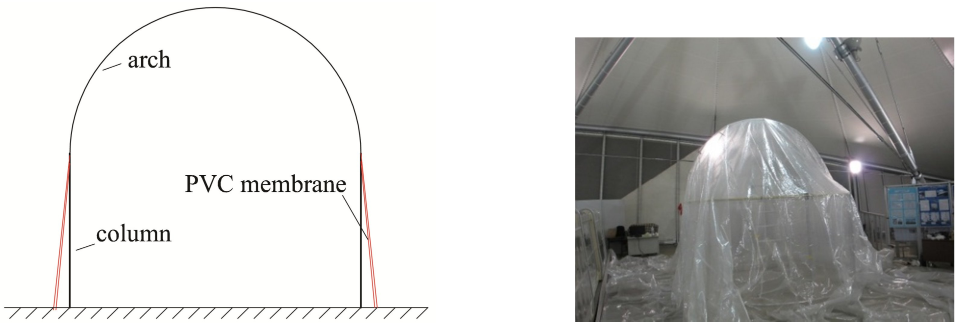

(d) Step four

Fig.7-27 Construction procedure

(a) Outside view (b) Inside view

Fig.7-28 Accomplished configuration at daytime

Fig.7-28 shows the accomplished structure. And we also extend the surplus PVC membrane in the boundary as long as possible (Fig.7-28(a)). The red type in Fig.7-28(a) is the location of door. We totally take four times deflating experiments. The minimum of draught head is about -60 Pa. We don't reduce the ultimate draught head make the skeleton buckling. Fig.7-29 shows one of the experimental configurations.

Fig.7-29 The experimental configuration

And Fig.7-30 shows dwelling experience in the round shelter during the night in January 10th, 2014.

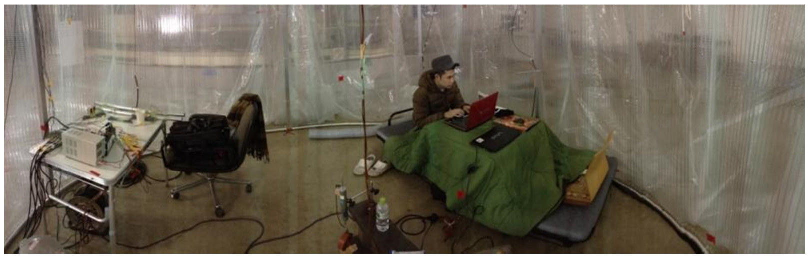

Fig.7-30 Dwelling experience in the night

Fig.7-31 Construction of shelter outdoors

In order to simulating the real construction outdoor, we built this round shelter on the grass in CHIBA campus of the University of Tokyo, shown in Fig.7-31. As there are too much gaps on the grass, even though we use the 400w blower to deflate, the draught head almost not changed. The purpose to realize the negatively pressured pneumatic structure fails outdoors.

2) Simulation of negatively pressured pneumatic structures

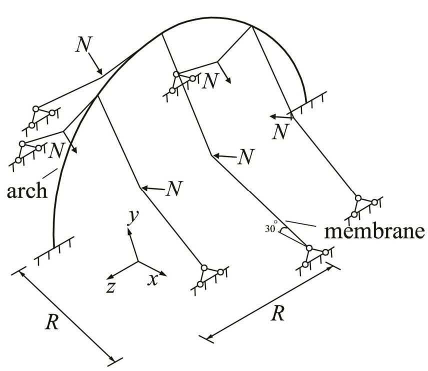

Fig.7-32 Model of the arch

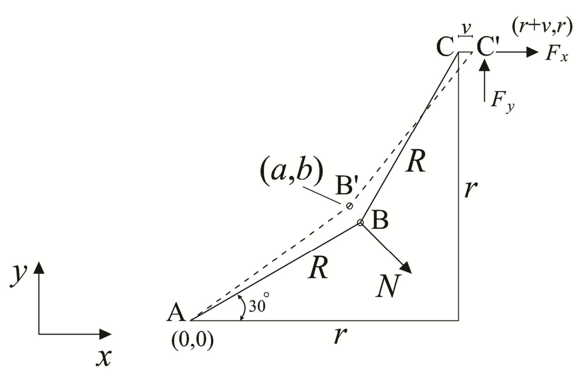

Fig.7-33 Mechanistic movements of the membrane

Now let's take discussion on the stiffening effect of membranes under negative draught head in round shelter.

We take the semi-circular arch at the top in Fig.7-23 as the research object. And other four semi-circular arches are taken into consideration this time.

We also make some assumptions. When membrane is under negatively draught head, we assume the angles between the membranes and horizontal plane are all 30°, and membranes are in curved shape under the concentrated loads N, as shown in Fig.7-32. The total loads of negative draught head are simplified as several same concentrated loads applied in membranes, and membranes are assumed be curved lines.

The configuration in Fig.7-33 is parts of the membranes in Fig.7-32. In Fig.7-33, membranes (seen as curved lines) experience mechanistic movements of membrane in x direction. The coordinates of A, B' and C' after movements are (0, 0), (a, b), and (r+v, r) respectively. The top circular arch in round shelter is 1.7m. Appendix D gives the stiffnesses of pseudo-springs by using the model in Fig.7-33.

Now the buckling problem of the arch considering the stiffening effect of membrane is analyzed. In numerical analysis, the entire arch is divided into 46 linear beam elements, and these elements have the same length. We use stiffness of pseudo-springs to substitute the curved membranes, and then model in Fig.7-32 will be equal to the one in Fig.7-34 (a).

In theoretical analysis in Chapter 4, the load pattern of the arch is assumed as uniform compression, but in practice external force may not always be this kind of load pattern, in Fig.7-34 (a), P_1~ P_{47} are the resultant forces transmits from membrane to the arch, and these loads are all in vertical direction. In order to comparing the results in Fig.7-34 (a), load pattern with uniform compression in radial direction is also assumed in Fig.7-34(b). And the loads and corresponding pseudo-springs in Fig.7-34(b) are as same as the ones in Fig.7-34(a).

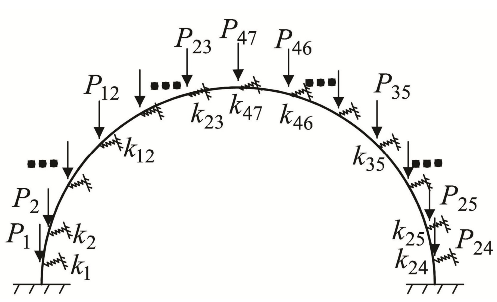

(a) Vertical load pattern

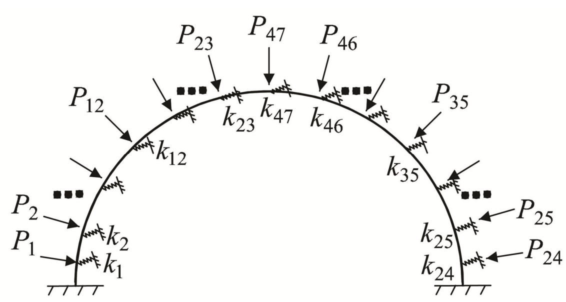

(b) Radial load pattern

Fig.7-34 Arch models with pseudo-springs

In order to obtain these resultant forces in Fig.7-34(a) and Fig.7-34(b), all the external forces in membranes are assumed to be equally distributed in to 49 concentrated loads N in Fig.7-32 at each side. The total external force is calculated by multiply of draught head and superficial area of one quarter sphere. By this assumption, when draught head is -1Pa and the radius R of the arch is 1.7m, the concentrated load N at all the nodes are 0.1853N. The relationships of the concentrated load N and P_1~ P_{47} are given in Appendix D. Here a line load q (unit: N/m) is assumed. And if the draught head is negative and equals -1Pa, the value of q can be calculated as 0.1853×3.3461×49/1.7/pi=5.6887N/m.

Table.7-2 Materials parameters of numerical example

	Young's modulus [GPa]	Poisson's ratio	Internal diameter [mm]	External diameter [mm]
Pipe	68.6	0.34	26	32

The materials parameters of pipes are given in Table.7-2. In numerical analysis, the boundary conditions of pipes are assumed to be fixed ended both in-plane and out-of-plane. The moments of inertias I_x and I_y in local coordinate referring to toFig.4-2 in Chapter 4 are the same, and I_x=I_y =I is established. Table.7-3 shows the comparison of the first order critical loads and buckling models in vertical load pattern and radial load pattern.

Table.7-3 Comparison of the first order critical loads and buckling modes

	(a) Vertical load pattern	(b) Radial load pattern
Models without pseudo-springs	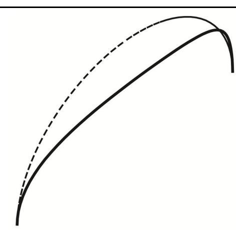 $q_{cr} = 2.23\frac{EI}{R^3}$	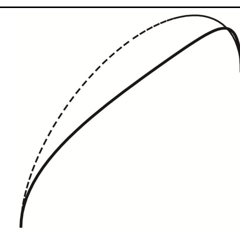 $q_{cr} = 2.51\frac{EI}{R^3}$
Models with pseudo-springs	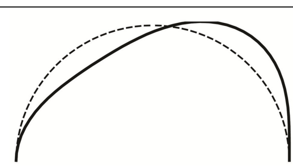 $q_{cr} = 8.67\frac{EI}{R^3}$	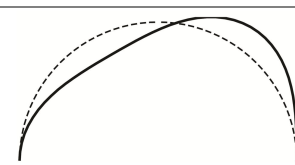 $q_{cr} = 8.15\frac{EI}{R^3}$

7.3 Loading test experiment

In Chapter 6, a concept called external force stiffening method is proposed. And in Section 7.2.3, simulation of curved membranes under negative draught head is discussed. In this chapter in-plane stability of a column featuring with curved cables is studied through loading test experiment.

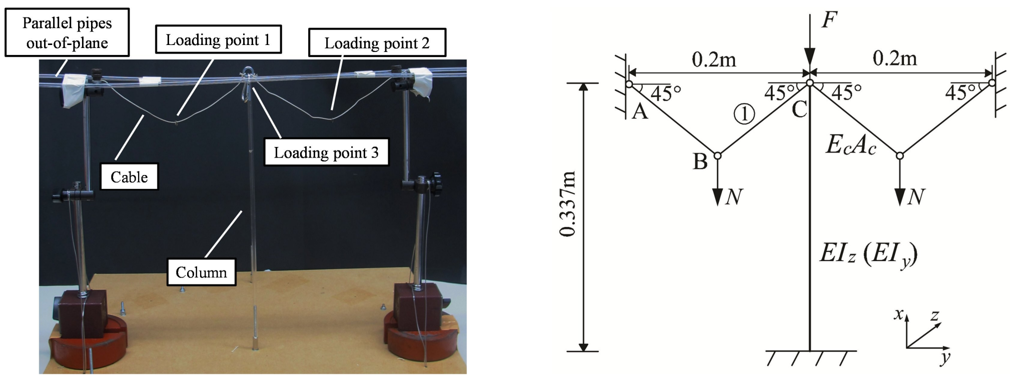

(a) Experimental model (b) Numerical model

Fig.7-37 Experimental model and numerical model

We carry out a loading test experiment of column with curved cables in 15th November, 2012 in the Laboratory. Fig.7-37(a) shows the experimental model. The column is made of a PVC pipe, the external diameter of PVC pipe is 6mm, its internal diameter is 4mm. We insert one side of the column into a screw to fix it. Two curved cables connect to the top of column symmetrically. At the same time, two parallel pipes are set up at the top of the column to prevent the out-of-plane movement of column. The material of cables is cotton, its diameter is 1mm. During the experiment, same weights are applied at loading point 1 and loading point 2 in Fig.7-37(a). Then another weight is applied at loading point 3 gradually until buckling of the column happens.

According the Japan PVC Pipe and Fittings Association, the Young's modulus of PVC Pipe is 3.33GPa, and the Poisson's ratio is 0.37~0.38. Pre-experiment is carried out to determine the Young's modulus of the PVC pipe. The length of PVC pipe excluding the support boundary is about 83.2cm, and the model of simply supported beam is used. A 30g weight is applied at the center of the PVC pipe. The measurements of vertical displacements at the center are 2.6cm, 2.5cm and 2.5cm, the average value of displacements is assumed as 2.5cm. For a simply supported beam with a length L, the vertical displacement with the concentrated load F at the middle position can be obtained through formulation $\Delta u = FL^3/48EI$. By using this formulation the approximate Young's modulus of PVC pipe is obtained as 2.82GPa. And the Poisson's ratio is assumed as 0.38.

Fig.7-37(b) shows the numerical model. The length of column is 0.337m excluding the length of screw in the boundary. The angel of the curved cable and the horizontal line is about 45°. In numerical analysis, the column is divided into 30 geometric nonlinear beam elements, and each of elements has the same length. And one cable is divided into one geometric nonlinear truss element. Referring to Reference [23], the Young's modulus of the cotton cable is assumed as 10.8GPa.

When there is no preexisting imperfection of column, by nonlinear FE analysis we can obtain at N=15.0N, F=8.4N, buckling of the column happens. In another aspect, by using the theoretical procedures in Section 6.5, we can obtain at N=15.0N, F=8.47N, buckling of the column happens.

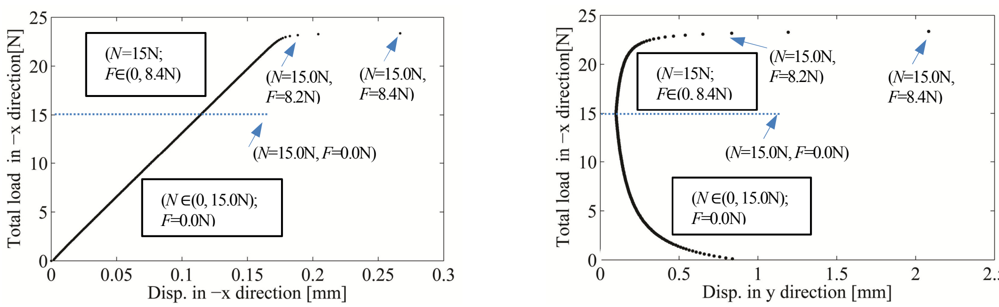

(a) (b)

Fig.7-38 Relationship of displacement and total load

In another aspect, the preexisting imperfection of the column is considered, in FE analysis a disturbing load with value 0.01N is applied in y direction at the position C in Fig.7-37(b). Fig.7-38(a) and Fig.7-38(b) show the relationship of displacements in -x direction/ y direction and total load respectively. Here the total load means the absolute value of resultant force at the position C in –x direction, which comes from N and F.

From Fig.7-38(a) we can observe the displacement in –x direction is monotone increasing during the loading process. And when N=15N, if F is larger than 8.2N, the displacement in x direction increase very quickly, we can suppose the column starts to collapse at the conditions when N=15.0N, and F=8.2N. Comparing to the case without preexisting imperfection, as the results of critical loads in these two cases are closed to each other, in the latter analysis only the numerical results in the case without preexisting imperfection are given.

From Fig.7-38(b), because of the preexisting imperfection, when N and F are both 0N, the displacement in y direction is 0.886 mm. Then in numerical analysis, firstly we keep F=0.0N, then N is increased from 0N to 15.0N, we can observe the preexisting displacement in y direction is decreasing, this phenomenon can be seen as that the curved cables begin to provide the stiffening effect. And when N arrives 15.0N, we keep N constant then we increase the F from 0N to 8.4N, then the displacement in y direction increases again.

Table.7-4 Comparison of results in experiment and numerical results

No.	Experimental results	Numerical results (no-preexisting imperfection)
1	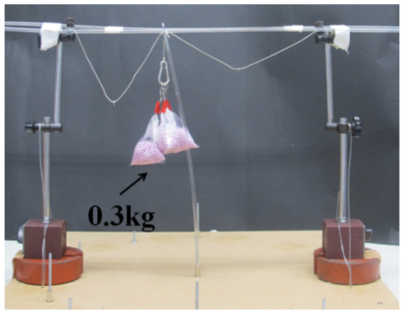 N=0kg; F_{cr}=0.3kg	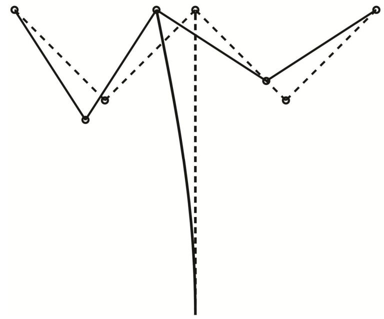 N=10$^{(-2)}$N; F_{cr}=3.1N
2-1	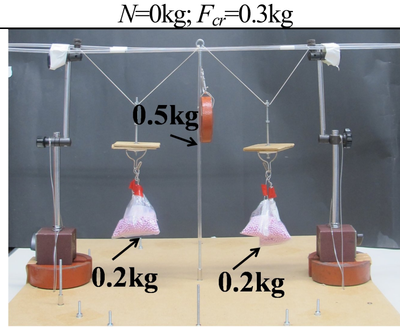 N=0.2kg; F=0.5kg	
2-2	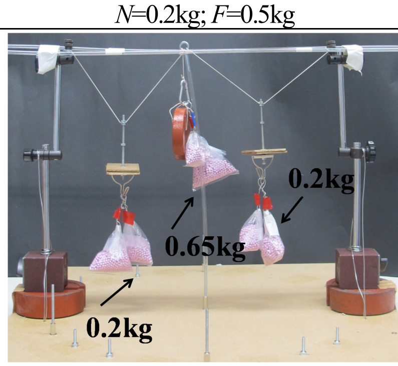 N=0.2kg; F_{cr}=0.65kg	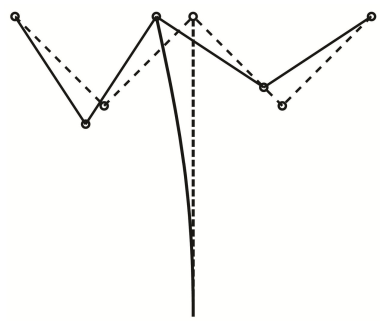 N=2N; F_{cr}=6.4N
3	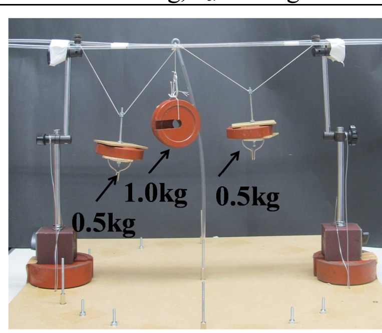 N=0.5kg; F_{cr}=1.0kg	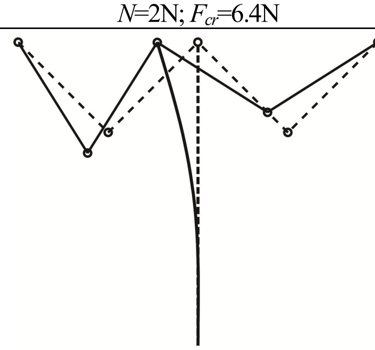 N=5N; F_{cr}=10.2N

4-1	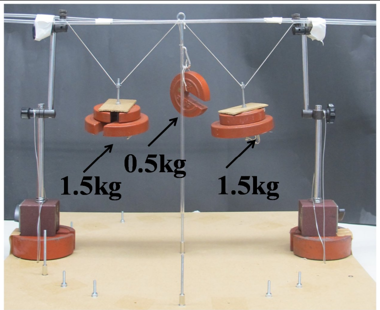 N=1.5kg; F=0.5kg	
4-2	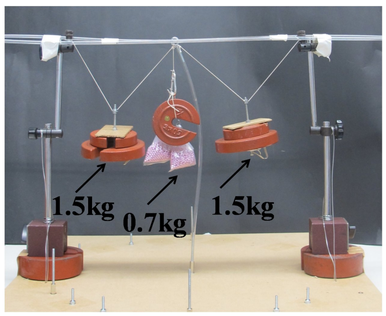 N=1.5kg; F_{cr}=0.7kg	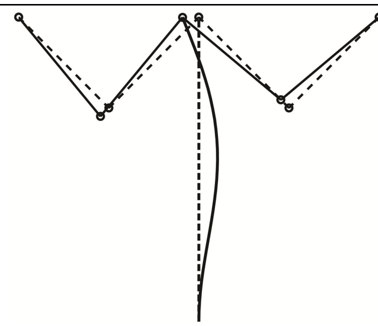 N=15N; F_{cr}=8.4N
5	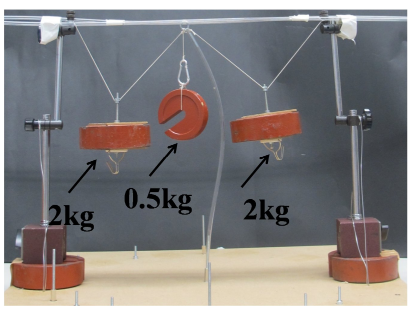 N=2kg; F_{cr}=0.5kg	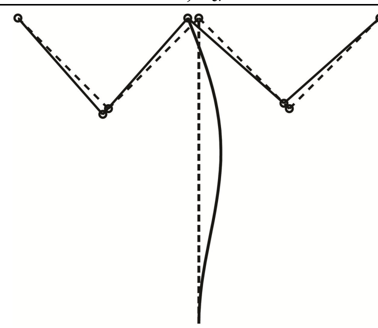 N=20N; F_{cr}=4.2N

Table.7-4 shows the comparison of results of the critical loads and buckling modes in experiment and FE analysis. From Table.7-4, the buckling modes in experiment and numerical examples can be observed to be very similar to each other.

7.4 Summaries

In this chapter, experiments of three negatively pressured pneumatic structures used as first-aid shelters are introduced, and their skeletons are mainly made of semi-circular arches. In addition, a column experiment is used to show the stiffening effect of curved cables under direct loads. The major achievements are summarized as follows:

1) In the experiment of hemispheric shelter, when there is no stiffening cables, although the critical load in

numerical analysis is about 17% of experimental one, their buckling modes are both rotational modes. In another aspect, when ropes are used to stiffen the skeleton, the critical load in numerical analysis is about 36% of experimental one. In experiment, the buckling phenomenon of skeleton is local buckling, while in numerical analysis the buckling mode of skeleton is global buckling behavior translating along one symmetrical axis.

2) In the experiment of rectangle shelter, light-weight infrastructures are proved to be available in the negatively pressured pneumatic structures. And in the experiment of round shelter, arch models with pseudo-springs for the simulation of negatively pressured pneumatic structure are proposed.

3) A loading test experiment is processed in a column structure featuring with curved cables. And study work shows loading on curved cables can change the buckling behavior of columns, and the critical loads and buckling modes in experiment and in FE analysis are very similar to each other. In addition, the existences of stiffnesses of pseudo-springs in flexible components are also verified.

Chapter 8 Conclusions

8.1 Main conclusions

The main conclusions are as follows:

1) Theoretical formulations based on arch-spring models show that spring ratios of elastic stiffnesses of the braces and the arches can determine the buckling behaviors of arches, and when the spring ratios are large than limiting spring ratios, these ratios almost cannot increase the critical loads of arches anymore.

2) The stiffening effects of various types of single arch and cross arch, which are stiffened by straight braces, are compared and summarized. The stability of hoop-ring structure stiffened with spokes is also analyzed. Study work shows restraining the buckling modes of these structures by straight constraint components can increase critical loads efficiently, and limiting spring ratios are also proved to be existing.

3) Flexible components such as curved cables have a similar characteristic, that is, their elastic stiffenesses cannot provide stiffening effect to the main structure as what the straight components do, only internal forces in these flexible components can provide a stiffness of pseudo-spring to stiffen the main structures. And the assumption of stiffness of pseudo-spring is proved by formulations based on a column model featuring with curved cables.

4) There are optimal internal forces of curved cables generating by external forces applied on them to provide best stiffening effects. Oversize external loads on curved cables will lower the stability of stiffened structure. And the phenomenons of optimal internal forces are also observed in the applications of a guyed mast structure and an arch structure featuring with curved cables.

5) The experiment of hemispheric shelter of negatively pressured pneumatic structures shows that curved membranes under negative draught head may provide stiffening effect, and by restraining the buckling modes of skeleton through straight components has greatly increased the critical loads about 40%. And the light-weight infrastructures in this type of pneumatic structures are available during the practice construction of rectangle shelter. And based on the model of round shelter, arch model with pseudo-springs is proposed to simulate the stiffening effect of membranes under negatively draught head.

6) A loading test experiment is processed in a column structure featuring with curved cables. And study work shows loading on curved cables can change the buckling shapes of the column, and the critical loads and

buckling modes in experiments and in FE analysis are similar to each other. In addition, the existences of stiffnesses of pseudo-springs in flexible components are also verified.

8.2 Future work

Arch structure is a kind of structure with brief shape and high-strength quality. Constraint components can effectively enhance the stability of arches, and the researches in this field are innovative and important. Researches can be continuously done in several aspects as follows:

1) Arches with symmetrical closed cross section are mainly taken as the research objects in this thesis. While for practical usage in the projects of arch structures, researches on other types of cross sections such as “I” type cross section and “T” type cross section are needed.

2) In linear FE buckling analysis, the in-plane buckling modes and out-of-plane buckling modes of arches are observed to happen independently. Then in theoretical procedures in this thesis the buckling control equations for in-plane stability and out-of-plane stability are divided separately. In future work, the coupling effect of these two kinds of buckling modes should be studied.

3) Although some works are carried out in studying the stiffening effects of flexible components, for efficiently utilizing of negatively draught head in negatively pressured pneumatic structures, new reliable pseudo-spring models according to the accurate experimental monitoring dates should be built. In addition, the optimal prestresses of cables in arch structures stiffened with cable-nets in practice in engineering fields should be studied.

REFERENCES

1. Kawaguchi K.. Theory of unstable structures and its applications. Ph.D Thesis of the University of Tokyo, 1990 (in Japanese: 川口健一：不安定構造物の理論とその応用に関する研究。東京大学学位請求論文，1990)

2. Hangai Y., Kawaguchi K.. Morphological analysis-generalized inverse matrix. Baifukan Co., Ltd., 1991 (in Japanese: 半谷裕彦，川口健一：形態解析−一般逆行列とその応用。培風館，1991)

3. Kawai T., Hujitani Y.. Buckling problems analysis. Basement and application of finite element method-Series 11, Baifukan Co., Ltd., 1991 (in Japanese: 川井忠彦，藤谷義信：座屈問題解析。有限要素法の基礎と応用シリーズ 11，培風館，1991)

4. Hisada T.. Basement of tensor analysis for nonlinear finite element method. Maruzen Co., Ltd., 1992 (in Japanese: 久田俊明：非線形有限要素法のためのテンソル解析の基礎。丸善株式会社，1992)

5. Noguchi H., Hisada T.. Integrated FEM formulation for total/updated-lagrangian method in geometrically nonlinear problem. The Japan Society of Mechanical Engineers (A), Vol. 59, No. 559, pp. 332-338, 1993 (in Japanese: 野口裕久，久田俊明：幾何学的非線形問題における total/updated Lagrange 総合形有限要素法定式化。日本機械学会論文集（A），Vol. 59，No. 559，pp. 332-338，1993)

6. Noguchi H., Hisada T.. Development of a sensitivity analysis method for nonlinear buckling load. The Japan Society of Mechanical Engineers (A), Vol. 59, No. 561, pp. 181-188, 1993 (in Japanese: 野口裕久，久田俊明：幾何学的非線形問題における座屈荷重感度解析手法の開発。日本機械学会論文集（A），Vol. 59，No. 561，pp. 181-188，1993)

7. Abe M., Tatemichi I., Kawaguchi M.. Thin-walled domes stiffened by tensegrig systems. AIJ J. Technol. Des., No. 1, pp. 96-101, 1995 (in Japanese: 阿部優，立道郁生，川口衛：テンセグリック・システムにより補剛された薄肉ドームの提案。日本建築学会技術報告集，No. 1，pp. 96-101，1995)

8. Miyamura T.. Bifurcation analysis of wrinkling on tension membrane and the experiment. Ph.D Thesis of the University of Tokyo, 1995 (in Japanese: 宮村倫司：張力膜におけるしわの分岐解析および実験。東京大学学位請求論文，1995)

9. Ishihara M.. Large-rotation and large-strain analysis of a beam by finite-element method. The Japan

Society of Mechanical Engineers (A), Vol. 62, No. 599, pp. 174-180, 1996 (in Japanese: 石原昌文 : 有限要素法による梁の大回転・大歪解析。日本機械学会論文集（A），Vol. 62，No. 599，pp. 174-180，1996)

10. Wu Minger. A basic study on a hybrid structure consisting of cables and rigid structures. Ph.D Thesis of the University of Tokyo, 1997 (in Japanese: 呉明児：ケーブルと剛体構造による複合構造の構造挙動に関する基礎的研究。東京大学学位請求論文，1997)

11. Fujii F., Mori A., Kawahara K.. Tracing the bifurcation points of a pinned circular arch subjected to stepwise changing loading modes. Journal of Structural Engineering (AIJ), Vol. 44A, pp. 293-298, 1998 (in Japanese: 藤井文夫，森明子，川原克美：座屈モードの変動に対する面内アーチの分岐点座屈の連続計算法。構造工学論文集 (AIJ)，Vol. 44A，pp. 293-298，1998)

12. Kaneko M.. Inflation analysis of pneumatic structure by using molecules of included gas. Master Thesis of the University of Tokyo, 2000 (in Japanese: 金子雅彦：内包気体の分子数制御による空気膜構造のインフレート解析。東京大学学位請求論文，2000)

13. Kuwamura H.. Mechanics in architecture-theory of elastic and its applications. Gihodo Shuppan Co., Ltd., 2001 (in Japanese: 桑村仁：建築の力学—弾性論とその応用。技報堂出版株式会社，2001)

14. Tabata H., Okada A., Saitoh M.. Study on structural characteristics of tensegric truss arch. J. Struct. Contr. Eng., AIJ, No. 549, pp. 91-98, 2001 (in Japanese: 田畑博章，岡田章，斎藤公男：テンセグリック・トラスアーチの構造特性に関する研究。日本建築学会構造系論文集，No. 549，pp. 91-98，2001)

15. Wu Minger, Sasaki M., Ohmori H.. Buckling behavior of a compressive member stiffened by tensile members: geometrically nonlinear analysis and buckling test. J. Struct. Contr. Eng., AIJ, No. 556, pp. 93-99, 2002 (in Japanese: 呉明児，佐々木睦朗，大森博司：テンション材により補剛された圧縮材の座屈性状に関する研究 : 幾何学非線形解析及び座屈実験。日本建築学会構造系論文集，No. 556，pp. 93-99，2002)

16. Nakashino K.. Study on the analysis method for structures constituted by membranes and cables. Ph.D Thesis of Institute of Space and Astronautical Science, 2002 (in Japanese: 中篠恭一：膜面やケーブルからなる構造物の解析法に関する研究。宇宙科学研究所学位請求論文，2002)

17. Kanayama T.. Stiffening effect of supplementary parts for orthogonal grid single-layer lattice shell. Ph.D Thesis of the University of Tokyo, 2003 (in Japanese: 金山敬：直交二方向グリッドの単層ラチスシ

ェルに対するパーツ補剛の効果に関する研究。東京大学学位請求論文，2003)

18. Wu Minger, Komatsu H., Sasaki M.. Experimental studies on an arch stiffened by cables. J. Struct. Contr. Eng., AIJ, No. 584, pp. 87-94, 2004 (in Japanese: 呉明児，小松宏年，佐々木睦朗：ケーブルにより補剛されたアーチに関する実験的研究。日本建築学会構造系論文集，No. 584，pp. 87-94，2004)

19. Fukushima T., Saitoh M.. Study on the buckling behavior of grid dome stiffened by strings. 2004 AIJ Kanto Research Report, pp. 109-111, 2004 (in Japanese: 福島孝志，斉藤公男：ストリング補剛された二方向格子ドームの座屈挙動に関する基礎的研究。2004 年度日本建築学会関東支部研究報告集，pp. 109-111，2004)

20. Katoh C., Uchiyama M., Nakajima H., Miyasato N., Kita S., Okada A., Nishiya T., Saitoh M.. Research on buckling behavior of beam string structures consisting of arched beam. 2008 AIJ Kanto Research Report, pp. 145-148, 2008 (in Japanese: 加藤千博，内山学，中島肇，宮里直也，北茂紀，岡田章，西谷隆之，斎藤公男：アーチ構造型張弦梁構造の座屈性状に関する研究。2008 日本建築学会関東支部研究報告集，pp. 145-148，2008)

21. Kawaguchi M.. Structure and emotion Ⅱ (membrane and pneumatic structure). Hosei University Architectural Institute Alumni Association, 2008 (in Japanese: 川口衛：構造と感性Ⅱ（膜と空気の構造）。法政大学建築学会同窓会，2008)

22. Kawaguchi K., Ke Wang-ling, Miki M.. Minimal surface with constraint conditions and steepest descent method. J. Struct. Contr. Eng., AIJ, Vol. 73, No. 632, pp. 1773-1777, 2008 (in Japanese: 川口健一，柯宛伶，三木優彰：付帯条件付き極小曲面と一般化最急降下法に関する研究。日本建築学会構造系論文集，Vol. 73，No. 632，pp. 1773-1777，2008)

23. Sekijima K., Kawakami K., Tamaru T., Izumo J.. Evaluation of properties of continuous fiber rope (part 2). Journal of Institute of Science and Technology, Kanto Gakuin University, No. 36, pp. 11-20, 2008 (in Japanese: 関島謙蔵，川上清陛，田丸武，出雲淳一：連続繊維ロープの性能評価（第 2 報）。関東学院大学工学総合研究所報 36，pp. 11-20，2008)

24. Kawaguchi K., Ozawa Y.. Linear inverse analysis of stress and shape control of structures with members of variable length. J. Struct. Contr. Eng., AIJ, Vol. 74, No. 639, pp. 849-856, 2009 (in Japanese: 川口健一，小澤雄樹：アクチュエータやターンバックルを有する構造物の形態・応力制御の線形逆解析法。日本建築学会構造系論文集，Vol. 74，No. 639，pp. 849-856，2009)

25. Frei Otto. Natural structure. [Iwamura Kazuo (Trans.)]. Kajima Institute Publishing Co., Ltd., 2010 (in Japanese: フライ・オットー（著）【岩村和夫（訳）】: 自然な構造体。鹿島出版会，2010)

26. Architectural Institute of Japan. Buckling and proof stress of lattice shells. Maruzen Co., Ltd., 2010 (日本建築学会：ラチスシェルの座屈と耐力。丸善株式会社，2010)

27. Nakajima H., Uchiyama M., Nishiya T., Okada A., Miyasato N., Katoh C., Saitoh M.. Research on buckling behavior of beam string structures consisting of arched beam. J. Struct. Constr. Eng., AIJ, Vol. 76, No. 659, pp. 89-96, 2011 (in Japanese: 中島肇，内山学，西谷隆之，岡田章，宮里直也，加藤千博，斎藤公男 : アーチ型張弦梁構造の座屈性状に関する研究。日本建築学会構造系論文集，Vol. 76，No. 659，pp. 89-96，2011)

28. Kawaguchi K.. Generalized inverse matrix and its applications in structural engineering (Computational Engineering Series 1). Corona Publishing Co., Ltd., 2011 (in Japanese: 川口健一: 一般逆行列と構造工学への応用（計算工学シリーズ 1）。コロナ社，2011)

29. Fujii F., Ohsaki M., Ikeda K.. Bifurcation mechanics of structures and materials. (Computational Engineering Series 3), Corona Publishing Co., Ltd., 2011 (in Japanese: 藤井文夫，大崎純，池田清宏：構造と材料の分岐力学（計算工学シリーズ 3）。コロナ社，2011)

30. Chen Kun, Hong Wenhan, Kawaguchi Ken'ichi,. Fundamental study on the buckling behavior and reinforcement for the skeleton supporting a negatively pressured pneumatic structure. Research Report on Membrane Structure 2011, No. 25, pp. 17-24, 2012 (in Japanese: 陳坤，洪文汗，川口健一：負圧型空気膜構造の支持骨組の座屈挙動と補強方法についての基礎的考察。膜構造研究論文集 2011，No. 25，pp. 17-24，2012)

31. Miki M.. Searching of the equilibrium shapes of structures by three-term method and dual estimate. Ph.D Thesis of the University of Tokyo, 2012 (in Japanese: 三木優彰：三項法と双対推定による構造物の釣り合う形状の探索。東京大学学位請求論文，2012)

32. Inoue K.. Fundamental study on deployable planar network and ultra-thin structure to be utilized in space. Master Thesis of the University of Tokyo, 2012 (in Japanese: 井上健一：宇宙利用を目指した展開型平面ネットワークと超薄膜に関する基礎的研究。東京大学学位請求論文，2012)

33. Chen Kun, Kawaguchi Ken'ichi. Fundamental study on stiffening effect of tensioned components under load. Research Report on Membrane Structure 2012, No. 26, pp. 13-19, 2013 (in Japanese: 陳坤，川口健

一：張力材経由の載荷による座屈補剛効果についての基礎的考察。膜構造論文集 2012，No. 26，pp. 13-19，2013)

34. Furuichi S.. Fundamental study on ultra-light large planar structure to be utilized for space solar power system. Master Thesis of the University of Tokyo, 2013 (in Japanese: 古市渉平：宇宙太陽光発電システムへの応用を目指した超軽量大型平面構造物に関する基礎的研究。東京大学学位請求論文, 2013)

35. Afra Pradana Rahman. Development of disaster relief first-aid shelters in Asia. Master Thesis of the University of Tokyo, 2013 (in Japanese: ラフマン・アフラ・プラダナ：アジアの災害後における応急仮設住宅の開発に関する研究。東京大学学位請求論文，2013)

36. Hong Wenhan. Basic study on negatively pressured pneumatic structures by using solar power system. Master Thesis of the University of Tokyo, 2013 (in Japanese: 洪文汗：太陽発電システムを用いた負圧型空気膜構造に関する基礎的研究。東京大学学位請求論文，2013)

37. C. Oran. Tangent stiffness in space frames. ASCE J Structure Div., Vol. 99, pp. 987-1001, 1937

38. A. E. H. Love. A treatise on the mathematical theory of elasticity (4th Edition). New York, 1944

39. S. P. Timoshenko, D. H. Young. Theory of structures. McGraw-Hill book company, 1945

40. L. Östlund. Lateral stability of bridge arches braced with transverse bars. Transactions of Royal Institute of Technology, Stockholm, Sweden, No. 84, pp. 27-33, 1954

41. Winter G.. Lateral bracing of columns and beams. Transactions of ASCE, Vol. 125, pp. 807-845, 1960

42. S. P. Timoshenko, J. M. Gere. Theory of Elastic Stability. McGraw-Hill, 1961

43. Vlasov. V. Z.. Thin-walled elastic beams (2nd edition). Israel Program for Scientific Translation, Jerusalem, 1961

44. Taylor A.C., Ojalvo M.. Torsional restraint of lateral buckling. Journal of the Structural Division, Vol. 92, pp. 115-129, 1966

45. Lay M. G., Galambos T. V.. Bracing requirements for inelastic steel beams. Journal of the Structural Division, Vol. 92, No. 1, pp.207-227, 1966

46. C. R. Calladine, S.Pellegrino. First-order infinitesimal mechanism. International Journal of Solids and

Structures, Vol. 27, No. 4, pp. 471-488, 1967

47. Thein Wah. Buckling of thin circular rings under uniform pressure. International Journal of Solids and Structures, Vol. 3, pp.967-974, 1967

48. George E. Weeks. Buckling of a pressurized toroidal ring under uniform external loading. National Aeronautics and Space Administration, 1967

49. Almeida, N. F. Lateral bucking of Twin arch ribs with transverse bars. Thesis presented to Ohio State University, at Columbus, Ohio, 1970

50. Column Research Committee of Japan. Handbook of structure stability. Corona Publishing Company, 1971

51. Bruce. C. Mutton. Stiffness requirement for lateral bracing. Journal of the Structural Division, Vol. 99, No. 10, pp. 2167-2182, 1973

52. Nethercot, D A. Buckling of laterally of torsionally restrained beams. Journal of Engineering Mechanics, Vol. 99, No. EM4, pp. 773-791, 1973

53. D. J. Dawe. Curved finite elements for the analysis of shallow and deep arches. Computer& Structures, Vol. 4, pp. 559-580, 1974

54. C. T. Li, N. K. Srivastava. Analysis of pneumatic shells with or without cable net; general finite- element formulation. Computer & Structures, Vol. 4, pp. 813-828, 1974

55. R.F. Jones, JR, M. G. Costello, T. E. Reynolds. Buckling of pressure loaded rings and shells by the finite element method. Computers & Structures, Vol. 7, pp. 267-274, 1975

56. M. Epstein, D. W. Murray. Three-dimensional large deformation analysis of thin walled beams. International Journal of Solids and Structures, Vol. 12, pp. 867-876, 1976

57. Ojakvi. M., Chambers, R. S., Effect of warpring restraints on I beam Buckling. Journal of the Structural Division, Vol. 103, pp. 2351-2360, 1977

58. R. D. Wood, O. C. Zienkiewicz. Geometrically nonlinear finite element analysis of beams, frames, arches, and axisymmetric shells. Computers & Structures, Vol. 7, pp. 729-735, 1977

59. R. F. Jones, M. G. Costello, T. E. Reynolds. Buckling of pressure loaded rings and shells by the finite

element method. Computer & Structure, Vol. 7, pp.267-274, 1977

60. T. Belytschko, L. Schwer, M. J. Klein. Large displacement, transient analysis of space frames. International Journal for Numerical Methods in Engineering, Vol.11, pp. 65-84, 1977

61. A. K. Noor, W. H. Greene, S. J. Hartley. Nonlinear finite element analysis of curved beams. Computer Methods in Applied Mechanics and Engineering, Vol. 12, pp. 289-307, 1977

62. J. H. Argyris, P. C. Dunne, M. Haase, J. Orkisz. Higher-order simplex elements for large strain analysis-natural approach. Computer Methods in Applied Mechanics and Engineering, Vol. 16, pp. 369-403, 1978

63. Thomas Michael Juliano. Inplane and out of plane buckling of thick rings subjected to hydrostatic pressure. Ph.D Thesis of New Jersey's Science & Technology University in USA, 1979

64. K. J. Bathe, S. Bolourchi. Large displacement analysis of three-dimensional beam structures. International Journal for Numerical Method in Engineering, Vol. 14, pp. 961-986, 1979

65. E. Riks. An incremental approach to the solution of snapping and buckling problems. International Journal of Solids and Structures, Vol. 15, pp. 529-551, 1979

66. Medland L C.. Buckling of interbraced beam systems. Engineering Structures, Vol. 2, No. 2, pp. 90-96, 1980

67. José Mario Martínez. Solving nonlinear simultaneous equations with a generalization of brent's method. Bit, Vol. 20, pp. 501-510, 1980

68. S. I. Oh. Finite element analysis of plane-strain sheet bending. International Journal of Mechanical Sciences, Vol. 22, pp. 583-594, 1980

69. N. Yamaki, A. Mori. Non-linear vibrations of a clamped beam with initial deflection and initial axial displacement, part Ⅰ: theory. Journal of Sound Vibration, Vol. 71, No. 3, pp. 333-346, 1980

70. M. Papadrakakis. Post-buckling analysis of spatial structures by vector iteration methods. Computers Mechanics, Vol. 14, No. 5-6, pp. 393-402, 1981

71. M. A. Crisfield. A fast increment/iterative solution procedure that handles "snap-through". Computers & Structures, Vol. 13, pp. 55-62, 1981

72. Tatsuro Sakimoto, Sadao Komatsu. Ultimate strength of arches with bracing systems. Journal of the Structural Divisions, Vol. 108, No. 5, pp. 1064-1076, 1982

73. Chai Hang Yoo, M. ASCE. Flexural-torsional stability of curved beams. Journal of the Engineering Mechanics Divisions, Vol. 108, No. 6, pp. 1351-1369, 1982

74. Robert D. Cook, Feng Zhaohua. Deflection and buckling of rings with straight and curved finite elements. Computers & Structures, Vol. 15, No. 6, pp. 647-651, 1982

75. John Argyris. An excursion into large rotations. Computer Methods in Applied Mechanics and Engineering, Vol. 32, pp. 85-155, 1982

76. J. Donea, S. Giuliani, J. P. Halleux. An arbitrary Lagrangian-Eulerian finite element method for transient dynamic fluid-structure interactions. Computer Methods in Applied Mechanics and Engineering, Vol. 33, pp. 689-723, 1982

77. Svensson, S.E., Plum, C, M.. Stiffener effects on torsional buckling of column. Journal of Structural Engineering, Vol. 109, No. 3, pp. 758-772, 1983

78. R. Rubinstein, S. N. Atluri. Objectivity of incremental constitutive relations over finite time steps in computational finite deformation analyses. Computer Methods in Applied Mechanics and Engineering, Vol. 36, pp. 227-290, 1983

79. M. A. Crisfield. An arc-length method including line searches and accelerations. International Journal for Numerical Methods in Engineering, Vol. 19, pp. 1269-1289, 1983

80. Karl Schweizerhof, Ekkehard Ramn. Displacement dependent pressure loaded in nonlinear finite element analysis. Computers & Structures, Vol. 18, No. 6, pp. 1099-1114, 1983

81. B. A. Schrefler, S. Odorizzi, R. D. Wood. A total lagrangian geometrically non-linear analysis of combined beam and cable structure. Computers & Structures, Vol. 17, No. 1, pp. 115-127, 1983

82. E. N. Dvorkin, K. J. Bathe. A continuum mechanics based four-node shell element for general nonlinear analysis. Engineering Computations, Vol. 1, pp. 77-88, 1984

83. Karl Schweizerhof, Ekkehard Ramm. Displacement dependent pressure loads in nonlinear finite element analyses. Computers & Structures, Vol. 18, No. 6, pp. 1099-1114, 1984

84. E. F. Punch, S. N. Atluri. Development and testing of stable, invariant, isoparametric curvilinear 2- and 3-D hybrid-stress elements. Computer Methods in Applied Mechanics and Engineering, Vol. 47, pp. 331-356, 1984

85. J. L. Meek, Hoon Swee. Tan. A stiffness matrix extrapolation strategy for nonlinear analysis. Computer Methods in Applied Mechanics and Engineering, Vol. 43, pp. 181-194, 1984

86. J. L. Meek, Hoon Swee Tan. Geometrically nonlinear analysis of space frames by an incremental iterative technique. Computer Methods in Applied Mechanics and Engineering, Vol. 47, pp. 261-282, 1984

87. G. Prathap, C. Ramesh Babu. An isoparametric quadratic thick curved beam element. Journal for Numerical Methods in Engineering, Vol. 23, pp. 1583-1600, 1986

88. Peter Gerstoft, A. G. Davenport. A simplified method for dynamic analysis of a guyed mast. Journal of Wind Engineering and Industrial Aerodynamics, Vol. 23, pp. 487-499, 1986

89. Yeong-Bin Yang, A. M. ASCE, Shyh-Rong Kuo. Static stability of curved thin-walled beams. Journal of Engineering Mechanics, Vol. 112, pp. 821-841, 1986

90. K. Kondoh, S. N. Atluri. A simplified finite element method for large deformation, post-buckling analyses of large frame structures, using explicitly derived tangent stiffness matrices. International Journal for Numerical Method in Engineering, Vol. 23, pp. 69-90, 1986

91. J. Oliver, E. Ońate. A total lagrangian formulation for the geometrically nonlinear analysis of structures using finite elements. Part Ⅱ: arches, frames and axisymmetric shells. International Journal for Numerical Method in Engineering, Vol. 23, pp. 253-274, 1986

92. John P. Papangelis, Nicholas S. Trahair, M. ASCE. Flexural-torsional buckling of arches. Journal of Structural Engineering, Vol.113, No. 4, pp. 889-906, 1987

93. S. L. Chan, S. Kitipornchai. Geometric nonlinear analysis of anti-symmetric thin-walled beam-columns. Engineering Structures, Vol. 9, pp. 243-254, 1987

94. Robert K. Wen, M. ASCE, Khaled Medallah. Elastic stability of deck-typed arch bridges. Journal of Structural Engineering, Vol. 113, No. 4, pp. 757-768, 1987

95. Yeong-Bin Yang, A. M. ASCE, Shyh-Rong Kuo. Effect of curvature of stability of curved beams. Journal of Structural Engineering, Vol. 113, No. 6, pp. 1185-1202, 1987

96. P. Wriggers, W. Wagner, C. Miehe. A quadratically convergent procedure for the calculation of stability points in finite element analysis. Computer Methods in Applied Mechanics and Engineering, Vol. 70, pp. 329-347, 1988

97. Siulai Chan. Geometric and material nonlinear analysis of beam-columns and frames using the minimum residual displacement method. International Journal for Numerical Methods in Engineering, Vol. 26, pp. 2657-2669, 1988

98. Y. M. Desai, N. Popplewell, A. H. Shah, D. N. Buragohain. Geometric nonlinear static analysis of cable supported structures. Computers & Structures, Vol. 29, No. 6, pp. 1001-1009, 1988

99. Tong G. S., Chen S. F. Buckling of laterally and torsionally braced beams. Journal of Constructional Steel Research, Vol. 11, No. 1, pp. 41-55, 1988

100. Tong G. S., Chen S. F. The elastic buckling of inter-braced girders. Journal of Constructional Steel Research, Vol. 14, No. 2, pp. 87-105,1989

101. J. L. Meek, S. Loganathan. Large displacement analysis of space-frame structures. Computer Methods in Applied Mechanics and Engineering, Vol. 72, pp. 57-75, 1989

102. K. S. Surana, R. M. Sorem. Geometrically non-linear formulation for three dimensional curved beam elements with large rotations. International Journal for Numerical Methods in Engineering, Vol. 28, pp. 43-73, 1989

103. Sunaramoorthy Rajasekaran, S. Padmanabhan. Equations of curved beams. Journal of Engineering Mechanics, Vol.115, No.5, pp. 1094-1111, 1989

104. W. R. Spillers. Geometric stiffness matrix for space frames. Computers & Structures, Vol. 36, No. 1, pp. 29-37, 1990

105. J. L. Meek, S. Loganathan. Geometric and material non-linear behavior of beam-columns. Computers & Structures, Vol. 34, No. 1, pp. 87-100, 1990

106. M. A. Crisfield. A consistent co-rotational formulation for non-linear, three-dimensional, beam-elements. Computer Methods in Applied Mechanics and Engineering, Vol. 81, pp. 131-150, 1990

107. Robert K. Wen, Member ASCE, Bambang Suhendro. Nonlinear curved beam element for arch structures. Journal of Structural Engineering, Vol. 117, No. 11, pp. 3496-3515, 1991

108. Haifan Xiang, Guangdong Liu. Stability and vibration of arch structures. China Communications Press, 1991 (in Chinese：项海帆，刘光栋：拱结构的稳定与振动。人民交通出版社，1991)

109. Roddeman DG. Finite element analysis of wrinkling membrane. Communications in Applied Numerical Methods, Vol. 7, pp. 299-307, 1991

110. Andrew Kwok Wai So, Siulai Chan. Buckling and Geometrically nonlinear analysis of frames using one element/member. Journal of Constructional Steel Research, Vol. 20, pp. 271-289, 1991

111. G. A. Holzapfel, Graz. A shear deformation shell theory for finite rotations and its numerical solution with the finite-difference method. Acta Mechanica, Vol. 92, pp. 193-207, 1992

112. Siulai Chan. Large deflection kinematic formulations of three-dimensional framed structures. Computer Methods in Applied Mechanics and Engineering, Vol. 95, pp. 17-36, 1992

113. Trahair, N. S. Flexural-torsional buckling of structures. E & FN Spon, London, 1993

114. L. A. Crivelli, C. A. Felippa. A three-dimensional nonlinear timoshenko beam based on the core-congruential formulation. International Journal for Numerical Methods in Engineering, Vol. 36, pp. 3647-3673, 1993

115. Siulai Chan. A non-linear numerical method for accurate determination limit and bifurcation points. International Journal for Numerical Methods in Engineering, Vol. 36, pp. 2779-2790, 1993

116. Young J. Kang, Chai H. Yoo. Thin-walled curved beams Ⅰ: Formulation of nonlinear equations. Journal of Engineering Mechanics, Vol. 120, No. 10, pp. 2072-2101, 1993

117. Young J. Kang, Chai H.Yoo. Thin-walled curved beams Ⅱ: Formulation of nonlinear equations. Journal of Engineering Mechanics, Vol. 120, No. 10, pp. 2102-2125, 1994

118. A. Becker, L. Kramer. Linear stability analysis for bifurcations in spatially extended systems with fluctuating control parameter. Physical Review Letters, Vol. 73, No. 7, pp. 955-958, 1994

119. Zhuyan Shen, Yongfeng Luo. Transition matrix of coordinate of beam-column element under large rotation. Shanghai Journal of Mechanics, Vol. 15, No. 4, pp. 13-19, 1994 (in Chinese：沈祖炎，罗永峰：节点大位移条件下的梁−柱单元坐标转换矩阵。上海力学，Vol. 15，No. 4，pp. 13-19，1994)

120. R. Reitinger, Kai-Uwe. Bletzinger, E. Ramm. Shape optimization of buckling sensitive structures.

Computing Systems in Engineering, Vol. 5, No. 1, pp. 65-75, 1994

121. Masashi Iura. Effects of coordinate system of the accuracy of co-rotational formulation for bernoulli-euller's beam. International Journal of Solids and Structures, Vol. 31, No. 20, pp. 2793-2806, 1994

122. Levy R, Spillers W. Analysis of geometrically nonlinear structures. Chapman and Hall, 1995

123. E. Ońate. On the derivation and possibilities of the secant stiffness matrix for nonlinear finite element analysis. Computers Mechanics, Vol. 15, pp. 572-593, 1995

124. K. J. Bathe. Finite Element Procedures. Prentice Hall, 1996

125. Yong-Lin Pi, N. S. Trahari. In-plane inelastic buckling and strengths of steel arches. Journal of Structural Engineering, Vol. 122, pp. 734-747, 1996

126. R. Sygulski. Dynamic stability of pneumatic structures in wind: theory and experiment. Journal of Fluids and Structures, Vol. 10, pp. 945-963, 1996

127. Siulai Chan. Large deflection dynamic analysis of space frames. Computers & Structures, Vol. 58, No. 2, pp. 381-387, 1996

128. M. A. Crisfield. Nonlinear Finite Element Analysis of Solids and Structures. Vol.1~2, Wiley, 1997

129. A. S. Nazmy. Stability and load-carrying capacity of three dimensional long-span steel arch bridges. Computers & Structures, Vol. 65, No. 6, pp. 857-868, 1997

130. R. Sygulski. Numerical analysis of membrane stability in air flow. Journal of Sound and Vibration, Vol. 207, No. 3, pp. 281-292, 1997

131. J. G. Teng, T. Hong. Nonlinear thin shell theories for numerical buckling predictions. Thin-walled Structures, Vol. 31, pp. 89-115, 1998

132. J. L. Meek, Qiang Xue. A study on the instability problem for 3D frames. Computer Methods in Applied Mechanics and Engineering, Vol. 158, pp. 235-254, 1998

133. L. Gründig. Minimal surfaces for finding forms of structural membranes. Computers& Structures, Vol. 30, No. 3, pp. 679-683, 1998

134. Lip H. I, Murray J. Clarke. Co-rotational and lagrangian formulations for elastic three-dimensional beam

finite elements. Journal of Constructional Steel Research, Vol. 48, pp. 123-144, 1998

135. K. Kebiche, M. N. Kazi-Aoual, R. Motro. Geometrical non-linear analysis of tensegrity systems. Engineering Structures, Vol. 21, pp. 864-876, 1999

136. P. Raveendranath, Gajbir Singh, B. Pradhan. A two-noded locking free shear flexible curved element. International Journal for Numerical Methods in Engineering, Vol. 44, pp. 265-280, 1999

137. Junming Chen. Nonlinear study on static and dynamic properties and stability for single-layer reticulated shells. Ph.D Thesis of Wuhan University of Technology in China, 2000

138. Marcus Rüter, Erwin Stein. Analysis, finite element computation and error estimation in transversely isotropic nearly incompressible finite elasticity. Computer Methods in Applied Mechanics and Engineering, Vol. 190, pp. 519-541, 2000

139. P. F. Pai, T. J. Anderson, E. A. Wheater. Large-deformation tests and total-lagrangian finite-element analyses of flexible beams. International Journal of Solids and Structures, Vol. 37, No. 21, pp. 2951-2980, 2000

140. Jinsan Ju, Yanglin Guo. Instability behavior in the plane of cable-arch structure. Journal of Building Structures, Vol. 22, No. 2, pp. 84-87, 2001 (in Chinese：剧锦三，郭彦林。索-拱结构的平面内稳定性研究。建筑结构学报，Vol. 22，No. 2，pp. 84-87，2001)

141. Hyo-Gyoung Kwak, Do-Yeon Kim, Hwan-Woo Lee. Effect of warping in geometric nonlinear analysis of spatial beams. Journal of Constructional Steel Research, Vol. 57, pp. 729-751, 2001

142. Wenyi Lin, Kuo Mo Hsiao. Co-rotational formulation for geometric nonlinear analysis of doubly symmetric thin-walled beams. Computer Methods in Applied Mechanics and Engineering, Vol. 190, pp. 6023-6052, 2001

143. S. Reese, T. Raible, P. Wriggers. Finite element modeling of orthotropic material behavior in pneumatic membranes. International Journal of Solids and Structures, Vol. 38, pp. 9525-9544, 2001

144. Y.-L. Pi, M. A. Bradford. Elastic flexural-torsional buckling of continuously restrained arches. International Journal of Solids and Structures, Vol. 39, pp. 2299-2322, 2001

145. Y.-L. Pi, M. A. Bradford, B. Uy. In-plane stability of arches. International Journal of Solids and Structures, Vol. 39, pp. 105-125, 2002

146. Jinsan Ju, Yanlin Guo. In-plane elastic buckling of arch. Tsinghua Science and Technology, Vol. 7, No. 3, pp. 322-325, 2002

147. P. Harikrishna, A. Annadurai, S. Gomathinayagam, N. Lakshmanan. Full scale measurements of structural response of a 50 m guyed mast under wind loading. Engineering Structures, Vol. 25, pp. 859-867, 2003

148. Xiaoming Yang. Study on the type and stability of cable-arch structure. Ph.D Thesis of Xi'an University of Architecture and Technology in China, 2004

149. Jinjun Li, Siulai Chan. An integrated analysis of membrane structures with flexible supporting frames. Finite Elements in Analysis and Design, Vol. 40, pp. 529-540, 2004

150. Young-Lin Pi, Mark Andrew Bradford. Elastic flexural-torsional buckling of fixed arches. Quarterly Journal of Mechanics & App. Maths., Vol. 57, No.4, pp. 551-569, 2004

151. Hongxia Wan. Theory research on form finding of cable nets and membrane structures. Ph.D Thesis of Wuhan University of Technology in China, 2004

152. X. Q. Peng, J. Cao. A continuum mechanics-based non-orthogonal constitutive model for woven composite fabrics. Composites: Part A, Vol. 36, pp. 859-874, 2005

153. Jianxin Gu, Siulai Chan. A refined finite element formulation for flexural and torsional buckling of beam-columns with finite rotations. Engineering Structures, Vol. 27, pp. 749-759, 2005

154. Xiaoming Yang. Study of the type and stability of cable-arch structure. Ph.D Thesis of Xi’an University of Architecture and Technology in China, 2005

155. K.-U. Bletzinger, R. Wüchner, F. Daoud, N. Camprubí. Computational methods for form finding and optimization of shells and membranes. Computer Methods in Applied Mechanics and Engineering, Vol. 194, pp. 3438-3452, 2005

156. Wenqing Zhang, John L. Leonard, Michael L. Accorsi. Analysis of geometrically nonlinear anisotropic membranes theory and verification. Finite Elements in Analysis and Design, Vol. 41, pp. 963-988, 2005

157. Xihu Jiang. The procedure and model technology analysis of pneumatic membrane structure. Ph.D Thesis of Tongji University in China, 2006

158. Yasuyuki Miyazaki. Wrinkled/slack model and finite element dynamics of membrane. International

Journal for Numerical Methods in Engineering, Vol. 66, pp. 1179-1209, 2006

159. Linyuan Zhou, Qiao Li. Updated lagrangian co-rotational formulation for geometrically nonlinear FE analysis of 3-D beam element. Journal of Southwest Jiaotong University, Vol. 41, No. 6, pp. 690-695, 2006 (in Chinese：周凌远，李乔：基于 UL 法的 CR 列式三维梁单元计算方法。西南交通大学学报，Vol. 41，No. 6，pp. 690-695，2006)

160. A. J. Gil, J. Bonet. Finite element analysis of prestressed structural membranes. Finite Element in Analysis and Design, Vol. 42, pp. 683-697, 2006

161. A. J. Gil. Structural analysis of prestressed Saint Venant-Kirchhoff hyperelastic membranes subjected to moderate strains. Computers & Structures, Vol. 84, pp. 1012-1028, 2006

162. Xinmin Wang. ANSYS engineering structure analysis. China Communications Press, 2007 (in Chinese：王新敏：ANSYS 工程结构数值分析。人民交通出版社，2007)

163. P. Mata, S. Oller, A. H. Barbat. Static analysis of beam structures under nonlinear geometric and constitutive behavior. Computer Methods in Applied Mechanics and Engineering, Vol. 196, pp. 4458-4478, 2007

164. R. A. Arciniega, J. N. Reddy. Tensor-based finite element formulation for geometrically nonlinear analysis of shell structures. Computer Methods in Applied Mechanics and Engineering, Vol. 196, pp. 1048-1073, 2007

165. Houjun Kang. The research on stability and vibration of cable-arch structure. Ph.D Thesis of Hunan University in China, 2007

166. J. Bonet, R. D. Wood. Nonlinear continuum mechanics for finite element analysis (2nd Edition). Cambridge University Press, 2008

167. Pan Zeng. Fundamentals of finite element analysis. Higher Education Press, 2009 (in Chinese：曾攀：有限元基础教程。高等教育出版社，2009)

168. Yan Xu. Precision and deployment analysis research for membrane inflatable antenna. Ph.D Thesis of Zhejiang University in China, 2009

169. J. G. Valdés, J. Miquel, E. Oñate. Nonlinear finite element analysis of orthotropic and prestressed membrane structure. Finite Elements in Analysis and Design, Vol. 45, pp. 395-405, 2009

170. Y.-L. Pi, M. A. Bradford. Effects of prebuckling analyses on determining buckling loads of pin-ended circular arches. Mechanics Research Communications, Vol. 37, pp. 545-553, 2010

171. Wentao Qiao. Study of cable supported structure system. Ph.D Thesis of Tianjin University in China, 2010

172. Hongbo Liu. Study on the construction control theory and temperature effect of suspen-dome structure. Ph.D Thesis of Tianjin University in China, 2011

173. Kun Wang. Research and design of the architectural form of the spoke structure. Master Thesis of Tsinghua University in China, 2011

174. Kun Chen, Ken'ichi Kawaguchi Preliminary research on stiffening effect of tensioned members with mechanism system and its applications. Journal of Structural Engineering (AIJ), Vol. 60B, pp. 179-187, 2014

Appendix A

Calladine [46] has discussed a first order infinitesimal state, in which small mechanism movements will bring the system from mechanism to a structure. For example, plane membrane or straight cable without prestress.

If a concentrated load which is perpendicular to the plane membrane or straight cable is applied to them, when we use FE method, we know that tangential elastic stiffness of plane membrane or straight cable is singularity, so it is difficult to get the solution of elastic displacement. The following passage introduces two methods in A.1 and A.2 to obtain the displacement.

A.1 Hypothesis damping term method [16]

The discretization of equilibrium equation can be written as follows:

$$\mathbf{Q}(\mathbf{u}) = \mathbf{F} \tag{A-1}$$

Here $\mathbf{Q}$ is the internal force vector, $\mathbf{F}$ is external vector, and $\mathbf{u}$ is the displacement vector. By using Newton-Raphson method to solve Eq.(A-1), the reiterative calculation at m-th step can be expressed as

$$\mathbf{K}({}^{m}\mathbf{u})\bullet({}^{m+1}\mathbf{u} - {}^{m}\mathbf{u}) = \mathbf{F} - \mathbf{Q}({}^{m}\mathbf{u}) \tag{A-2}$$

In Eq.(A-2), $\mathbf{K}({}^{m}\mathbf{u})$ is a tangential stiffness matrix at m-th step.

Here a plane membrane without prestress is taken for example. In the initial state the presstress is 0, when external load which is perpendicular to the membrane is applied to the plane membrane, the components of tangential stiffness matrix in the same direction of the external load is 0. As the tangential stiffness matrix is a singular matrix, the process of iteration in Eq.(A-2) cannot go on. At this time, the method in quasi dynamic problem is utilized. A damping term matrix $\mathbf{D}$ is added to Eq.(A-1), and Eq.(A-1) becomes

$$\mathbf{D}\bullet\dot{\mathbf{u}} + \mathbf{Q}(\mathbf{u}) = \mathbf{F} \tag{A-3}$$

The damping term matrix $\mathbf{D}$ can be calculated as follows.

$$\mathbf{D} = {}^{m}\mu\mathbf{I} \tag{A-4}$$

In Eq.(A-4), ${}^{m}\mu$ is a damping coefficient at m-th step, and $\mathbf{I}$ is a unit matrix. The increment of $\mathbf{u}$ is

$$\dot{\mathbf{u}} = \frac{{}^{m+1}\mathbf{u} - {}^{m}\mathbf{u}}{\Delta t} \tag{A-5}$$

Substituting Eq.(A-5) into Eq.(A-3), and utilizing Eq.(A-2), then we can obtain

$$[\mathbf{K}({}^{m}\mathbf{u}) + \frac{1}{\Delta t}\mathbf{D}]\bullet({}^{m+1}\mathbf{u} - {}^{m}\mathbf{u}) = \mathbf{F} - \mathbf{Q}({}^{m}\mathbf{u}) \tag{A-6}$$

If the numerical solution becomes convergence, there is

$${}^{m+1}\mathbf{u} - {}^{m}\mathbf{u} = (\dot{\mathbf{u}}\Delta t) \to 0 \tag{A-7}$$

Then Eq.(A-6) returns to Eq.(A-1).

In the numerical calculation, the damping coefficient ${}^{1}\mu$ at the first step of iteration can be 1. And damping coefficient ${}^{m}\mu$ at m-th step can be 0.5 time of damping coefficient ${}^{m\text{-}1}\mu$ at (m-1)-th step as follows:

$${}^{m}\mu = 0.5\bullet{}^{m-1}\mu \tag{A-8}$$

A.2 No elongation displacement method [1], [2], [28]

Researchers Hangai[2] and Kawaguchi[1], [2], [28] have used the Moore-Penrose generalized inverse matrix in the morphological analysis. If a matrix **A** can satisfy the following four conditions at the same time, then $\mathbf{A}^{+}$ is called Moore-Penrose generalized inverse matrix.

Condition 1: $\mathbf{A}\mathbf{A}^{+}\mathbf{A} = \mathbf{A}$

Condition 2: $\mathbf{A}^{+}\mathbf{A}\mathbf{A}^{+} = \mathbf{A}^{+}$

Condition 3: $(\mathbf{A}\mathbf{A}^{+})^{T} = \mathbf{A}\mathbf{A}^{+}$

Condition 4: $(\mathbf{A}^{+}\mathbf{A})^{T} = \mathbf{A}^{+}\mathbf{A}$

Then the usage of Moore-Penrose generalized inverse matrix in the FE program is introduced. When there is no prestress in the initial state, components of internal force vector $\mathbf{Q}({}^{1}\mathbf{u})$ are all 0. Here assuming the following two equations

$$\mathbf{f} = \mathbf{F} - \mathbf{Q} \tag{A-9}$$

$$\Delta^{m+1}_{m}\mathbf{u} = {}^{m+1}\mathbf{u} - {}^{m}\mathbf{u} \tag{A-10}$$

Then substituting Eq.(A-9) and Eq.(A-10) into Eq.(A-2), we can obtain

$$\mathbf{K}({}^{m}\mathbf{u}) \bullet \Delta^{m+1}_{m}\mathbf{u} = \mathbf{f} \tag{A-11}$$

Using the Moore-Penrose generalized inverse matrix, we can obtain the general solution of Eq.(A-11)

$$\Delta^{m+1}_{m}\mathbf{u} = \mathbf{K}({}^{m}\mathbf{u})^{+}\mathbf{f} + [\mathbf{I} - \mathbf{K}({}^{m}\mathbf{u})^{+} \bullet \mathbf{K}({}^{m}\mathbf{u})]\alpha \tag{A-12}$$

At the right side of Eq.(A-12), the first term is called particular solution, and the second term is called complementary solution. Here α is an arbitrary small scalar.

Firstly, the component of external force corresponding to the elastic elongation is noted as $\mathbf{f}_1$, and the component of external force to the no elongation displacement method is noted as $\mathbf{f}_2$, these two parameters are given as follows:

$$\mathbf{f}_1 = \mathbf{K}({}^{m}\mathbf{u}) \bullet \mathbf{K}({}^{m}\mathbf{u})^{+} \bullet \mathbf{f} \tag{A-13}$$

$$\mathbf{f}_2 = [\mathbf{I} - \mathbf{K}({}^{m}\mathbf{u})^{+} \bullet \mathbf{K}({}^{m}\mathbf{u})] \bullet \mathbf{f} \tag{A-14}$$

The no elongation displacement $\Delta^{m+1}_{m}\mathbf{u}$ can be obtained by using the following equation.

$$\Delta^{m+1}_{m}\mathbf{u} = \alpha \mathbf{f}_2 \tag{A-15}$$

In the initial state, prestress in the membrane is 0, so when external force perpendicular to the membrane is applied, $\mathbf{f}_1$=0. Then we can use Eq.(A-15) to get the no elongation displacement $\Delta^{m+1}_{m}\mathbf{u}$. After updating the shape of membrane with this no elongation displacement, the tangential stiffness matrix is no longer singularity, then Eq.(A-2) can be used to get the elongation displacement.

Comparing to the hypothesis damping term method in A.1 and no elongation displacement method in A.2, it is more convenient to utilize the latter one. Because there is no additional damping term matrix needed to be added to tangential stiffness matrix, only thing we do is to use Eq. (A-15) in the calculation.

A.3 Numerical example

Fig.A-1 shows a quadrangular plane membrane under a concentrated load in perpendicular direction. The plane of membrane is parallel to plane *uv*. The size of plane membrane is 6.096m×6.096m. The thickness is 0.1058mm. And the Young's modulus of the membrane is 206Gpa, Poison's ratio is 0.3. A concentrated load with magnitude 44458N is applied in –*w* direction. The initial prestress of the membrane is 551.6MPa. And in FE analysis, the membrane is divided into 32 isoparametric triangular elements [5], [16].

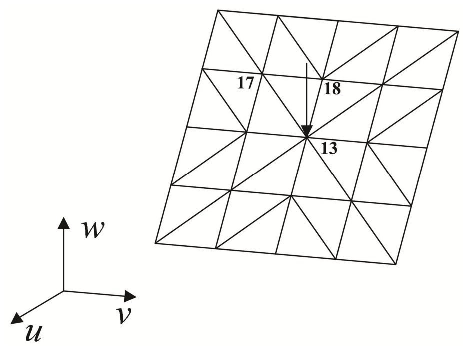

Fig.A-1 Quadrangular plane membrane [122], [161], [169]

Table.A-1 shows the comparison of results with past researches. We can observe the numerical results of displacements by this appendix is very approaching to the ones in the past researches.

Table.A-1 Comparison of results with past researches (with prestress)

Node	Displacement [mm]	Prestress [551.6Pa]			
		Levy [122]	Gil [161]	Valdés [169]	This appendix
17	*u*	0.38	0.36	0.36	0.37
	v	0.38	0.36	0.36	0.37
	w	-36.35	-36.14	-36.30	-36.36
18	*u*	0.43	0.43	0.43	0.43
	v	0	0	0	0
	w	-66.17	-66.04	-66.17	-66.18
13	*u*	0	0	0	0
	v	0	0	0	0
	w	-168.71	-168.30	-168.30	-168.78

In another aspect, when there is no prestress in the membrane in the initial state, then the methods introduced in A.1 and A.2 can be used to get the displacement. In the latter calculation of Eq.(A-15), the parameter α is assumed to be 10^{-4}. In the same numerical example, Valdés[169] utilizes generalized-α integral method to obtain the displacement when there is no prestress in the initial state. The comparison of the results obtained by using the methods in appendix and past research is shown in Table.A-2.

Fig.A-2 shows the relationship of displacement and concentrated load with and without prestress. In the case of no prestress, the results obtained by the hypothesis damping term method and the no elongation method are almost identical to each other.

Table.A-2 Comparison of results with past research (without prestress)

<table>
<tr><td rowspan="3">Node</td><td rowspan="3">Displacement [mm]</td><td colspan="3">Prestress [0 Pa]</td></tr>
<tr><td>Valdés [169]</td><td colspan="2">This appendix</td></tr>
<tr><td>Generalized-α integral method</td><td>Hypothesis damping term method</td><td>No elongation displacement method</td></tr>
<tr><td>13</td><td>w</td><td>234.75</td><td>235.92</td><td>235.91</td></tr>
</table>

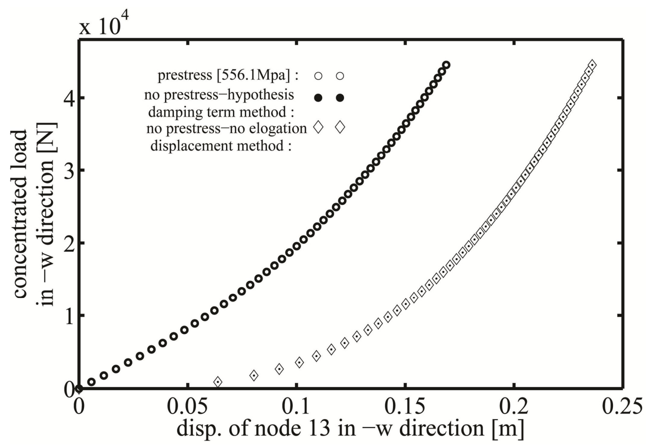

Fig.A-2 Relationship of displacement and concentrated load

Appendix B

B.1 Simple methods for in-plane stability of the arch

In Section.4.4.1 of Chapter 4, we have obtained the general solution of displacements v and w, and then calculated the critical loads of circular arch with hinged ended and fixed ended. Here by taking the example of arch with hinged ended boundary conditions, we introduce other two methods in the past researches. Firstly, we talk about a method by using approximate functions of buckling modes [103], [108], [165]. The boundary conditions are assumed as hinged ended: v=0, v''=0 at φ=0 and $\varphi=\alpha$. Then a function of buckling mode satisfying the boundary conditions can be assumed as [103], [108], [165].

$$v = A\sin\frac{2\pi}{\alpha}\varphi \tag{B-1}$$

Then Substituting Eq.(B-1) into buckling controlling equation Eq.(4.20) in Chapter 4, we can obtain

$$[(\frac{2\pi}{\alpha})^2 - 1 - \frac{qR^3}{EI_x})][(\frac{2\pi}{\alpha})^2 - 1]A\cos\frac{2\pi}{\alpha}\varphi = 0 \tag{B-2}$$

As A is an arbitrary number, then the solution of Eq.(B-2) is

$$q_{cr} = [(\frac{2\pi}{\alpha})^2 - 1]\frac{EI_x}{R^3} \tag{B-3}$$

Especially, when $\alpha = \pi$, the first order critical load q_{cr} is

$$q_{cr} = \frac{3EI_x}{R^3} \tag{B-4}$$

Another method to obtain critical load of the circular arch with hinged ended is introduced by Timoshenko [42], given in Eq.(B-5)~ Eq.(B-12).

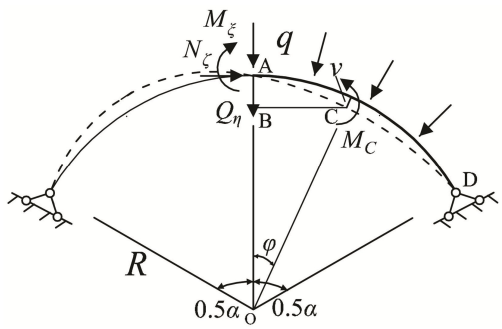

Fig.B-1 Circular arch with hinged ended boundaries

Fig.B-1 shows a circular arch with hinged ended. From the first term of Eq.(4.5) and Eq.(4.8) in Chapter 4, the expression of moment M_ξ can be obtained as

$$M_\xi = -EI_x K_x = -EI_x\left(\frac{d^2v}{ds^2} + \frac{1}{R}\frac{dw}{ds}\right) \tag{B-5}$$

Substituting the pre-establish condition $\frac{dw}{ds} = \frac{v}{R}$ in Eq.(4.17) into Eq.(B-5), we can obtain

$$\frac{d^2v}{ds^2} + \frac{v}{R^2} = -\frac{M_\xi}{EI_x} \tag{B-6}$$

As the shape of the arch is assumed as circular, then $ds = Rd\varphi$ is a pre-established condition, then the same expression of Eq.(B-6) is

$$\frac{d^2v}{d\varphi^2} + v = -\frac{R^2}{EI_x}M_\xi \tag{B-7}$$

From Eq.(B-1) we can obtain the moment M_C in arbitrary cross section C is

$$M_C = qRv \tag{B-8}$$

Substituting Eq.(B-8) into Eq.(B-7), we can obtain

$$\frac{d^2v}{d\varphi^2} + \left(1 + \frac{qR^3}{EI_x}\right)v = 0 \tag{B-9}$$

The general solution of Eq.(B-9) is

$$v = A\cos\tau\alpha + B\sin\tau\alpha \tag{B-10}$$

The expression of τ can be found in Eq.(4.22) in Chapter 4. Then from the boundary conditions, we can obtain

$$\begin{cases} 0 = A \\ 0 = -A \\ 0 = A\cos(\pi\tau) + B\sin(\pi\tau) \\ 0 = -A\tau^2\cos(\pi\tau) - B\tau^2\sin(\pi\tau) \end{cases} \tag{B-11}$$

Then we can obtain A=0, at this time B cannot be 0, the buckling control equation is

$$\sin(\pi\tau) = 0 \tag{B-12}$$

Because τ is larger than 1, then the minimum positive value of τ which satisfies Eq.(B-12) is 2. The corresponding critical load is same as the one in Eq.(B-4).

B.2 Approach to solve the fifth order linear differential equation

Another method to obtain the general solution of the five order linear differential equation in Eq.(4.20) in Chapter 4 is introduced. We assume the general solution of displacement v as

$$v = e^{r\varphi} \tag{B-13}$$

Then substituting Eq.(B-13) into Eq.(4.20), and utilizing the expression of τ in Eq.(4.22), we can obtain

$$[r^4 + (\tau^2+1)r^2 + \tau^2]re^{r\varphi} = 0 \tag{B-14}$$

The characteristic equation can be obtained as

$$[r^4 + (\tau^2+1)r^2 + \tau^2]r = 0 \tag{B-15}$$

Then we know the solution of r in Eq.(B-15) is r=0 or $r^4 + (\tau^2+1)r^2 + \tau^2 = 0$. From the latter equation, we know

$$r^2 = \frac{-(1+\tau^2) \pm \sqrt{(1+\tau^2)^2 - 4\tau^2}}{2} = \frac{-(1+\tau^2) \pm (\tau^2-1)}{2} = \begin{cases} -1 \\ -\tau^2 \end{cases} \tag{B-16}$$

The four solutions of r in Eq.(B-16) are $r_1 = i$, $r_2 = -i$, $r_3 = \tau i$, $r_4 = -\tau i$. Then including r=0 in above narrative, the general solution of Eq.(4.20) can be expressed as

$$v = A\sin\varphi + B\cos\varphi + C\sin\tau\varphi + D\cos\tau\varphi + E \tag{B-17}$$

Eq.(B-17) is identical to Eq.(4.27) in Chapte4.

B.3 Buckling of the arch out-of-plane

Now another kind of boundary conditions in Fig.4-10 in Chapter 4 is considered. The boundary conditions are assumed as hinged ended in-plane and out-of-plane, that is, among the six DOF of the node at each side of the arch, three translation DOF are constrained, and the other three rotational DOF are free. This kind of boundary conditions can be expressed as

(1) $M_\eta = 0$ at $\varphi = 0$ and $\varphi = \alpha$

(2) $M_\zeta = 0$ at $\varphi = 0$ and $\varphi = \alpha$

(3) $u = 0$ at $\varphi = 0$ and $\varphi = \alpha$

Firstly, the boundary condition (1) is identical to $K_y = 0$. From Eq.(4.6) and identical relation $ds = Rd\varphi$, we can obtain $K_y = \dfrac{d^2u}{ds^2} + \dfrac{\theta}{R} = 0 \to \dfrac{1}{R}\dfrac{d^2u}{d\varphi^2} + \theta = 0$ at $\varphi = 0$ and $\varphi = \alpha$. In addition, Eq.(4.58) is substituted into previous equation, then $\dfrac{d^2\theta}{d\varphi^2} + \theta = 0$ is obtained. Then boundary condition (1) can be expressed as

$$\begin{cases} 0 = B + D - Bk_1^2 + Dk_2^2 \\ 0 = A\sin(\alpha k_1) + B\cos(\alpha k_1) + C\sinh(\alpha k_2) + D\cosh(\alpha k_2) \\ \quad - Ak_1^2\sin(\alpha k_1) - Bk_1^2\cos(\alpha k_1) + Ck_2^2\sinh(\alpha k_2) + Dk_2^2\cosh(\alpha k_2) \end{cases} \tag{B-18}$$

Similarly, the boundary condition (2) is identical to curvature $K_z = 0$. From Eq.(4.7) and $ds = Rd\varphi$, we can obtain $K_z = \dfrac{d\theta}{ds} - \dfrac{1}{R}\dfrac{du}{ds} = 0 \to \dfrac{d\theta}{d\varphi} - \dfrac{1}{R}\dfrac{du}{d\varphi} = 0$ at $\varphi = 0$ and $\varphi = \alpha$. Substituting Eq.(4.59) into previous equation, then $\dfrac{d\theta}{d\varphi} + \int \theta d\varphi = 0$ is obtained. Then boundary condition (2) can be expressed as

$$\begin{cases} 0 = Ak_1 + Ck_2 - \dfrac{A}{k_1} + \dfrac{C}{k_2} + E \\ 0 = Ak_1\cos(\alpha k_1) - Bk_1\sin(\alpha k_1) + Ck_2\cosh(\alpha k_2) + Dk_2\sinh(\alpha k_2) \\ \quad -\dfrac{A}{k_1}\cos(\alpha k_1) + \dfrac{B}{k_1}\sin(\alpha k_1) + \dfrac{C}{k_2}\cosh(\alpha k_2) + \dfrac{D}{k_2}\sinh(\alpha k_2) + E \end{cases} \tag{B-19}$$

Finally, from boundary condition (3), we can obtain

$$\begin{cases} 0 = B + D - \lambda(-\dfrac{B}{k_1^2} + \dfrac{D}{k_2^2} + F) \\ 0 = A\sin(\alpha k_1) + B\cos(\alpha k_1) + C\sinh(\alpha k_2) + D\cosh(\alpha k_2) \\ \quad -\lambda(-\dfrac{A}{k_1^2}\sin(\alpha k_1) - \dfrac{B}{k_1^2}\cos(\alpha k_1) + \dfrac{C}{k_2^2}\sinh(\alpha k_2) + \dfrac{D}{k_2^2}\cosh(\alpha k_2) + \alpha E + F) \end{cases} \tag{B-20}$$

According to the sequence of A, B, C, D, E and F, a matrix $\mathbf{S_{3D\text{-}P2}}$ is assumed as

$$\mathbf{S_{3D\text{-}P2}} = \begin{bmatrix} 0 & 1-k_1^2 & 0 & 1+k_2^2 & 0 & 0 \\ (1-k_1^2)\sin(\alpha k_1) & (1-k_1^2)\cos(\alpha k_1) & (1+k_2^2)\sinh(\alpha k_2) & (1+k_2^2)\cosh(\alpha k_2) & 0 & 0 \\ k_1 - \dfrac{1}{k_1} & 0 & k_2 + \dfrac{1}{k_2} & 0 & 1 & 0 \\ (k_1 - \dfrac{1}{k_1})\cos(\alpha k_1) & (-k_1 + \dfrac{1}{k_1})\sin(\alpha k_1) & (k_2 + \dfrac{1}{k_2})\cosh(\alpha k_2) & (k_2 + \dfrac{1}{k_2})\sinh(\alpha k_2) & 1 & 0 \\ 0 & 1 + \dfrac{\lambda}{k_1^2} & 0 & 1 - \dfrac{\lambda}{k_2^2} & 0 & -\lambda \\ (1+\dfrac{\lambda}{k_1^2})\sin(\alpha k_1) & (1+\dfrac{\lambda}{k_1^2})\cos(\alpha k_1) & (1-\dfrac{\lambda}{k_2^2})\sinh(\alpha k_2) & (1-\dfrac{\lambda}{k_2^2})\cosh(\alpha k_2) & -\lambda\alpha & -\lambda \end{bmatrix}$$

(B-21)

Then the buckling control equation can be expressed as

$$\det(\mathbf{S_{3D\text{-}P2}}) = 0 \tag{B-22}$$

Here a numerical model with same parameters in Section 4.3.1 in Chapter 4 is used. By using Eq.(B-22), the first order critical load is $q_{cr} = 1.13\dfrac{EI_y}{R^3}$.

B.4 The critical load of stiffening pattern C in Section 5.4.1

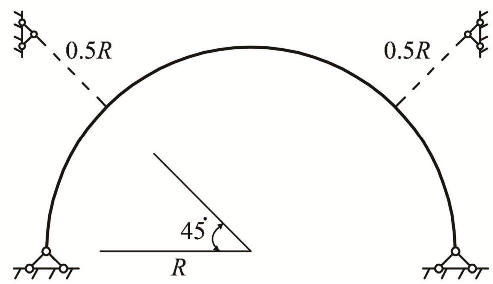

Fig.B-2 Pattern C

As complement in Section 5.4 in Chapter 5, here the critical load of stiffening pattern C in Fig.B-2 when the buckling mode is symmetric in-plane in 2D space is deduced. The boundary conditions of the arch are hinged ended. A spring ratio r is defined as

$$r = \left(\frac{EA}{0.5R}\right) / \frac{EI_x}{R^3} \tag{B-23}$$

In Section 5.4.1, a spring ratio r_p has been noted, and by its definition we should be aware that r_p=0.5r. Fig.B-3(a) shows the configuration of the arch when symmetric buckling mode happens. And Fig.B-3(b) shows the equilibrium state of forces at the position of the spring. Here ϕ in Fig.B-3(a) is assumed as 0.25α.

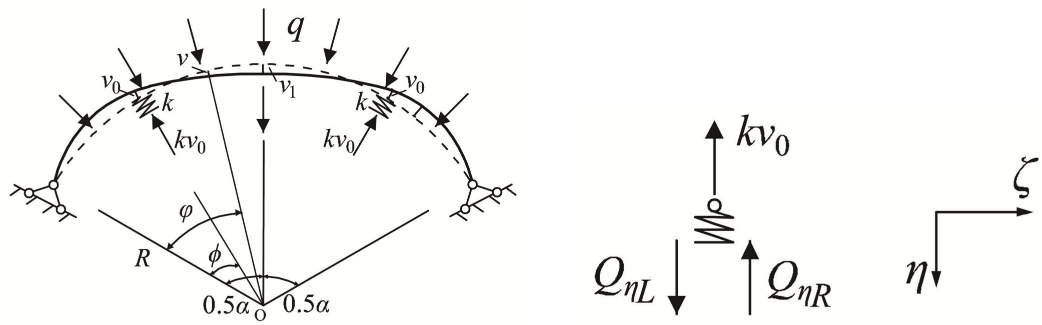

(a) (b)

Fig.B-3 Circular arch with hinged ended boundary conditions

When the boundary conditions of the arch are hinged ended, the boundary conditions can be expressed as

(1) $v_L = 0$, $v_L'' = 0$, $w_L = 0$ at $\varphi = 0$

(2) $Q_{\eta R} = 0$, $v_R' = 0$, $w_R = 0$ $\varphi = 0.5\alpha$

(3) $v_L = v_R = v_0$, $Q_{\eta L} = kv_0 + Q_{\eta R}$, $v_L' = v_R'$, $v_L'' = v_R''$, $w_L = w_R$, $(Q_L)' = (Q_R)'$ at $\varphi = 0.25\alpha$

From the boundary condition (2), we can obtain

$$0 = -A_2 \cos 0.5\alpha + B_2 \sin 0.5\alpha - C_2\tau^3 \cos 0.5\alpha\tau + D_2\tau^3 \sin 0.5\alpha\tau \tag{B-24}$$

$$0 = A_2 \cos 0.5\alpha - B_2 \sin 0.5\alpha + C_2\tau \cos 0.5\alpha\tau - D_2\tau \sin 0.5\alpha\tau \tag{B-25}$$

$$0 = -A_2 \cos 0.5\alpha + B_2 \sin 0.5\alpha - C_2 \frac{\cos 0.5\alpha\tau}{\tau} + D_2 \frac{\sin 0.5\alpha\tau}{\tau} + 0.5\alpha E_2 + F_2 \tag{B-26}$$

The expression of boundary condition (1) and (2) are omitted here. A matrix $\mathbf{S_{2D\text{-}SHC}}$ is assumed as

$$\mathbf{S_{2D\text{-}SHC}} = \begin{bmatrix}
0 & 1 & 0 & 1 & 1 & 0 & \vdots \\
0 & 1 & 0 & \tau^2 & 0 & 0 & \vdots \\
1 & 0 & \dfrac{1}{\tau} & 0 & 0 & -1 & \vdots \\
0 & 0 & 0 & 0 & 0 & 0 & \vdots \\
0 & 0 & 0 & 0 & 0 & 0 & \vdots \\
0 & 0 & 0 & 0 & 0 & 0 & \vdots \\
\sin 0.25\alpha & \cos 0.25\alpha & \sin 0.25\alpha\tau & \cos 0.25\alpha\tau & 1 & 0 & \vdots \\
0 & 0 & 0 & 0 & 0 & 0 & \vdots \\
\cos 0.25\alpha & -\sin 0.25\alpha & \tau^3 \cos 0.25\alpha\tau & -\tau^3 \sin 0.25\alpha\tau & 0 & 0 & \vdots \\
\cos 0.25\alpha & -\sin 0.25\alpha & \tau \cos 0.25\alpha\tau & -\tau \sin 0.25\alpha\tau & 0 & 0 & \vdots \\
\sin 0.25\alpha & \cos 0.25\alpha & \tau^2 \sin 0.25\alpha\tau & \tau^2 \cos 0.25\alpha\tau & 0 & 0 & \vdots \\
\cos 0.25\alpha & -\sin 0.25\alpha & \dfrac{\cos 0.25\alpha\tau}{\tau} & -\dfrac{\sin 0.25\alpha\tau}{\tau} & -0.25\alpha & -1 & \vdots \\
\sin 0.25\alpha & \cos 0.25\alpha & \tau^4 \sin 0.25\alpha\tau & \tau^4 \cos 0.25\alpha\tau & 0 & 0 & \vdots
\end{bmatrix}$$

$$
\left.\begin{matrix}
\vdots & 0 & 0 & 0 & 0 & 0 & 0 & 0 \\
\vdots & 0 & 0 & 0 & 0 & 0 & 0 & 0 \\
\vdots & 0 & 0 & 0 & 0 & 0 & 0 & 0 \\
\vdots & -\cos 0.5\alpha & \sin 0.5\alpha & -\tau^3 \cos 0.5\alpha\tau & \tau^3 \sin 0.5\alpha\tau & 0 & 0 & 0 \\
\vdots & \cos 0.5\alpha & -\sin 0.5\alpha & \tau \cos 0.5\alpha\tau & -\tau \sin 0.5\alpha\tau & 0 & 0 & 0 \\
\vdots & -\cos 0.5\alpha & \sin 0.5\alpha & -\dfrac{\cos 0.5\alpha\tau}{\tau} & \dfrac{\sin 0.5\alpha\tau}{\tau} & 0.5\alpha & 1 & 0 \\
\vdots & 0 & 0 & 0 & 0 & 0 & 0 & -1 \\
\vdots & \sin 0.25\alpha & \cos 0.25\alpha & \sin 0.25\alpha\tau & \cos 0.25\alpha\tau & 1 & 0 & -1 \\
\vdots & -\cos 0.25\alpha & \sin 0.25\alpha & -\tau^3 \cos 0.25\alpha\tau & \tau^3 \sin 0.25\alpha\tau & 0 & 0 & \dfrac{kR^3}{EI_x} \\
\vdots & -\cos 0.25\alpha & \sin 0.25\alpha & -\tau \cos 0.25\alpha\tau & \tau \sin 0.25\alpha\tau & 0 & 0 & 0 \\
\vdots & -\sin 0.25\alpha & -\cos 0.25\alpha & -\tau^2 \sin 0.25\alpha\tau & -\tau^2 \cos 0.25\alpha\tau & 0 & 0 & 0 \\
\vdots & -\cos 0.25\alpha & \sin 0.25\alpha & -\dfrac{\cos 0.25\alpha\tau}{\tau} & \dfrac{\sin 0.25\alpha\tau}{\tau} & 0.25\alpha & 1 & 0 \\
\vdots & -\sin 0.25\alpha & -\cos 0.25\alpha & -\tau^4 \sin 0.25\alpha\tau & -\tau^4 \cos 0.25\alpha\tau & 0 & 0 & 0
\end{matrix}\right]
$$

(B-27)

The buckling control equation is

$$\det(\mathbf{S}_{\mathbf{2D\text{-}SHC}}) = 0 \tag{B-28}$$

Here the same example in Section. 5.4.1 is used, the central angel of the arch is $\alpha=\pi$. The results obtained by using Eq.(B-18) and by FE method are shown in Fig.B-4. From Fig.B-4, we can observe that the maximum difference of the two results is about 2.2%.

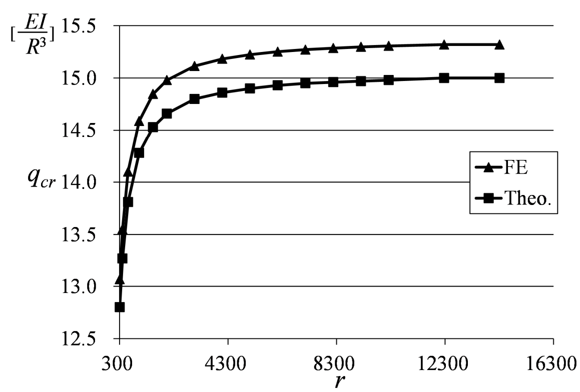

Fig.B-4 Comparison of the results by theoretical method and FE method

B.5 Coupling effect of in-plane stability and out-of-plane stability

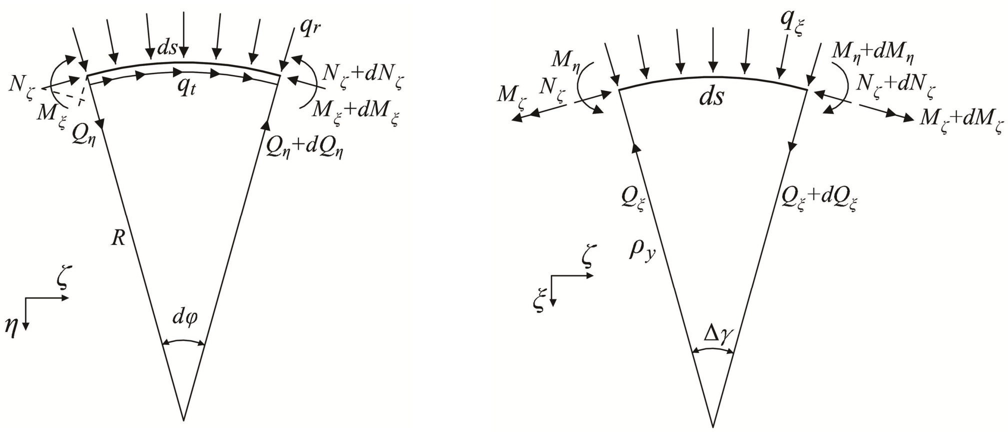

(a) In-plane (b) Out-of-plane

Fig.B-5 Isolated infinitesimal body of the arch (in Chapter 4) [108]

In Chapter 4, the in-plane stability and out-of-plane stability of the arch are discussed respectively. In analyzing the out-of-plane stability, the assumptions in past researches are used, which are $M_\xi = 0$ and $N_\varsigma = qR$. If we do not consider these assumptions but consider all the equilibrium forces, we can obtain

$$\begin{cases} \sum F_\varsigma = 0 \\ \sum F_\eta = 0 \\ \sum M_\xi = 0 \\ \sum F_\xi = 0 \\ \sum M_\eta = 0 \\ \sum M_\varsigma = 0 \end{cases} \tag{B-29}$$

From (B-29), we can obtain

$$\begin{cases} \sum F_\varsigma = N_\varsigma + dN_\varsigma - N_\varsigma \cos d\varphi - Q_\eta \sin d\varphi - q_t ds + \underline{Q_\xi \sin\Delta\gamma} = 0 \\ \sum F_\eta = Q_\eta + dQ_\eta - Q_\eta \cos d\varphi + N_\varsigma \sin d\varphi - q_r ds = 0 \\ \sum M_\xi = M_\xi + dM_\xi - M_\xi \underline{\cos\Delta\gamma} + Q_\eta ds + m_\xi ds + \underline{M_\zeta \sin\Delta\gamma} = 0 \\ \sum F_\xi = Q_\xi + dQ_\xi + q_\xi ds - N_\varsigma \sin\Delta\gamma - Q_\xi \cos\Delta\gamma = 0 \\ \sum M_\eta = M_\eta + dM_\eta - M_\eta \cos d\varphi + M_\zeta \sin d\varphi + m_\eta ds + Q_\xi ds = 0 \\ \sum M_\varsigma = M_\varsigma + dM_\varsigma - M_\varsigma \cos d\varphi - M_\eta \sin d\varphi - \underline{M_\xi \sin\Delta\gamma} + m_\varsigma ds = 0 \end{cases} \tag{B-30}$$

The underline terms in Eq.(B-30) are the ones considering the coupling effect of all moments and forces in equilibrium, and these terms are not taken into consideration in Chapter 4.

In Eq.(B-30), we neglect the effect of m_ξ, m_η, m_ς and q_t, and as $d\varphi$, $\Delta\gamma$ is very small, here we suppose $\cos d\varphi\approx 1$, $\sin d\varphi\approx d\varphi$, $\cos\Delta\gamma\approx 1$, $\sin\Delta\gamma\approx\Delta\gamma$, then Eq.(B-30) transforms into

$$\begin{cases} \dfrac{dN_\varsigma}{ds}-\dfrac{Q_\eta}{R}+\underline{Q_\xi K_y}=0 \\ \dfrac{dQ_\eta}{ds}+\dfrac{N_\varsigma}{R}-q_r=0 \\ \dfrac{dM_\xi}{ds}+Q_\eta+\underline{M_\zeta K_y}=0 \\ \dfrac{dQ_\xi}{ds}+q_\xi-N_\varsigma K_y=0 \\ \dfrac{dM_\eta}{ds}+\dfrac{M_\zeta}{R}+Q_\xi=0 \\ \dfrac{dM_\varsigma}{ds}-\dfrac{M_\eta}{R}-\underline{M_\xi K_y}=0 \end{cases} \tag{B-31}$$

Now let's talk about the solution of Eq.(B-31). Firstly, from the third term and fifth term in Eq.(B-31), we can obtain Q_η and Q_ξ as

$$\begin{cases} Q_\eta=-\dfrac{dM_\xi}{ds}-\underline{M_\zeta K_y} \\ Q_\xi=-\dfrac{dM_\eta}{ds}-\dfrac{M_\zeta}{R} \end{cases} \tag{B-32}$$

Secondly, from the combination of first term and second term in Eq.(B-30), at the same time utilizing the expression of Q_ξ in Eq.(B-32) we can obtain

$$-R^2\frac{d^2Q_\eta}{ds^2}+R^2\frac{dq_r}{ds}-Q_\eta+R\underline{Q_\xi K_y}=0 \tag{B-33}$$

Substituting Eq.(B-32) in to Eq.(B-33), we can obtain

$$R^2\frac{d^3M_\xi}{ds^3}+R^2\underline{\underline{\frac{d(M_\zeta K_y)}{ds}}}+R^2\frac{dq_r}{ds}+\frac{dM_\xi}{ds}+\underline{M_\zeta K_y}+\underline{R(-\frac{dM_\eta}{ds}-\frac{M_\zeta}{R})K_y}=0 \tag{B-34}$$

In another aspect, the combination of the fourth term and fifth term in Eq.(B-31), we can obtain

$$-\frac{d^2 M_\eta}{ds^2} - \frac{1}{R}\frac{dM_\zeta}{ds} + q_\xi - N_\varsigma K_y = 0 \tag{B-35}$$

Then the independent equations of Eq.(B-31) are as follows:

$$\begin{cases} R^2 \dfrac{d^3 M_\xi}{ds^3} + R^2 \dfrac{\underline{d(M_\zeta K_y)}}{ds} + R^2 \dfrac{dq_r}{ds} + \dfrac{dM_\xi}{ds} + \underline{M_\zeta K_y} + \underline{R(-\dfrac{dM_\eta}{ds} - \dfrac{M_\zeta}{R})K_y} = 0 \\ -\dfrac{d^2 M_\eta}{ds^2} - \dfrac{1}{R}\dfrac{dM_\zeta}{ds} + q_\xi - N_\varsigma K_y = 0 \\ \dfrac{dM_\varsigma}{ds} - \dfrac{M_\eta}{R} - \underline{M_\xi K_y} = 0 \end{cases} \tag{B-36}$$

When consider the unlined terms in Eq.(B-36), multiply term of moment and curvature makes it different to get closed form solutions of the critical loads.

Appendix C

C.1 Comparison of two stiffening effects

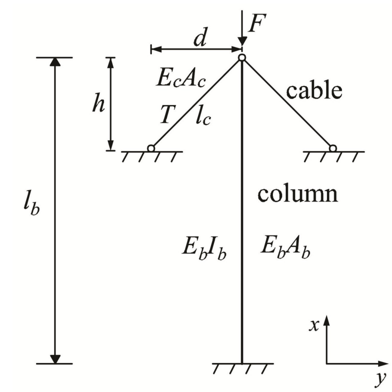

Fig.C-1 Column stiffened by straight cables [174]

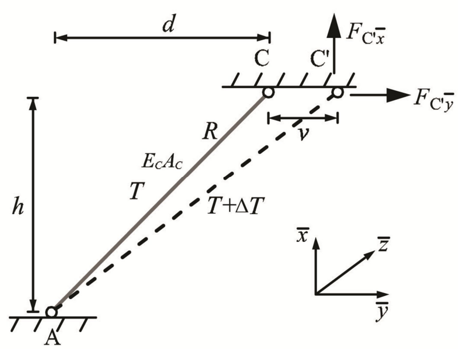

Fig.C-2 Movement of straight cable

Fig.C-1 shows a column stiffened by two straight cables. Symbols in Fig.(C-1) refer to Section 6.2 in Chapter 6. Fig.C-2 shows the movements of cable in $\bar{y}$ direction. Here symbol "R" is used to substitute for symbol "l_c" in Fig.C-1. In Fig.C-2, position C moves in $\bar{y}$ direction to a new position C' with a small displacement v. T is assumed as the internal force of the cable before buckling. Then from the geometrical relationship after movement, the increment of the length in cable is

$$\Delta R = \sqrt{h^2 + (d+v)^2} - R = \sqrt{R^2 + 2dv + v^2} - R \tag{C-1}$$

And the increment of internal force of the cable after movement is

$$\Delta T = \frac{E_C A_C}{R}\Delta R \tag{C-2}$$

1) Case 1: T=0

The reaction force at position C' after movement is

$$\begin{cases} F_{C'\bar{y}} = \Delta T \dfrac{d+v}{\sqrt{R^2+2dv+v^2}} = \dfrac{E_C A_C}{R}\dfrac{d+v}{\sqrt{R^2+2dv+v^2}}(\sqrt{R^2+2dv+v^2}-R) \\ F_{C'\bar{x}} = \Delta T \dfrac{h}{\sqrt{R^2+2dv+v^2}} = \dfrac{E_C A_C}{R}\dfrac{h}{\sqrt{R^2+2dv+v^2}}(\sqrt{R^2+2dv+v^2}-R) \end{cases} \tag{C-3}$$

Then considering the symmetry of cables in Fig.C-1, the resultant force F_y in y direction can be obtained as

$$F_y = F_{C'\bar{y}}(v) - F_{C'\bar{y}}(-v)$$

$$= \frac{E_C A_C}{R}\frac{d+v}{\sqrt{R^2+2dv+v^2}}(\sqrt{R^2+2dv+v^2}-R) - \frac{E_C A_C}{R}\frac{d-v}{\sqrt{R^2-2dv+v^2}}(\sqrt{R^2-2dv+v^2}-R) \tag{C-4}$$

When the value of v approaches to 0, the limiting ratio of F_y and v is

$$\lim_{v\to 0}\frac{F_y}{v} = \frac{2d^2}{R^2}\frac{E_c A_c}{R} \tag{C-5}$$

Here a parameter k_E is assumed as

$$k_E = \frac{2d^2}{R^2}\frac{E_C A_C}{R} \tag{C-6}$$

In another aspect, the resultant force in global Cartesian coordinate in x direction is

$$F_x = F_{C'\bar{x}}(v) + F_{C'\bar{x}}(-v) \tag{C-7}$$

When the value of v is small value, the limiting value of F_x is

$$\lim_{v\to 0} F_x = \lim_{v\to 0}\frac{E_C A_C h}{R}\left(2 - R\frac{\sqrt{R^2+v^2+2dv}+\sqrt{R^2+v^2-2dv}}{\sqrt{R^2+v^2+2dv}\sqrt{R^2+v^2-2dv}}\right) = 0 \tag{C-8}$$

2) Case 2: $T \neq 0$

Here the stiffening effect of elastic stiffnesses of cables is temporarily ignored, let's only talk about the stiffening effect of internal force T. Assuming T keeps constant after movement. Then from the geometrical relationship of the cable, we can obtain the reaction forces at position C' are

$$\begin{cases} F_{C'\bar{y}} = T\dfrac{d+v}{\sqrt{R^2+2dv+v^2}} \\ F_{C'\bar{x}} = T\dfrac{h}{\sqrt{R^2+2dv+v^2}} \end{cases} \tag{C-9}$$

Similarly, the resultant force F_y in global Cartesian coordinate in y direction can be obtained as

$$F_y = F_{C'\bar{y}}(v) - F_{C'\bar{y}}(-v) = T\frac{d+v}{\sqrt{R^2+2dv+v^2}} - T\frac{d-v}{\sqrt{R^2-2dv+v^2}} \tag{C-10}$$

Then the limiting ratio of F_y and v when v approaches to 0 is

$$\lim_{v\to 0}\frac{F_y}{v} = T\lim_{v\to 0}\left(\frac{\dfrac{d+v}{\sqrt{R^2+2dv+v^2}} - \dfrac{d-v}{\sqrt{R^2-2dv+v^2}}}{v}\right) = \frac{2h^2}{R^2}\frac{T}{R} \tag{C-11}$$

When the value of v is very small, assuming a parameter k_T as

$$k_T = \frac{2h^2}{R^2}\frac{T}{R} \tag{C-12}$$

The sign of k_T is

$$\begin{cases} k_T > 0, & if\ T\ is\ tension. \\ k_T < 0, & if\ T\ is\ compression. \\ k_T = 0, & if\ T\ is\ 0. \end{cases} \tag{C-13}$$

The resultant force F_x in global Cartesian coordinate in x direction is

$$F_x = F_{C'\bar{x}}(v) + F_{C'\bar{x}}(-v) = T\frac{h}{\sqrt{R^2+2dv+v^2}} + T\frac{h}{\sqrt{R^2-2dv+v^2}} \tag{C-14}$$

When the value of v is small, the limiting value of resultant force F_x is

$$\lim_{v\to 0}F_x = \lim_{v\to 0}Th\left(\frac{1}{\sqrt{R^2+2dv+v^2}} + \frac{1}{\sqrt{R^2-2dv+v^2}}\right) = \frac{2Th}{R} \tag{C-15}$$

In another aspect, comparing k_E in Eq.(C-6) and k_T in Eq.(C-12), we can obtain

$$\frac{k_T}{k_E} = \frac{\frac{2h^2}{R^2}\frac{T}{R}}{\frac{2d^2}{R^2}\frac{E_C A_C}{R}} = (\frac{h}{d})^2 \frac{T}{E_C A_C} \tag{C-16}$$

In usual, $E_C A_C \gg T$, then the stiffening effect of T can be ignored. And Table.C-1 is a summary of three stiffening patterns.

Table.C-1 Comparison of three kind stiffening patterns

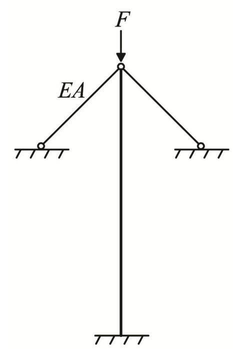 (a) Stiffening pattern Ⅰ	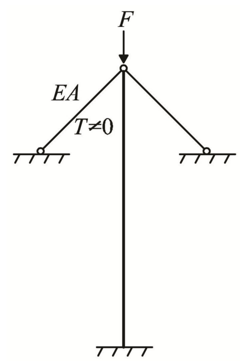 (b) Stiffening pattern Ⅱ	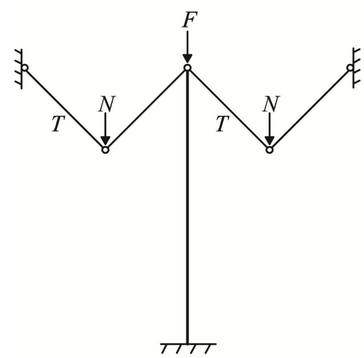 (c) Stiffening patternⅢ
Stiffening effect is aroused by *EA*.	Stiffening effect is aroused by *EA* and *T*, but stiffening effect of *T* can be ignored.	Stiffening effelct is only aroused by *T*, and *EA* does not provide stiffening effect.

C.2 Stability of a column stiffened by one spring

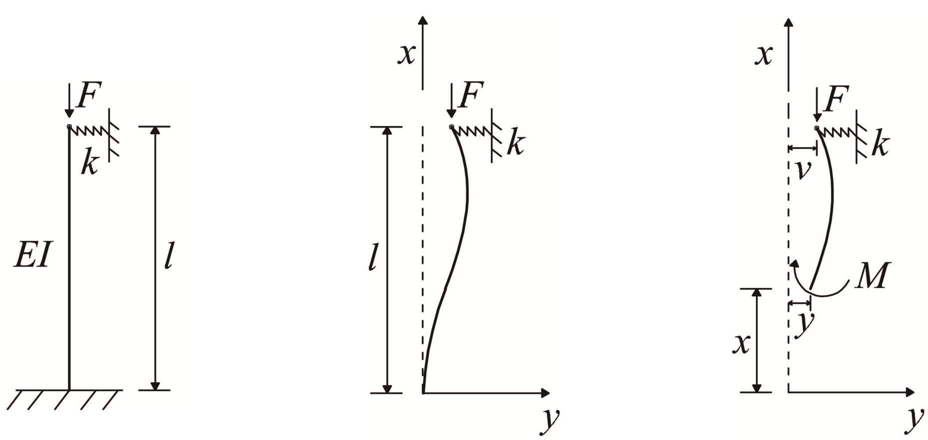

(a) (b) (c)

Fig.C-3 Column stiffened by one spring at top

Fig.C-3(a) shows a column stiffned by one spring at top. Fig.C-3(b) shows the shape of the column after buckling happens. And Fig.C-3(c) shows the isolated infinitesimal body of the column. The relationship between curvature and moment can be expressed as

$$EIy'' = -M \tag{C-17}$$

And from Fig.C-3(c), moment at abritary cross section is

$$M = kv(l-x) - F(v-y) \tag{C-18}$$

Substituting Eq.(C-18) into Eq.(C-17), we can obtain

$$y'' + \frac{F}{EI}y = \frac{-kv(l-x)+Fv}{EI} \tag{C-19}$$

Here a parameter λ is assumed as

$$\lambda^2 = \frac{F}{EI} \tag{C-20}$$

Then Eq.(C-19) transforms into

$$y'' + \lambda^2 y = -\frac{kv}{EI}(l-x) + \lambda^2 v \tag{C-21}$$

The general solution of Eq.(C-21) is

$$y = A\cos\lambda x + B\sin\lambda x + v - \frac{kv}{\lambda^2 EI}(l-x) \tag{C-22}$$

The boundary conditions are : y=0, y'=0 at x=0; y=v at x=l. By using these boundary conditions, we can obtain

$$\begin{cases} A + v - \dfrac{kvl}{\lambda^2 EI} = 0 \\ \lambda B + \dfrac{kv}{\lambda^2 EI} = 0 \\ A\cos\lambda l + B\sin\lambda l + v = v \end{cases} \tag{C-23}$$

Substituting A in the first term and B in the second term into the third term in Eq.(C-23), we can obtain

$$((1 - \frac{kl}{\lambda^2 EI})\cos\lambda l + \frac{k}{\lambda^3 EI}\sin\lambda l)v = 0 \tag{C-24}$$

Eq.(C-24) is the buckling control equation.

1) If elastic stiffness of the spring $k = 0$, Eq.(C-24) transforms into

$$(\cos \lambda l)v = 0 \tag{C-25}$$

As value of v is an arbitrary number, there is

$$\cos \lambda l = 0 \tag{C-26}$$

As the minimum positive value (λl) satisfying Eq.(C-26) is 0.5π, then we can obtain

$$\lambda = \frac{\pi}{2l} \tag{C-27}$$

Substituting Eq.(C-27) into Eq.(C-20), the critical load F_{cr} is

$$F_{cr} = \frac{\pi^2 EI}{(2l)^2} \tag{C-28}$$

2) If elastic stiffness of the spring $k \neq 0$, the solution of Eq.(C-24) is

$$(1 - \frac{kl}{\lambda^2 EI})\cos \lambda l + \frac{k}{\lambda^3 EI}\sin \lambda l = 0 \tag{C-29}$$

Here noting two non-dimensional parameters u and r as

$$\begin{cases} u = \lambda l \\ r = \dfrac{k}{EI / l^3} \end{cases} \tag{C-30}$$

Substituting u and r into Eq.(C-29), we can obtain

$$\tan u = u - \frac{u^3}{r} \tag{C-31}$$

Numerical method can be used to get the solution of u in Eq.(C-31). Especially, when k is infinity, u=4.493 can be obtained. The corresponding critical load F_{cr} is

$$F_{cr} = u^2 \frac{EI}{l^2} \tag{C-32}$$

Table C-2 Materials parameters of the column

	Young's modulus	Poisson's ratio	Internal diameter	External diameter	Length
Column	205[GPa]	0.3	10[cm]	30[cm]	10[m]

Table.C-3 First order buckling modes of column by FE method

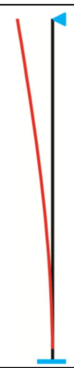		
r=0 $F_{cr}=0.25\dfrac{\pi^2 EI}{l^2}$	r=62.11 $F_{cr}=1.96\dfrac{\pi^2 EI}{l^2}$	r=1.24×10^5 $F_{cr}=2.05\dfrac{\pi^2 EI}{l^2}$

Table.C-2 shows the materials parameters of the column in numerical analysis. And Table.C-3 gives the results obtained by FE methods. In another aspect, the critical loads calculated by Eq.(C-31) are almost identical to the ones obtained by FE methods, so their values are omitted here.

Appendix D

D.1 Approximate approach for the stiffness of pseudo-spring

From Eq.(6.9) in Section 6.3.1 of Chapter 6, reaction forces $F_{C'\bar{y}}$ and $F_{C'\bar{x}}$ are given as follows:

$$\begin{cases} F_{C'\bar{y}} = \dfrac{N((\bar{y}_C+v)^4-(R_1^2-R_2^2)^2)}{2(\bar{y}_C+v)^2\sqrt{4(\bar{y}_C+v)^2R_1^2-(R_1^2-R_2^2+(\bar{y}_C+v)^2)^2}} \\ F_{C'\bar{x}} = \dfrac{N}{2}(\dfrac{R_1^2-R_2^2}{(\bar{y}_C+v)^2}+1) \end{cases} \tag{D-1}$$

Especially, when R_1=R_2, Eq.(D-1) transforms into

$$\begin{cases} F_{C'\bar{y}} = \dfrac{N(\bar{y}_C+v)}{2\sqrt{4R_1^2-(\bar{y}_C+v)^2}} \\ F_{C'\bar{x}} = \dfrac{N}{2}(\dfrac{1}{(\bar{y}_C+v)^2}+1) \end{cases} \tag{D-2}$$

Here the same example in Section 6.6 of Chapter 6 is used. Assuming N=1, $R_1=\dfrac{\sqrt{2}}{10}$, $\bar{y}_C=\sqrt{2}R_1=\dfrac{1}{5}$.

According to Eq.(6.15), the accurate value of stiffness of pseudo spring is

$$k_{accurate} = \frac{4NR_1^2}{(4R_1^2-\bar{y}_C^2)^{(3/2)}} = 10 \tag{D-3}$$

On contrast, here an approximate of stiffness of pseudo-spring is defined as follows:

$$k_{appro.} = [F_{C'\bar{y}}(+v)-F_{C'\bar{y}}(-v)]/v \tag{D-4}$$

Table. D-1 Approximate value of $k_{\text{appro.}}$

v	10^{-4}	10^{-3}	10^{-2}
$F_{C'\bar{y}}$ (+v)	0.50050038	0.50503788	0.55416880
$F_{C'\bar{y}}$ (-v)	0.49950037	0.49503712	0.45341026
$k_{\text{appro.}}$	10.0001	10.0008	10.0759

If the value of v is known, then by static method the reaction forces $F_{C'\bar{y}}(+v)$ and $F_{C'\bar{y}}(-v)$ can be obtained. Table.D-1 shows the results of three different values of v. From table.D-1, we can obtain when v is 10^{-4} or 10^{-3}, the approximation of $k_{\text{appro.}}$ is close to the accurate value in Eq.(D-3), therefore this approximate approach can be used to obtain the stiffness of pseudo-spring.

D.2 Extension of approximate approach

Next the approximate approach to get the stiffness of pseudo-spring in numerical example in Section 7.2.3 of Chapter 7 will be introduced.

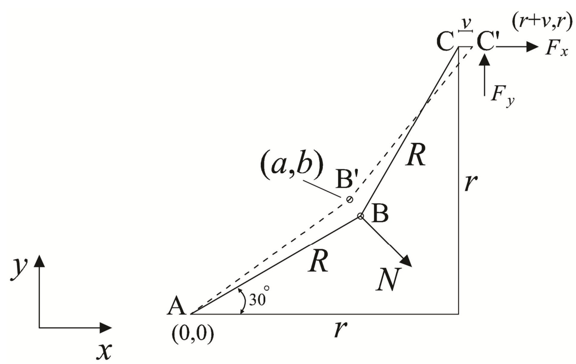

Fig.D-1 Mechanistic movement of the membrane

Fig.D-1 shows the mechanistic movement of the membrane (seen as a curved line) in x direction. The coordinates of A, B' and C' after movements are (0, 0), (a, b), and ($r+v$, r) respectively. The distances of line AB and line BC are assumed to keep constant after movement. Then from the geometric relationship we can obtain

$$\begin{cases} a^2 + b^2 = R^2 \\ (a - r - v)^2 + (b - r)^2 = R^2 \end{cases} \tag{D-5}$$

The solution of (a, b) in Eq.(D-5) is

$$\begin{cases} a = \sqrt{R^2 - b^2} \\ b = \dfrac{-2a(r + v) + (r + v)^2 + r^2}{2r} \end{cases} \tag{D-6}$$

In another aspect, the relationship between F_x and F_y is

$$\frac{F_y}{F_x} = \frac{r - b}{r + v - a} \tag{D-7}$$

Meanwhile, from the equilibrium condition of the moment at the position A, we can obtain

$$\frac{N}{\sqrt{2}} \bullet (a+b) + F_x \bullet r = F_y \bullet (r+v) \tag{D-8}$$

Substituting the expression of F_y in Eq.(D-7) into Eq.(D-8), the expression of F_x can be obtained as

$$F_x = \frac{\frac{N}{\sqrt{2}} \bullet (a+b)}{\frac{r-b}{r+v-a} \bullet (r+v) - r} \tag{D-9}$$

In Fig.D-1, assuming r=1.7, then the value of R in Fig.D-1 is R=1.24448637. For these conditions the approximate stiffness of pseudo-spring is noted k_1. And N is assumed as 1(N). By using Eq.(D-9) and Eq.(D-4), $F_x\,(+v)$, $F_x\,(-v)$ and k corresponding to different values of v are shown in Table.D-2.

Table.D-2 Approximate values of k

v	10^{-4}	10^{-3}	10^{-2}
$F_x\,(+v)$	0.96654714	0.97217320	1.03208550
$F_x\,(-v)$	0.96530527	0.95975404	0.90736341
k	12.4187	12.4192	12.4722

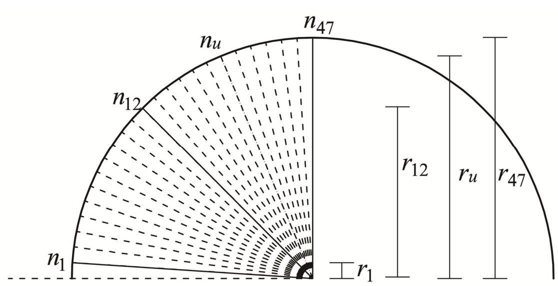

Fig.D-2 Heights of nodes in the circular arch

In FE analysis, the entire arch is divided into 48 linear beam elements along circumferential direction, and each element has the same length. Fig.D-2 shows the heights of nodes in the circular arch.

In Table.D-2, the approximate stiffnesses of pseudo-spring when r is 1.7m have been obtained. By using the same method in equations above and assuming v as 10^{-4} and N=1, we can get other stiffnesses of pseudo-springs at different nodes. The results are given in Table.D-2. In Table.D-3, symbol r_u is means the height of the u-th node.

Table.D-3 Approximate stiffnesses of pseudo-springs

	r_{47}=1.7m	r_{12}=1.2021m	r_1=0.1112m	r_u
k_n	12.4187N/m	17.5624N/m	189.8542 N/m	$k_1\times r_{47}/ r_u$

In another aspect, if v=0, from Eq.(D-7) and Eq.(D-9), we can obtain

$$F_y = \frac{\frac{N}{\sqrt{2}}\bullet(a+b)}{\frac{r-b}{r-a}\bullet r - r}\bullet\frac{r-b}{r-a} = \frac{N}{\sqrt{2}}\frac{(a+b)(r-b)}{(a-b)r} \tag{D-10}$$

Considering the symmetric of mechanistic membrane, the resultant force P_n in y direction is $2F_y$, and their values are given in Table D-4 (assuming N=1.).

Table.D-4 Resultant forces in y direction

	r_{47}	r_{12}	r_1	r_u
P_n	3.3461	3.3461	3.3461	3.3461

Appendix E

E.1 Arch-spring models

a) In-plane

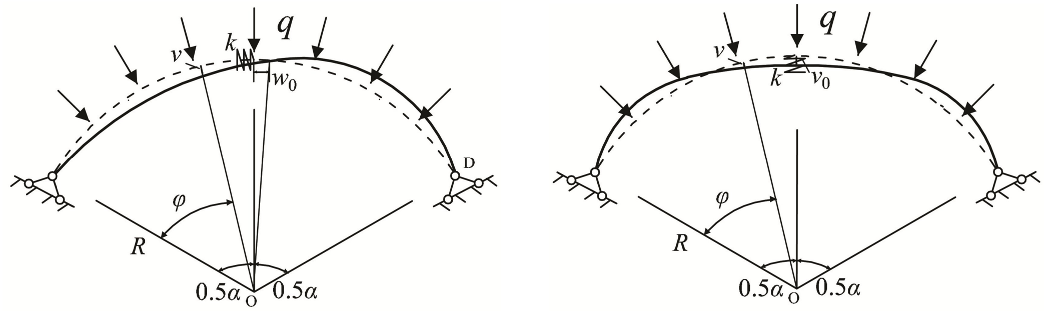

(a) Anti-symmetric arch-spring model (b) Symmetric arch-spring model

Fig.E-1 Arch-spring models in-plane

The arch has a hollow circular constant cross section with external diameter equaling 12mm and internal diameter equaling 6mm. The Young's modulus is 205Gpa and the Poisson's ratio is 0.3. The entire arch is divided into 48 linear beam elements, and each beam element has the same length. One brace is divided into one linear truss element. The radius of the arch is 1m. The central angular of the arch is π. The external force is assumed as uniform compression. Spring ratios r_x and r_y are assumed as $r_x = k/(\frac{EI_x}{R^3})$, $r_y = k/(\frac{EI_y}{R^3})$ respectively.

Table.E-1 Critical loads q_{cr} (unit: EI_x/R^3-hinged ended boundaries)

r_x	(a) Anti-symmetric	(b) Symmetric
0	3.06	8.15
5.11	4.16	8.88
10.22	5.26	9.59
15.34	6.36	10.29
20.45	7.46	10.98
25.56	8.15	11.65
30.67	8.15	12.29
40.90	8.15	13.53
51.12	8.15	14.67
61.34	8.15	15.30
66.45	8.15	15.30

Table.E-2 Critical loads q_{cr} (unit: EI_x/R^3-fixed ended boundaries)

r_x	(a) Anti-symmetric	(b) Symmetric
0	8.15	13.15
5.11	8.88	13.89
10.22	9.59	14.61
20.45	10.98	16.05
30.67	12.29	17.45
40.90	13.15	18.82
51.12	13.15	20.16
61.34	13.15	21.45
71.57	13.15	22.69
81.79	13.15	23.89
92.01	13.15	24.50
97.13	13.15	24.50

b) Out-of-plane

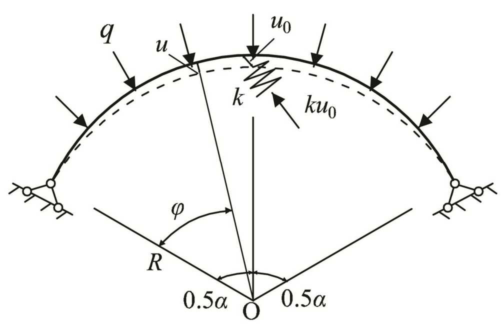

Fig.E-2 Arch-spring model out-of-plane

Table.E-3 Critical loads q_{cr} (unit: EI_y/R^3)

r_y	(a) Hinged ended in-plane and fixed ended out-of-plane	(b) Fixed ended in-plane and out-of-plane
0	2.52	2.52
0.51	2.85	2.85
1.53	3.06	3.50
2.56	3.06	4.15
3.58	3.06	4.79
4.60	3.06	5.43
7.67	3.06	5.83
15.34	3.06	5.83
25.56	3.06	5.83

E.2 Single arch stiffened by braces

a) In-plane

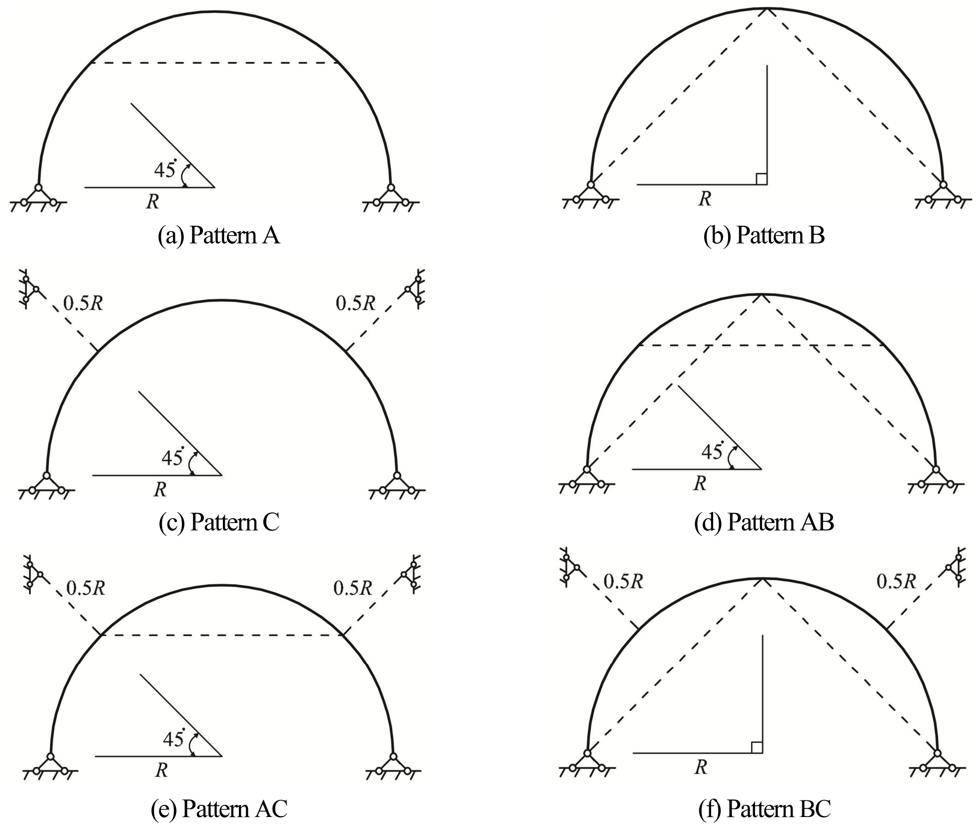

(a) Pattern A (b) Pattern B (c) Pattern C (d) Pattern AB (e) Pattern AC (f) Pattern BC

Fig.E-3 Stiffening patterns of single arch in-plane

Parameters: R-radius of the arch; E_C-Young's modulus of the brace; A_C-area of cross section of the brace; E-Young's modulus of the arch; I-inertia of moment, and I=I_x=I_y. Spring ratio of the brace and the arch is assumed as $r_p = (\frac{E_C A_C}{R})/(\frac{EI}{R^3})$.

Table.E-4 Critical loads q_{cr} (unit: EI/R^3-hinged ended boundaries)

r_p	Pattern A	Pattern B	Pattern C	Pattern AB	Pattern AC	Pattern BC
0	3.06	3.06	3.06	3.06	3.06	3.06
5.11	3.06	3.84	7.41	3.84	7.41	8.20
20.45	3.06	6.17	9.46	6.17	11.28	11.36
51.12	3.06	10.83	10.87	10.83	14.49	14.79
76.68	3.06	14.68	11.69	14.68	15.31	15.32
102.24	3.06	15.30	12.28	15.30	15.31	15.33
153.35	3.06	15.30	13.07	15.30	15.31	15.34

Table.E-5 Critical loads q_{cr} (unit: EI/R^3-fixed ended boundaries)

r_p	Pattern A	Pattern B	Pattern C	Pattern AB	Pattern AC	Pattern BC
0	8.15	8.15	8.15	8.15	8.15	8.15
5.11	8.15	8.67	11.20	8.67	11.20	11.66
20.45	8.15	10.18	15.88	10.18	16.58	17.42
51.12	8.15	12.97	19.01	12.97	19.01	19.71
76.68	8.15	15.00	19.51	15.00	19.51	20.22
102.24	8.15	16.70	19.74	16.70	19.74	20.51
153.35	8.15	19.03	19.97	19.03	19.97	20.87
204.47	8.15	20.27	20.07	20.27	20.07	21.13

b) Out-of-plane

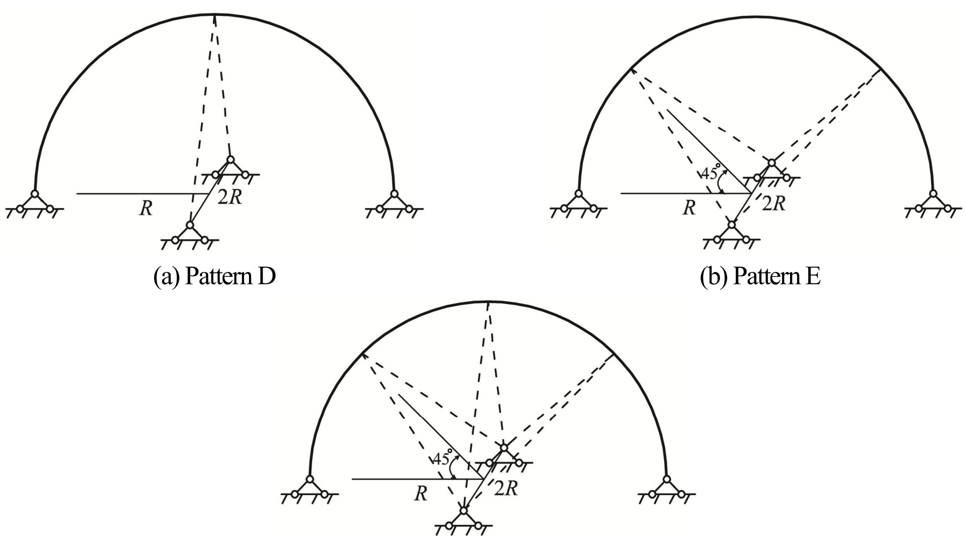

(a) Pattern D (b) Pattern E

(c) Pattern DE

Fig.E-4 Stiffening patterns of single arch out-of-plane

1) Hinged ended in-plane and fixed ended out-of-plane

Table.E-6 Critical loads q_{cr} (unit: EI/R^3)

r_p	Pattern D	Pattern E	Pattern DE
0	2.52	2.52	2.52
0.51	2.75	2.62	2.85
1.53	3.06	2.82	3.52
5.11	3.06	3.45	4.61
25.56	3.06	5.44	10.09
51.12	3.06	6.29	13.04
76.68	3.06	6.65	14.75
102.24	3.06	6.85	15.32
153.36	3.06	7.05	15.32

2) Fixed ended both in-plane and out-of-plane

Table.E-7 Critical loads q_{cr} (unit: EI/R^3)

r_p	Pattern D	Pattern E	Pattern DE
0	2.52	2.52	2.52
0.51	2.75	2.62	2.86
1.53	3.21	2.82	3.52
5.11	4.82	3.45	5.68
25.56	5.83	5.44	10.09
51.12	5.83	6.29	13.04
76.68	5.83	6.65	14.75
102.24	5.83	6.85	15.70
153.36	5.83	7.05	16.63

E.3 Cross arch stiffened by braces

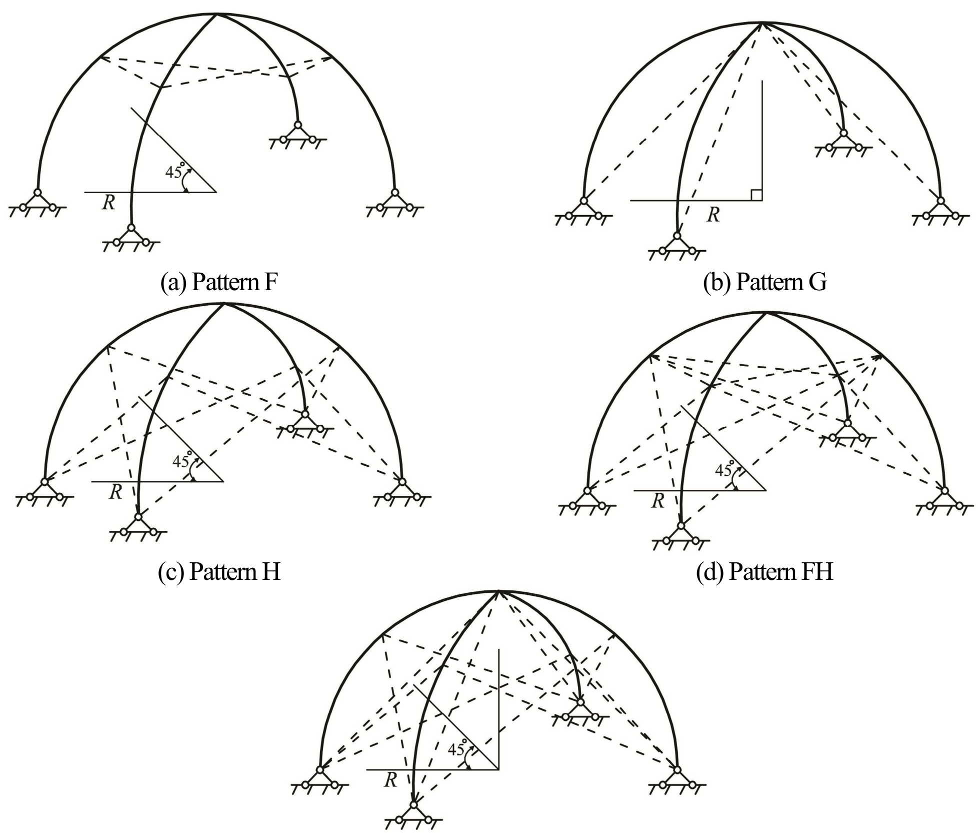

(a) Pattern F (b) Pattern G

(c) Pattern H (d) Pattern FH

(e) Pattern GH

Fig.E-5 Stiffening patterns of cross arch

Table.E-8 Critical load q_{cr} (unit: EI/R^3-hinged ended boundaries)

r_p	Pattern F	Pattern G	Pattern H	Pattern FH	Pattern GH
0	1.16	1.16	1.16	1.16	1.16
5.11	1.16	1.16	2.30	2.30	2.30
20.45	1.16	1.16	5.61	5.61	5.61
51.12	1.16	1.16	9.23	10.99	9.91
76.68	1.16	1.16	9.81	11.80	11.36
102.24	1.16	1.16	10.25	11.89	11.90
153.35	1.16	1.16	10.98	11.94	11.96
204.47	1.16	1.16	11.56	11.96	11.99

Table.E-9 Critical loads q_{cr} (unit: EI/R^3-fixed ended boundaries)

r_p	Pattern F	Pattern G	Pattern H	Pattern FH	Pattern GH
0	5.83	5.83	5.83	5.83	5.83
5.11	5.83	5.83	6.77	6.77	6.77
20.45	5.83	5.83	9.33	9.33	9.34
51.12	5.83	5.83	13.03	13.03	13.04
76.68	5.83	5.83	14.74	14.74	14.75
102.24	5.83	5.83	15.69	15.69	15.70
153.35	5.83	5.83	16.61	16.61	16.63
204.47	5.83	5.83	17.03	17.03	17.07